Landscape Susceptibility to Large Fires

by

Nicholas Gellie

Submitted in fulfilment of the requirements for the degree of
Masters of Philosophy
of the Australian National University
October 2009

THE AUSTRALIAN NATIONAL UNIVERSITY

Candidate's Declaration

This thesis contains no material that has been accepted for the award of any other degree or diploma in any university. To the best of the author's knowledge, it contains no material previously published or written by another person, except where due reference is made in the text.

Nicholas Gellie Date:

Acknowledgements

This study was made possible through support of a scholarship from the Australian National University.

I would like to thank my principal supervisor Dr. Geoffrey Cary at the Fenner School of Environment and Society for his overarching support of my research endeavour.

I would also like to thank my supervisors, Dr. Sandy Berry, Dr. Janette Lyndesay, and Mr. Ken Johnson, for their unwavering and enthusiastic direction, comments, and support. In particular, I acknowledge the support of Mr. Ken Johnson in the detail of time series analysis and classification, and more generally for his enthusiasm in encouraging inquiring discourse.

Dr Sue Holzknecht provided advice on the earlier drafts of the manuscript and proofread the final version. Dr. Alan Wade undertook editing of the later drafts of the manuscript. Dr Kim Wells undertook detailed scientific editing of the penultimate draft. I am indebted to them for their patience and thoroughness in helping me to prepare the manuscript for publication.

Dr. Kevin Tu provided an advanced copy of a scientific paper containing a model of soil evaporation, which turned out to be invaluable in this study. Dr. Anthony Fowler of the University of Auckland provided the software to run his soil water balance model, as well as a background manual to help understand the model parameters. Dr. Michael Roderick and Mr. Michael Hobbins were exceedingly helpful with the supply of short-wave and long-wave radiation flux data obtained from the Research School of Biological Sciences weather station at Canberra Airport. Similarly, Mr. Norm Mueller of Ecowise Environmental provided me with weather data and streamflow records from the upper Cotter River and Queanbeyan River catchments that proved very useful in checking global irradiance estimates and the components of the daily soil water balance models, such as modelled evaporation and run-off. The Bureau of Meteorology freely provided the weather datasets for this study without which would not have made this study possible. Canadian Forest Service provided a spreadsheet for calculating the Canadian Fire Weather Index (FWI) and its components, which was invaluable for creating the time series of potential fire spread.

I also want to thank my partner Helen Rivero for her unwavering and dedicated support.

Finally, I especially wish to acknowledge my parents' insistence that I pursue my dream of postgraduate study. I dedicate this study to my much-loved father, Geoffrey Gellie.

Abstract

The aim of my study is twofold: (1) to develop a methodology to investigate the temporal variation in susceptibility of a landscape to fire and (2) to identify possible critical thresholds at which landscapes becomes predisposed to large landscape fires. Critical thresholds are based on two key indicators: landscape dryness and potential fire spread. The study of these susceptibility factors uses both medium and long-term weather datasets: 65 years of three-hourly and daily weather data from Canberra airport and 136 years of daily rainfall records from Queanbeyan. Landscape dryness and fire weather are examined in a medium-term study, whereas only landscape dryness is used in the long-term study.

Based on the soil dryness index (MSDI) derived by Mount (1972), a new version of a seasonal dryness index (RSDI) was derived from thermodynamic equations, using net radiation and rainfall as the two major pre-determinants of the soil water balance at any point in the landscape. The RSDI model is based on the heat and water balance concepts (Budyko, 1974; Oke, 1987), as well as more recent remote sensing studies of gross primary productivity and transpiration (Berry, 2001; Berry and Roderick, 2002; 2004) and soil evaporation (Priestley and Taylor, 1972; Fisher *et al.*, 2008). The RSDI model requires a minimal number of input weather parameters: daily rainfall, maximum and minimum temperature and relative humidity, as well as projective foliage cover of functional leaf types for any given vegetation (Berry, 2001; Berry and Roderick, 2004; Fisher *et al.*, 2008).

When assessed by independent tests using comparable studies and streamflow data, the RSDI model performed as well as the original MSDI model. The RSDI model was selected to produce a medium-term landscape dryness using data from Canberra airport. The Fowler daily soil water balance model (Fowler, 1992) was employed for the long-term time series of landscape dryness because it only requires rainfall data and an annual profile of average daily evaporation.

A new fire season calendar is developed by averaging 65 years of modelled indices of landscape dryness (SWD), fuel moisture and potential fire spread. Five instead of the four traditional seasons in the fire seasons calendar were identified: winter, spring, high summer, late summer, and autumn with readily identifiable changes in the seasons. The calibrated RSDI and Fowler daily soil water balance model were then used to classify the fire seasons by the annual profiles of soil water deficit over both the medium and long-term. The annual profiles of fire seasons were also classified using the Fire Weather Index (FWI) from the Canadian Forest Fire Danger Rating System. The Fire Weather Index was selected as the preferred model for potential fire spread after comparing it with the FFDI using two methods: (1) an annual profile of a daily potential fire spread anomaly and (2) classification trees of daily potential fire spread. The classification of annual profiles of soil water deficit and FWI distilled down to six and

seven readily identifiable profiles respectively. For both indices, there is considerable heterogeneity in the profiles of fire seasons because of the variability of the synoptic weather patterns, producing rainfall in any given year. The long-term study provided an important set of fire susceptibility benchmarks for recently extreme fire seasons, 1982/83, 2002/03 and 2006/07. The analysis reaffirmed the need for calibrated and validated models of landscape dryness and potential fire spread because the results of the classification technique is dependent on the shape of the annual profiles produced by each index. The analysis also showed that these calibrated models could be used to identify the high-risk fire seasons since the 1870s.

A lightning ignition model, using a decision tree modelling approach, successfully modelled the temporal likelihood of lightning ignition using thunderstorm-days, precipitation, landscape dryness and fire weather. The model indicated that there have been 104 days in the 65 year record at Canberra Airport that have had the potential to start fires. Out of these, only three large landscape fires have occurred in 1951/52, 1982/83, and 2002/03 in the ACT region, which had the right combination of landscape dryness and potential fire spread conditions.

Finally, this study suggests possible relationships between the more severe patterns of landscape dryness and potential fire spread, and the broader continental and sub-global climatic factors important to the development of severe fire conditions.

Further improvement to the models of landscape dryness and fire weather is recommended for future evaluation of fire susceptibility. The all-wave net radiation model (RSDI) shows considerable potential for evaluation of landscape dryness in other regions in south eastern Australia as long as there are accurate and continuous records of the key weather variables that drive the models including: precipitation, minimum and maximum temperature and relative humidity. The Canadian Fire Weather Index model could be further adapted as an index of fire weather and potential fire spread in south eastern Australia by calibrating and validating the algorithms for Drought Code (DC), Duff Moisture Content (DMC), and Fine Fuel Moisture Content (FFMC).

Table of Contents

List of Figures

List of Tables

Appendices

List of Equations

Acronyms, Symbols, and Indices

Acronym	*Quantity*	*Units*
a	year	
A	Priestley-Taylor coefficient	
AWC	available soil water capacity	mm
AWS	automatic weather station	
Cp_d	specific heat of oven-dry dry wood	kJ kg^{-1}
Cp_w	specific heat of water	kJ kg^{-1}
C_{AV}	mean daily cloud cover	Octas
C_P	heat capacity of water	kJ kg^{-1}
δMS	change in soil moisture storage	mm
D_{SR}	days since rain	
DTR	daily temperature range	^{o} C
d_N	day number of the year, starting on 1 January	
$1/d^2$	correction for the eccentricity of the earth's orbit	
D	diffuse radiation	Wm^{-2}
DP_{1500}	dew point at 1500 hr	^{0}C
D_{SR}	days since rain	Day
D_Y	total number of days in a year	Day
e_S	saturation vapour pressure	HPa
e_A	actual vapour pressure	HPa
$e_S\,(T_{MAX})$	water vapour pressure at T_{MAX}	HPa
$e_A\,(T_{MIN})$	water vapour pressure at T_{MIN}	HPa
E_A	actual total evaporation ($E_S + E_T + E_I$) or ($E_{T+S}+E_I$)	mm
E_I	evaporation of water intercepted by vegetation	mm
E_T	transpiration flux	mm
E_P	potential evaporation	mm
E_{PT}	potential transpiration of turgor leaf type (T)	mm
E_{PM}	potential transpiration of mesophyllous leaf type (M)	mm
E_{PS}	potential transpiration of sclerophyllous leaf type (S)	mm
E_S	soil evaporation	mm
E_{TT}	actual transpiration of turgor leaf type (T)	mm
E_{TM}	actual transpiration of mesophyllous leaf type (M)	mm
E_{TS}	actual transpiration of sclerophyllous leaf type (S)	mm
E_{T+S}	evapotranspiration ($=E_S+E_T$)	mm
F	fraction of the AWC at which $E_{T+S}=E_P$ is not limiting for E_S or E_T	

FR	flash run-off	mm
F_M	the fraction of *Mesophyllous* leaf type as a proportion of total TMS cover	
F_S	the fraction of *Sclerophyllous* leaf type as a proportion of total TMS cover	
F_T	the fraction of *Turgor* leaf type as a proportion of total TMS cover	
F_V	the fraction of photosynthetic radiation absorbed by vegetation (FPAR)	
δG	soil heat flux	Wm^{-2}
H	sensible heat flux	Wm^{-2}
HY	heat yield of dry fuel	$J\ g^{-1}$
I	heat output of fire line	Wm^{-1}
k_λ	light attenuation coefficient at a given wavelength	
$L_\downarrow$	downwelling long-wave radiation	Wm^{-2}
$L_\uparrow$	upwelling long wave radiation	Wm^{-2}
L^*	net long wave radiation	Wm^{-2}
m	distance	m
mnth	month of the year	
M_F	fuel fractional moisture content	
M_E	fuel moisture of extinction	
MC_S	upper surface fuel moisture content	
MC_L	lower surface fuel moisture content	
Mf	fractional fuel moisture content	
MJ	megajoules	
n	the number of daily hours of sunshine	
N	number of days in year	day
P_{0900}	precipitation measured at 0900 hours	mm
PFC	projective foliage cover	%
Q_{IG}	heat required for pre-ignition	$kJ\ kg^{-1}$
Q_D	deep sub-surface flow	$mm\ d^{-1}$
Q_{IG}	energy required to bring fuel up to ignition temperature	Wm^{-2}
Q	total run-off	$mm\ d^{-1}$
Q_O	overland water flow	$mm\ d^{-1}$
Q_T	soil water through-flow	$mm\ d^{-1}$
R_A	Extra-terrestrial irradiance	Wm^{-2}
RH	relative humidity	
RH_{1500}	relative humidity measured at 1500 hours	^oC
R_N	net all-wave radiation	Wm^{-2}
R_N	net irradiance for a given wavelength	Wm^{-2}
R_{NS}	net all wave radiation at the soil surface	Wm^{-2}
ROS	rate of spread	$m\ sec^{-1}$
R_S	surface irradiance, global irradiance	Wm^{-2}

$R_{S\lambda}$	net surface irradiance for a given wavelength (λ)	Wm^{-2}
SWD	soil water deficit	mm d^{-1}
T_A	mean daily temperature atmospheric air temperature	^oC, K
T_F	fuel temperature	^oC, K
T_{IGW}	wood ignition temperature	^oC, K
T_{1500}	temperature measured at 1500 hours	^oC
T_{MAX}	maximum daily temperature	^oC, K
T_{MEAN}	mean daily temperature	^oC, K
T_{MIN}	minimum daily temperature	^oC, K
T_S	surface temperature	^oC, K
VPD	vapour pressure deficit	HPa
W	weight of available fuel per square metre	kg m^{-2}
WD_{1500}	wind direction at 1500 hr	
WS	Wind speed	km hr^{-1}
WS_{1500}	wind speed measured at 1500 hours	km hr^{-1}
a	year	

Symbol	***Quantity***	***Units***
α	surface reflectivity, surface albedo	
δ	declination angle in degrees	
ε_A	emissivity of air	
ε_S	emissivity of earth's surface	
Γ	day length	decimal hr
k_λ	radiation attenuation coefficient at a given wavelength	
λ	latent heat of evaporation	J kg^{-1}
μ	optical path length	m
ρ_W	is the density of water	Kg m^{-3}
τ_{CF}	atmospheric transmittance	
τ_D	dust and aerosol atmospheric transmittance	
τ_G	atmospheric gas transmittance	
τ_O	atmospheric ozone transmittance	
τ_W	atmospheric water vapour transmittance	
υ	wind speed	m sec^{-1}

Abbreviation	*Full name*
BIAS	Bias in the estimate
BUI	Build-up Index
CFFDRS	Canadian Forest Fire Danger Rating System
DC	Drought Code
DMC	Duff Moisture Code
DSR	Daily severity rating estimated as a function of the FWI
DSWBM	Daily Soil Water Balance Model
F-DSWBM	Fowler Daily Soil Water Balance Model
FFDI	Forest Fire Danger Index (0-100 scale)
FFMC	Fine Fuel Moisture Code
FPAR	Fraction PAR (Photosynthetically Active Radiation) absorbed by the plant canopy
PFSI	Potential Fire Spread Index
FWI	Fire Weather Index
IOD	Indian Ocean Dipole
ISI	Initial Spread Index, a component of the FWI model
KBDI	Keetch-Byram Drought Index
LLF	Large Landscape Fire
LLMC	Live Leaf Moisture Content
LOESS	Locally weighted smoothing of values in a time series (LOWESS)
MAE	Mean absolute error
MBE	Mean bias error
MSDI	Mount Soil Dryness Index
MDSR	Monthly Total DSR
MSWD	Monthly Mean SWD
NCEP	National Centre for Environmental Prediction
Niño3	Sea surface temperature index in the central Pacific
Niño4	Sea surface temperature index in the western Pacific
PMRE	Percent mean relative error
RMSE	Root mean squared error
RSDI	All-wave net radiation model of Mount Soil Dryness Index (MSDI)
SFWI	Standardised FWI (scaled 0-100 to FFDI)
SAM	Southern Annular Mode
SOI	Southern Oscillation Index
SWD	Soil Water Deficit
WMO	World Meteorological Organisation

Chapter 1: Introduction

1.1 Background

The Black Saturday fires in Victoria in February 2009 were devastating in their impact upon life, property, vegetation and wildlife, occurring under extremes of landscape dryness and fire weather. A key issue is how the Victorian landscapes became so flammable and susceptible to fires burning at such extreme intensities, catching local communities and fire authorities off guard. These fires, together with those that preceded them in 1851, 1898, 1914, 1926, 1939, 1982, 2003 and 2006, can be regarded as large landscape fires (Council of Australian Governments, 2003; Foley, 1947). A LLF is defined here as a fire that burns a significant proportion of a regional landscape, somewhere between 20 and 100% of its area. The area burnt in an LLF is generally over 20,000 hectares in size and likely to be more than 100,000 hectares in size.

This study of landscape susceptibility to large fires is about the historical potential for large landscape fires (LLFs) to develop in the ACT study region, based on the seasonal coincidence of fire susceptibility factors: seasonal landscape dryness, potential fire spread, and sources of ignition (Figure 1.1). Once the longer-term dry landscape conditions are established, the occurrence and potential size of a LLF depend on sources of fire ignition and the daily nature of fire weather. Causes of fire ignition can be from either lightning or human-caused ignitions. Daily weather encompasses diurnal variation in factors such as temperature, atmospheric moisture, wind speed, and atmospheric instability. The synoptic weather processes that drive the extremes of daily weather, such as dry thunderstorms and the hot, dry and windy weather conditions are related to large-scale processes that are an order of magnitude larger in scale than a landscape.

In this study, the three fire susceptibility factors are viewed primarily in a temporal, rather than a spatio-temporal perspective. The first two factors of landscape dryness and potential fire spread predispose a landscape to a LLF while ignition in some form realises the risk of occurrence of a LLF. As Malcolm Gill (2005:67) states: 'The greatest chance of large and destructive fires occurs when the fuels have reached maximum quantity, are continuous over a large region, are in an extremely dry state, and are subject to a strong dry wind in an unstable atmosphere.'

This study thus assumes that the biophysical variation in a landscape, such as variation in topography, vegetation, and disturbance history, is a constant while examining the temporal nature of landscape susceptibility to LLFs from one or two representative points in a landscape. A key factor relating to the spatial aspect of landscape dryness is that of fuel continuity across a landscape. It is assumed that once landscape dryness has reached critical levels, high spatial continuity of dry and available fuels exists across a heterogeneous landscape with highly varied

terrain, vegetation, and climate. That is, even the damper and moister areas in the landscape, such as sheltered wet forests, become dry and available to burn as part of a LLF.

The first predisposing factor of landscape dryness is a seasonal process governed by the levels of dryness reached in vegetation and soil domains. The level of dryness attained in a year is a cumulative function of seasonal daily levels of solar radiation and rainfall. Whilst the drying out of soils and vegetation is a seasonal annual process, accumulated levels of dryness in the soils and underlying regolith can last for several years, generally termed extended drought. Landscape dryness encompasses two critical factors in fire susceptibility at the landscape scale: fuel combustibility and vegetation flammability. The first term 'fuel combustibility' refers to the ease at which dead forest fuels can catch fire and sustain flaming combustion. The second term 'flammability' refers to the ease with which live forest fuels, particularly leaves and small twigs, can ignite and burn, upon being heated from the flames produced by dead forest fuels (Anderson, 1970). Therefore, it is imperative to know when these highly combustible and flammable conditions exist in a landscape in order to anticipate when a LLF might occur. These fire-susceptible conditions take time to develop – usually over a season and occasionally across seasons and years.

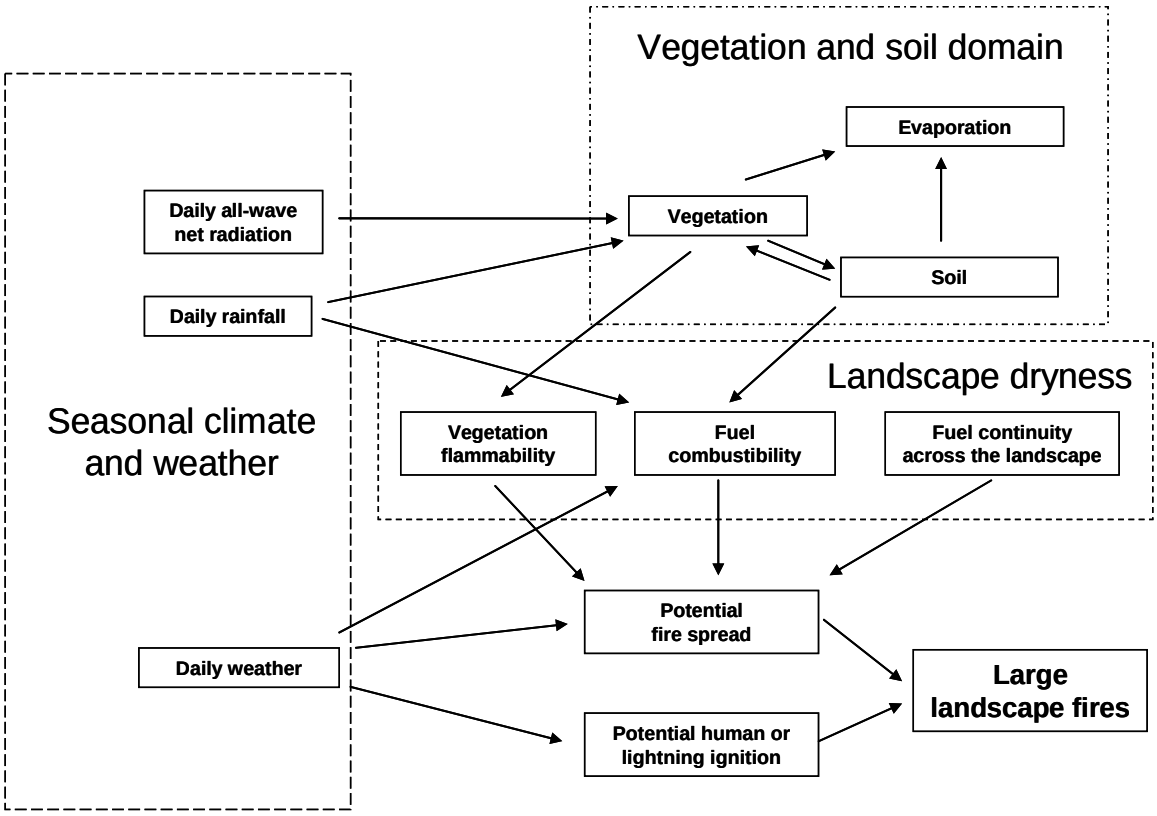

Figure 1.1 Key factors in landscape susceptibility to large fires

Notes: (1) Soil dryness is used as an indirect measure of fuel combustibility and vegetation flammability, given that these factors are not estimated directly.

(2) The predisposing fire susceptibility factors of vegetation flammability, fuel combustibility, and fuel continuity in the landscape are in the box termed landscape dryness in the centre of the diagram.

The approach in this study necessitates monitoring the state of historical conditions of the seasonal factor in landscape susceptibility to large fires — landscape dryness. A daily soil water balance model (DSWBM) is one simple way to assess the state of historical soil dryness and hence vegetation and landscape dryness, based on weather data from one or more representative weather stations.

The equation for a DSWBM takes the general form:

$$\delta MS = P - E_A - (Q_O + Q_T) \quad (mm\ d^{-1}). \qquad \text{Equation 1.1}$$

where δMS is the change in soil moisture store, P is the daily precipitation, E_A is actual total evaporation; Q_O is the runoff via overland flow above the soil surface; and Q_T is the runoff via through-flow within the soil and the immediate sub-soil.

Equation 1.1 represents the state of balance between the processes of rainfall, evaporation, and run-off at a landscape scale. This soil moisture balance can be monitored using a variety of drought or soil moisture indexes, such as the Keetch-Byram Drought Index (KBDI) (Keetch and Byram, 1968), the Palmer Drought Index (PDI) (Palmer, 1965), the Mount Soil Dryness Index (Mount, 1972) and the Fowler soil water balance model (F-SWDBM) (Fowler, 1992; 1994). These soil water balance models (DSWBMs) can be set up at a representative point in a catchment or a region to model hydrological processes using one set of model parameters (Fowler and Adams, 2004). The change of soil moisture conditions can be monitored through time using an index of soil moisture deficit, termed the Soil Dryness Index (SDI) in the MSDI model, or Soil Water Deficit (SWD) in the F-SWDBM model. In this study, the term SWD is used and is defined similarly to the SDI as 'the amount of effective rainfall required to bring the soil back up to field capacity' (Mount, 1972:4).

Daily interactions between atmospheric moisture, such as water vapour pressure and cloud cover, and extra-terrestrial radiation (R_A), drive all-wave net radiation (R_N) (Budyko, 1974; Oke, 1987; Ward and Robinson, 2000). The fraction of the all-wave net radiation reaching the forest canopy and the soil surface governs potential evaporation (E_P). E_P is the maximum evaporation that can take place from a surface fully saturated with water over a specified time (Lhomme, 1997). It is affected by: (1) the stage in the seasonal cycle, (2) the latitudinal position (Budyko, 1974; Iqbal, 1983; Oke, 1987; Roderick, 1993), (3) the position in the landscape such as topographic position, slope, and aspect (Iqbal, 1983), and (4) the vegetation and soil cover (Budyko, 1974; Berry, 2001; Berry and Roderick, 2004; Berry *et al.*, 2006). The proportion of E_P converted into actual evaporation (E_A) is in turn influenced by the seasonal patterns of rainfall that regulate soil moisture and vegetation conditions, such as vegetation canopy cover and plant vigour.

The second factor is fire weather. Brown and Davis (1973) defined fire weather as: 'weather conditions which influence fire ignition, fire behaviour or control'. Daily fire weather incorporates a number of factors that vary from day to day including temperature, air moisture,

atmospheric instability, and wind speed. Day-to-day fire weather is generally difficult to forecast over periods longer than a week, although the weather patterns during the year conform to a natural range of means and expected variability based on our knowledge of historical climate in a region. The daily fire weather can be at times quite stable yet at other times quite chaotic and unpredictable. The influence of fire weather is considerable given that it can cause dry vegetation and fuels to dry out in the lead-up to the peak period of fire susceptibility and drive severe fires if ignited.

Monitoring the interactions between landscape dryness and daily fire weather is achieved using an index of potential fire spread, which functions at much shorter time scales than the seasonal landscape dryness factor. A potential fire spread index (PFSI) estimates rate of spread and potential fire intensity at a given place through time. A potential fire spread index combines three factors: fuel availability, fuel moisture levels in fine and coarse fuels, and average wind speed (McArthur, 1967; Van Wagner, 1987).

A drought index, hereafter in this study referred to as a landscape dryness index, indirectly estimates the first factor in a PFSI: availability of both fine and coarse dead fuels for a representative vegetation type. As there is no direct physical correlation between fuel availability and a drought or soil moisture index, the relationship has to be created empirically. This necessity led McArthur to devise a simple drought factor based on the Keetch-Byram Drought Index (KBDI) and the number of days since rain (McArthur, 1967). The Soil Dryness Index model (SDI) was developed in 1972 in response to research concerns about the applicability of the KBDI to Australian conditions (Mount, 1972). Judging by the absence of papers in the literature, the KBDI has never been formally calibrated in south eastern Australia. The Mount Soil Dryness (MSDI) model was calibrated first at Lidsdale near Lithgow in New South Wales, based on a comparison of soil moisture and run-off data, and then on a limited number of catchments in Tasmania (Mount, 1972).

The second factor in a PFSI, fuel moisture, is one measure of the ignitability and combustibility of the surface dead fuels on the forest floor. Ambient temperature, relative humidity, recent rainfall effects, and, to some extent, solar radiation and wind speed govern fuel moisture levels of the different fuel components on the forest floor (Byram and Jemison, 1943; Van Wagner, 1987).

The third factor in a PFSI is wind speed. Under extreme wind conditions, a PFSI indicates levels of extreme fire behaviour once soil, vegetation, and coarse fuels moisture content (landscape dryness) as well as fine fuel moisture have fallen below critical levels. Knowing when in which part of the fire season, the extremes of fire weather might occur are thus fundamental for understanding the fire susceptibility of a given forested catchment or region.

The terms for PFSI used in fire science studies are: (1) Forest Fire Danger Index (FFDI) or, (2) Fire Weather Index (FWI). Neither term represents the real function and meaning of a PFSI

and hence is potentially misleading. When estimating potential fire spread, a PFSI assumes a basic constant set of fuel conditions, such as fuel loads, fuel arrangement, and fuel compaction. Other factors affecting fire spread, such as elevation, slope, aspect, and topographic position, are kept constant.

The Forest Fire Danger Index (FFDI) has served as an index of fire danger in forest settings in Australia since the 1960s (McArthur, 1966; 1967). The FFDI is a simple numeric index, scaled from 0-100, representing the range of potential fire spread for a constant set of fuel conditions. Much of McArthur's fire behaviour research was based on point observations of the relationships between fuel, fire weather and fire behaviour and then extrapolated to a range of forest environments in Australia (Dudley, 2003). Field-testing and verification of the Australian models of potential fire spread have not been undertaken in different regional and local situations as would appear warranted.

A possible alternative to the FFDI is the Fire Weather Index (FWI) — a component of the Canadian Forest Fire Danger Rating System (CFFDRS) used in the boreal and wet temperate forests of Canada. The FWI was originally derived to assess fire behaviour potential in Canadian boreal pine forests (Van Wagner, 1987). It has since been adapted to forecast fire danger in a wide variety of environments in the world including: boreal forests in Alaska and Sweden, tropical rainforests in Indonesia and Malaysia; grasslands, shrublands and exotic pine plantations in New Zealand and Fiji; Mediterranean pine forests and shrublands in Portugal, Spain, Italy and Greece (Taylor and Alexander, 2006; Wotton, 2008). The FWI incorporates indices of landscape dryness, fuel moisture, fuel availability and fire weather as separate discrete modules (Van Wagner, 1987). This type of approach enables parts of the FWI system to be tested and validated independently and then combined later. While the CFFDRS system has been adapted to New Zealand conditions (Fogarty *et al.*, 1998a), limited testing of the CFFDRS has been done for Australian pine plantations (Alexander, 1998), but not for Australian eucalypt forests. The distinct advantage of the FWI in the CFFDRS over the FFDI model of fire weather is the simplicity, generality and transparency of the tightly integrated fuel moisture and fuel availability components of the FWI.

The basic shortcomings of soil water deficit and potential fire spread models used in Australia are:

(1) they have not been adequately tested in a range of spatial and temporal conditions;

(2) these models have not been tested within a process-based framework and they should not be extrapolated beyond known equations and observed data;

(3) the models have been applied in widely varying conditions without firstly being calibrated;

(4) the data and field studies on which the models were based is sometimes unavailable or missing (for example, KBDI and FFDI); and,

(5) an uncalibrated untested model may lead to false assumptions and decisions being made in field applications.

The errors associated with the use of models could lead to a failure to recognise severe fire conditions characteristic of LLFs, with potentially catastrophic consequences. This is an example of a type II error (errors of omission or false negative result) causing a failure to forecast a LLF (Taylor and Alexander, 2006). Thus, it is vital that the models of landscape dryness and potential fire spread are calibrated or checked before they are applied under operational conditions.

To overcome the above model limitations and shortcomings, this study selects models that represent the biophysical processes of landscape dryness and potential fire spread as closely as possible. For instance, landscape dryness models should be founded on tightly integrated eco-hydrological processes within vegetation ecosystems in a region. By relating the indices of fire susceptibility to biophysical processes in a landscape, critical values can be identified that mark significant changes in fuel combustibility and vegetation flammability. The critical thresholds of fire susceptibility then have some basis in reality. For instance, when a value of an index of landscape dryness has been surpassed, we can expect to find deeply dried soil profiles, cured grasses and herbs, recognisable plant stress in vegetation and negligible water flow in major streams. By monitoring and recognising these features in the landscape through simple landscape dryness indices, we should be better able to anticipate the tipping point in landscape susceptibility to large fires that lead to a high risk of LLFs. We can also anticipate when severe fire weather conditions, when combined with very dry landscape conditions, can lead to severe and destructive fires, as evidenced by the loss of life and property in the February 2009 fires in Victoria.

1.2 Significance and relevance of the study

The south eastern corner of Australia has been subject to large, if sometimes catastrophic, fires since European fires since European settlement. Most of the largest and most damaging fires have occurred in the dry and wet sclerophyll forests in the coastal and hinterland mountain ranges along the Great Dividing Range between Melbourne and Sydney. The two most severe fires have been the February 6th 1851 and January 13th 1939, mainly in Victoria but extending into southern New South Wales. These fires are estimated to have burnt five and three million hectares respectively. The three factors involved were prolonged drought, followed by a searing prolonged heat wave, and culminating with a day of extremes temperatures (45-47 ^{o}C) and gale force winds. Just recently, the February 7th 2009 fires in Victoria had comparable fire weather to that of the 1851 and 1939 fires but only had few fires alight either prior to or on the day of extreme fire weather.

There have been other fire seasons in southern eastern Australia with LLFs but with not quite the severity and impact of the fire seasons of 1851/52, 1938/39, and 2008/09. In these cases, extensive droughts and short spells of severe to extreme fire weather resulted in LLFs in 1897/98, 1905/06, 1925/26, 1931/32, 1943/44, 1951/52, 1964/65, 1968/69, 1982/83 up until 1993.

Since 1994, there has been a run of relatively frequent fire seasons at intervals from two to four years in south eastern Australia. In the northern part, in the Sydney sandstone basin, between 500,000 and 1,000,000 ha of forest were burnt during the 1993/94, 1997/98, 2001/02, and 2002/03 fire seasons. Further south, in the Victorian and NSW Alps, between 1,200,000 and 1,300,000 ha of montane and sub-alpine forest were burnt on two occasions, in 2002/03 and 2006/07 , and most recently, 430,000 hectares were burnt on a single day on February 7th in 2008/09 (Australian Bureau of Statistics, 2003; Department of Sustainability and the Environment, 2009). Because of the recent LLFs in the last decade, large areas of burnt-over forest are now in a highly vulnerable condition requiring decades of protection and management to facilitate their reversion to more mature forests. Their protection from future devastating LLFs will become increasingly important in the years to come. Otherwise, large areas of forest will remain in a permanent regrowth state that will facilitate future LLFs.

At a global scale, LLFs have become more widespread and more frequent in sub-tropical, temperate, and boreal forests in the last 20 years, compared with the last one hundred years. This trend is expected to continue with the most recent International Panel of Climate Change report concluding that forest fires are likely to become more frequent, larger and more intense in these regions (IPCC, 2007a; IPCC, 2007b). In the forests of Northern America and Canada a significant increase in the occurrence of LLFs has been reported in the last 25 years (Flannigan and Wotton, 2001; Westerling *et al.*, 2003). The IPCC report also concluded that there could be an increase in frequency of droughts in many parts of the world, including SE Australia, with a likely increase in frequency and severity of LLFs.

A medium or long-term retrospective view of the full range of landscape dryness, potential fire spread, and lightning ignition in a regional landscape can increase our knowledge and understanding of the conditions under which LLFs have developed in the past. This long-term view could then assist in the anticipation and preparation of such events by:

(1) interpreting the potential for LLFs in any given fire season by comparing the present conditions of landscape dryness and fire spread potential with the historical seasonal profiles of these factors in past fire seasons;

(2) monitoring landscape conditions to see whether the thresholds of the first two susceptibility factors, landscape dryness and potential fire spread, have been reached or exceeded; and

(3) knowing when lightning ignition has coincided with very dry landscapes and runs of severe fire weather, and using this knowledge to predict when dry thunderstorms are likely to start fires on any given day during a fire season.

This study seeks to develop a deeper knowledge of the temporal variations in conditions of landscape dryness, fire weather and lightning ignition, which together shape the potential for a LLF in any given fire season, using locally calibrated indices. The study also uses the concepts of threshold values of landscape dryness and potential fire spread to find out in what part of a fire season the potential for a LLF exists. To derive these threshold values requires appropriate and accurate models of landscape dryness and potential fire spread.

The philosophy behind this study is that the concepts and methods can be applied to other regions in south eastern Australia to anticipate potential lethal combinations of highly flammable landscapes with extremes of fire weather, which devastated Victoria and elsewhere in south eastern Australia in recent fire seasons: 2002/2003, 2006/07, and 2008/2009. The practical application to field management is via three key steps: first, the careful evaluation of the weather data and suitable models; second, the verification and validation of the outputs from the models; third, the analysis and interpretation of landscape susceptibility to fire, based on the models; and fourth, relating the results to the wider temporal and spatial context.

1.3 Thesis topic

This dissertation develops a method for analysing and interpreting reconstructed historic fire susceptibility of the ACT region's forested landscape, using two daily indicators of fire susceptibility: landscape dryness and potential fire spread. The other factor in a landscape's susceptibility to large fires, fire ignition, is considered briefly in terms of daily lightning ignition potential.

The thesis represents an exploration of the seasonal and longer-term temporal views of landscape susceptibility to large fires based on (1) landscape dryness and (2) potential fire spread, based on the most realistic models and data available within a region.

The approach taken and the philosophy underlying are to examine and then combine the different temporal views to assess:

(1) how landscape susceptibility to LLFs has varied through time;

(2) to find out specifically in which fire seasons and in what part of these seasons the highest potential for LLFs has existed; and

(3) to determine any discernible trends in year-to-year or decade-to-decade potential for LLFs in the fire season record.

The approach taken in this study is presented in Figure 1.2. Landscape susceptibility to large fires is examined from a medium and long-term perspective, necessitating models and weather data to support the integrated analyses conducted in this study.

The thesis sets out to model fire susceptibility using the most reliable and accurate weather records available locally. The yearly fire seasonal profiles, based on year-day number, serve as a standard basis for short, medium, and long-term comparison of the trends, sequences, and types of fire seasons. These annual profiles also support classification methods allowing classification of fire seasons into a small number of categories or types. Two views of the yearly profiles are developed: one is based on an index of landscape dryness and the other is based on an index of potential fire spread. These two factors are not independent – potential fire spread indices take into account landscape dryness, which is an indirect surrogate for fuel availability and continuity, and to a lesser extent vegetation flammability (McArthur, 1962a; McArthur, 1967; Deeming *et al.*, 1978; Van Wagner, 1987).

Where possible, calibrated and validated models, used to evaluate landscape susceptibility to large fires, are employed. The approach is based on the selection and development of models of the indices that reflect biophysical processes as closely as possible. For instance, the process of daily evaporation equates to known or estimated evaporation from soil and vegetation, and this leads to levels of soil moisture in a catchment that produce known levels of water run-off.

This means testing the validity of hydrological processes within a daily soil water balance model such as soil evaporation, plant transpiration, and interception of rainfall. In the case of an index of potential fire spread, this has meant selecting one that best represents the state of seasonal fuel and fire weather in any given part of a fire season.

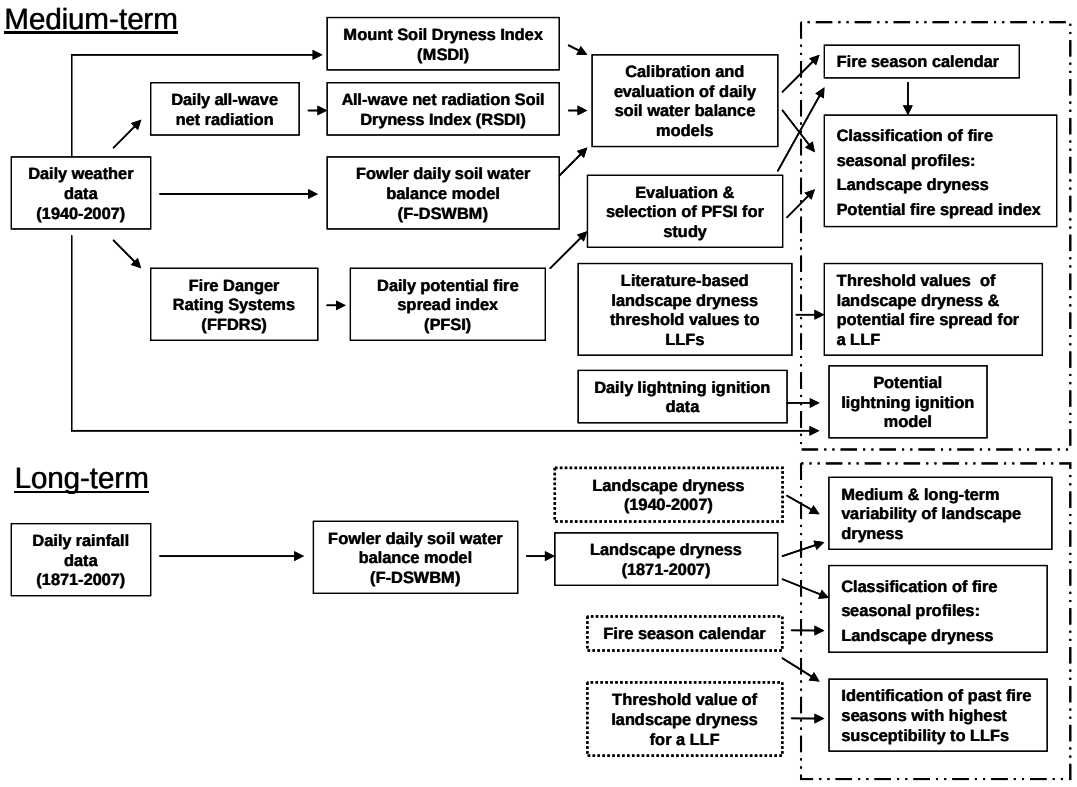

Figure 1.2 The methodology employed in this study to analyse and interpret landscape susceptibility to large fires

1.4 Research questions and organisation of the remainder of the thesis

The study is organised into 10 chapters that detail the steps and processes required to model and interpret the key indicators of landscape susceptibility to large fires. The organisation of the study is based on the approach shown in Figure 1.2 and the key research questions that relate to the development of the model of landscape susceptibility to large fires. Each chapter is based upon one or more key research questions that together provide the research framework for the topic (Table 1.1). Chapters 3-7 involve the selection of models and collation of the necessary data in order to prepare the time series of the fire susceptibility datasets for analysis. Chapters 8-9 involve the detailed interpretation of landscape susceptibility to large landscape fires in the medium and long-term perspectives.

In subsequent chapters, the topic of landscape susceptibility to large fires is dealt with as follows.

Chapter 2 describes the study setting in terms of local climate, topography, vegetation, and soils. Despite the heterogeneity of the ACT region's landscapes, the study aims to model landscape dryness in at least two of its three climatic provinces (modified Koëppen provinces Cfa and Cfb) and potential fire spread in at least one (Cfa).

Chapter 3 first outlines which daily soil water balance models are best suited to the study of medium and long-term landscape dryness. Next, a net radiation-based daily soil water balance model is developed from the Mount Soil Dryness Index (MSDI), using equations for soil evaporation and plant transpiration sourced from the literature that best replicates real world processes and conditions. The models for these two evaporation processes are shown to substitute successfully for the more general evaporation evapotranspiration model used in the MSDI model.

Chapter 4 outlines the ideal modelling framework and assesses which weather stations have the necessary data at the standard specified for this study. Based on those weather stations with suitable weather datasets, the modelling framework is modified to fit the best available weather data. The last part of the chapter focuses on (1) the standards of weather data standards, (2) the availability of weather datasets that meet those standards, (3) the completeness of the weather datasets, and (4) methods used to collate continuous and complete medium and long-term datasets for the fire susceptibility models.

Table 1.1 Research questions dealt with in subsequent chapters

Chapter	Research Question
Chapter 2	(1) How feasible is it to apply a simple temporal model of landscape susceptibility to large fires to a region with wide ranging climate, topography, vegetation, soils, and fire history?
Chapter 3	(2) Which daily soil water balance model (DSWBM) is best suited to the study of landscape dryness over the medium and long term?
	(3) Can simple and elegant sub-models of soil evaporation and plant transpiration replace evapotranspiration models?
Chapter 4	(4) As part of the ideal modelling framework for this study, what datasets for medium and long-term indices of landscape dryness and potential fire spread can be constructed for each of the three climate zones?
Chapter 5	(5) Can all-wave net radiation (R_N) and its components be estimated to sufficient levels of accuracy as a precursor to estimating potential evaporation (E_P)?
Chapter 6	(6) Which daily soil water balance models best approximate the hydrological processes of evaporation, run-off, and soil water deficit and should be used for further analysis of landscape susceptibility to large fires?
Chapter 7	(7) Can a threshold of soil water deficit (SWD) indicate a realistic threshold for fuel availability, combustibility, and vegetation flammability in a forested landscape?
	(8) Which of the PFSI models is the most transparent and explicit, and best integrates the factors involved in estimating potential fire spread?
Chapter 8	(9) Does redefining the season and the periods within a fire season using fire susceptibility criteria, such as landscape dryness, fine fuel moisture, and potential fire spread, produces a more meaningful definition than previous definitions?
	(10) What can classification and time series analysis of landscape dryness and potential for high fire spread reveal about landscape susceptibility to LLFs in the medium-term?
	(11) Can a model based on particular combinations of landscape dryness and weather predicts the potential for lightning ignition in the ACT region?
Chapter 9	(12) What does a broader temporal and spatial view of fire susceptibility tell us about its long-term history, climatic factors and influences contributing to it?

In Chapter 5, models of short wave and long-wave radiation are evaluated to ensure that all-wave net radiation could be estimated to a high degree of accuracy with least bias for two climate zones. The resultant estimates of daily short-wave and all-wave net radiation are then verified against estimates from other comparable studies and site-based measurements of these fluxes. Accurate estimates of all-wave net radiation are seen as crucial for accurate estimates of potential evaporation, which is a key input parameter into models of both soil evaporation and plant transpiration, developed in Chapter 4.

Chapter 6 first describes the methods used to calculate Soil Water Deficit (SWD) based on the three daily soil water balance models selected for this study. The validity of the estimates of soil evaporation and plant transpiration produced by the new radiation-based soil water balance model (RSDI) is then assessed. Finally, the daily soil water balance models are evaluated to determine which of these produce the most consistent and representative annual profiles of landscape dryness for a medium and long-term analyses in Chapters 8 and 9.

Chapter 7 first examines how daily soil water balance models are used to estimate indirectly availability of fuels to burn in a forest, which is a critical component of a potential fire spread index. Thresholds for very dry to extreme levels of landscape dryness drawn from the literature are formulated from known studies from Australia and overseas. These studies demonstrate that availability of fuels to burn and vegetation flammability can suddenly change once critical moisture levels in vegetation and fuel are reached after extended dry periods. The last part of the chapter outlines the structure and variables of the two potential fire spread indices, FFDI and FWI, for interpreting landscape susceptibility to large fires based on medium-term time weather datasets.

The first part of Chapter 8 proposes a new fire season calendar for the ACT region based on average daily values of fire susceptibility criteria: landscape dryness, fine fuel moisture, and potential fire spread. The new definition of seasons within a fire season is then used to derive a seasonal marker for determining when extremes of landscape dryness and potential fire spread occur within a fire season. Hierarchical classification of the annual profiles in each fire season since 1951 is then applied to both medium-term datasets of landscape dryness and potential fire spread to investigate the number, type, and severity of groups and sub-groups of fire seasons. The sequence of the groups of fire seasons based on the preferred fire potential index was then analysed to determine two aspects of landscape susceptibility to large fires: (1) what has been the sequences of groups of fire seasons and (2) which fire seasons in what fire season groups have had the highest likelihood for LLFs. Threshold values for landscape dryness and potential fire spread are then identified for this region, and are used to determine which months in the fire calendar are most prone to LLFs and in which fire seasons there has been the highest likelihood for LLFs. The last part of the chapter investigates a model of the landscape and weather conditions conducive to lightning ignition, as well as other concurrent indicative information about the state of the atmosphere, such as vertical profiles of temperature and air moisture content. Detailed conclusions derived from the medium-term interpretation of landscape susceptibility to fire are provided at the end of the chapter.

Chapter 9 places the results of the medium-term time series of landscape dryness and potential fire spread into a longer-term context. The medium and long-term time series of landscape dryness are first broken down into their constituent parts using time series analysis. The analysis is used to uncover any underlying trends in landscape dryness at sub-decadal, decadal, and inter-decadal time scales. The long-term landscape record is then classified using

the Fowler daily soil water balance model and rainfall records from Queanbeyan weather station, which is closely correlated to the Canberra Airport medium-term rainfall dataset. This chapter presents the findings of the longer-term classification of fire seasons and compares the major fire seasons extracted from the analysis to those found in historical fire chronologies in and adjoining the ACT region. Finally, this chapter discusses the results of the medium-term and long-term time series of landscape dryness and potential fire spread in relation to the climatic and weather processes that produce dry landscapes, potential for high fire spread, and lightning ignition.

Chapter 10 first summarises the principal findings from each of the chapters (Chapters 2-9). Limitations of the research method, as wells as the models and data, are reviewed. Recommendations for future research are outlined. Finally, conclusions are reached as to how to best apply the study's methodology for determining landscape susceptibility to large fires to other regions in south eastern Australia.

Chapter 2: Study Region

This chapter describes the study region at a continental and regional scale, and discusses other factors such as the recent climate, topography, dominant vegetation and soil types, and fire history. Apart from providing a context, these contextual factors show why the ACT region is well suited to a study of fire susceptibility, even though its landscapes, vegetation, and fire history are highly heterogeneous.

2.1 Description of study area and landscape

The study area (1,518,000 hectares within a rectangle with sides 110 km wide and 138 km long) is centred on the city of Canberra (longitude: 149.130; latitude: 35.276 south) in the Australian Capital Territory (ACT) (Figure 2.1). The ACT is located in south eastern Australia about 100 km from the coast and located on a peneplain with a belt of mountain ranges to the west and east ranging in elevation between 600 and 2000 m.

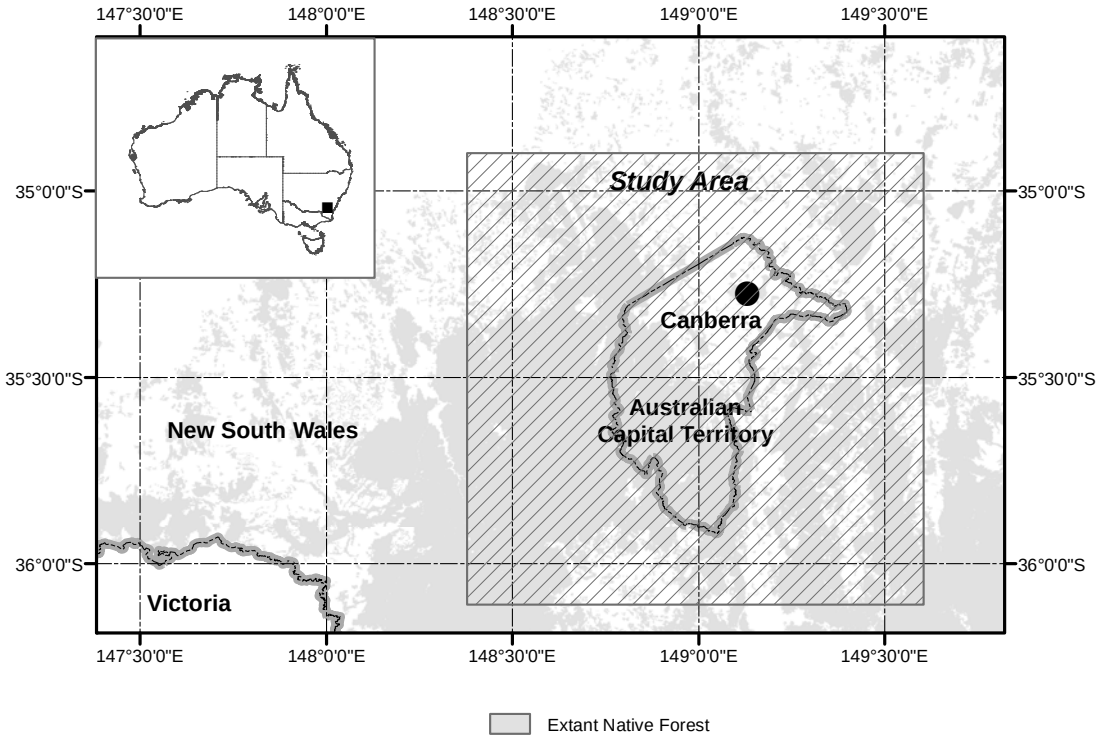

Figure 2.1 The study area shown in inset (top left hand corner) and in relation to the ACT and surrounding land in New South Wales (main diagram)

2.2 Climate

The ACT region at an approximate latitude 35.5°S has a semi-continental climate (Sturman and Tapper, 2006). Its latitudinal position is the key determinant of both incoming solar radiation and day length during the course of the annual cycle, and its climate. This places it more or less under the sub-tropical ridge which dominates the weather patterns during the course of a year (Hobbs, 1998; Sturman and Tapper, 2006). The sub-tropical high-pressure cells, most dominant in summer, predispose the region to a dry continental climate. During the cooler months of the year, these high-pressure cells are less dominant, resulting in relatively cool and moist conditions. The maritime influence is intermittent, despite the proximity of the eastern coastline of Australia, largely because the Great Dividing Range and coastal ranges to the east trap some of the moisture borne by easterly winds. Occasional incursions of polar maritime air masses set in at eight to 10 day intervals from the south and south-west bringing about changes to temperature and to rainfall. The region's temperate climate is thus characterised by highly variable intra-annual temperature and intra- and inter-annual rainfall.

The study area can be divided into three climate zones (Figure 2.2) using a regional scale classification of climate, such as that proposed by Gentilli (1972) adapted from Koëppen (1936):

(1) Cfa in the sub-montane hills and plains in and around Canberra between 600 and 800 m;

(2) Cfb in the montane ridges and escarpment to the west of Canberra between 800 and 1400 m; and

(3) Csc in the high country above an elevation of 1400 m.

The lower tableland plains at Canberra are characterised by a warm climate with uniform summer/winter rainfall and a long mild summer (Cfa). The adjoining Brindabella Ranges are characterised by a uniform rainfall with a cool to mild summer (Cfb). In strong contrast, the high country in the Snowy Mountains further to the west and south west of the Brindabella Ranges have winter-dominated rainfall and a short cool to mild summer (Csc). Therefore, the climate varies markedly in terms of amount and seasonality of rainfall as well as temperature between the high sub-alpine mountainous region to the far west and south-west, the montane-sub alpine ranges to the west, and the sub-montane hills and plains in the centre and east.

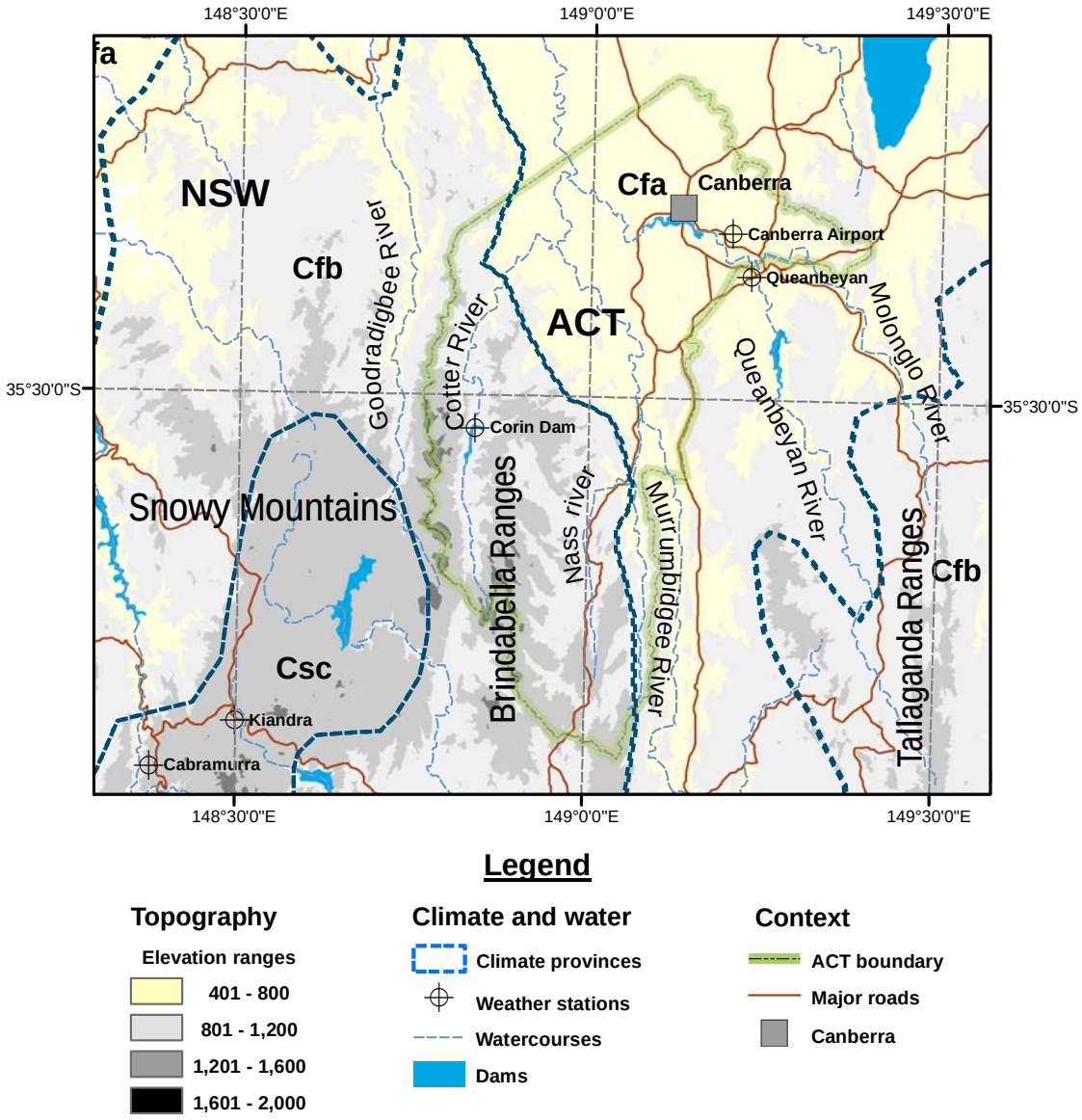

Figure 2.2 The ACT region, showing Gentilli climate zones, topography, dams, rivers, and important weather stations sites referred to in text

Source: Map prepared on Arcview GIS using GIS data supplied by the NSW Department of Environment and Climate Change (2005) and Geoscience Australia (Geoscience Australia, 2003).

Note: The modified Koëppen climate zones were drawn by the author based on field knowledge of vegetation and climate in the study area.

The seasonal variation in climate for the last 60 to 140 years is first illustrated with a combined plot of monthly and daily mean monthly temperature and rainfall in Figure 2.3(a) and is based on climate data recorded at Canberra Airport. The mean monthly rainfall ranges from 42 to 65 mm, with a monthly average of 50 mm. The high spring rainfall results from moister north westerly continental air interacting with colder air behind cold fronts and low pressure cells coming up from the Southern Ocean. A decrease in rainfall is evident in December as these low pressure cells move further south, away from the Australian continent. Rainfall

during the later summer months (January-March) is the result of convective thunderstorms developing over the heated land to the west of the ACT ranges with the passage of heat troughs emanating from the centre of the continent. The decline in rainfall in winter reflects the more limited atmospheric moisture associated with the passage of cold fronts from the southwest.

The station of Cabramurra lies in the heart of the Csc climate zone at 1485m, being 900 metres higher than Canberra Airport. As a result mean monthly daily temperatures are about six degrees lower on average than that at Canberra in any typical year (Figure 2.3(b)). The rise and fall in mean daily temperature at both Canberra Airport and Cabramurra reflect the seasonal rise and fall in solar radiation in the southern hemisphere, with mean daily monthly temperature falling to a low of 5^{o}C in winter and rising to 21^{o}C in summer at Canberra Airport. Mean daily temperatures at Cabramurra range between 1 and 15^{o}C, reflecting the cooler and moister climate in the high country.

The much higher rainfall at Cabramurra is the result of orographic uplift of air over the high mountain ranges during the passage of pre-frontal troughs and polar maritime cold fronts. The mean monthly rainfall ranges from 68 to 200 mm, with a monthly average of 137 mm. During the cooler months of the year, mean monthly rainfall at Cabramurra is two to three times that at Canberra Airport. However, mean monthly rainfall falls dramatically from November to April, reflecting a shift towards more stable weather patterns then.

Canberra Airport lies within the middle of the Cfa climate zone, overshadowed by the high mountains to the west with a vertical relief from 1000 to 1500 m. It thus lies in a rain shadow in the lee of the ranges, resulting in less rainfall from the rain-producing weather systems that come in predominantly from the north-west or south-west.

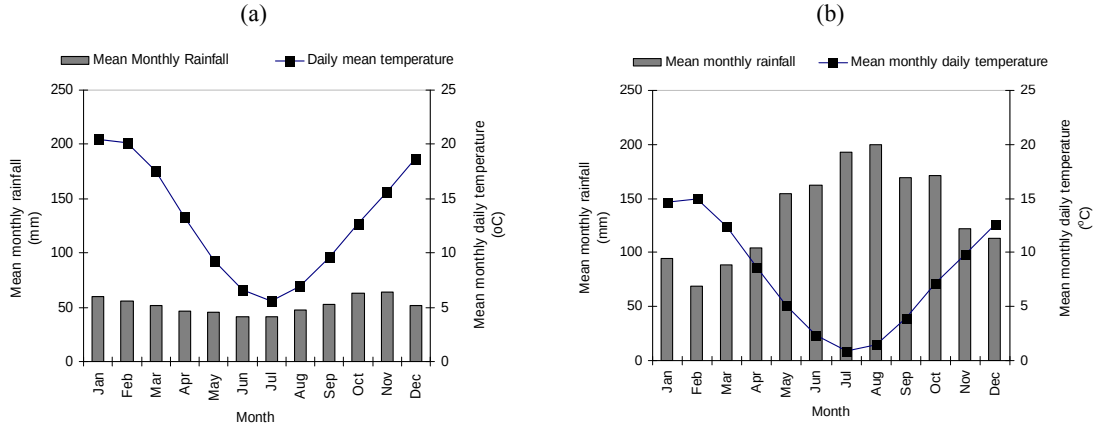

Figure 2.3 Mean monthly rainfall and mean daily temperature at (a) Canberra Airport (585 m ASL) and (b) Cabramurra (1485 m ASL)

Source: Medium-term weather data for Canberra (1940-2007) and Cabramurra (1955-2007) from Bureau of Meteorology (1940-2007)

Following a dry winter near Canberra, even with a typical follow-up spring and summer rainfall (Figure 2.3(a)), the amount of rainfall may be insufficient for annual recharge of soils on the sub-montane plains to occur (see Figure 6.15). In contrast, the vegetation and soils in the moister climate at Cabramurra usually have ample soil water for plant growth in most fire seasons — because of the high winter rainfall from 150 to 200 mm on average (see Figure 6.16). In most years, the high monthly rainfall in winter and spring at the cooler time of the year in effect recharges the deeper loams and gradational soils beneath the forests. These soils have a much higher soil water holding capacity and take up most of the incoming rainfall. The remainder is discharged into streams and rivers as run-off. During periods of below-average rainfall in winter and spring, there may be insufficient precipitation to recharge these deeper soils found in the high country. Once the vegetation and soils dry out in spring, this can lead to drier landscapes than usual and to an increased likelihood of LLFs.

An examination of the long-term rainfall record shows years with significantly lower annual rainfall amongst the years with median or high annual rainfall (Figure 2.4). The rainfall stations of Queanbeyan, Corin Dam on the upper Cotter River and Kiandra/Cabramurra composite are representative of an east to west altitudinal cline: 580 m at the lowest station at Queanbeyan, rising to 1395 m at the highest station at Kiandra. Inter-annual rainfall at Kiandra has the greatest variability, and it is least variable at Queanbeyan. Since 1938, the very low rainfall years are in sequence at all the stations. There is a distinctive pattern of a three to four year cycle of high and low rainfall evident, particularly in the Cabramurra record. From 1996 onwards, this seesaw oscillation in rainfall changes to a much dampened variation, seen in the records from all three stations. This may indicate a change in the climatic factors controlling rainfall though this inference should be treated with caution: Cabramurra winter rainfall has been consistently below the level that might have been reasonably anticipated and it is possible that snow and ice have not been intercepted by the pluviometer installed at the Automatic Weather Station (AWS) (see section 4.3.2).

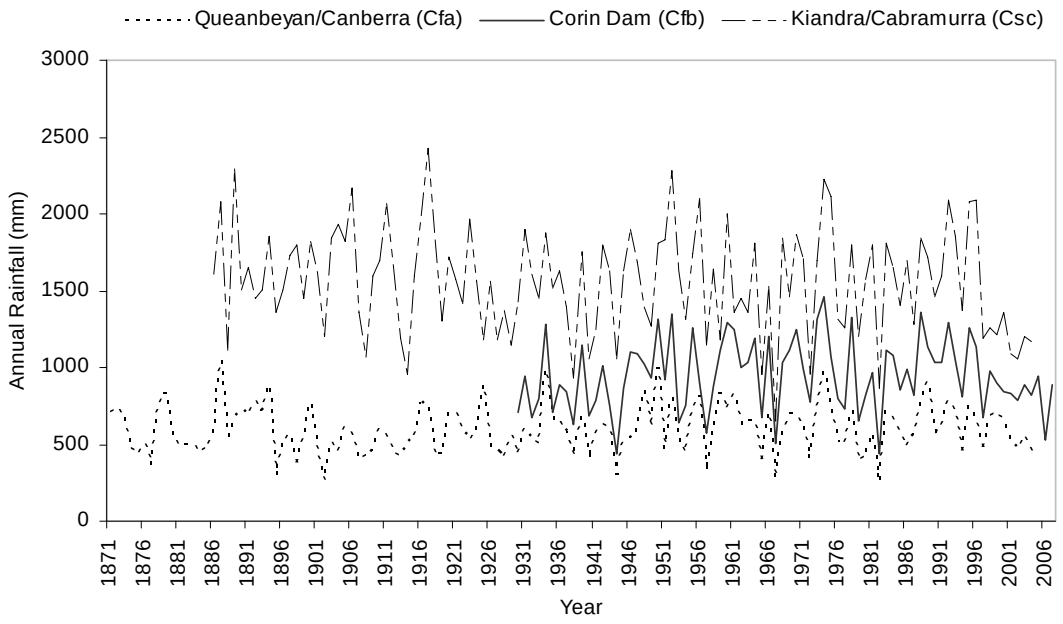

Figure 2.4 Trends in rainfall at rainfall stations representative of the three climate provinces in the study region

Source: The annual rainfall values are derived from averaging daily weather records of three long-term and currently operational weather stations, Queanbeyan and Canberra airport, and one medium term weather station, Cabramurra (Bureau of Meteorology, 2007a).

Notes: (1) Elevations of the weather stations above sea level are: Queanbeyan (560 m), Canberra (585 m), Corin Dam (932 m) and Kiandra (1395 m).

(2) Kiandra rainfall dataset was extended from 1972 to the present using adjusted rainfall records from the closely located weather station at Cabramurra (correlation with Kiandra (R^2=0.89).

(3) Monthly rainfall at weather station at Queanbeyan is highly correlated with that at Canberra airport (R^2=0.918).

2.3 Topography

The topography of the study area is depicted in Figure 2.2. Canberra and its immediate surrounds, in the centre of the study area, comprise undulating plains, interspersed with hills. Immediately to the west, and across the Murrumbidgee River, the precipitous Tidbinbilla, Brindabella and, further west, the northern Snowy Mountains (Bogong Peaks and Fiery Ranges) ranges rise. To the east and southeast of Canberra lies the much lower relief of the Queanbeyan, Tinderry, and Tallaganda ranges. The area is thus surrounded by hills and mountains on three sides to the west, south, and east and is only open to the north via undulating hills and plains.

The difference in average height above sea level between the high country to the west and the lower plains on which Canberra is located is over 1200 m. The mountainous ranges comprising, in the main, the Brindabella Ranges and Snowy Mountains pose a major barrier to

the movement of air masses originating from either the west or the east. The regular formation of lenticular clouds over these ranges is indicative of their significant influence on the local climate.

To the west, the mountainous terrain comprising Bimberi-Scabby Ranges, Tidbinbilla Ranges, and Clear Hills-Gudgenby Ranges, is highly dissected by the Naas, Cotter, and Goodradigbee rivers that drain into the Upper Murrumbidgee River that flows in a northerly direction. The Cotter River flows north along a steep sided valley fault line between the Tidbinbilla and Brindabella ranges draining the territory's highest mountains. The catchment of the upper Cotter River comprises a rugged mountainous landscape with a vertical relief of more than 1000 m in places. The highly dissected nature of the mountain ranges creates topographic variation in slope and aspect, which then affects insolation, soil type and soil moisture regimes, and consequently distribution of montane and sub-alpine vegetation (Moore *et al.*, 1993).

To the west, the Goodradigbee, Cotter, Paddys, and Naas Rivers drain the higher mountain catchments of the Brindabella Ranges. Just to the north of the Cotter with the Murrumbidgee River confluence, the Molonglo River joins the Murrumbidgee River. The Molonglo River system drains the Googong catchment to the east and southeast of Canberra and is joined by the Queanbeyan River 20 kilometres to the west. To the north of Canberra, minor streams drain the depositional plains and low hills.

Records of rainfall and streamflow exist for the upper Cotter River catchment dating back to the mid 1930s. These valuable instrument records can be used to validate daily soil water balance models (see section 6.4.2, Chapter 6).

2.4 Vegetation and soils

The vegetation (Figure 2.5) and soils largely reflect the climate and geology in the three climatic zones described in section 2.2.

The more elevated parts of the study area are dominated by sub-alpine vegetation comprising *Eucalyptus pauciflora* (Snow Gum) low forests and sub-alpine moorland complex (Costin, 1954; Gellie, 2005), overlying alpine humus soils (Talsma, 1983; McKenzie *et al.*, 2004). These are predominantly located in the Csc climatic province. Annual average rainfall is over 1500 mm per annum with snow settling at the higher elevations during winter and early summer. The combination of a cool-to-cold climate and the humic shallow soils promote the development of sub-alpine herbfields, bogs, and heathlands at the expense of trees above 1650 metres on the flatter more exposed sub-alpine terrain (Costin, 1954; Costin *et al.*, 1964).

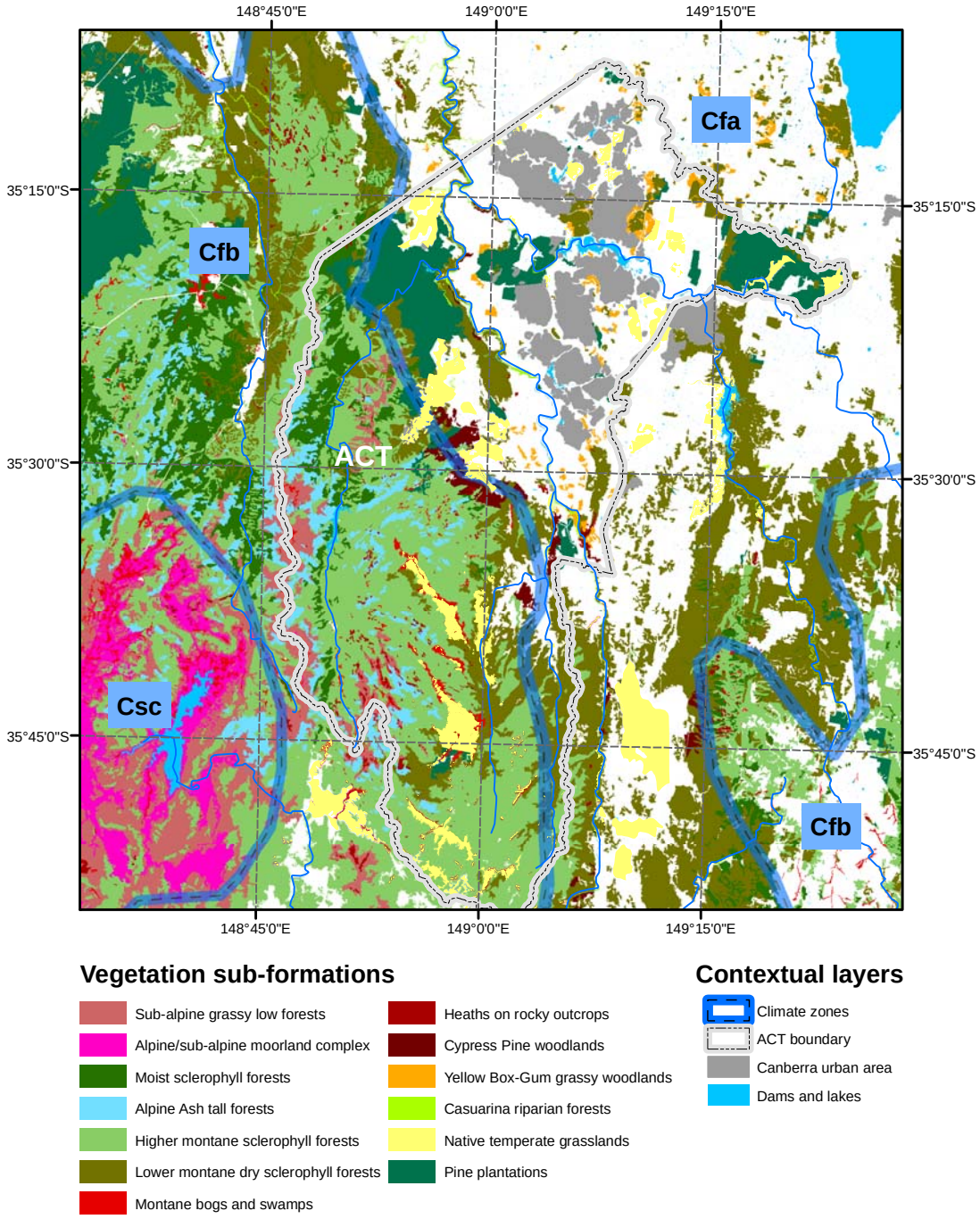

Figure 2.5 Vegetation sub-formations in relation to Gentili's climate zones

Source: Vegetation map is extracted from regional vegetation map prepared by Gellie (2005).

Note: Classification of vegetation is based on vegetation sub-formations defined by Gellie (2005).

Below this, in the Cfb province, productive montane moist sclerophyll forests of *Eucalyptus fastigata* (Brown Barrel), *E. delegatensis* (Alpine Ash) – *E. dalrympleana* (Mountain Gum), and *E. robertsonii* ssp. *robertsonii* (Narrow-leaved Peppermint) – *E. viminalis* (Ribbon Gum) predominate on sheltered easterly and southerly facing slopes. Beneath these moist sclerophyll forests, deeply weathered kraznozems and red earths occur on sheltered slopes while on the more exposed slopes weathered yellow podzolic soils are found (Talsma, 1983; McKenzie *et al*., 2004). On the northerly and westerly drier higher slopes, higher montane sclerophyll forests of *E. dalrympleana* ssp. *dalrympleana* (Mountain Gum), *E. pauciflora, E. robertsonii* ssp. *robertsonii,* and *E. dives* (Broad-leaved Peppermint) predominate. At lower elevations grassy/shrubby forests of *E. dives E.mannifera* ssp. *mannifera* (Brittle Gum) along with forests of *E. rubida* ssp. *rubida* (Candlebark) and *E. dives* (ANU Forestry Department, 1973; Gellie, 2005). Shallower red and yellow podzolics soils underlie these dry sclerophyll forest types (Talsma, 1983; McKenzie *et al*., 2004).

At lower elevation and to the east of the Brindabella Ranges, within the Cfa province, dry lower montane sclerophyll forests, comprising *E. rossii* (Scribbly Gum), *E.mannifera ssp. mannifera* (Brittle Gum) and *E.macroryncha* are located on shallow infertile soils on outcropping hills. On the lower hillslopes and tableland plains, *E.melliodora* (Yellow Box) – *E. blakelyii* (Blakely's Red Gum) grassy woodlands occur on deeper yellow podzolic soils, while native temperate grasslands occur on shallow less well drained, red podzolic soils within the valley floors (Talsma, 1983). In Figure 2.5, the Yellow Box-Gum woodlands are depicted in orange while patches of native grasslands are depicted in yellow. Both vegetation types are now largely cleared for grazing or modified by urban settlement (Gellie, 2005). Some small areas of swamps, bogs, and swamp forest are found in flatter open valleys in the Namadgi and Brindabella Ranges. The remainder of the vegetation on the sub-montane plains and hills around the city of Canberra, depicted as white areas in Figure 2.5, comprises cleared and semi-cleared grassland, degraded woodland and forest (shown as a white colour in Figure 2.5).

The soil types and their soil water holding capacities under the more widespread vegetation types are presented in Table 2.1. The shallow red podzolic soils under dry sclerophyll forests have low water holding capacity - between 100 and 165 mm (Talsma, 1983) - that makes these forests highly prone to drought stress (Pook *et al*., 1965) and potentially more susceptible to crown fire because of a lower tree canopy between 12 and 25 m in height. Montane eucalypt forests with canopies ranging from 25 to 40 m in height are generally found on deeper yellow podzolic soils, which have better soil water holding capacities, between 200 and 300 mm. These forests are less prone to drought stress yet they may still be predisposed to drought stress in dry years because of coarse textured A horizons, particularly on soils derived from granite rocks. Moist sclerophyll forests with canopies ranging from 35 m to 50 m in height overlie deep friable gradational soils up to four metres in depth. These forests have the highest water retention capacity, between 250 and 400 mm and are also capable of drawing water from deep

within the profile and within the weathered sub-soil (Costin *et al.*, 1964; Leuning *et al.*, 2005). As a result, moist sclerophyll forests are potentially least flammable in moist fire seasons. However, in dry-very dry fire seasons, these forests become much more prone to burn as their deep litter beds become more available (Luke and McArthur, 1978).

Table 2.1 Vegetation, soils and soil water holding capacities in the study area

Vegetation Type	Crown Canopy Height (m)	Soil Type	Soil water holding capacity (mm)
Montane and sub-montane grasslands	0.3-1.0	Sub-humic podzol	100-150
Subalpine low forests/woodlands	5-15	Red earth, sub-humic podzol	150-200
Lower montane Yellow Box-Gum grassy woodlands	18 -30	Yellow earth	200-250
Lower montane dry sclerophyll forests	12-25	Red podzol	100-150
Higher montane sclerophyll forests	25-35	Yellow podzols & yellow earths	200-300
Sub-alpine and montane moist sclerophyll forests (includes Brown Barrel and Alpine Ash tall forests)	30-45	Red & Yellow Earths	300-400

Source: Vegetation type is adapted from Gellie (2005); soil type is based on Talsma (1983); and values of soil water holding capacity are based on fire and catchment studies in the ACT (O'Loughlin *et al.* (1986).

Note: Estimates of canopy height are extracted from Appendix 5 Vegetation Profiles in Gellie (2005).

2.5 Fire history

Records of large landscape fires have been collated for the ACT region (ANU Forestry Department, 1973; Environment ACT, 2004) and southern New South Wales (Foley, 1947; Council of Australian Governments, 2003). These records indicate that LLFs have occurred at varying intervals, and locations, of between 11 and 20 years since 1906, with some intervening periods longer than 20 years. Large landscape fires in the study region, as defined in section 1.1, can be categorized into three categories of fires, according to starting place and spread:

(1) started on the sub-montane plains and hills, burning in grassland and forest there (1918/19, 1925/26, 1956/57, 1978/79, 1984/85 and 2001/02);

(2) started in the Brindabella Ranges and did not spread beyond there (1905/06, 1938/39, and 1982/83); and

(3) started in the Brindabella Ranges and spread onto the sub-montane plains and hills (1951/52 and 2002/03).

Large landscape fires (LLFs) that fall into the last category are the most difficult to control and manage, particularly if severe fire weather immediately follows lightning ignition in the more remote and rugged parts of the Brindabella ranges. The January 2003 fires that ignited the Brindabella Ranges certainly followed this pattern. Large fires resulted from five separate ignitions following the passage of dry thunderstorms on 8 January (McLeod, 2003). Almost two weeks later under extreme weather conditions, these fires burnt rapidly eastwards onto the sub-montane plains. The rapid spread was exacerbated by the total lack of any significant moisture barriers, the complex terrain, and areas being left long unburnt in the more productive moist and sub-alpine forests in the Brindabella Ranges.

Historical reports in the first part of the 20th century reveal a higher frequency of fire seasons than listed above, with LLFs occurring from the early 1900s to the early 1940s in the high country to the west of Canberra. Brackenreg (1926) recorded major fires in the ACT as occurring in 1905/06, 1914/15, 1917/18, 1918/19, 1920/21, and 1925/26. Foley (1947) assessed the fire seasons in the study region as being severe in 1918/19, 1928/29, 1931/32, 1939/40, and 1941/42. In an earlier study done by Pryor (1939) from fire scars on Snow Gums, the fire seasons with severe fires were documented as occurring in 1875/76, 1881/82, 1882/83, 1892/93, 1898/99, 1905/1906, 1910/11, 1918/19, 1925/26, 1931/32, and 1938/39. The fire scars on Snow Gums may also reflect less severe fires lit by graziers in the autumn following removal of stock (Banks, 1982). In his study, Banks found that severe fire seasons occurred in 1876/77, 1899/900, 1919/20, 1925/26, and 1938/39. The severe fire seasons identified by Banks in 1899/1900 and 1919/20 were most likely to have occurred in 1898/99 and 1918/19, which makes them correspond more closely with the reports of Brackenreg (1926) and the research findings of Pryor (1939). Both Banks (1982) and Pryor (1939) contend that the intense fires between the 1870s and the 1940s induced structural change in the sub-alpine forests, from a more open oldgrowth forest to dense, thicket-like regrowth stands.

Since the 1938/39 fire, annual reports of the Bushfire Council collated by the ANU Forestry Department (1973) suggest that fire seasons with LLFs occurred in 1939/40, 1943/44, 1956/57, 1957/58, 1964/65, 1967/68 and 1972/73. Since then, large landscape fires have occurred in 1978/79, 1982/83, and 2002/03. Prior to the 1970s, it is difficult to say whether some fire seasons did indeed have LLFs, with the possible exception of the fires in 1938/39, the impacts of which were well documented by Pryor (1939). This study may help to elucidate which of the reportedly severe fire seasons had the potential to carry large landscape fires based solely on an index of landscape dryness (See Chapter 9).

This retrospective study of natural susceptibility of mountainous landscapes to fire was made possible by the existence of fire history records and by the fact that mainly naturally ignited LLFs have occurred, at intervals of between 11 and 20 years, since the start of reliable records of fire in the 1950s. LLFs between the 1880s and the late 1930s were more frequent due to the fact that many were lit by pastoralists and campers (Banks, 1982; Pulsford, 1991).

Prior to the 1880s, LLFs may have been less frequent but the record is incomplete and hence inconclusive. A significant common feature of the most catastrophic LLFs is that they may all have started as small multiple fires (Stretton, 1939). The pre 1939 record indicates that some landscape scale fires followed a pattern of systematic burning off where at least several fires were deliberately lit, but in most instances, these burning practices were conducted towards the end of summer.

2.6 Findings

Despite being in a relatively moist and cool mountain environment, the study area has been subject to periods of low rainfall at intervals between three and ten years. These dry periods have created the necessary pre-conditions for landscape in the study region for LLFs to occur at intervals from 11 to 25 years.

This study aims to delineate critical thresholds of landscape dryness and potential fire spread beyond which the mountain ranges and the plains became highly susceptible to occurrences of LLFs. Predisposition to landscape scale fire is predicated on (1) most of the vegetation and soils drying to critical thresholds following long spells without rain, (2) a source (and most likely multiple sources) of ignition, and (3) existence of extreme fire weather conditions. The complexity of terrain, vegetation, and soils in the region provides a real test as to whether a simple temporal model of landscape susceptibility to large fires can be formulated. The remainder of the study will address the first research question in Section 1.4 (Table 1.1): 'How feasible is it to apply a simple temporal model of landscape susceptibility to large fires to a region with wide ranging climate, topography, vegetation, soils, and fire history?'. The applicability of point-based landscape dryness indices to this complex study region will be further examined in Chapters 5 and 6.

The next chapter describes the structure and function of daily soil water balance models suitable for this study and proposes a DSWBM driven by potential evaporation based on all-wave net radiation. The all-wave net radiation based DSWBM (RSDI) employs separate soil evaporation and plant transpiration sub-models to replace the evapotranspiration term in the MSDI model.

Chapter 3: Daily Soil Water Balance Models

The climatic variability of the study area described in Chapter 2 can lead to sustained low rainfall at intervals from three to six years in all three climate provinces in the study area: Cfa, Cfb, and Csc. Depending on the time of the year, these extended dry spells could produce near extremes in landscape dryness. Extremes in landscape dryness is defined as when the landscape is entirely dry with little if any soil moisture remaining in any of the major widespread vegetation types, even the higher montane and sub-alpine forests found in cooler and wetter environments. Examining seasonal landscape dryness conditions, in the lead-up to critical levels of landscape dryness, can be done using a daily soil water balance model (DSWBM). These models are designed to operate at a representative point in the landscape to reflect changes in average soil water over time for a given water catchment (Fowler and Adams, 2004). A daily soil water balance model simulates the key hydrological processes using two key inputs: (1) daily rainfall and (2) potential evaporation, producing Soil Water Dryness (SWD) as the principal output (section 1.1; Equation 1.1).

Landscape dryness is the cumulative seasonal factor in fire susceptibility that takes into account the annual cycle of evaporation that rises and falls, according to the seasonal rise and fall in all-wave net radiation, and seasonal rainfall conditions. The seasonal variation in SWD is pivotal to this study and requires robust and accurate DSWBMs to simulate the partition of daily rainfall into evaporation and run-off. Furthermore, the components of estimated evaporation and run-off can be verified against other models and data to ensure that it reflects the biophysical processes in the soil and vegetation domains as closely as possible (See Chapter 6).

The first part of this chapter outlines the existing and proposed DSWBMS that could be used to derive medium (up to 60-70 years) and a long-term (100-150 years) time series of Soil Water Deficit.

The second part of this chapter provides the theoretical basis for the derivation of R_N from its short-wave and long-wave components. These generic algorithms are crucial for estimating potential and actual soil evaporation and plant transpiration discussed in the last part of the chapter.

3.1 Daily soil water balance models

Two daily soil water balance models were identified from the literature for use in this study: (1) the Fowler Daily Soil Water Balance Model (F-DSWBM) (Fowler, 1992; 2002); and (2) the Mount Soil Dryness Index model (MSDI) (Mount, 1972; Mount, 1980). Both models require few weather data inputs and run on daily weather data. Both models have been previously tested in their respective countries of origin: the F-DSWBM in New Zealand and the MSDI in Australia. The Keetch-Byram Drought Index (KBDI) was excluded as a possible DSWBM on the following grounds. First, its evapotranspiration function has not been

calibrated to Australian conditions and evapotranspiration is assumed to occur at a rate proportional to the level of soil moisture. Second, the interception of daily rainfall is fixed as a constant rather than being varied according to overstorey and understorey cover, and whether the previous day was wet or dry. Lastly, it has fewer inbuilt hydrological functions than either the F-DSWBM or the MSDI. Burrows (1987) concluded that the MSDI estimated the state of landscape dryness better than the KBDI in Jarrah Forests in Western Australia and therefore recommended the MSDI for forest fire control applications.

The Fowler daily soil water balance model (Fowler, 1992; Fowler, 1999) is straightforward yet all-encompassing. In this model, Fowler (1992) incorporated the principal hydrological factors and processes; gross rainfall, interception, infiltration excess, surplus, and drainage with output water storages expressed as soil water, quickflow, and base flow (Figure 3.1).

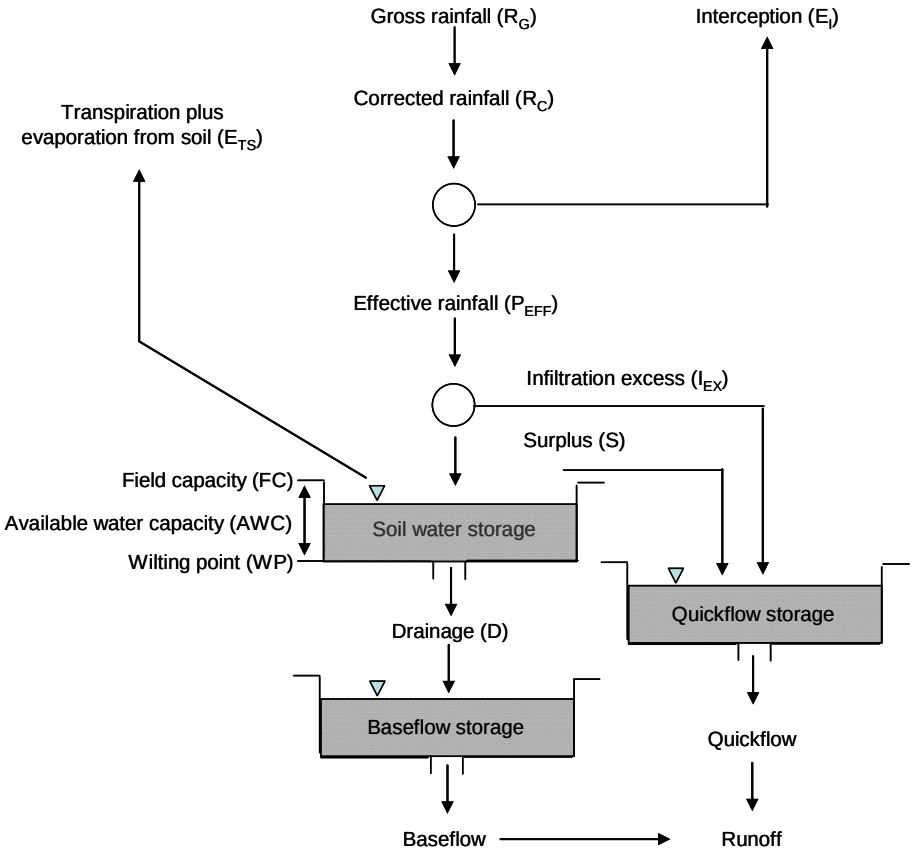

Figure 3.1 Elements of a daily soil water balance model (DSWBM)

Source: Adapted from Fowler, 2002:252.

The Fowler daily soil water balance model (F-DSWBM) is based on daily inputs of two weather variables: corrected daily rainfall (R_C); and a measure of daily mean E_P for each Julian Day (JD) in the annual cycle. R_C is defined as the measured rainfall adjusted to take into account the local environmental conditions surrounding a rainfall gauge (Fowler, 1999). For the purposes of this study, it is assumed that R_C is equal to the daily rainfall measured in a standard

rain gauge at 0900 hours (P_{0900}). It is best suited to long-term study of landscape dryness because only historical rainfall data are needed, once daily average evaporation values over a year have been estimated from actual data (see section 6.1.3). This assumes that the annual profile of daily average evaporation stays constant over the full length of a long-term time series.

The Soil Dryness Index model (MSDI) (Mount, 1972) (Figure 3.2), includes most of the hydrological processes and factors used in the F-DSWBM. Like the F-DSWBM, the key processes of evapotranspiration and rainfall drive the MSDI. The hydrological sub-models in the MSDI include the following water balance processes: evaporated of intercepted water, flash run-off and soil capacity over-flow and evapotranspiration from the soil water store at different rates governed by the soil water content.

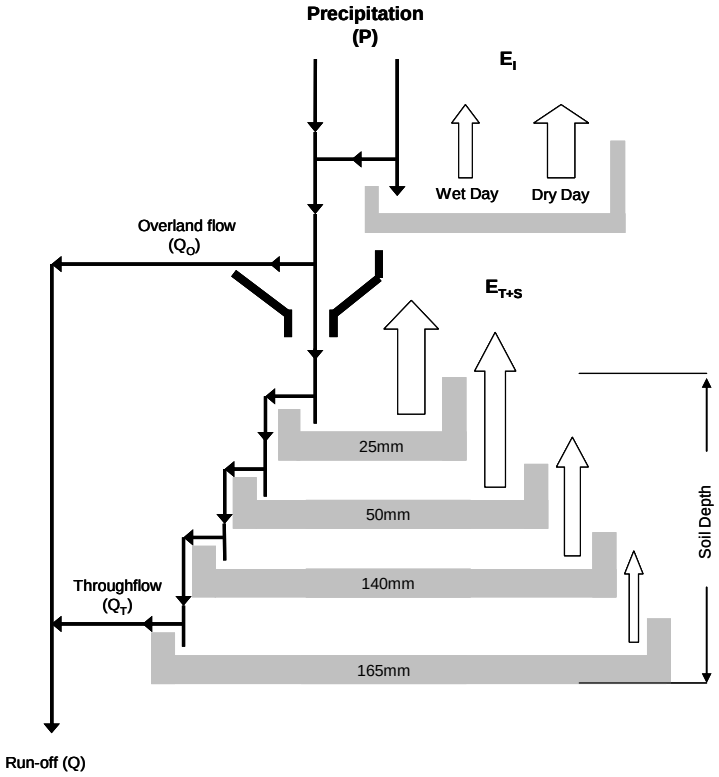

Figure 3.2 The MSDI model and its components

Source: The above figure is adapted from Mount (1972).

Notes: (1) Overland flow and throughflow are termed flash run-off and soil capacity overflow in the description of the MSDI model (Mount, 1972; Mount, 1980).

(2) The four different levels in the soil moisture store reflect the thresholds of SWD that govern the evapotranspiration rate attained at different daily maximum temperatures.

Unlike the Fowler daily soil water balance model (F-DSWBM), only the soil water storage is included in the MSDI model although a more elaborate version of it includes the quickflow and baseflow storage parameters (Kuczera, 1988). Flash-run-off can be regarded as an

approximation of the process of infiltration excess leading to surface water flow over a forested soil. It is defined as 'that produced by rain falling on the soil, not already at field capacity, faster than it is absorbed by some layer in the profile' (Mount, 1972:4). Flash run-off is calculated using a linear equation, and is in proportion to the amount of daily precipitation and the density of both overstorey and understorey vegetation. It is equivalent to overland flow (Q_O) in the F-DSWBM. Soil capacity overflow in the MSDI model combines the slower elements of through-flow (Q_T) and ground-flow (Q_B) once the soil is saturated. In the MSDI model, a lag period is not specified for these two elements of streamflow.

The soil water deficit (SWD) in the MSDI model is estimated as:

$$SWD_{(t)} = SWD_{(t-1)} - P_{EFF(t-1)} + E_{T+S(t)} \quad \text{(mm)} \qquad \text{Equation 3.1}$$

where $SWD_{(t)}$ is the soil water deficit at the end of the day, $SWD_{(t-1)}$ is the soil water deficit on the previous day, $E_{T+S\,(t)}$ is the actual evaporation estimated from a lookup table of daily maximum temperature (T_{MAX}) for that day and $SWD_{(t)}$.

Only one parameter, E_{T+S}, needs to be changed to convert the MSDI into a radiation-based soil dryness index model (RSDI model). Evapotranspiration (E_{T+S}) is split into two separate components:

$$SWD_{(t)} = SWD_{(t-1)} - P_{EFF(t-1)} + E_{S(t)} + E_{T(t)} \quad \text{(mm)} \qquad \text{Equation 3.2}$$

where $E_{S(t)}$ is soil evaporation and $E_{T(t)}$ is evaporation from plant transpiration on that day.

Soil evaporation (E_S) and plant transpiration (E_T), are modelled using potential evaporation derived from all-wave net radiation. See section 3.2 later in this chapter.

Effective rainfall (P_{EFF}) is estimated as:

$$P_{EFF\,(t)} = P_{(t-1)} - E_{I(t)} - Q_{O(t)} \quad \text{(mm)} \qquad \text{Equation 3.3}$$

where $P_{(t-1)}$ is the rainfall on the previous day, measured at 9 am (Eastern Standard Time), $E_{I(t)}$ is the evaporation of intercepted water from vegetation and soil surfaces, and $Q_{O(t)}$ is the overland flow, which was originally termed flash runoff in the MSDI model.

The method for estimating E_I remains unchanged in the new RSDI model for three reasons. First, modelling E_I using thermodynamic energy principles was considered far too complex for this study. Second, the existing model was considered accurate enough for this study. For example, Langford *et al.* (1978) showed that the MSDI provided satisfactory estimates of E_I for wet sclerophyll forests in Victoria. Third, no comparative or recent studies of E_I in and adjacent to the study area could be found to validate the E_I model so no further attempt was made to improve it.

Total run-off ($Q_{(t)}$) is estimated from the following set of equations:

If $P_{EFF(t)} \geq SWD_{(t)}$ then $Q_{(t)} = Q_{T(t)} + Q_{O(t)}$ (mm) Equation 3.4

else $Q_{(t)} = Q_{O(t)}$

where $Q_{T(t)}$ is flow of water through the soil.

3.2 Estimation of potential soil evaporation and plant transpiration

The methodology for calculating potential soil evaporation (E_S) and plant transpiration (E_T) from all-wave net radiation (R_N), and its derivative, potential evaporation (E_P), is now outlined. Estimating R_N from its short- and long-wave radiation components is outlined in section 3.2. Subsequently, the equations to estimate E_P from R_N is described in section 3.3.1. Finally E_P is used to estimate E_S and E_T in section 3.3.2.

3.2.1 Estimation of extra-terrestrial and surface irradiance (R_A)

Incoming solar radiation at the top of the atmosphere is termed extra-terrestrial irradiance (R_A), defined as the intensity of the sun's energy received at the top of the earth's atmosphere (Iqbal, 1983). R_A fluctuates according to the orbit of the Earth on its annual journey around the sun, being determined by geometrical relationships between the earth and the sun (Figure 3.3). The orbit of the earth around the sun follows an annual cycle, equivalent to 365.25 days on the 'plane of the ecliptic', which is the plane on which all the planets, including the earth, rotate around the sun.

The present tilt of the earth on its axis is 23.5^o (Linacre and Geartz, 1997). The earth's tilt on its axis is also termed the angle of declination; this refers to the highest angle observed at noon of a celestial body at a given latitude and time of the year (Iqbal, 1983; Linacre and Geartz, 1997). The angle of declination as shown in Figure 3.3 gives rise to the seasons experienced by the earth.

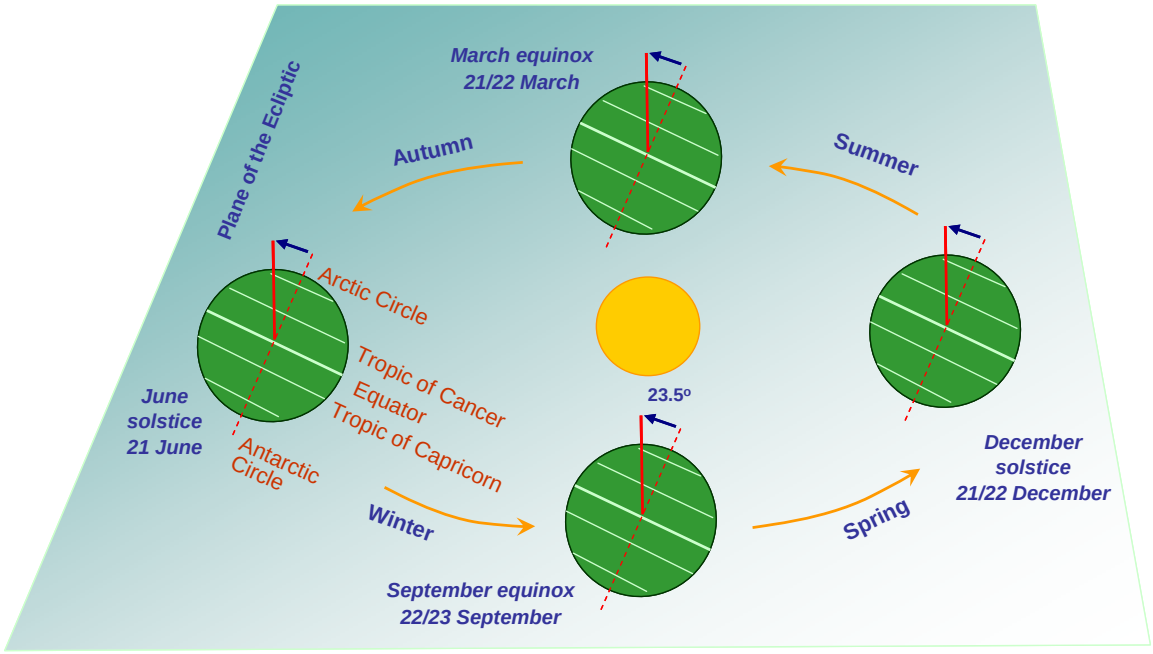

Figure 3.3 Orbit of the Earth around the sun on the plane of the ecliptic during the course of the annual cycle

The following series of equations (Equations 3.5-3.8) were employed to estimate the daily values of the radiation at the top of the atmosphere (R_A) through the annual cycle (Roderick, 1999).

Day angle Γ, is the apparent angle of declination for a given day of the year, relative to the sun, and is estimated as follows (Roderick, 1999):

$$\Gamma = \frac{360}{D_Y}(d_N - 1) \qquad \text{Equation 3.5}$$

where Γ is the day angle in degrees and d_N is the day number of the year commencing 1st January and D_Y is the total number of days in the year.

The declination angle of the earth, relative to the sun, is estimated from Γ, and is expressed as (Roderick, 1999):

$$\delta = \frac{180}{\pi}\left(\begin{array}{l} 0.006918 - 0.399912\cos\Gamma + 0.070257\sin\Gamma - 0.006758\cos 2\Gamma \\ + 0.000907\sin 2\Gamma = 0.0026973\cos 3\Gamma + 0.00148\sin 3\Gamma \end{array}\right) \qquad \text{Equation 3.6}$$

where δ is the declination angle in degrees.

A correction for the eccentricity of the earth's orbit is estimated thus (Roderick, 1999):

$$\frac{1}{d^2} = \left(\begin{array}{l} 1.000110 + 0.034221\cos\Gamma + 0.001280\sin\Gamma + \\ 0.000719\cos\Gamma + 0.00077\sin 2\Gamma \end{array}\right) \qquad \text{Equation 3.7}$$

where $\frac{1}{d^2}$ is a correction for the eccentricity of the earth's orbit.

Finally, R_A is estimated from Γ, δ and $\frac{1}{d^2}$ as:

$$R_A = \frac{37.595}{d^2}\left(\sin\phi\sin\delta\left((\omega_{ss}\frac{\pi}{180}\right)+\cos\phi\cos\delta\sin\omega_{ss}\right) \quad \text{(MJ m}^{-2}\text{ d}^{-1}\text{)} \qquad \text{Equation 3.8}$$

where ϕ is the latitude of the point on the earth's surface in decimal degrees and ω_{ss} is the hour angle at sunset.

As solar radiation passes through the earth's atmosphere, a proportion of it is reflected back into space by clouds, some is absorbed by clouds and small dust particles called aerosols. The balance of incoming solar radiation flux reaching the earth's surface is called the surface irradiance (R_S): this comprises both direct and diffuse radiation (Oke, 1987; Linacre and Geartz, 1997). The direct component of R_S comprises that irradiance that has not been subject to scattering while passing through the earth's atmosphere. The scattered component is termed 'diffuse' radiation.

The principal factors affecting R_S are the concentration of aerosols and water vapour, and the amount of cloud cover (Iqbal, 1983). Because few weather stations record surface irradiance, R_S is instead estimated from R_A using empirical attenuation equations. Therefore it is simple a matter of choosing the best empirical equations for deriving R_S from R_A (Bristow and Campbell, 1984; Kimball *et al.*, 1997; Supit and van Kappel, 1998; Liu and Scott, 2001; Trnka *et al.*, 2005). Estimating R_S using empirical equations will be examined further in Chapter 5.

3.2.2 Estimation of all-wave net radiation (R_N)

The net radiation at the earth' surface (R_N) is defined as:

$$R_N = R_S(1-\alpha) + L_{\downarrow} - L_{\uparrow} \qquad \text{(W m}^{-2}\text{)} \qquad \text{Equation 3.9}$$

where R_S is the surface irradiance , α is the albedo or surface reflectivity to short-wave radiation and $L_{\downarrow}$ and $L_{\uparrow}$, are the downward and upward long wave radiation components.

The albedo (α) is the ratio of incoming to outgoing shortwave radiation and is dependent on surface properties. Typical values of α in a forest are between 0.15 and 0.17, whereas in a grassland values lie between 0.22 and 0.25, depending on levels of vegetation growth and seasonal light conditions (Oke, 1987; Linacre, 1992).

The other terms in Equation 3.9, the long wave radiation components $L_{\downarrow}$ and $L_{\uparrow}$, can be estimated from the Stefan-Boltzman law, assuming that the earth and atmosphere approximate black bodies (Linacre, 1968; Linacre, 1992; Sturman and Tapper, 2006).

The estimation of $L_{\uparrow}$ in a clear sky atmosphere is:

$$L_{\uparrow} = \varepsilon_s \sigma T_s^{\,4} \quad (\text{W m}^{-2}) \qquad \text{Equation 3.10}$$

where ε_s corresponds to the emissivity of the surface (0.97-0.98 for forests ; 0.90-0.95 in grasslands (Oke, 1987)) which is the ratio of the radiant energy emitted by the earth's surface or atmosphere over the incoming radiant energy, σ is the Stefan-Boltzman Proportionality Constant (5.67×10^{-8} $Wm^{-2}K^{-4}$), and T_s is the absolute temperature (degrees Kelvin) of the earth's surface.

The estimation of $L_{\downarrow}$ in a clear sky atmosphere is:

$$L_{\downarrow} = \varepsilon_a \sigma T_A^{\,4} \quad (\text{W m}^{-2}) \qquad \text{Equation 3.11}$$

where ε_s corresponds to the emissivity of the atmosphere (0.95) whose value is close to that of a black body (0.95), and T_A is the mean daily temperature (degrees Kelvin) of the earth's atmosphere.

The net long-wave radiation flux (L^*) is therefore estimated as:

$$L^* = L_{\uparrow} - L_{\downarrow} \quad (\text{W m}^{-2}) \qquad \text{Equation 3.12}$$

Cloud cover generally decreases L^*. If the cloud cover is low down, dense and persistent enough during a 24 hour period, ε_s is increased because of the downward emission of $L_{\downarrow}$. Higher altitude cloud emits lower $L_{\downarrow}$ and hence L^* is not reduced as much as for low cloud, for the same given amount of cloud cover. However, the difference in cloud type cannot be taken into account in the development of the RSDI model as continuous records of detailed cloud data are have not been collected at Canberra Airport.

All the equations and coefficients needed to model R_N have been described in this section. The empirical equations for R_S and $L_{\downarrow}$ are evaluated later for use in this study in sections 5.1 and 5.3.

3.3 Derivation of soil evaporation (E_S) and plant transpiration (E_T) sub-models

This section outlines the models and sub-models to estimate soil evaporation (E_S) and plant transpiration (E_T) for an all-wave net radiation-based RSDI model. These models are based on potential evaporation estimated from R_N, that are then, along with soil and vegetation factors, used to produce estimates of E_S and E_T. The classical approach has been to treat soil evaporation and plant transpiration as a single evapotranspiration entity, though as different processes they warrant independent estimation. Fortunately E_P, which forms the basis of the separate models of E_S and E_T can be estimated directly from R_N (Penman, 1948; Monteith,

1965; Priestley and Taylor, 1972; Budyko, 1974; Linacre, 1992; Linacre and Geartz, 1997; Berry, 2001; Berry and Roderick, 2002; Linacre, 2004).

3.3.1 Potential evaporation (E_P)

To model E_S and E_T using R_N requires suitable and appropriate simple and elegant models of E_P from either a soil or a plant surface. This section explores some of the possible models sourced from the literature for this purpose.

The estimation of E_P involves either:

(1) a thermodynamic approach, or

(2) a combination of thermodynamic and aerodynamic approaches (Ward and Robinson, 2000).

The classic study of Penman (1948) derived the following equation based on a combination of thermodynamic and aerodynamic approaches:

$$E_P = \left(\left(\frac{s}{\gamma}\right)R_n + E_D\right) \Big/ \left(\left(\frac{s}{\gamma}\right)+1\right) \qquad \text{(mm d}^{-1}\text{)} \qquad \text{Equation 3.13}$$

where s is the slope of the saturated vapour pressure curve for a given temperature T_A, E_D is the drying power of the air, and γ is the psychometric constant.

The dimensionless factor s/γ partitions the relative contribution of R_N and E_D in determining E_P (Ward and Robinson, 2000).

E_D is estimated from:

$$E_D = 0.35(e_S - e_A)\left(1 + \frac{\upsilon}{100}\right) \qquad \text{(mm d}^{-1}\text{)} \qquad \text{Equation 3.14}$$

where e_S is the saturation vapour pressure at the mean air temperature, e_A is the actual vapour pressure, and υ is the wind speed in m sec^{-1} measured two metres above the ground (Ward and Robinson, 2000:127).

Monteith (1965) further adapted this to take account of plant and soil moisture resistances to limit potential evaporation:

$$E_P = \frac{s(R_n - \delta G) + \rho c(e_S - e_A)/r_A}{s + \gamma[1 + r_S/r_A]} \qquad \text{(mm d}^{-1}\text{)} \qquad \text{Equation 3.15}$$

where ρ is the air density, c is the specific heat of the air, r_A is the aerodynamic resistance, r_S is the surface resistance.

Equation 3.15, also known as the Penman-Monteith equation, requires a detailed set of meteorological variables such as: R_N and Q_G, e_S and e_A, average wind speed and the resistances r_A and r_S, derived from hourly weather measurements. Therefore, Equation 3.15 is not well suited to this study for three reasons. First, taking hourly measurements is too short a time-scale for estimation of a medium or a long-term time series of soil water deficit (SWD) based on daily

weather measurements. Second, the resistances of air, soil, and plant surfaces are not well known for eucalypt forests. They would have to be determined from field studies for all vegetation types in the study region. Third, long-term datasets of hourly or even three-hourly weather are not available from most Australian weather stations. For these reasons, this approach is not feasible because of the type and amount of data involved and the complexity of estimating some of the input parameters.

A preferred alternative is to use a simple thermodynamic approach is to estimate the available energy at an evaporating surface, either a plant leaf or a soil surface and then to estimate the amount of latent heat evaporating off both surfaces in response to the available energy (Ward and Robinson, 2000). E_P can be estimated in this way from Budyko (1974).

$$E_P = R_N \lambda \rho_W \qquad (\text{mm d}^{-1}) \qquad \text{Equation 3.16}$$

where R_N is all-wave net-radiation (MJ m^{-2} d^{-1}), λ is the latent heat of evaporation (J Kg^{-1}), and ρ_W is the density of water (Kg m^{-3}).

In the case of E_T, it is assumed that that plants need to maintain leaf water content to survive. If the leaf water content of plants can be used to classify the plants in Australian vegetation into a few functional types, R_N can be partitioned into E_P for each functional leaf type. This approach is further outlined in section 3.3.3.

In the case of E_S, the available R_N at the soil surface (R_{NS}) can be estimated from a combination of three factors: the shading effects of the various plant layers in a forest, the drying power of the air close to the soil surface, and the soil surface wetness. This approach is described further in section 3.3.2.

3.3.2 Soil evaporation (E_S)

The remote sensing-based model of E_S, developed by Fisher *et al.* (2008), was assessed as the most feasible method for estimating E_S. Although Fisher's model requires monthly input data, it is amenable to use of daily time steps required here. The Fisher equation for estimating E_S is:

$$E_S = (F_{\text{WET}} + F_{SM} \times (1 - F_{\text{WET}})) \times (R_{NS} - \delta G_S) \quad (\text{mm}) \qquad \text{Equation 3.17}$$

where F_{WET} is the relative surface wetness and F_{SM} is the soil water constraint, both terms have been defined by Fisher *et al.* (2008).

F_{WET} in Equation 3.19 is defined by Fisher *et al.* as 'the fraction of time that surface is wet' The authors state that the estimation of F_{WET} is '...scaled to relative humidity (RH) using a power function to reflect the time scale at which it changes ($F_{WET} = RH^4$). This function effectively predicts 0% wet surfaces at RH<70%, 50% wet surfaces at RH=93% and 100% wet surfaces at RH=100%.'

The term F_{WET} in Equation 3.17 is estimated as

$$F_{WET} = RH_{MIN}^{4} \qquad \text{Equation 3.18}$$

where RH_{MIN} is the daily minimum relative humidity.

Fisher's F_{SM} sub-model reflects the close association between atmospheric and soil water conditions. After R_{NS}, the vapour pressure deficit (VPD) is the next most important factor affecting evaporation conditions. The reason for choosing the warmest part of the day (T_{MAX}, RH_{MIN}) to estimate F_{SM} is because it is assumed that this is when soil water is most likely to be in dynamic equilibrium with near surface air moisture levels.

The second term F_{SM} in Equation 3.17 is estimated as:

$$F_{SM} = RH^{VPD/\beta} \qquad \text{Equation 3.19}$$

where VPD is the vapour pressure deficit taken at mid-day conditions (e_S-e_A), β is a coefficient that determines the relative sensitivity of F_{SM} to VPD. In this study the warmest conditions of the day will be based on T_{MAX}, determining VPD and RH_{MIN}.

Having determined R_N, the net radiation at the forest floor (R_{NS}) can now be estimated from R_N, with adjustments being made for the attenuation of light through forest canopy layers using Beer-Lambert's Law (Jarvis *et al.*, 1976):

$$R_{NS} = (1 - \alpha)R_N \times e^{(1-kL)} \qquad (Wm^{-2}) \qquad \text{Equation 3.20}$$

where k is the canopy light extinction coefficient and L is the combined leaf area index (LAI) of the all the vegetation layers above the soil surface. R_N above the forest canopy has been estimated previously using Equation 3.9.

The final term δG_S is estimated based on an adaptation of the equations developed in the Jarrah Forest study by Silberstein *et al.* (2001):

Between December and March	$\delta G_S = 0.09 * R_{NS}$	(Wm^{-2})	
For the intervening spring (Sep-Nov) and autumn months (Apr-May)	$\delta G_S = 0.05 * R_{NS}$		Equation 3.21
Between June and August	$\delta G_S = -0.03 * R_{NS}$		

where δG_S is the seasonally adjusted soil heat flux.

An unvalidated assumption is that δG_S varies between -0.03 and 10 percent of R_{NS} during the course of the solar cycle even though δG_S should more or less balance out to zero over an annual time scale. In a first approximation Lhomme (1997) found that δG_S for grasslands is about 5% of R_N throughout the year. From a detailed short-term energy and water balance study

in a *Eucalyptus marginata (*Jarrah) forest in Western Australia, Silberstein *et al.* (2001) estimated δG_S to be during daylight hours between 8 and 9% of R_N.

Now that all the terms have been estimated, E_S can be calculated from Equation 3.17.

3.3.3 Plant transpiration (E_T)

A wealth of models to describe and estimate the rate of ecosystem processes has become available with the advent of remote sensing. For example, it is now possible to monitor gross primary productivity and evapotranspiration at a landscape scale (Berry, 2001; Berry and Roderick, 2004; Berry, 2007). The key issue in modelling E_T is how to estimate the ratio of E_P over E_T using transpiration models that take account of projective foliage cover of the overstorey and understorey in a given vegetation type at the same time factoring in the effect of soil water availability on each of the overstorey and understorey components.

Calculating E_T is a two-step process. Estimates of potential E_T for three dominant leaf types (TMS) are outlined in section 3.3.3.1. To calculate E_T for each leaf type, potential E_T is multiplied by a soil moisture resistance function. This takes account of the effect of SWD on relating E_T to the variation in soil water from field capacity to wilting point (3.3.3.2).

3.3.3.1 Potential plant transpiration model for each TMS leaf surface

The Turgor-Mesic-Sclerophyll leaf type (TMS) scheme developed in a recent remote sensing study, partitions E_T into its separate components, based on leaf functional types (Berry, 2001; Berry and Roderick, 2004). The scheme developed by Berry (2001; 2004) uses three broad leaf types:

(1) derive structural support from the turgor pressure of water, such as grasses and herbs — the Turgor (T) leaf type;

2) are mainly found in found in trees and shrubs where water and nutrients are readily available — the Mesophyllous (M) leaf type; and

(3) are found in sclerophyll shrubs adapted to low nutrient and often low water availability — the Sclerophyll (S) leaf type.

A T leaf type has a relatively high mass fraction of water (0.9) compared to the other two leaf types, M (0.6) and S (0.45). The higher the leaf water content, the higher is the water demand to maintain plant function. According to Berry (2001; 2004) the three leaf types present entirely distinctive ecological strategies that plants can adopt to water and nutrient availability. Thus, a T leaf type has evolved in response to highly variable soil water regime, under conditions of relatively high nutrient availability, whereas an M leaf type has evolved in response to optimal moisture and nutrient conditions. An S leaf type reflects an adaptation to low nutrient status and periodic water stress due to highly variable soil water conditions in more shallow impoverished soils.

The TMS scheme uses estimates of the fraction of photosynthetically active radiation (FPAR) and the relative contributions of the TMS components to partition R_N into E_T for each TMS component (Berry, 2001; Berry and Roderick, 2004). Instead of using relative contributions of each TMS leaf type, Projective Foliage Cover (PFC) for each TMS leaf types is used here to estimate the fraction of E_T for each of the TMS components. This relationship has not been independently validated in this study.

Based on their respective mass fractions of water, projective foliage cover (PFC) the potential transpiration flux of the mesophyllous M leaf type (E_{PM}) can be estimated from:

$$E_{PM} \equiv E_P \times 0.60 \times PFC_M \quad (\text{mm d}^{-1}) \qquad \text{Equation 3.22}$$

where PFC_M is the projective foliage cover of an M leaf type.

Because the turgor (T) leaf type is mainly found on the forest floor in these landscapes, and because sclerophyll (S) leaf type can be found in any forest sub-stratum, Equation 3.20 must first be applied to estimate the reduction in R_N caused by the interception of a tree or shrub canopy. Forest canopy Leaf Area Index (LAI) is only applied to estimate R_N and E_P for the understorey component in a forest:

$$E_{PT} \equiv E_P \times 0.90 \times PFC_T \quad (\text{mm d}^{-1}) \qquad \text{Equation 3.23}$$

$$E_{PS} \equiv E_P \times 0.45 \times PFC_S \quad (\text{mm d}^{-1}) \qquad \text{Equation 3.24}$$

where PFC_T and PFC_S are the projective foliage cover of T and S leaf surfaces for a given vegetation type.

Projective foliage covers, PFC_T, PFC_M, and PFC_S are kept constant estimating E_{PT}, E_{PM}, and E_{PS} over the full length of the time series. This is unlike the method used by Berry (2001; 2004), in which FPAR and the relative contribution of each TMS leaf type changes constantly over time, according to seasonal conditions or recent disturbances, such as grazing, clearing, or fire. The models for soil moisture resistance outlined in section 3.3.3.2 provide a useful mechanism for estimating E_T for each of the TMS leaf types, instead of FPAR.

3.3.3.2 Actual plant transpiration models for each TMS leaf surface

Potential E_T is the amount of transpiration that might occur from a constantly green canopy that is well supplied with water. Potential E_T is also dependent on the PFC of the T, M, and S leaf surfaces, as demonstrated in the previous section. As the soil dries out, the contribution to E_T from each of the leaf types is assumed to reduce according to some form of soil moisture resistance equation. Essentially, an equation for soil water resistance simulates the effect of available water for plant transpiration between field capacity and wilting point. The amount of available water between these two limits in one metre of forest soil has been defined as 165mm (Mount, 1972) although this may vary between 200 and 400 mm (Talsma, 1983; Raupach *et al.*, 2001; Fowler and Adams, 2004) in wet forest types in Australian and New Zealand. The

amount of available water in the soil can be fixed for a given vegetation type. In the MSDI model the amount of available water was set as a constant 165 mm in both forests and grasslands (Mount, 1972), somewhat lower than that used in other studies. However, it appears to work satisfactorily in a range of forest types (Mount, 1972). The level of available soil water was however increased to 250 mm in wet sclerophyll forests in Victoria's water catchments (Langford *et al.*, 1978) to take account of the deeper soils. Increasing the soil depth generally increases the evapotranspiration flux for a given daily maximum temperature.

Three equations have been used to model the effect of soil moisture resistance on E_T (Table 3.1). Equation 3.25 assumes a straight-line relationship between E_A and E_P as soil moisture decreases over time. Equation 3.26 assumes that this relationship takes a quadratic form. The last equation, Equation 3.27 employs several simple linear equations to arrive at E_T at different levels of SWD.

Table 3.1 List of soil moisture resistance models

General description	Equation formula	Equation number
Linear soil water resistance model	$E_A = \frac{1-\left(\frac{SWD}{AWC)}\right)}{1-F} \times E_P$	Equation 3.25
Quadratic soil water resistance model	$E_A = \left(1-\frac{SWD}{AWC}\right)^2 \times E_P$	Equation 3.26
Mount linear E_T model with different soil moisture resistances applying at different SWD levels through the soil profile	If SWD <25mm, $E_A = 1.0 \times E_P$	Equation 3.27
	else if 25<SWD <50mm, $E_A = 0.8 \times E_P$	
	else if 50<SWD <140mm, $E_A = 0.65 \times E_P$	
	else if 140.5<SWD <165 mm, $E_A = 0.27 \times E_P$	
	else SWD >165 mm $E_A = 0.10 \times E_P$	

Note: SWD is the Soil Water Deficit, AWC is the available water capacity and F is a certain fraction of the available water supply when E_T matches E_P under non-limiting soil moisture conditions.

The effect of these three soil moisture resistance models over the full range of SWD from zero to 165 mm is presented in Figure 3.4. As can be seen, Equation 3.27 and Equation 3.28 model the ratio of $\frac{E_T}{E_P}$ in a similar fashion to each other over the full range of SWD.

In contrast, Equation 3.29 appears to differ markedly from the other two equations. However, Equation 3.29 will be used in the RSDI on the following grounds. First, it has already been tested and used to estimate E_{T+S} in a variety of forest environments in Australia (Mount,

1972; Langford *et al*., 1978). Second, the thresholds at which each of the linear equations applies, as well as the ratio of $\frac{E_T}{E_P}$ can be adjusted to suit different depths and types of soils. Equation 3.29 originally applied to the estimation of E_{T+S} in the MSDI model. Thus it is assumed that the same ratio can be applied to the estimation of plant transpiration (E_T) in the RSDI model.

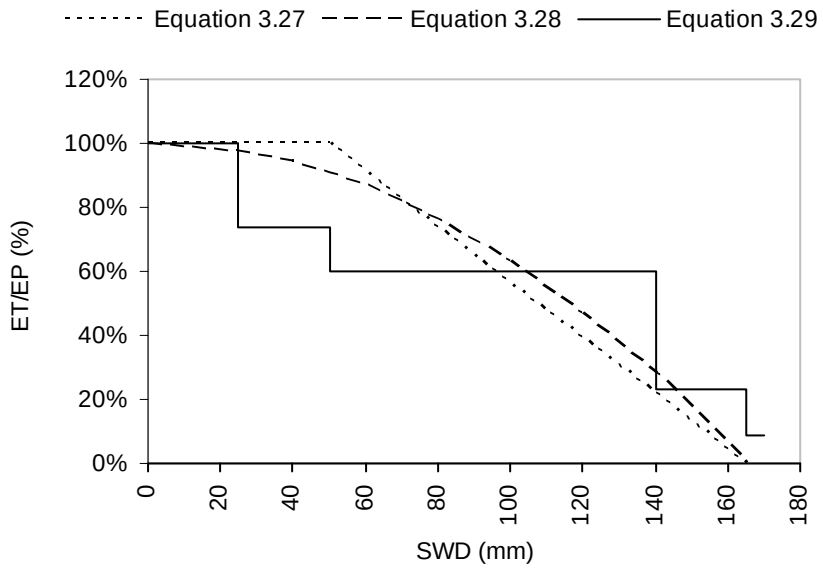

Figure 3.4 $\frac{E_T}{E_P}$ ratios estimated using different soil water resistance models across the range of soil water deficit (0-165 mm)

The ratio of $\frac{E_T}{E_P}$ estimated from Equation 3.27 at any SWD can be applied to estimate E_T of M and S leaf surfaces:

$$E_{TM+S} = E_T / E_P \times \left(E_{PM} + E_{PS}\right) \quad \text{(mm d}^{-1}\text{)} \qquad \text{Equation 3.28}$$

Because T leaf types are associated with shallow rooted ephemeral grasses and forbs in the forests in this study area, E_T was curtailed at SWD=100 mm. It is assumed that high curing levels occur above this threshold in the RSDI model. As a result, transpiration from T type leaf surfaces is estimated as:

$$E_{TT} = E_T / E_P \times E_{PT} \quad \text{(mm d}^{-1}\text{)} \qquad \text{Equation 3.29}$$

The estimation of E_T for all the TMS leaf components has now been derived. This then completes the estimation of E_S and E_T components within the RSDI model.

3.4 Findings

Three preferred DSWBMs were selected from the literature based on their parsimonious requirements for medium and long-term weather data and their closeness to biophysical reality (Section 3.1). The MSDI and the RSDI model appear suited for medium-term studies of SWD over time because the sub-models of $E_{\mathbf{I}}$ and $E_{\mathbf{T+S}}$ closely approximate evaporation processes in south eastern Australian forests. The Fowler (F-DSWBM) model is more suited potentially to estimate a long-term time series of SWD, because of its minimal data requirements of precipitation and E_P based on Julian days (JD). Once either of the two medium-term DSWBMs is calibrated, then the F-DSWBM can be calibrated to the medium-term SWD index before further analysis is undertaken.

The modelling of R_N based on its separate components R_A, R_S, albedo and net long-wave radiation, $L\downarrow$ and $L\uparrow$ was presented in Section 3.2, based on previous studies (Budyko, 1974; Oke, 1987; Roderick, 1999). It can be estimated from a minimum dataset of T_{MIN}, T_{MAX}, P_{0900} although supply of additional variables such as cloud cover or sunshine hours can improve the accuracy of the estimate. However, the latter two variables are not always measured or estimated continuously at manned or automatic weather stations. The Budyko equation (Equation 3.16) can be used to estimate potential evaporation (E_P) from all-wave net radiation (R_N) to form the basis for modelling $E_{\mathbf{S}}$ and $E_{\mathbf{T}}$.

The estimation of E_{T+S} from models of $E_{\mathbf{S}}$ and $E_{\mathbf{T}}$ was advanced in Section 3.3, based on remote sensing studies (Section 3.3), using a minimal set of weather variables including T_{MAX}, $T_{MIN,}$ and RH_{MIN}. Models of $E_{\mathbf{S}}$ and $E_{\mathbf{T}}$ can therefore be used instead of the more general evapotranspiration term in the RSDI daily soil water balance model.

This chapter therefore answers the second and third questions posed in section 1.4 (Table 1.1): 'What daily soil water balance models (DSWBMs) are most suited to the study of landscape dryness over the medium and long-term? Can simple and elegant sub-models of soil evaporation and plant transpiration replace evapotranspiration models?'

Having determined which soil water balance models are suited to the purposes of this study, the next chapter investigates what datasets and weather stations are available in the study region to drive these models, as well as those of potential fire spread.

Chapter 4: Datasets for the Landscape Susceptibility Models

This chapter sets out to create medium and long-term weather datasets that are necessary to drive the models of landscape dryness and potential fire spread for three climate zones in the study region (Cfa, Cfb, Csc) (Figure 1.2). The weather datasets needed for deriving, calibrating, and then analysing these two fire susceptibility factors are:

(1) calculated daily R_N and hence daily E_P, to enable estimation of E_S and E_T in the RSDI model (Chapter 5) for each of the three weather stations, representing the climate zones identified in Chapter 2;

(2) medium (50-70 yrs) and long-term (> 100 yrs) daily SWD time series datasets for two distinct climate zones. These will be needed for calibration and validation studies (Chapter 6), and for time series analysis and classification (Chapters 8 and 9); and

(3) medium-term time series data for daily FWI and FFDI for at least one location (Chapter 8).

The first part of the of chapter examines the weather datasets from weather stations in the study area that meet the modelling requirements of the selected landscape dryness and potential fire spread models for the three climate zones (see Section 2.2). The second part of the chapter reviews the data standards and available weather data for the study. The third part of the chapter demonstrates how continuous and relatively error-free datasets are compiled for each of the models from the available weather data.

4.1 Modelling requirements based on study purposes

4.1.1 Modelling plan

An idealised modelling plan is presented in Figure 4.1. While only one medium-term SWD dataset will be used in time series analysis and classification, the additional SWD datasets produced by the other two daily soil water balance models are needed to support calibration, validation, and cross-comparison of the models. They need to perform well and have practical applicability. Medium-term indices of landscape dryness are required for each of the three climatic zones: Sub-montane plains, Montane and Sub-alpine (see section 2.2).

Medium-term landscape dryness indices can be produced for each of the three climate regions, but modelling is limited by the range and quality of data, and by the length of the record. Stations representative of these distinctive climatic regions are Canberra Airport (Cfa), Corin Dam (Cfb) in the upper Cotter River catchment, and Cabramurra (Csc). Queanbeyan weather station, close to Canberra Airport, has long-term rainfall records. Judicious melding of

the Queanbeyan and Canberra Airport records enabled construction of a long-term sub-montane plains weather dataset.

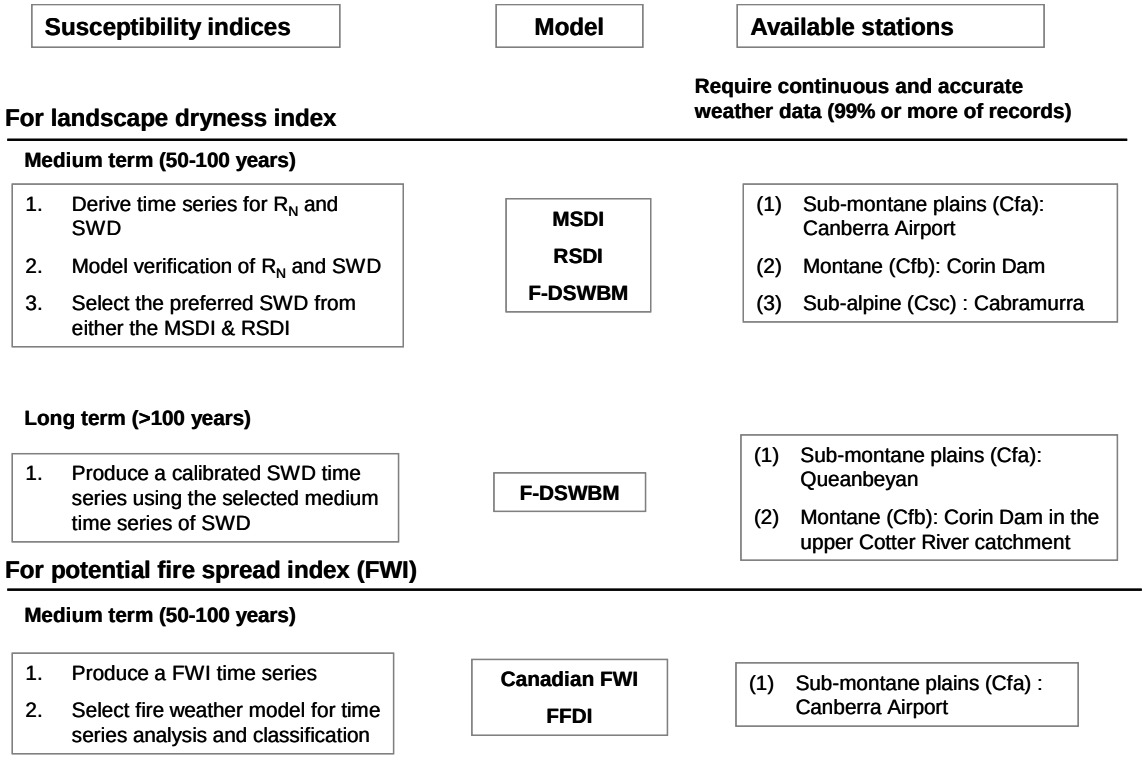

Figure 4.1 Modelling plan for thesis

Note: Plan assumes availability of comprehensive, consistent, and accurate long-term climate records for time series analysis in all three climate zones. For example, it was not practicable to estimate directly all-wave net radiation (R_N) at the sub-alpine weather station at Cabramurra.

The compiled weather data and models of landscape dryness are used for two purposes in preparing a medium-term time series. First, calibration and validation of sub-models for E_S and E_T in the RSDI model are performed to align the RSDI model with other sources of published scientific data, including ground or remotely sensed data. Second, the calibrated RSDI, along with the Fowler and MSDI models, is tested using evaporation and run-off data to check the calibrations and make any further adjustments to the models. Once the models are sufficiently calibrated, the preferred models can be compiled as a succession of annual SWD profiles, commencing on 1st July to correspond with the annual solar cycle and the start and finish of fire seasons.

For medium-term time series of potential fire spread, the requisite daily weather data are only available at Canberra Airport. The technology to record continuous weather data in more remote regions has only become available in the last 10 years, and anyway remote telemetric data recording systems will always have problems recording weather data on a continuous and accurate basis. Because no independent method for testing the validity or accuracy of the FWI

or the FFDI is available, their capacity to model potential fire spread during the course of a fire season is discussed in Chapter 8. The same process is also used to select the preferred model of PFSI in time series analysis and classification of annual profiles of potential fire spread.

The modelling plan requires at least two landscape dryness models initially to estimate landscape dryness for two climate zones: sub-montane (Cfa) and montane (Cfb). The key weather station for the long-term time series of landscape dryness is that of Queanbeyan whose length of record exceeds 100 years. The Corin Dam weather station record, which is a representative weather station in the montane climate zone, only goes back to 1936, which is only five years longer than that of Canberra. The net result is that only one long-term time series of landscape dryness can be implemented.

4.1.2 Weather variables for the indices of landscape dryness and potential fire spread

A minimal weather variable data set was used for modelling landscape dryness and potential fire spread. Those variables required for modelling landscape dryness (P_{0900}, T_{MAX}, T_{MIN}, C_{AV}, $T_{1500,}$ and RH_{1500}) are depicted in Figure 4.2 and are used to calculate potential and actual evaporation rates in daily time steps. In particular, the RSDI model requires the derived modelling variable R_N, the equations of which were formulated in the previous chapter. The estimation of R_N and its input variables requires the following weather variables, C_{AV}, P_{0900}, T_{MAX} and T_{MIN}.

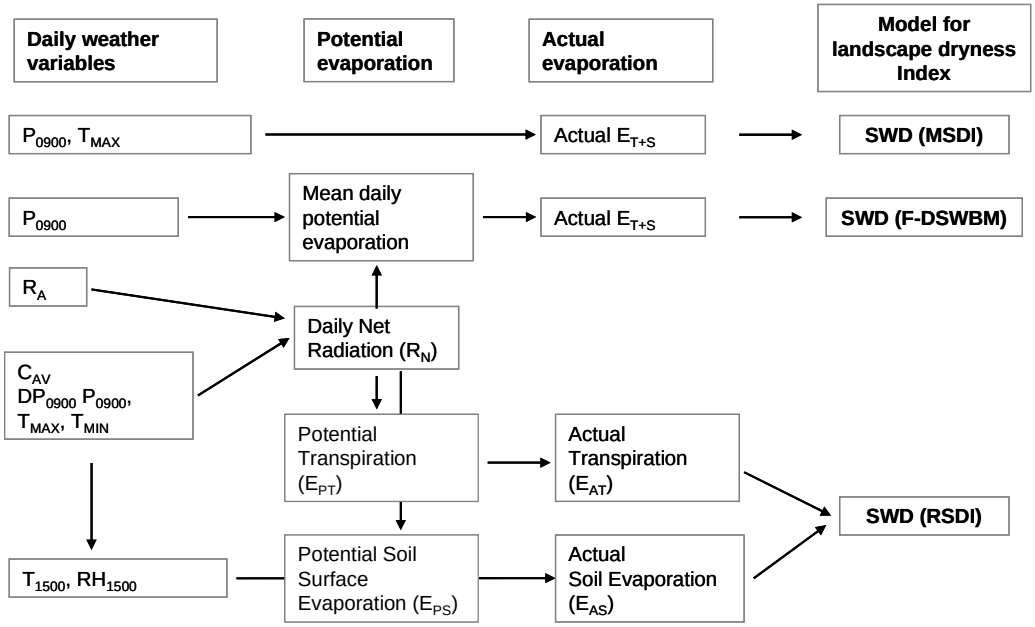

Figure 4.2 Weather variables and sub-models for estimating landscape dryness index

where T_{MAX} is the maximum daily surface temperature, T_{MIN} is the minimum daily temperature, E_{T+S} is the daily evapotranspiration rate, P_{0900}, is the amount of precipitation to 9am; C_{AV} is the mean daily cloud cover, T_{1500}

and RH_{1500} are the temperature and relative humidity. T_{1500} and RH_{1500} approximate the conditions at the warmest and driest part of the day (sometime between 1400 and 1800 hrs).

Notes: (1) Extra-terrestrial irradiance (R_A) is also needed for estimation of all-wave net radiation (R_N)

(2) To estimate soil water deficit (SWD) in the upper Cotter River catchment using the RSDI model, all-wave net radiation from Canberra Airport as a first approximation was used to model R_N.

The two potential fire spread models, FWI and FFDI, require a range of weather variable inputs (Figure 4.3). Four daily weather variables (P_{0900}, T_{1500}, RH_{1500} and WS_{1500}) are required inputs for the fuel moisture, fuel availability, and potential fire spread models. The fuel availability indices require estimates of intermediate medium and long-term fuel moisture levels using the DMC and DC codes embedded in the FWI model whereas the FFDI model requires days since rain (D_{SR}) and drought index (DI) estimated from one of the DSWBMs.

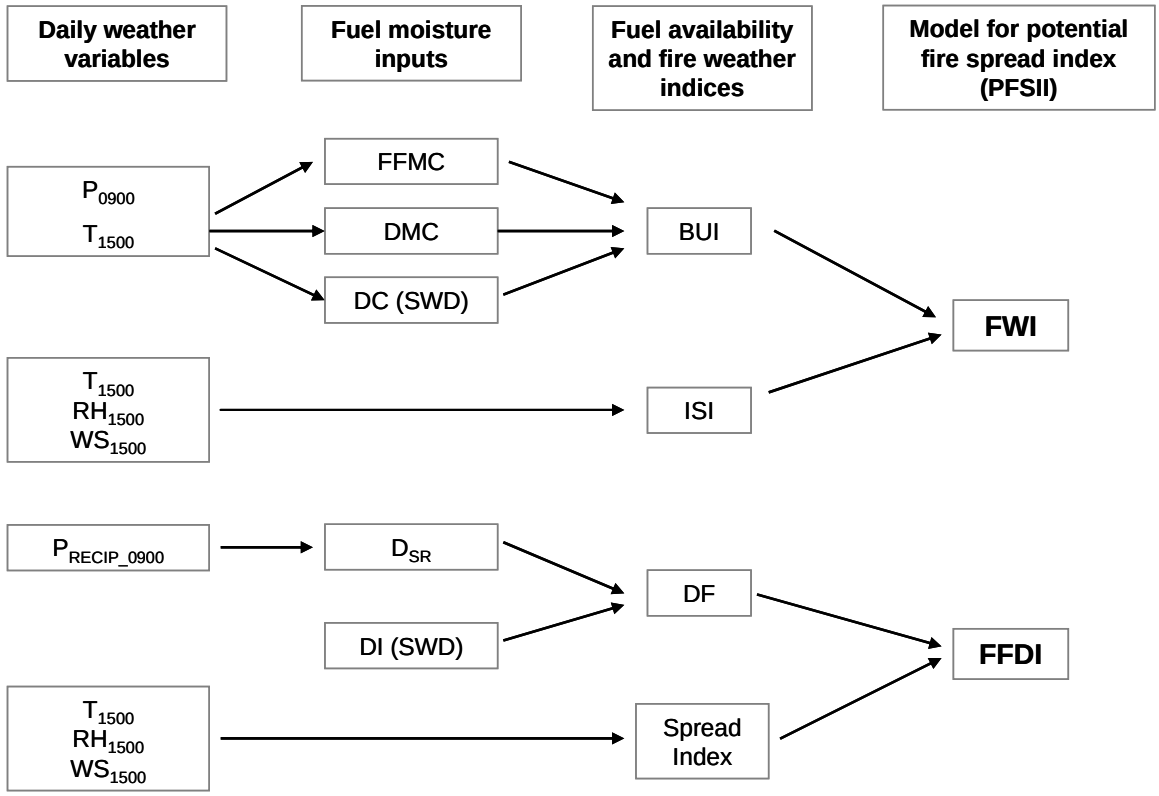

Figure 4.3 Weather variables and sub-models for estimating potential fire spread

where D_{SR} is the number of days since rain; P_{0900} is daily precipitation measured at 0900 hr; T_{1500}, RH_{1500}, and $WS1_{500}$ are the temperature, relative humidity and wind speed measured (or estimated) at 1500 hr close to the warmest part of any given day (by mid summer, the hottest part of the day is late afternoon, after 1500 hours).

Notes: (1) The two PFSI models can only be estimated from Canberra Airport weather data (see Table 5.1)

(2) The FFDI is based on a standard fuel load of 12.5 t ha^{-1}, which is assumed to be constant in this study.

In summary, nine weather variables are required as inputs into the three landscape dryness and two potential fire spread models (Table 4.1). The variables, dewpoint and wind direction at 1500 hrs (DP_{1500} and WD_{1500}), were included for contextual purposes as they provide information about the type of atmospheric air mass moving over the region at the time.

Table 4.1 Weather variables needed for modelling of all-wave net radiation, landscape dryness, and potential fire spread

Weather variables	All-wave net radiation	Landscape dryness			Potential fire spread indices (PFSI)	
	R_N	MSDI	RSDI	F- DSWBM	FFDI	Canadian FWI
P_{0900}	●	●	●	●	●	●
C_{AV}	●					
T_{MAX}	●	●	●			
T_{MIN}	●		●			
DP_{0900}	●					
DP_{1500}	●					
T_{1500}					●	●
RH_{1500}			●		●	●
WS_{1500}					●	●
WD_{1500}					●	●

Notes: (1) ● indicates variable needed to run model.

(2) As well as P_{0900} data, the F-DSWBM requires mean daily evaporation from estimates taken over a 20 to 30 year period (see section 6.1.3).

The weather variables needed for the daily soil water balance models are summarised below (Table 4.2).

Table 4.2 Canberra Airport and Corin Dam input weather variables for F-DSWBM, MSDI and RSDI models

Model	Time scale (yrs)	Data requirements
RSDI	56+	C_{AV}, P_{0900}, T_{MAX}, T_{MIN}, RH_{MIN} and VPD_{MIN} and mean daily e_A
MSDI	65+	P_{0900} and T_{MAX}
F-DSWBM	130 -150	P_{0900} and average E_P for each JD in a year estimated from the last 30 years.

Note: The RSDI model needs additional variables to estimate R_N and its components that are recorded at standard weather stations, although cloud cover should be estimated at intervals across the day to obtain accurate estimates of R_S used in the estimation of R_N.

Input weather variables for the two potential fire spread models are summarised in Table 4.3.

Table 4.3 Weather variables needed to estimate potential fire spread (from Canberra Airport)

Model	Time scale of study (yrs)	Data requirements
FFDI	65+	SWD, P_{0900}, T_{1500}, RH_{1500}, WS_{1500}
FWI	65+	SWD, P_{0900}, T_{1500}, RH_{1500}, WS_{1500}

Note: SWD is estimated from any one of the DSWBMs. The scale of SWD is set to, or scaled up to, 200 mm for use in both potential fire spread indices. The standard scale of SWD in the MSDI and RSDI models is 165 mm.

4.2 The weather data

4.2.1 Weather stations and data standards

The Australian Bureau of Meteorology (BOM) collects and collates high quality weather data across a network of Reference Climate Stations (RCS) meeting quality standards set down by the World Meteorological Organisation (WMO) (Bureau of Meteorology, 1997; World Meteorological Organization, 1983; World Meteorological Organization, 1988). Nevertheless, actual weather records contain data errors, due to the changes in reporting requirements and the quality of instrumentation. More specifically, changes have included:

- the number, location, and regularity of maintenance of weather stations;
- changes in instrumentation and technology;
- frequency of instrumentation calibration and measurement; and
- observer or instrument bias (Linacre, 1992).

The data collection standards are designed to keep instrument and human error within acceptable and stated quality standards over the long-term (Bureau of Meteorology, 1997).

Weather data requirements for this study conform to the following criteria:

- they have been collected in accordance with standards set down by the WMO;
- they have few missing records in the record from the start of reliable record-keeping, defined as having less than 1-3% of total number of records missing; and
- they have been collected using comparable and consistent methods and instrumentation.

Other factors important in the selection of a weather station for long-term study include external and internal site factors. Based on the BOM's observation specification (Bureau of Meteorology, 1997), the external site factors include:

- site permanency;
- avoidance of site relocation;
- the site environment remaining largely unchanged over the period of record; and
- the site is located well away from the influence of urban settlement and lakes, and the surrounds have a stable land use.

It is desirable that:

- the weather recording instruments be sited according to WMO layout requirements;
- the instruments are of the highest quality; and
- the instruments are maintained and calibrated on a regular basis.

BOM standards for data quality and weather station standards (Table 4.4) are drawn from the WMO standards for weather recording and weather stations (World Meteorological Organization, 1983; World Meteorological Organization, 1988; Bureau of Meteorology, 1997).

4.2.2 Effects of weather data and modelling errors on fire susceptibility indices

The proclivities of weather stations to malfunction aside, the principal errors in long-term datasets arise from:

- magnitude and variation of the absolute and relative errors in the measurement of weather data;
- possible measurement biases due to the recording instruments or attributable to the weather observer; and
- errors in the formulation of any model of a particular index of fire susceptibility.

Absolute error is defined as error associated with the physical measurement of a weather variable (Linacre, 1992). For instance, the absolute error in the physical measurement of temperature is ± 0.1 °C. This absolute error represents the best possible accuracy to which a weather variable can be measured using a particular instrument or method of observation.

Relative error is defined as the absolute error expressed as a percentage of the weather variable that will vary according to the magnitude of the recorded values. Relative error is used for estimating the comparative accuracy of weather variables at the opposite ends of the scale of the reported range of expected values. In the case of temperature, the relative error of 1°C at 30^{o}C(284K) is 0.067%, and at 0^{o}C (303K) it is 0.073%.

Table 4.4 Contemporary standards for weather data collected at accredited reference climate stations in Australia

Factor	Variable	Measurement	Recording range	Reported resolution	Required accuracy	Remarks
Precipitation	Daily rainfall	T	0 – 400 mm	0.1 mm	±0.1 mm up to 5mm ±2% > 5mm	
Solar Radiation	Surface irradiance	T	0 – 50	0.5 Wm^{-2}	1 Wm^{-2}	
	Net radiation	T	0 – 30	1 $MJm^{-2}d^{-1}$	±1 $MJm^{-2}d^{-1}$ up to 8 $MJm^{-2}d^{-1}$ ±5% > 8 $MJm^{-2}d^{-1}$	Daily average net radiation values
Temperature	Air temperature	I	-60 – +60 °C	0.1 °C	±0.1 °C	
Relative humidity	Dewpoint	I	-60 – +60 °C	0.1 °C	±0.5 °C	Error in estimating relative humidity tends to ±1% when nearing saturation
	Relative humidity	I	5 – 100%	1%	±3%	
Clouds	Cloud cover	I	0 – 8/8	1/8	±1/8	
Wind	Wind speed	A	0 – 75 ms^{-1}	0.5 ms^{-1}	±0.5ms^{-1} up to 5 ms^{-1} ±2% > 5 ms^{-1}	Average over 2 or 10 min
	Wind direction	A	0 – 360°	5°	±10°	Average over 2 or 10 min
Evaporation	Pan evaporation	T	0 – 10 mm	0.1 mm	±0.1 mm up to 5 mm ±2% > 5 mm	

Where I = Instantaneous reading; A = Averaging – averaged values over a fixed time period as specified for the weather station; T = Totals over a fixed time period(s) as specified for the weather station

Source: Documentation contained in Observation Specification 2013.1 (Bureau of Meteorology, 1997) based on WMO standard.

Seasonal variations and the particular characteristics of a weather station can also affect the size of relative error in the estimation of a weather variable (Table 4.5). This table is adapted from Linacre (1992:33) where absolute and relative tolerable errors of commonly measured weather variables at a manned operating weather station or an automatic weather station are presented using some typical seasonal values.

In practice, the relative error will depend on the size and range of the seasonal values for each of the key input variables. If, for example, the total absolute acceptable measurement error for R_N is $\pm$ 0.9 MJ m^2 d^{-1}, then the maximum tolerable relative error will range between 4 and 9%, depending on season. Similarly, if the absolute total acceptable error for maximum daily temperature is 0.8^oC, then the seasonal total relative error will vary between 0.8 and 1.8% while the relative error in minimum daily temperature varies much more widely (between 1.5 and 100%). Rainfall records are particularly prone to high relative errors for low rainfall (< 5 mm) and can be compounded by both systematic and observer errors. Since light rainfall events occur frequently in the records, there is a potential cumulative error in estimates of water available for evaporation, a key estimating variable for modelling SWD in a DSWBM.

High landscape susceptibility to fire only occurs towards the top end of the scales of landscape dryness and adverse fire weather conditions. Hence, any interpretation of the potential for a large landscape fire during a fire season, predicated on thresholds of soil water deficit (SWD) and the potential fire spread index (FWI) is critically dependent on the quality of historical weather records. As SWD is a cumulative index that is intended to seasonally reduce to zero during the cooler periods of the year, the index self-corrects in most years, except those leading into any periods of high fire susceptibility. A critical factor, too, is the estimate of evaporation rate. Estimates of moisture loss must be within 0.1 mm per day to ensure that potential cumulative evaporation is not grossly in error.

Temperature measurements fall within a 5% error threshold for most of the year, except during the coldest periods in winter. An automatic weather station may provide somewhat less accurate estimates of daily minimum and maximum temperature in winter compared to the more accurate values measured at a manned observation weather station. The reason for this is that the thermometers used at an automatic weather station are less precise (Table 4.5) and are also not maintained as often given their remote locations. For that reason, manned operating weather stations, like Canberra Airport, should be used instead of automatic weather stations because of the lower absolute and relative errors for most of weather variables (Table 4.5). Another factor is that there are usually gaps in automatic weather station records of minimum and maximum temperature that make it difficult to produce continuous records for daily soil water balance models.

Table 4.5 Range in absolute and relative errors for weather variables at manned observing and automatic weather stations

Weather factors		Relative errors			
Weather variable	**Mean or typical values**	**Manned observing weather station**		**Automatic weather station**	
		Absolute value	(%)	Absolute value	(%)
Surface irradiance (R_S) (MJ m^2 d^{-1})	25.7 (Jan)	0.9	3.5	NA	NA
	10.0 (Jul)	0.9	9	NA	NA
Rainfall (mm)	below 5	0.2	4-20	0.5	10-20
	5-10	0.2	2-4	0.5	10
	above 10	0.2	<2	0.5	<10
Maximum temperature (T_{MAX}) (°C)	25.5 (Jan)	0.2	0.07%	0.5	0.17%
	11.2 (Jul)	0.2	0.07%	0.5	0.18%
Minimum temperature (T_{MIN}) (°C)	13.0 (Jan)	0.2	0.07%	0.5	0.17%
	0.2 (Jul)	0.2	0.07%	0.5	0.18%
Relative humidity (%)	10	1	10	2	20
	70	1	1.7	2	3.4
Wind speed (km hr^{-1})	5	0.5	10	0.5	10
	30	0.5	2	0.5	2

Source: Adapted from Linacre (1992:33).

Notes: (1) The values of irradiance and maximum and minimum temperature (column 2) are based on mean Canberra Airport values for the period 1981 to 1991.
(2) The estimates for relative error in maximum and minimum temperature are based on temperatures in Kelvin (K).

Extremes of temperature and wind speed at the upper end of a potential fire spread index critically influence the potential for spread of fire. Relative humidity is low under extreme fire weather conditions, typically 5 to 10%, so relative error is likely to be high (10 and 20%). This has ramifications for estimation of fuel moisture content when this is low and for estimating fire spread and fire intensity (Rothermel, 1972; Cheney, 1981; Van Wagner, 1987; Trevitt, 1989). Fortunately, relative errors for both temperature and wind speed are likely to be lower at the high end of FWI. The adoption of cup anemometer technology, replacing the old Beaufort estimation of wind speed, in particular has improved records (Bessell, 2006). Bessell (2006) found that The Beaufort scale underestimated wind speed compared to those taken with electronic cup anemometers. This signals a need for adjustments to the older wind speed records taken with the Beaufort scale to make them consistent with the more recent wind speed records.

While relative and absolute errors in weather data are important, errors that are embedded in a model can produce biases in index values as well. These modelling errors result from the

formulation of empirical models to cover the range of landscape dryness or potential fire spread, rather than from errors associated with the weather data. For instance, the RSDI model is dependent on estimates of evaporation from soil and plants that are themselves dependent on the value of R_N, temperature and relative humidity (Penman, 1948; Mount, 1972; Fisher *et al.*, 2008). Not all the data are available for calculation of each of the above weather variables, particularly in the more remote parts of the study area. Proxy estimation of missing records of weather variables lowers the confidence in the final estimate of daily evaporation because of an unknown level of inaccuracy and/or bias. As an example, the daily soil water balance models are based on a cumulative soil water deficit being calculated from each day's evaporation values. A consistent bias in evaporation would result in a significant deviation from the true value of soil water deficit. The biased value would thus affect the period during which the threshold of fire susceptibility was exceeded during a fire season, and hence the degree to which the landscape was potentially exposed to large landscape fires (LLFs).

Errors in a potential fire spread index are influenced by the relationships between soil water deficit, fuel moisture and wind speed. A key issue is how well mathematical formulae model this relationship (see section 1.1 for discussion of type 1 or type 2 errors). The combined effect of the errors in measurement of fuel moisture and wind speed on FFDI has been studied by Trevitt (1989). The potential size of errors in estimating rate of spread was assessed using fuel moisture and wind speed in the FFDI (Noble *et al.*, 1980), assuming that the variables of fuel moisture and wind speed are largely independent of each other. The uncertainty of the estimate of rate of spread was found to increase with increase in wind speed and decrease in fuel moisture content. Thus errors associated with combinations of low fuel moisture and high wind speeds could lead to higher levels of uncertainty at the extreme end of the scale of a potential fire spread index. This uncertainty poses an issue for the accuracy of values of potential fire spread indices in the earlier part of the time series, prior to the installation of improved wind speed instrumentation in the mid 1990s. Prior to that, estimates of wind speed made using the Beaufort scale were more prone to possible human error.

4.2.3 Weather station data suitable for estimating medium and long-term indices of fire susceptibility

Weather stations with suitable weather records determining the indices of fire susceptibility must have continuous, consistent and complete records over the medium-term (50-70 yrs) and long-term (> 100 yrs) time scales. Continuity of records means having few, if any, gaps in the records. Consistency refers to consistent measurement of weather records without a major change to weather station conditions or method of recording, to limit possible bias in the estimate of a weather variable. Finally, accuracy of records refers to the records of each weather variable conforming to the accuracy standards of the World Meteorological Organisation (WMO) throughout the period of record (see Table 4.4).

The basic requirement for this study was to find suitable weather stations where analysis could be performed on two medium-term datasets of landscape dryness and potential fire spread and one long-term landscape dryness dataset. There was also a need to select the most representative weather station in each of the climatic zones to produce the respective fire susceptibility indices. An additional requirement was to locate additional weather stations either for filling gaps in the weather record or for validation of the indices.

The first step in locating suitable weather stations was to inspect in detail a set of weather variables collected at weather stations within and surrounding the study area. The two key variables in estimating landscape dryness are daily evaporation and precipitation (see Equation 1.1; Chapter 1). Given that the F-DSWBM requires only precipitation as an input variable to estimate an index of landscape dryness (Fowler, 1992; Fowler, 2002), the approach taken was to evaluate the length and completeness of precipitation records of weather stations that fell into the three climatic zones: sub-montane, montane and sub-alpine.

The evaluation of precipitation records was based on three criteria:

(1) length of records (greater than 50 years);

(2) completeness, based on the gaps in the precipitation records, from the start of records up to June 2007; and

(3) the overall percentage of complete records within the period of record defined in criterion (2) (had to exceed 97%).

The results of this evaluation are presented in Table 4.6.

In the sub-montane part of the study area (Cfa climate zone), four weather stations were found to be suitable for a medium-term record (47, 64, 69, and 72 years duration), and only two for a long-term one (117 and 136 years duration). For a medium-term study, Canberra Airport weather station was found to have the best overall data quality. For a long-term study, Queanbeyan weather station was found to have the longest continuous and consistently recorded set of precipitation records. Its overall data quality (97% of high quality records) was second to that at Gidleigh station near Bungendore. The advantage of both Canberra and Queanbeyan weather stations is that they fall in the centre of the sub-montane plains in close proximity to each other whereas the Gidleigh weather station lies on the eastern edge of the study area. The latter is however useful for filling short gaps in weather data in the Queanbeyan weather station record. As Canberra Airport is part of the Bureau of Meteorology's RCS network, it has the capability to support the two medium-term models of landscape dryness: RSDI and MSDI in the sub-montane climate zone (Cfa).

In the montane parts of the study area further to the west (Cfb climate zone), only four weather stations were found to have sufficient length and quality of record: Blundells Hill, Corin Dam, Fairlight Station, and Pierces Creek. Based on the set criteria, only the weather stations at Corin Dam and Fairlight Station possess the necessary length and quality of

precipitation records within the montane climate zone. The two other stations, at Blundells Hill and Pierces Creek, play an important role in filling in missing precipitation at: Corin Dam and Fairlight Station respectively. Of these latter two, the weather station at Corin Dam is the more suitable for estimating landscape dryness in the montane climate zone. It lies in the heart of the Cotter catchment and the Brindabella Ranges and is therefore a useful representative station for calculating a medium-term soil water deficit (SWD) in the montane climate zone.

In the sub-alpine climate zone (Csc), the data from the weather station at Kiandra, combined with that from Cabramurra manned operated and automatic weather stations, can be used to create a composite precipitation record for a long-term climate record. Like the Canberra Airport weather station, the weather records from the two Cabramurra stations contain data for key variables (T_{MAX}, T_{MIN}, DP_{1500} and RH_{1500}) needed to run the more data intensive MSDI and RSDI models. However, using a composite weather record is problematic because of some significant gaps in the weather record for DP_{1500} and RH_{1500}. In conclusion, a long-term SWD dataset estimated using the precipitation records from these weather stations might not be accurate or reliable enough for this study without further data evaluation.

Stations with data that can support a medium-term Potential Fire Spread Index (PFSI) for the three climatic regions also had to be identified. In addition to the precipitation data, the completeness, consistency, and accuracy of the weather variables recorded at 1500 hrs are critical for estimating the PFSI factor. A comparison of records from the three reference climate stations in the study area (Burrinjuck, Cabramurra, and Canberra Airport) showed that only the weather record at Canberra Airport had the completeness, consistency, and accuracy required to produce indices of landscape dryness and potential fire spread for the medium-term time scale (Table 4.7) from 1 July 1951 onwards. Between 1 March 1939 to 1 July 1951, the critical records of dewpoint and relative humidity are largely missing, the latter being a critical factor in the estimation of fine fuel moisture content used to derive either FFDI or FWI.

As for an index of potential fire spread, only one can be estimated for the sub-montane climate zone from the start of reliable and complete set of Canberra Airport weather records in 1951. Medium-term datasets are too short and incomplete for a medium-term PFSI in either the montane or sub-alpine climate zones (Cfb, Csc) using respectively either Corin Dam or Cabramurra weather station records.

Table 4.6 Precipitation weather station attributes in the study region

Gentilli Climatic region	Weather station	Station number	Elevation (m)	Start of continuous record	End of continuous record	Length of continuous record (yr)	High quality record (%)	Application in study
Cfa	Queanbeyan	70072	580	1 Jul 1871	30 Jun 2007	136	97.0	Long-term SWD time series
	Bungendore (Gidleigh)	70035	725	1 Jul 1886	30 Jun 2007	117	99.9	Filling small gaps in records in Queanbeyan time series
	Hall (Lochleigh)	70045	634	1 Jul 1903	30 Jun 2007	100	99.8	
	Canberra Airport	70014	578	1 Jul 1939	30 Jun 2007	64	99.9	Medium-term SWD time series
	Tharwa General Store	70083	595	1 July 1938	30 Jun 2007	69	75.9	
	Ainslie - Tyson Street	70000	585	1 Jul 1935	30 Jun 2007	72	98.1	
	Huntley	70093	580	1 Jul 1956	30 Jun 2007	47	98.9	
Cfb	Fairlight Station	70032	610	1 Jul 1884	31 Dec 2004	119	97.8	Precipitation record not that different from Canberra Airport as it lies on the boundary between the Cfa and Cfb climate zones
	Corin Dam	570947	962	1 Jul 1930	30 Jun 2007	77	93.0	Medium-term SWD series
	Pierces Creek	70070	585	1 Jul 1930	30 Jun 1991	61	100	Filling gaps in Corin Dam time series
	Blundells Hill	570955	1054	1 Jul 1963	30 Jun 2007	55	99.6	Filling gaps in Corin Dam time series

Table 4.6 continued

Gentilli Climatic region	Weather station	Station number	Elevation (m)	Start of continuous record	End of continuous record	Length of continuous record (yr)	High quality record (%)	Application in study
Csc	Cabramurra	72091	1475	1 Jul 1955	30 Apr 1999	44	99.7	Medium-term SWD, if combined with station 72161
	Cabramurra (AWS)	72161	1482	1 May 1999	30 Jun 2007	8	95.0	
	Kiandra	71010	1395	1 Jul 1909	30 Jun 1969	60	100	Long-term SWD, if combined with Cabramurra MOWS and AWS
	Yarrangobilly	72141	980	1 Jul 1977	30 Jun 2007	30	95.7	Filling gaps in weather records at Cabramurra manned operating weather station since 1999

Source: Internet database of weather stations (Bureau of Meteorology, 2006). The start of a continuous precipitation record was set to July 1st to coincide with a July-June year.

Notes: (1) Weather stations are manned operating weather stations unless otherwise specified as an Automatic Weather Station (AWS) in the first column.

(2) The grey shaded rows indicate weather stations central to the estimation of landscape dryness in each climate zone.

Table 4.7 Completeness of fire weather variables at Canberra Airport to produce a potential fire spread index

Time period	Weather variables	Start of continuous record	End of records	Length of record (days)	Number of missing records	Completeness of record	Comments
Daily	Precipitation to 9 am	1 Mar 1939	30 Jun 2007	24290	2	99.9	Complete set of records
Daily	Maximum temperature	1 Mar 1939	30 Jun 2007	24290	0	100	Complete set of records
Daily	Minimum temperature	1 Mar 1939	30 Jun 2007	24290	0	100	Complete set of records
0900,1500	Cloud cover	1 Mar 1939	30 Jun 2007	24290	487	97.5	Monthly blocks of data missing: Jan-Mar 1942; Sep-Dec 1942; Nov 1971-Feb 1972. Otherwise a small number of scattered records are missing since 1951
3 hourly	Cloud Cover	1 Mar 1939	30 Jun 1997	24290	307	98.4	Some 307 records are missing prior to April 1997. Thereafter, cloud cover is recorded less frequently but frequently enough to produce an average daily cloud cover
1500 hours	Temperature	1 Jul 1951	30 Jun 2007	19785	319	98.3	Monthly blocks of data are missing: Jan – Mar 1942; Oct –Dec 1942. Otherwise, 128 records are missing since July 1951
0900, 1500 hours	Dewpoint temperature	1 Mar 1939, 1 Jul 1951	30 Jun 2007	24290, 19785	4149, 129	79.0, 99.3	Complete block of data missing prior to July 1951. The 129 records missing since July 1951 include a monthly block of data: Nov 1971-Feb 1972
1500 hours	Relative humidity	1 Mar 1939, 1 Jul 1951	30 Jun 2007	24290, 19785	4047, 128	79.5, 99.3	Similar blocks of data missing as the DP1500 prior to July 1951
1500 hours	Wind speed	1 Jul 1951	30 Jun 2007	19785	339	98.2	Monthly blocks of data missing: Jan-Mar 1941; Nov-Dec 1942; Nov 1971-Feb 1972
1500 hours	Wind direction	1 Jul 1951	30 Jun 2007	19785	343	98.2	Same gaps in the weather records as WS_{1500}

Source: Canberra Airport weather records (Station number: 70014) 1 Mar 1939 to 30 August 2007 (Bureau of Meteorology, 2007b).

Notes: (1) The start of continuous complete records for most of the weather variables was July 1951, which aligns with the start of the fire season used in this study

(2) Grey shaded rows indicate significant blocks of missing records for that variable, particularly prior to 1951.

4.3 Compilation of consistent and complete weather datasets

Time series analysis and classification require consistent and complete weather datasets to model landscape dryness and fire spread potential.

The modelling framework (Figure 4.1) proposes that indices of fire susceptibility be modelled at three sites, one in each climate zone. However, based on the findings in section 4.2.3, only Canberra Airport has the requisite data to estimate all-wave net radiation, landscape dryness and potential fire spread indices for the sub-montane climate zone (Cfa). Similarly, only Queanbeyan weather station has the precipitation records to estimate long-term landscape dryness. For the montane climate zone (Cfb), Corin Dam contains reliable records of precipitation extending back to the mid 1930s. Using one or more of the methods described in the following sections, T_{MAX}, RH_{1500}, and R_N can be interpolated for Corin Dam from the data at Canberra Airport. Landscape dryness based on SWD can be estimated using any of the three proposed DSWBMs. Compilation of the weather datasets was therefore centred on: (1) Canberra Airport records, and (2) medium to long-term precipitation records at Corin Dam and Queanbeyan.

4.3.1 Filling gaps and creating proxy weather datasets

Linacre (1992) considers that there are four methods for filling gaps in records or creating proxy datasets for a given weather variable:

(1) climatological estimation — where the missing value is estimated from the average of values recorded at the same time in previous years;

(2) interpolation of missing records from mean monthly values in a year or monthly values for a number of years;

(3) parallel estimation — where a constant ratio or constant difference is derived from comparison of overlapping records from a nearby station; and

(4) proxy estimation — where the missing value is related to simultaneous values of related weather variables, using an empirical relationship.

Table 4.8 illustrates how parallel and proxy estimation will be used to fill missing records. The weather variables with the largest gaps are daily precipitation (P_{0900}) for Corin Dam and Cabramurra weather stations and relative humidity (RH_{1500}) records for weather stations at Cabramurra, Corin Dam, and Canberra Airport.

Large gaps in relative humidity (RH_{1500}) records at Cabramurra and Corin Dam preclude the use of the RSDI model at those stations especially since Canberra Airport is in a quite different climatic region. Canberra Airport records for precipitation (P_{0900}), temperature (T_{1500}),

and relative humidity (RH_{1500}) are nearly complete, requiring relatively small gaps in the records to be filled.

Table 4.8 Completeness of records of key weather variables with proposed method for estimating missing records

Fire susceptibility indicator	Weather station	Weather variable	Number (and percentage) of missing records	Method for estimating values of missing records
Landscape dryness (SWD)	Cabramurra	P_{0900}	2181 (9.9)	Parallel estimation of P_{0900} using Yarrangobilly weather station records from May 1999 to the present. Prior to that, parallel estimation is based on Kiandra weather station records
		T_{MIN}, T_{MAX}	436 (2.7)	Parallel estimation from either Kiandra or Tumbarumba weather station records
		RH_{1500}	1229 (95.1)	Proxy estimation based on T_{MAX} and DP_{0900} (~99.99% of records intact at Cabramurra weather station since 1962)
	Corin Dam	P_{0900}	2004 (7.0)	Parallel estimation using Pierces Creek weather station records prior to 1936 and infilling small gaps in data
		T_{MIN}, T_{MAX}	15885 (100)	Parallel estimation from either Cabramurra or Canberra Airport weather station records
		RH_{1500}	15885 (100)	Proxy estimation from records at either Cabramurra or Canberra Airport weather stations
	Canberra Airport	RH_{1500}	4175 (16.7)	Proxy estimation using T_{MAX} and T_{MIN} from Canberra Airport weather station records prior to 1 Jul 1951
Potential fire spread (FFDI, FWI)	Canberra Airport	T_{1500}	60 (1.3)	Proxy estimation using T_{MAX} from Canberra Airport weather station records prior to 1 Jul 1951
		RH_{1500}	4175 (16.7)	Proxy estimation using T_{MAX} and T_{MIN} from Canberra Airport weather station records prior to 1 July 1951
		WS_{1500}	339 (1.8)	Proxy estimation using Burrinjuck WS_{1500} records

Notes: (1) There was a gap in the weather record at Canberra Airport from November 1971 to February 1972, coinciding with the introduction of daylight saving in Australia. The missing records were filled using 1000 and 1600 hourly weather data, extracted from the Bureau of Meteorology's three-hourly weather record at Canberra Airport (Bureau of Meteorology, 2007c).

(2) Method of filling gaps in weather records is based on Linacre (1992).

4.3.2 Filling missing precipitation records

The parallel estimation method was used to fill major gaps in the Corin Dam and Cabramurra precipitation datasets shown in Table 4.8. Linear regression was based on matched monthly precipitation records of the target and the adjoining proxy station. Correlations are presented in Table 4.9.

Table 4.9 Correlation of monthly precipitation at different weather stations

Target weather station	Proxy weather station	Overlapping period	Slope	Correlation (R^2)
Cabramurra (MOWS)	Yarrangobilly	1 Feb 1978- 1 May 1999	1.37	0.71
Cabramurra (AWS)	Yarrangobilly	1 May 1999 – 30 Apr 2006	1.03	0.65
Corin Dam	Fairlight Station	1 Jul 1936 – 31 Dec 2004	1.06	0.69
Corin Dam	Pierces Creek	1 Jul 1936 – 31 May 1968	1.13	0.62

Note: The slope of the regression line is equivalent to the ratio of precipitation between the proxy and target station

There appears to have been a significant change in precipitation correlation between Yarrangobilly and Cabramurra since the installation of the AWS at Cabramurra. The new AWS site is within a kilometre of the previous manned operating weather station (Bureau of Meteorology, 2006). When comparing the records from the nearby Yarrangobilly rainfall station to those from the manned and automatic weather stations at Cabramurra, rainfall has decreased by 30% at Cabramurra relative to the Yarrangobilly weather station since the installation of the automatic weather station in 1999. This corresponds to the changeover from manual recording to an automatic tipping bucket rain gauge. The apparent discrepancy in precipitation at the Cabramurra automatic weather station might be explained by a loss of recorded precipitation due to ice and snow not being adequately recorded at the new Cabramurra pluviometer. As it stands, this finding reduces confidence in contemporary estimates of SWD at Cabramurra (Csc climate province).

An estimation of missing P_{0900} values at Corin Dam from Fairlight Station values can be made with reasonable confidence (R^2=0.69), and to a lesser degree from Pierces (R^2=0.62). Considerable gaps in the Corin Dam precipitation (P_{0900}) records were found to be in the early record, mainly between 1930 and 1936. However, since then there have been only small gaps in precipitation records. Therefore, the occasional small gap filled by a parallel estimation of precipitation from a nearby rainfall station should not significantly affect the values of SWD in a landscape dryness model for the montane ranges to the west of Canberra (Cfb climate province).

4.3.3 Construction of complete datasets for daily soil water balance models

It is important to have continuous and accurate datasets for the two indices of fire susceptibility: landscape dryness and potential fire spread. This section describes the process that was followed to create those datasets.

The modelling framework requires landscape dryness (SWD) to be modelled at two weather stations: Canberra Airport (Cfa climate zone) and Corin Dam in the upper Cotter River catchment (Cfb climate zone) (see Figure 4.1). The weather variables needed to model SWD using the MSDI are T_{MAX} and P_{0900}. A complete record for these two variables exists for Canberra Airport. However, daily maximum temperature (T_{MAX}) has only been recorded at Corin Dam since the 1990s. The absence of T_{MAX} records prior to then necessitates proxy estimation of T_{MAX}, using parallel estimation of T_{MAX} from Canberra Airport using a temperature correction factor.

The RSDI model requires the additional variables of T_{MIN} and RH_{1500} to model SWD at Corin Dam. The interpolation of both these variables is highly problematic for the following reasons. First, daily minimum temperature (T_{MIN}) varies considerably from one weather station to another, depending on local topography and climate regimes (Geerts, 2003). Minimum daily temperature (T_{MIN}) can be used to estimate RH_{1500}, together with T_{MAX}. However, this method is not entirely without error. The estimation of RH_{1500} can also be based on dewpoint temperatures recorded at Canberra Airport using either DP_{0900} or DP_{1500}. Yet again, the air moisture characteristics at Canberra Airport and in the upper Cotter River catchment can differ on a daily basis, leading to incorrect RH_{1500} values for the upper Cotter River catchment. However, this may be the only method of approximating the estimation of RH_{1500} in the absence of direct measurements at Corin Dam for the medium-term series from 1951 onwards.

Soil Water Deficit (SWD) can be estimated from the F-DSWBM model for both Canberra Airport and Corin Dam weather stations using daily mean potential evaporation based on the weather record at Canberra Airport. With all three DSWBMs, the complete precipitation record prepared for the Corin Dam weather station will be used (section 4.3.2). The Corin Dam record includes earlier precipitation records from Upper Cotter Hut, which is located 10 kilometres upstream at a similar elevation.

An attempt was made to interpolate the complete set of missing records of T_{MAX} and T_{MIN} at Corin Dam extending back as far as 1951, by adjusting the values of T_{MAX} and T_{MIN}, using the temperature correction value of -6.7^{o}C per 1000 m rise in elevation (Linacre, 1992). The results of the proxy estimation of T_{MAX} at Corin Dam from Canberra Airport and Cabramurra are presented in Figure 4.4 (a) and (b).

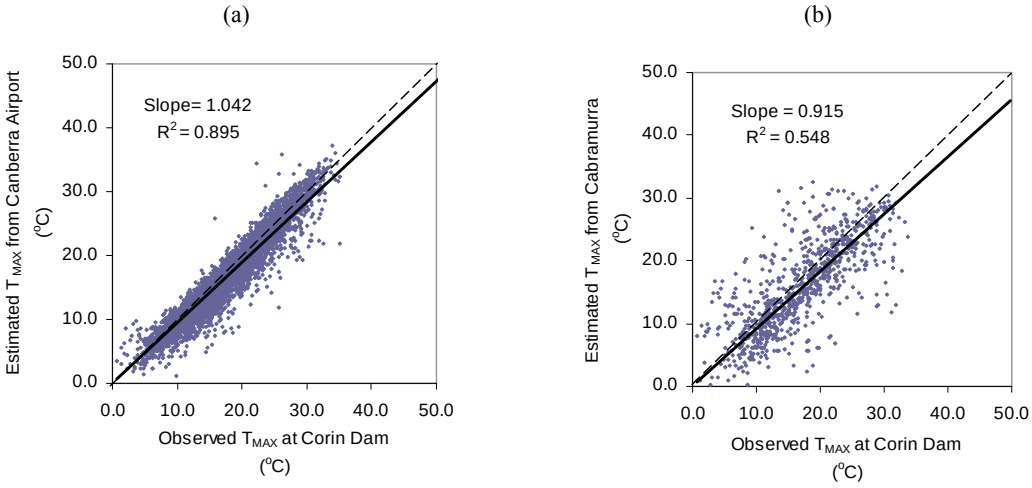

Figure 4.4 Estimation of T_{MAX} at Corin Dam, from (a) Canberra Airport and (b) Cabramurra records (18 August 1996 to 30 July 2008)

Source: T_{MAX} data between 18 August 1996 to 30 July 2008 is extracted from (Bureau of Meteorology, 2007b) and EcoWISE (2008).

Note: The solid line represents the results of the linear regression, while the dashed line represents a ''perfect-fit'' line.

The estimation of T_{MAX} at Corin Dam from Canberra Airport (Figure 4.4 (a) is more highly correlated with the observed T_{MAX} at Corin Dam than that at Cabramurra (Figure 4.4 (b). Given the high correlation (slope =1.042, R^2 = ~0.895) for estimating maximum temperatures at Corin Dam from Canberra Airport, it is possible to estimate T_{MAX} for a median elevation in the upper Cotter River catchment by adjusting the T_{MAX} records downwards by 4%.

The estimation of T_{MIN} at Corin Dam using T_{MIN} measured at Canberra Airport also is slightly less well correlated (slope=1.114, R^2 =0.846). The parallel estimation of T_{MIN} at Corin Dam is achieved by adjusting the records of T_{MIN} at Canberra Airport down by 11%. Therefore it is also possible to estimate T_{MIN} for a median elevation in the upper Cotter River catchment. Thus net long-wave radiation (L*), a key component of net radiation (Equation 3.9), can be estimated for the upper Cotter River catchment as both T_{MAX} and T_{MIN} can be estimated to a high degree of confidence given the very high R^2 (R^2>0.85).

Daily soil evaporation (E_S), based on the Fisher *et al.* (2008) model, uses minimum daily relative humidity, as well as T_{MAX} and T_{MIN}. In this study, minimum daily relative humidity is assumed the same as that recorded at 1500 hours (RH_{1500}). The relative humidity at 1500 hours (RH_{1500}) is estimated using the adjusted T_{MAX} for Corin Dam weather station and the DP_{0900} measured at Canberra Airport. The assumption made here is that the dewpoint temperature at Corin Dam is the same as that measured at Canberra Airport. The results of this parallel estimation of Corin Dam from Canberra Airport are presented in Figure 4.5 (b). While the results of the estimation of RH_{1500} are not quite as good as T_{MAX} and T_{MIN} (Slope=0.945,

R^2=0.652), they are satisfactory given that the Corin Dam weather station is located in a different climate province (Cfb) to that of Canberra Airport. The impact of the potential error in the estimate of RH_{1500} at Corin Dam is not quantifiable at this stage. This issue will be addressed later in Chapter 6 when the various DSWBMS are validated against other sources of data.

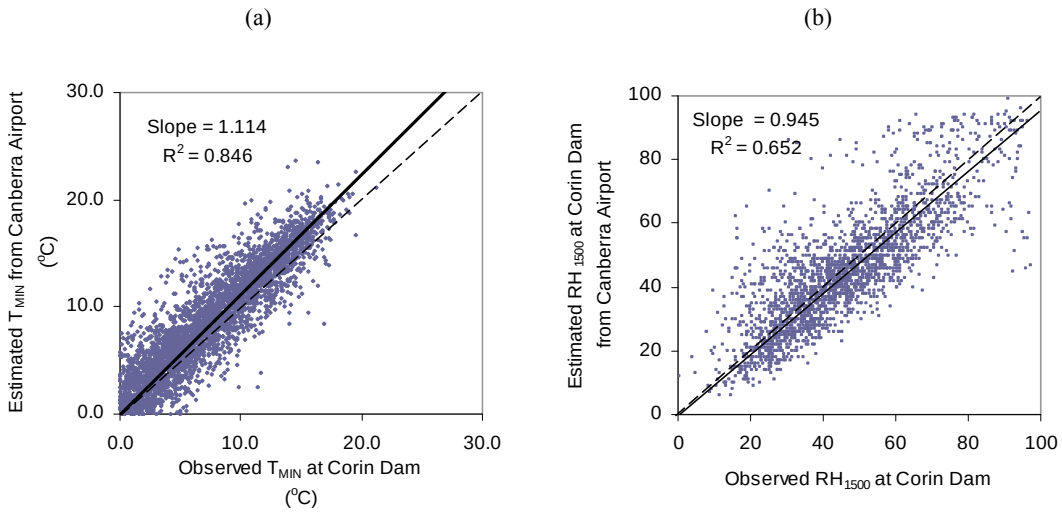

Figure 4.5 Estimation of (a) T_{MIN} and (b) RH_{1500} at Corin Dam, based on Canberra Airport records (18 August 1996 to 18 August 2002)

Source: T_{MIN} and RH_{1500} data recorded between 18 August 1996 and 18 August 2002 is extracted from Canberra Airport (Bureau of Meteorology, 2007b)and Corin Dam (EcoWISE (2008)).

Note: The solid line represents the results of the linear regression, while the dashed line represents a ''perfect-fit'' line.

The missing records for both weather stations were then estimated using the methods described above. This prepared the way for completing the weather datasets necessary for estimation of the three DSWBMs. A complete weather dataset was now ready for the estimation of the RSDI at two weather stations at Canberra Airport and Corin Dam, based on: (1) R_N and its input variables (Chapter 5), and (2) E_P and its derivatives (E_A, E_{T+S}, E_T, and E_S) (Chapter 6) as a precursor for the estimation of SWD.

4.3.4 Construction of complete datasets for potential fire spread indices

The estimation of fire spread potential using either the FFDI or FWI requires a complete weather dataset (P_{0900}, T_{1500}, RH_{1500}, WS_{1500} and WD_{1500}) to be based on Canberra Airport weather station records from 1951 to the present (Figure 4.3). As the weather records at Canberra Airport are 97-99% complete for these weather variables, filling the missing records is a small task based on the methods outlined below.

Since there is a very tight relationship between T_{1500} and T_{MAX}, given that maximum temperature is often reached by mid-afternoon on most days of the year, missing T_{1500} records can be easily estimated using linear regression (T_{1500} =0.951 T_{MAX} , R^2 = 0.969 see Figure 4.6).

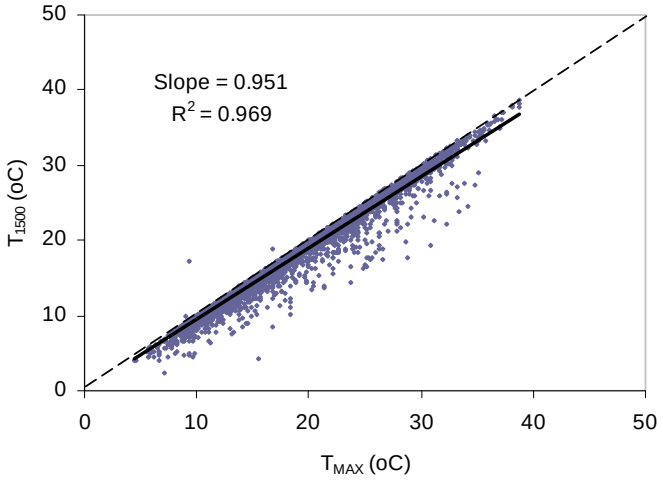

Figure 4.6 Relationship between T_{1500} and T_{MAX}

Source: Temperature data recorded at Canberra Airport weather station (1951- 2005).

Missing RH_{1500} records at Canberra Airport were filled using the following method. Where morning dewpoint (DP_{0900}) records were available, RH_{1500} was estimated from T_{MAX} and DP_{0900}, yielding the ratio of actual over saturated vapour pressure deficit (e_A/e_S). The value of e_A was estimated from Equation 4.1.

$$e_A = \exp(1.8096 + (17.269425 * DP_{0900})/(237.3 + DP_{0900})) \qquad \text{Equation 4.1}$$

where e_A is the actual vapour pressure in Hpa and DP_{0900} is the temperature at 0900 hours in Kelvin.

In the absence of DP_{0900} records, e_A was estimated from T_{MIN}.

The value of e_S was similarly estimated from Equation 4.1, substituting either T_{1500} or T_{1500} estimated from T_{MAX}, for DP_{0900}.

To estimate WS_{1500} or WD_{1500} for Canberra Airport, gaps in weather records were filled directly with wind speed records from another RCS station close to Canberra Airport, Burrunjuck station to the north-west of Canberra Airport. This station is about the same elevation and only 50 km in line with the dominant wind sector from the north-west. Given the small number of records missing at Canberra Airport, the possible error associated with a direct proxy without adjustment was considered minimal in the estimation of a PFSI model.

The above procedure resulted in a complete weather dataset being constructed for Canberra Airport and paves the way for deriving R_N and its input variables in the next chapter, as well as deriving E_P and its derivatives (E_A, E_{T+S}, E_T, and E_S) for landscape dryness models in

Chapter 6. Complete records of weather data needed to run the PFSI models of FFDI and FWI were similarly compiled.

4.4 Findings

This chapter has presented a modelling framework for the input weather data needed to estimate the key indices of fire susceptibility: landscape dryness and potential fire spread. The original plan to model R_N at three weather stations, each representative of a climate zone, had to be modified because continuous records of critical variables, such as RH_{1500} and C_{AV}, were not available in the Montane (Cfb) and Sub-alpine (Csc) climate zones. The only option therefore was to extrapolate the model of R_N at Canberra Airport to the upper Cotter River catchment. The validity of this approach is examined in the next chapter.

From section 4.1, it can be concluded that high quality weather data are only available from Canberra Airport to model R_N and E_P for the RSDI model. It is also presumed that this same R_N data can be used to model R_N and E_P for the Corin Dam site (upper Cotter River catchment) although L^* can be estimated because T_{MAX} and T_{MIN} at that site can be satisfactorily estimated from Canberra Airport records. The complete Corin dam precipitation dataset, together the modelled R_N from Canberra Airport, can then be used to estimate water runoff from the three daily soil water balance models for the upper Cotter River catchment (MSDI, RSDI, F-DSWBM). Daily complete stream flow records for the upper Cotter River catchment are available for the period 1964 - 2007. Modelled runoff can then be compared with measured runoff as part of the evaluation of these DSWBMs in Chapter 6.

A peculiar anomaly emerged in the P_{0900} data at Cabramurra after 1999, when the manned operating station was replaced with an automatic weather station. This casts doubt on the accuracy of the estimate of soil water deficit (SWD) made since that date. Given that there is no accurate or suitable method to correct this problem, the P_{0900} data there may contain some unquantifiable errors even if the records are adjusted using precipitation records from the nearby station of Yarrangobilly. The nearby station of Corin Dam has most of its precipitation records since 1936 intact so the proxy estimation of precipitation to fill missing precipitation records should not affect the analyses of landscape dryness that start from about 1964.

The weather dataset recorded at Canberra Airport has been almost complete since July 1951. Less than 2% of its records are missing in any one of the weather variables required to estimate either the FFDI or the FWI. It should therefore be more than adequate to derive accurate estimates of potential fire spread indices if the models themselves do not generate any major bias or inaccuracies in later analyses of the PFSI time series. The only variable likely to cause potential bias in estimates of either PFSI is that of wind speed because of the change from estimated to measured wind speed in the 1990s.

Even though the ideal modelling framework could not be fulfilled in all respects, the results and findings in this chapter have substantially addressed the fourth key research question posed in Section 1.3 (Table 1.1): 'As part of the ideal modelling framework for this study, what datasets for medium and long-term indices of landscape dryness and potential fire spread can be constructed for each of the three climate zones?'

The next chapter tests various empirical equations sourced from the literature than can be used to estimate the components of all-wave net radiation. After that, the validity of the estimates of daily all-wave net radiation for the sub-montane and montane climate zones are verified against other published studies (Cfa and Cfb).

Chapter 5: Derivation and Verification of All-wave Net Radiation

A number of studies (Monteith, 1965; Budyko, 1974; Roderick, 1999; Berry and Roderick, 2004; Berry *et al*., 2006) have pointed to the importance of net radiation (R_N) in governing key ecological landscape processes, notably transpiration, soil and plant respiration, photosynthesis and soil evaporation. This is nowhere better encapsulated than the observation of Priestly and Taylor (1972:90):'to encourage every meteorologist to accept net radiation into his or her daily thinking as one of the basic synoptic variables would be entirely appropriate in a modernized scientific approach to the subject.'

Chapter 3 outlined suitable models of soil evaporation and plant transpiration to replace the evapotranspiration term in the Mount Soil Dryness Index (MSDI), resulting in a new version — the all-wave net radiation version (RSDI). The pursuit of such evaporation models was driven by the fifth research question posed in Section 1.4 (Table 1.1): can all-wave net radiation (R_N) and its components be estimated to sufficient levels of accuracy as a precursor to estimating potential evaporation (E_P)?

The purpose of this chapter is to identify empirical models in the literature for estimating R_N with reasonable confidence. This is because there are no complete datasets for either surface irradiance or long-wave radiation components in the study region to fulfil the medium-term study requirements for an all-wave net radiation model of potential evaporation. Daily Surface irradiance has only been measured from 1991 to 1994 (Bureau of Meteorology, 2005) at Canberra Airport. Similarly, daily long-wave radiation has only been measured for a short period since January 2007 at Canberra Airport (RSBS, 2008).

The first part of the chapter outlines the methods and results employed to validate the input variables from which R_N is calculated, including surface irradiance (R_S), albedo (α) and net long wave radiation (L^*). The second part of the chapter relates the outputs of R_N and its components, based on the weather data recorded at Canberra Airport, with other comparable studies done in the ACT region, to evaluate whether the results of this study are in accord with those of previous studies.

5.1 Estimation of surface irradiance

This section is about testing the performance of empirical models that estimate R_S using equations that estimate R_S from R_A using formulae that mainly take into the effect of water vapour in the atmosphere.

The attenuation of R_A through the earth's atmosphere relates to the absorption properties of atmospheric gases across the solar radiation spectrum, in accordance with Beer's Law (Iqbal, 1983):

$$R_{S\lambda} = R_{A\lambda} \exp(-k_\lambda \mu)$$ Equation 5.1

where $R_{S\lambda}$ is the spectral irradiance for a given wavelength, $R_{A\lambda}$ is the incoming spectral top-of-atmosphere irradiance, k_λ is the radiation attenuation coefficient at a given wavelength, and μ is the optical path length.

Solar radiation is not absorbed evenly across the range of wavelengths between 0.3 and 3.0 μ m (Figure 5.1) due to the intermittent absorption of the principal atmospheric gas, water vapour, and, to a lesser extent, by other less strong absorption gases, such as ozone (O_3), oxygen (O_2) and carbon dioxide (CO_2) (Iqbal, 1983; Oke, 1987).

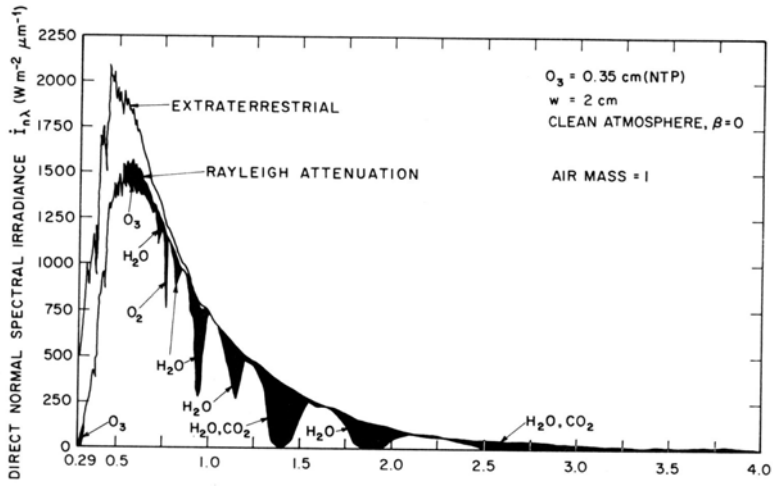

Figure 5.1 Attenuation of extra-terrestrial short wave radiation (0.1 and 3.1 μm) by ozone, carbon dioxide and water

Source: Iqbal (1983).

Note: The black areas under the curve represent attenuated short-wave radiation.

As well as the effect of the principal absorptive atmospheric gases, there are other transient influences such as dusts and aerosols in the atmosphere. The transmissivity of the atmosphere under cloud-free conditions can therefore be expressed as:

$$\tau_{CF} = \tau_O \times \tau_G \times \tau_W \times \tau_D$$ Linacre (1992) Equation 5.2

where τ_{CF} is the cloud-free transmittance combined attenuation coefficient from transmittance effects τ_O, τ_G, τ_W and τ_D due to ozone, atmospheric gases, water vapour. and dusts and aerosols, respectively.

R_S is then calculated:

$$R_S = R_A \times \tau_{CF} \qquad \text{(MJ m}^{-2}\text{ d}^{-1}\text{ or W m}^{-2}\text{)} \qquad \text{Equation 5.3}$$

Typical transmittance values for the contributing factors are: τ_O (0.98), τ_G (0.87-0.93), τ_W (0.85-0.91) and τ_D (0.93) (Linacre, 1992). Using Equation 5.2 gives a cloud-free transmittance value of 0.72. Essentially, the atmospheric ozone transmittance (τ_o) value is assumed to be constant since 1951, which constitutes the medium-term time series in this study. The atmospheric gas transmittance (τ_G) is a function of elevation and can be set as a constant at any given elevation (0.90 for Canberra) (Linacre, 1992).

The remaining factors in Equation 5.2, atmospheric water vapour transmittance (τ_W) and dust and aerosol atmospheric transmittance (τ_D) are time-dependent. Values of τ_w are determined by levels of water vapour in the lower atmosphere (Linacre, 1992; Winslow *et al.*, 2001). Atmospheric water vapour transmittance can be modelled using proxy variables for absorption and scattering of water vapour pressure: daily precipitation, relative humidity, minimum and maximum temperature (Liu and Scott, 2001; Winslow *et al.*, 2001).

Transmittance through dusts and aerosols (τ_D) varies with volcanic activity, dust storms, burning of vegetation and emission of industrial pollutants (Sturman and Tapper, 2006). Suspended material from these sources contains a complex mix of inorganic and organic compounds; volcanic, industrial, and mining sulphate particulates; carbonaceous particles from fires; mineral dust and organic compounds contributing to haze and smog. All of these can lead to temporary attenuation spiking of R_A. For example, volcanism can produce varying amounts of sulphur dioxide and ash that scatter and reflect back into space incoming shortwave radiation, leading to significant radiative cooling in the atmosphere and at the earth's surface for up to two years after an eruption (Sear *et al.*, 1987). Significant volcanic events in the last 50 years include Agung (1963), El Chichon (1982), and Pinatubo (1991). Over a 76 year period (1916-1992), volcanic eruptions at or near the equator have occurred at 5-15 year intervals. Thus, dusts and aerosols have a short-lived but an important effect on atmospheric transmissivity. Despite these variable influences and the remoteness of Australia from the main volcanic eruptions in the northern hemisphere, the value of τ_D for Canberra was left as a background constant (τ_D=0.93) because of the difficulty of modelling the effect of dust on τ_D through time.

A number of relationships for estimating surface irradiance (R_S) are discussed in the literature (Equations 5.10-5.18, Table 5.1). Most of these were sourced from Trnka *et al* (2005), which examined the efficacy of these equations in Central Europe. Only one equation, Equation 5.18, uses local Canberra Airport weather data to produce local coefficients. Equation 5.10 was omitted from further study due to the lack of high calibre sunshine hour records at Canberra Airport.

5.1.1 Evaluation method

In order to compare the performance of the empirical models, daily R_S data were extracted from the Bureau of Meteorology (BOM) records at Canberra Airport (Bureau of Meteorology, 2005). The most complete records available were for the period between January 1991 and December 1993. This data, together with other Bureau of Meteorology (2007b) records (Γ, rain-days R, where R=1, if P_{0900}>1 mm, else R=0), C_{AV}, T_{MAX}, T_{MIN} DP_{0900} and e_A) were compiled into a spreadsheet. Literature-based values for the coefficients for each of the empirical equations were employed.

For each of the attenuation equations, dates of the observed daily R_S data were carefully matched to the dates of the weather data. For missing daily R_S records, all estimated values from the empirical equations were set to null to exclude them from the performance tests. Surface irradiance (R_S) values were variously estimated employing Equation 5.13:

$$R_S = Eqn.formula \times R_A \qquad \text{Equation 5.4}$$

where $Eqn.formula$ corresponds to each of the nine empirical attenuation formulae under evaluation (Equations 5.10-5.18, Table 5.1).

5.1.2 Comparative performance of surface irradiance attenuation models

The models in Table 5.1 were evaluated using five performance criteria: (1) bias (BIAS), (2) root mean square error (RMSE), (3) mean absolute error (MAE), (4) percent mean relative error (PMRE) and (5) goodness of fit (R^2) between the estimated and the observed daily R_S. Equations for the first five performance criteria are given by:

$$BIAS = \frac{1}{n}\sum_{i=1}^{n}(y_i - x_i), \qquad \text{Equation 5.5}$$

$$RMSE = \sqrt{\frac{1}{n}\sum_{i=1}^{n}(y_i - x_i)^2}, \qquad \text{Equation 5.6}$$

$$MAE = \frac{100}{n}\sum_{i=1}^{n}\left|(y_i - x_i)\right|, \qquad \text{Equation 5.7}$$

$$PMRE = \frac{100}{n}\sum_{i=1}^{n}\left|\frac{(y_i - x_i)}{x_i}\right|, \text{ and} \qquad \text{Equation 5.8}$$

$$R^2 = 1 - \sum\left(y_{obs} - y_{pred}\right)^2 \Big/ \sum\left(y_{obs} - y_{mean}\right)^2 \qquad \text{Equation 5.9}$$

where n is the number of observations, x_i is an individual observed value, and y_i is an individual estimated value.

Table 5.1 Empirical models used to estimate surface irradiance on a daily basis

Equation Number	Surface irradiance relationships	Parameter notes	Source
Equation 5.10	$R_S = a_P + b_P\left(\frac{n}{\Gamma}\right)$	where n is sunshine hours (hr), Γ is the day length (hr). a_P and b_P are site-specific estimated coefficients	Prescott (1940)
Equation 5.11	$R_S = R_A\left(0.72 \times (1 - 0.75 \times \left(C_{AV}/8\right)^{3.4}\right)$	where C_{AV} is the fraction of the sky occupied by clouds, expressed in Oktas (eighths)	Reiff *et al.*(1984)
Equation 5.12	$R_S = R_A(0.85 - 0.047C_{AV})$	where C_{AV} is the fraction of the sky occupied by clouds, expressed in Oktas	Linacre (1992)
Equation 5.13	$R_S = R_A\left[a_S\sqrt{(T_{MAX} - T_{MIN})}\right] + b_S\left(\sqrt{(1 - C_{AV}/8)}\right)$	where a_S, b_S and c_S are estimated coefficients. C_{AV} is the average daily cloud cover, expressed in Oktas	Supit and Van Kappel (1998)
Equation 5.14	$R_S = R_A[\tau_{CF} D_W (1 - \beta e_S(T_{MIN})/e_S(T_{MAX}))]$	where τ_{CF} is the atmospheric transmittance defined by: τ_O the transmittance of clean dry air, τ_A the transmittance related to aerosols and ozone and τ_V the transmittance related to atmospheric water vapour. D_W is a day length correction factor and β is a site-specific correction factor (generally set to a value of 1.041, but equals 1.088 for Canberra)	Winslow *et al.*(2001)
Equation 5.15	$R_S = R_A a_B\left(1 - \exp(-b_B(T_{MAX} - T_{MIN})^{c_B}\right)$	where a_B, b_B and c_B are estimated coefficients from calibration and validation of the transmittance at a particular site	Bristow and Campbell (1984)
Equation 5.16	$R_S = R_A\sqrt{(T_{MAX} - T_{MIN})} + b_H$	where T_{MAX}-T_{MIN} is equivalent to the daily temperature range (DTR) and b_H is an estimated coefficient	Hargreaves *et al*. (1985)
Equation 5.17	$R_S = R_A\left[1 - \exp\left(-b_D f(T_{AVG})\Delta T^2 f(T_{MIN})\right)\right]$	where b_D is an estimated coefficient of Equation 2, $f(T_{AVG})$ and $f(T_{MIN})$ are functions of daily average and minimum temperatures	Donatelli and Campbell (1998)
Equation 5.18	$R_S = R_A a_L\left(1 - \exp(b_L DTR)^{c_L}\right)\left(1 + d_L R_{J-1} + eR_J + fR_{J+1} + G_L\right)$	where a_L, b_L, c_L, d_L, e_L, f_L and G_L are estimated site-specific coefficients calibrated to a particular weather station and where DTR=T_{MAX}-T_{MIN}	Liu and Scott (2001)

Finally, linear regression was used to test the co-linearity of estimated against observed R_S (Equation 5.19). Correlation coefficient (R^2) was produced as part of the linear regression.

$$y = ax + b \qquad \text{Equation 5.19}$$

where x is observed R_S, y is estimated R_S and a and b are calculated regression coefficients.

To assess the performance of the attenuation models, a table of summary statistics (Table 5.2) was compiled to determine which of the equations were best suited for the estimation of R_S.

The best correlations were obtained employing Equation 5.11 and 5.13 each having comparably low BIAS, RMSE, MAE, and PMRE. Equation 5.14 also performed well, especially when average daily DP_{0900}, instead of T_{MIN} values, were used to estimate actual vapour pressure. The remaining relationships had R^2 values less than 0.8. Equation 5.18 was comparable in performance to Equation 5.14 and has the advantage of not using DP_{0900} or T_{MIN}.

Table 5.2 Performance of surface irradiance (R_S) models

Relationship Equation	BIAS	RMSE	MAE	PMRE	Linear regression coefficients		
					a	b	R^2
Equation 5.11	-1.81	3.39	0.37	2.87	0.813	3.538	0.882
Equation 5.12	-1.37	3.80	1.44	3.75	0.735	5.946	0.828
Equation 5.13	-0.82	2.74	0.87	2.71	0.832	3.738	0.907
Equation 5.14	-0.44	3.95	0.55	3.61	0.976	1.008	0.834
Equation 5.15	0.44	3.86	2.92	25.52	0.71	5.460	0.783
Equation 5.16	0.96	3.93	2.93	26.67	0.731	5.639	0.783
Equation 5.17	-1.07	3.97	1.06	3.89	0.789	4.735	0.788
Equation 5.18	-0.36	3.49	0.61	3.45	0.747	4.988	0.834

Note: Units for BIAS, RMSE, MAE and PMRE are in MJ m^{-2} d^{-1}. The highest performing equations are shaded grey in the table.

To illustrate the scatter of points and the goodness of fit, the estimated and observed R_S were plotted onto a series of x-y graphs (Figure 5.2). The highest performing equations are shown (Equations 5.11, 5.12, 5.13, 5.14, 5.17, and 5.18).

(a) Equation 5.11 (Reiff *et al.*, 1984)

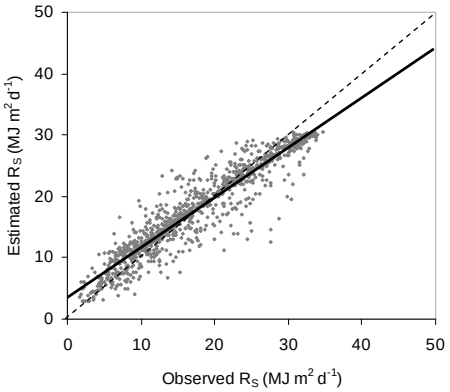

(b) Equation 5.12 (Linacre, 1992)

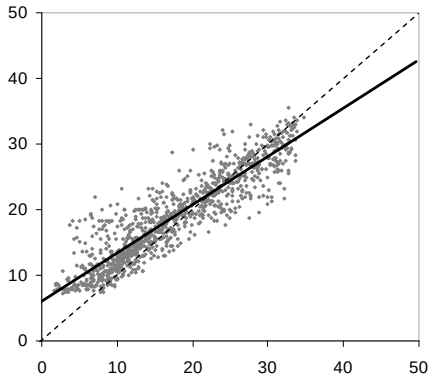

(c) Equation 5.13 (Supit and van Kappel, 1998)

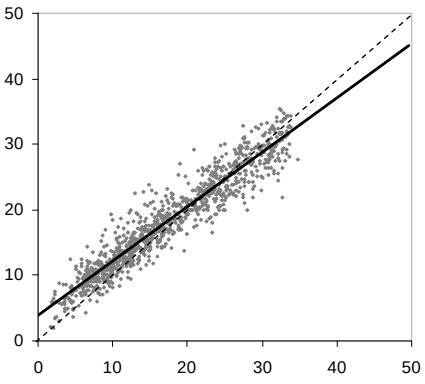

(d) Equation 5.14 (Winslow *et al.*, 2001)

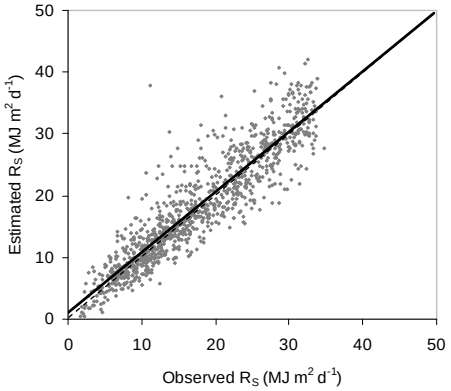

(e) Equation 5.17 (Donatelli and Campbell, 1998)

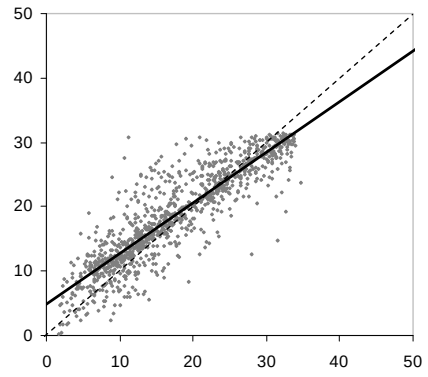

(f) Equation 5.18 (Liu and Scott, 2001)

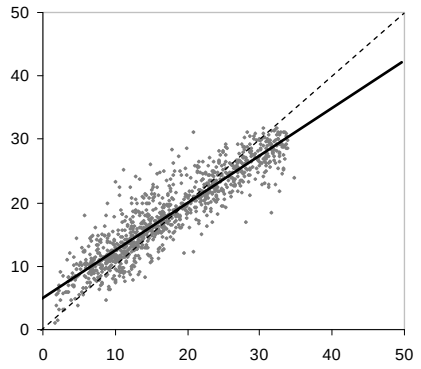

Figure 5.2 Performance of the six best relationships used to estimate surface irradiance

Note: The dotted line indicates a 1:1 relationship between the independent variable on the x-axis and the dependent variable on the y-axis.

Equations 5.11 and 5.13 exhibited the tightest scatter of points relative to the 1:1 line whereas Equations 5.12, 5.14, 5.17, 5.18 had a wider scatter with a greater number of outliers and achieved a lower R^2 less than 0.85. Increased scatter in these last four equations is because they employ a single variable to estimate τ_W, such as the daily temperature range, based on T_{MAX} and T_{MIN}, or daily cloud cover (Equations 5.13, 5.17); or the algorithms are not especially applicable to daily local atmospheric conditions (Equation 5.14). Less scatter was observed where a range of values and parameters (for example, daily temperature range, cloud cover, or rainfall events before, during and after a given day) was used to estimate τ_W.

Out of the three highest performing equations, Equation 5.13 was selected as the preferred equation for estimating R_S at Canberra Airport despite exhibiting a slightly positive and negative bias at low and high R_S values. Equation 5.13 showed the least bias of the three preferred R_S estimation equations but had a slightly wider scatter of points than Equation 5.11 but a narrower scatter than 5.18.

The ideal modelling framework requires the estimation of R_S and R_N at two weather stations, Canberra Airport and Cabramurra. However, continuous records of C_{AV}, TMAX and TMIN are not available at Cabramurra and thus preclude estimating of daily R_S values there or extrapolating them from there to the Corin Dam site in the upper Cotter River catchment.

Instead, daily R_S values can be inferred from Canberra Airport to the Corin Dam site. Data were obtained from EcoWISE Environmental Services (EcoWISE, 2008) for two nearby R_S recording stations, Googong and Corin Dam. A simple correlation between Canberra Airport records and those available for these stations yielded R^2 values of 0.834 and 0.732, and RMSEs of 39.7 and 52.9, respectively (Figure 5.3 (a) and (b)). R^2 values for R_S from 0.7 to 0.8 are considered adequate for this study given the high number of R_S observations at Googong and Corin Dam (4900, 3990) although the RMSEs between 30-50 W m^{-2} suggest that there can be a high error at times. Estimated R_S values at Googong and Corin Dam were correspondingly 12% lower and 6% higher on average than the observed values at these stations. A wide scatter of points with significant outliers was evident in both regressions, particularly at Corin Dam. This suggests that R_S values can be higher at Canberra Airport than at higher elevations in the Brindabella mountains to the west of Canberra where there can be more and denser cloud cover obscuring the land surface. Despite these potential limitations, the estimates of RS from Canberra Airport will be used to model R_S, and hence R_N at Corin Dam. The validity of this assumption will be tested further in section 6.4 by verifying the annual water balance in the upper Cotter River catchment using annual catchment runoff data.

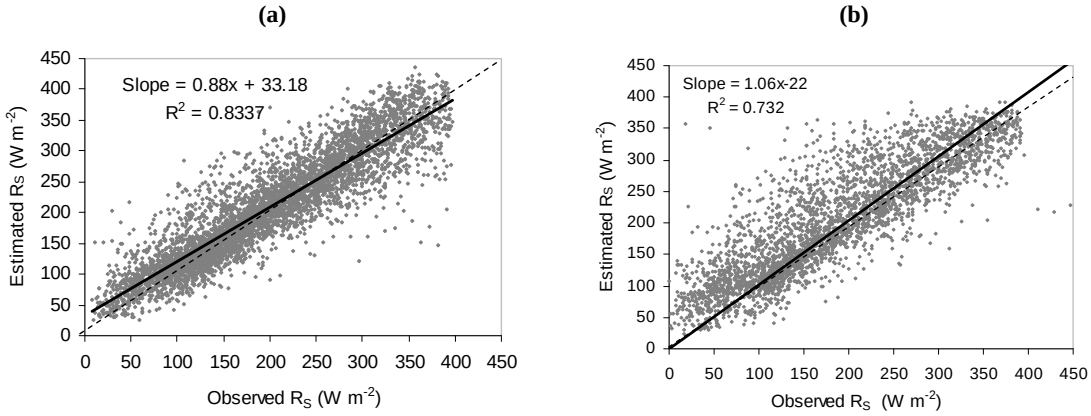

Figure 5.3 Comparison of estimated and observed surface irradiance (R_S) at (a) Googong and (b) Corin Dam in the upper Cotter River catchment

Note: The dotted line indicates a 1:1 relationship between the independent variable on the x-axis and the dependent variable on the y-axis.

Modelling R_S at nearby stations using the Canberra R_S model, indicates that Canberra Airport surface irradiance values can be extrapolated with reasonable levels of confidence to other nearby places including the surrounding sub-montane plains and hills, as well as to the montane and sub-alpine ranges in the western part of the study area. Cloud cover is estimated in Oktas at Canberra Airport, which includes estimation of cloud cover over the Brindabella Ranges and surrounding areas up to a radius of 50 km. Both weather stations at Googong Dam and Corin Dam lie well within that radius of Canberra Airport.

5.2 Estimation of surface albedo

The next factor to be determined in the estimation of R_N is the surface reflectivity of short-wave radiation at the earth's surface under clear skies, termed albedo (α). Measured clear-sky values for different vegetation and soils surfaces are presented in Table 5.3.

Table 5.3 Measured clear-sky albedo values

Coniferous forest	Broad-leaved forests, including rainforests	Grassland	Agricultural crop	Soils dry	Soils wet	Author (s)
0.10-0.18	0.13-0.18	0.16-0.28	0.15-0.24	0.08-0.19		Linacre (1992)
0.08-0.14						Stewart (1971)
0.11		0.24-0.27				Moore (1976)
0.08-0.10	0.15-0.20	0.16-0.26	0.18-0.24	0.05	0.40	Oke (1987)

Note: (1) The value obtained by Moore (1976) for pine forest was obtained in winter and spring in a one-year study.

Typical albedo values for forest vegetation range between 0.10 and 0.16; agricultural crops between 0.18 and 0.23 and dry soils and deserts between 0.37 and 0.45 (Gash and Shuttleworth, 1991).

The estimation of albedo is based on visible light (λ=0.2-0.7) (Equation 5.20) and for infra-red bands (λ=0.2-0.7) (Equation 5.21) based on published spectral reflectance data for vegetation and other surface covers (Berry and Roderick, 2004):

$$\alpha_{vis} = -0.27 * F_v + 0.31 \qquad \text{Equation 5.20}$$

where F_V is the fraction of photosynthetic radiation absorbed by the vegetation (FPAR). For a complete canopy of vegetation, F_V=0.95:

$$\alpha_{ir} = 0.40 + 0.05F_T - 0.21F_V \qquad \text{Equation 5.21}$$

where F_T is the fraction of turgor type plants as a proportion of the total TMS cover.

The proportional cover of T, M and S leaf functional types (See Chapter 3, section 3.3.3.1) was estimated for each of the principal vegetation types from personal field knowledge and experience in the study area (Table 5.4). The classification of vegetation types was based on Gellie (2005). They were also compared with the albedo values for grasslands, woodlands, and forests, obtained in Berry's (2002) study. The current study's values were found to be consistent with that study.

Values of α_{VIS} and α_{IR} are combined into a single α_{SW} using the estimates of the proportional cover of T, M, and S for each vegetation type:

$$\alpha_{sw} = 0.51\alpha_{vis} + 0.49\alpha_{ir} \qquad \text{Equation 5.22}$$

where α_{SW} is the estimated short-wave radiation albedo.

The ratios of 0.51 and 0.49 equate to the relative proportions of visible and infra-red radiation that are in the visible and infra-red bands of sunlight (Berry and Roderick, 2004).

Estimates for short-wave radiation albedo for forests and grassland (Table 5.4; values based on Equation 5.22) are internally consistent and reflect the values expected for these vegetation types.

Table 5.4 Proportions of leaf functional types and estimated albedo for the principal vegetation types in the study region

Vegetation Type	T	M	S	α_{VIS}	α_{IR}	α_{SW}
Temperate native grasslands	0.6	0	0.4	0.05	0.40	0.22
Southern Tablelands Yellow Box-Gum grassy woodland	0.3	0.5	0.2	0.05	0.27	0.16
Southern Tablelands sub-montane dry grassy forest	0.2	0.5	0.2	0.05	0.26	0.15
Southern Tablelands montane Mountain Gum grassy forest	0.3	0.6	0.1	0.05	0.27	0.16
Sub-alpine Ash shrubby forest	0.2	0.7	0.1	0.05	0.24	0.15

Note: The names for vegetation types in column are based on the descriptions for vegetation formations in Gellie (2005). Scientific names for plants are not included in those descriptions.
The TMS values were obtained using a best guess for each of the vegetation types.

As well as vegetation canopy albedos, the albedo of the forest floor is needed to estimate net soil surface radiation and hence evaporation at the soil surface (E_S). Silberstein *et al.* (2001) working in *Eucalyptus marginata* (Jarrah) forests in Western Australia, found a soil surface albedo of 0.29, and in the absence of other published estimates, this 'under canopy' value was adopted in the present research for estimating soil evaporation (E_S).

5.3 Estimation of downwelling long-wave radiation

Estimating and validating net long-wave radiation (L^*) (Equation 3.9) complete the estimation of R_N. The first term in the estimation of L^*, the upwelling component ($L_{\uparrow}$) is the product of the Stefan Boltzmann constant, air temperature (K) and the emissivity constant for a given vegetation surface given by Equation 3.10). Emissivity (ε) from forests is estimated to be between 0.97 and 0.98, whereas ε from grassland is estimated to be 0.90 and 0.95 (Stull, 2000).

The more significant term in Equation 3.9 is the downwelling component ($L_{\downarrow}$) affected by water vapour pressure, cloud cover of the atmosphere, and atmospheric gases such as carbon dioxide that contribute to an enhanced $L_{\downarrow}$. The estimation of $L_{\downarrow}$ uses one or more weather variables: the effective temperature of the overlying ambient air and the bulk emissivity of the column of air above the earth's surface (Iziomon *et al.*, 2003). A generalised equation for estimating downwelling radiation under clear-sky conditions (C_{AV}=0) takes the form:

$$L_{\downarrow(0)} = \varepsilon_0(T_A, e)\sigma {T_A}^4 \qquad (\text{W m}^{-2}) \qquad \text{Equation 5.23}$$

where ε_O is the effective emissivity of the atmosphere, T_A is the mean daily temperature, e_A is the mean daily vapour pressure respectively, and where either T_A or e_A can be used to estimate $L_{\downarrow}$.

Because depth and type of cloud cover affect $L_{\downarrow}$, the clear-sky formulas needs to accommodate a cloud cover factor. Iziomon *et al.* (2003) developed a simple formula (Equation 5.24) using just cloud cover (Equation 5.24) that can be applied to montane and sub-alpine environments.

$$L_{\downarrow} = \varepsilon_0(T_A, e)\sigma {T_A}^4 \times (1 + 0.005 {C_{AV}}^2) \qquad (\text{W m}^{-2}) \qquad \text{Equation 5.24}$$

where C_{AV} is the average cloud cover in Oktas

This is similar to the generalised equation formulated by Linacre (1992) except that he adopted a lower leading coefficient 0.0034 (in lieu of 0.005). With a formula that accommodates both clear sky and cloudy conditions, empirical formulas can now be tested using observed weather $L_{\downarrow}$ measurements.

5.3.1 Evaluation method

A number of ways to estimate atmospheric emissivity (ε_o) and hence $L_{\downarrow}$ under clear sky conditions can be found in the literature (Table 5.5). The simple formula (Equation 5.25) developed by Brunt (1932) takes account of mean near-surface daily vapour pressure. Swinbank (1963) developed an equation for downwelling long-wave radiation based on absolute ambient temperature (Equation 5.26). Idso and Jackson (1969) further refined

Swinbank's equation (Equation 5.27). Based on radiative transfer theory, Brutsaert (1975) devised a generalised model of clear sky transmissivity that took into account ambient temperature and average daily water vapour pressures (Equation 5.28). Idso (1981) developed a similar model using the same two variables (Equation 5.29). Prata (1996) questioned the theoretical basis of Equation 5.28 arguing that at low water vapour contents, $L_{\downarrow}$ did not tend to a constant because of the additional effects of greenhouse gases CO_2 and O_3 on $L_{\downarrow}$. Prata's (1996) formula developed a new formulation (Equation 5.30). Iziomon *et al.* (2003) went further and proposed a relationship Equation 5.31 that took account of the variability of air water vapour content at different elevations and is a further elaboration of Equation 5.28.

Measurements of downwelling radiation ($L_{\downarrow}$) were made at Canberra Airport for the period 24 January 2007 to 24 July 2008 using the Research School of Biological Sciences pyranometer, and were complemented by daily weather data records for the corresponding period. Mean daily vapour pressure (e_A) was estimated from DP_{0900} and ambient daily temperature based on the average of T_{MAX} and T_{MIN} for that day. Cloud cover (C_{AV}) was estimated by averaging three-hourly cloud cover data dating back to 1951.

Observed $L_{\downarrow}$ measurements, and calculated values of $L_{\downarrow}$ using each of the clear sky transmissivity formulas were entered into a long-wave calculation worksheet devised in this study, taking care to match weather data, derived weather variables and observed and estimated values of downwelling radiation ($L_{\downarrow}$) with the spreadsheet date field.

Summary statistics were prepared using the approach developed in section 5.1.1. The same performance criteria were adopted in the assessment of the best performing downwelling long wave radiation formula. The performance criteria in order again were: (1) bias (BIAS), (2) root mean square error (RMSE), (3) mean absolute error (MAE), (4) percent mean relative error (PMRE), and (5) goodness of fit (R^2) between the estimated and the observed daily values of R_S.

An initial evaluation of the empirical formulas outlined in Table 5.5 was completed first to exclude those formulas that did not meet the required performance standards for this study. The $L_{\downarrow}$ observations and estimates were filtered using a C_{AV} of less than 1.0 to make a straightforward comparison between observed clear sky measurements and those estimated using empirical equations.

The empirical models (Table 5.5) were then evaluated for cloudy sky conditions by multiplying the clear sky values of $L_{\downarrow}$ by the cloud effect factor implicit in Equation 5.24 and then comparing these findings back to the corresponding observed set of $L_{\downarrow}$ measurements. The same set of performance criteria was then reapplied to this data subset to determine the most applicable $L_{\downarrow}$ formula for cloudy sky conditions.

Table 5.5 Empirical models used to estimate daily downwelling long wave radiation

Equation Number	Equation formula	Comments	Authors
Equation 5.25	$\varepsilon_a = a + b\varepsilon^{1/2}$	where a and b are site-specific coefficients. Based on Sellers (1965) a=0.605 and b=0.048	Brunt (1932)
Equation 5.26	$\varepsilon_a = k \times T_a^{\,6}$	where T_A is the mean daily temperature (K)	Swinbank (1963)
Equation 5.27	For Ta >280K $\varepsilon_a = 1 - 0.261 \times \exp\left(-7.77 \times 10^{-4} \times (2.73.16 - T_a)\right)$	where T_A is the mean daily temperature (K)	Idso and Jackson (1969)
Equation 5.28	$\varepsilon_a = 1.24\left[\frac{e_a}{T_a}\right]^{1/7}$	where e_a is the mean daily water vapour pressure (HPa) and T_A is the mean daily temperature (K)	Brutsaert (1975)
Equation 5.29	$\varepsilon_a = 0.7 + 5.95 \times 10^{-5} \times e_a \exp(1500/T_a)$	where e_a is the mean daily water vapour pressure (HPa) and T_A is the mean daily temperature (K)	(Idso, 1981)
Equation 5.30	$\varepsilon_a = 1 - (1+\xi) \times \exp\left(-(1.2 + 3.0 \times \xi)^{1/2}\right)$	where ξ is an empirical constant which equals $46.5e_A/T_A$ for a typical scale water vapour height and lapse rate in the overlying atmosphere	(Prata, 1996)
Equation 5.31	$\varepsilon_a = 1 - X_S \times \exp\left(\frac{-Y_s \times e_a}{T_a}\right)$	where X_S is a site-specific calibration parameter, e_a is the mean daily water vapour pressure (HPa), T_A is the mean daily temperature (K)	Iziomon *et al.*(2003)

5.3.2 Comparative performance of downwelling long wave radiation models

The performance of the $L_{\downarrow}$ attenuation models was evaluated using the same five criteria as for the R_S models. Summary statistics were compiled to determine which of the empirical equations were best suited for the estimation of $L_{\downarrow}$ (Table 5.6).

Table 5.6 Summary statistics of clear sky transmissivity models

Equation	BIAS	RMSE	MAE	PMRE	Linear regression coefficients		
					a	b	R^2
Equation 5.25 (Brunt, 1932)	15.3	49.8	35.1	13.1	0.957	2.207	0.909
Equation 5.26 (Swinbank, 1963)	26.0	56.9	42.3	15.9	0.758	52.29	0.848
Equation 5.27 (Idso and Jackson, 1969)	34.0	61.1	46.8	17.7	0.759	46.16	0.854
Equation 5.28 (Brutsaert, 1975)	12.6	48.4	35.6	13.1	0.87	30.19	0.916
Equation 5.29 (Idso, 1981)	30.9	54.2	42.5	16.1	0.971	-17.0	0.909
Equation 5.30 (Prata, 1996)	20.6	49.6	37.2	14.0	0.952	-1.32	0.908
Equation 5.31 (Iziomon *et al*., 2003)	6.8	52.0	37.2	13.6	0.693	85.51	0.819

Note: Analysis is based on 48 clear sky observations made between 24 January 2007 and 24 July 2007 at the Canberra Airport when the daily C_{AV} was less than one Okta.

The best performing equations were Equation 5.25, Equation 5.28, and Equation 5.30 each having an R^2 value exceeding than 0.9 (grey shaded rows, Table 5.6). All had comparable RMSEs, MAEs and PMREs although Equation 5.25 and Equation 5.28 expressed less BIAS than Equation 5.30. Equation 5.25 was selected as the best performing equation under clear sky conditions.

When downwelling radiation was adjusted for cloud cover using Equation 5.24, all seven equations predicted levels close to observed $L_{\downarrow}$ (Table 5.7). As in the clear sky evaluation, Equations 5.25, 5.28, and 5.30 outperformed the other equations on most of the criteria.

The high root mean square errors (RMSEs) found in all the seven equations could be related to the high variability of e_A and to the quality of the cloud cover data, which does not take into account the amount, type and height of cloud cover. Other more detailed daily studies of $L_{\downarrow}$, using hourly e_A and cloud cover, achieve RMSEs closer to 15-30 W m^{-2} (Jimenez *et al.*, 1987; Duarte *et al*., 2006). It is unlikely that an RMSE below 15 W m^{-2} could be achieved with any of these simple $L_{\downarrow}$ formulas, given that effective emissivity of the atmosphere is only sampled near the surface and not in the various levels in the atmosphere.

Table 5.7 Summary statistics of cloudy sky transmissivity models

Equation	BIAS	RMSE	MAE	PMRE	Linear Regression		
					a	b	R^2
Equation 5.25 (Brunt, 1932)	-1.2	48.0	38.5	12.8	0.921	24.826	0.842
Equation 5.26 (Swinbank, 1963)	-7.2	54.6	44.5	14.6	0.811	50.109	0.737
Equation 5.27 (Idso and Jackson, 1969)	23.9	57.0	45.9	15.7	0.815	42.020	0.741
Equation 5.28 (Brutsaert, 1975)	7.6	50.8	40.9	13.7	0.8454	40.44	0.855
Equation 5.29 (Idso, 1981)	26.0	55.0	44.7	15.4	0.877	14.260	0.856
Equation 5.30 (Prata, 1996)	19.5	52.8	42.5	14.4	0.907	16.355	0.845
Equation 5.31 (Iziomon *et al.*, 2003)	-5.8	55.0	44.2	14.6	0.747	81.00	0.761

Note: Coefficients of 0.005 and 1.6, rather than 0.005 and 2 gave a better estimate of cloudy sky transmissivity in Equation 5.24.

To illustrate their performance graphically, the three best equations, Equation 5.25, Equation 5.28, and Equation 5.30 are shown side by side in clear sky and cloudy conditions (Figure 5.4).

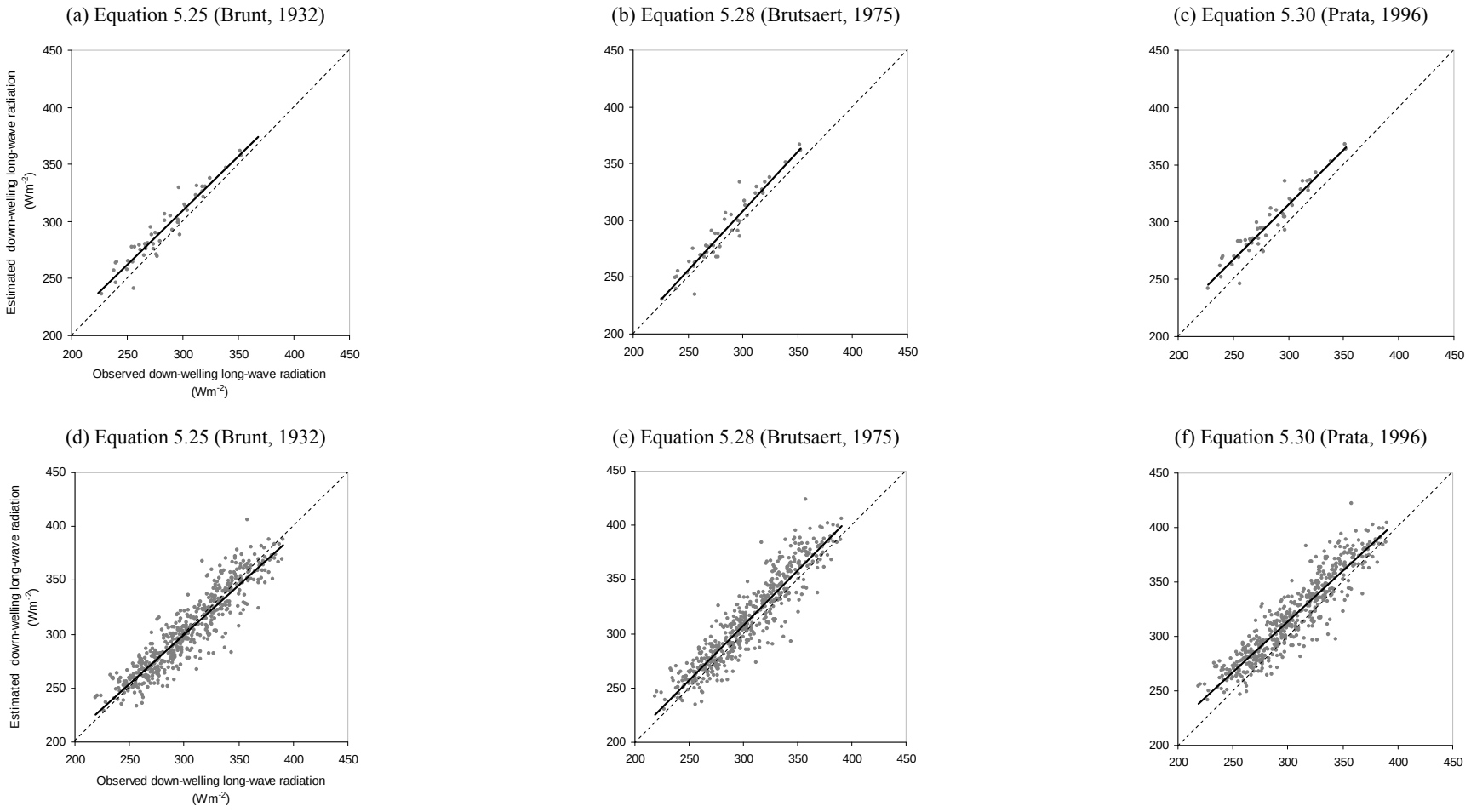

Figure 5.4 Performance of the three best downwelling radiation equations in clear skies (a), (b), and (c) and cloudy skies (d), (e), and (f)

Source: Observed daily $L_{\downarrow}$ data taken from the RSBS pyranometerr set up at Canberra Airport weather station between January 2007 and July 2008.

Note: The dotted line indicates a 1:1 relationship between the independent variable on the x-axis and the dependent variable on the y-axis.

The Brunt Equation (Equation 5.25) shows least bias under either clear or cloudy sky conditions. Equation 5.29 and Equation 5.30 show a slight positive bias throughout the range of $L_{\downarrow}$.

The Brunt formulation (Equation 5.25) was found to be the best performing equation for estimating $L_{\downarrow}$ as it worked well in both clear and cloudy sky conditions although it still has relatively high RMSE errors. This equation will be used to estimate $L_{\downarrow}$ at Canberra Airport and at Corin Dam in the upper River catchments since average daily cloud cover (C_{AV}) and daily average vapour pressure (eA) data measured at Canberra Airport can be used in the estimation of $L_{\downarrow}$.

5.4 Compilation and comparison of all-wave net radiation models

5.4.1 Method

The Supit-Van Kappel (Equation 5.8) and the Brunt (Equation 5.25) equations were found to be the best performing ones for estimating R_S and $L_{\downarrow}$. Along with the albedos estimated for forest types in the study area (Table 5.3), these equations were used to estimate all-wave net radiation for representative forest types at Canberra Airport and in the upper Cotter River catchment using Equation 3.9 (see section 3.2.2).

Because of the lack of suitable data to drive the R_S sub-model at Cabramurra or in the Upper Cotter River catchment, estimates of R_S at Canberra Airport are extrapolated to estimate R_N for the Upper Cotter River catchment.

A series of connected worksheets within an Excel workbook was set up to estimate R_N and its components, based on 65 years of Canberra Airport weather records. The values of R_N and its components were then tabulated and compared on a monthly basis within years with data obtained from other similarly based studies in the ACT region.

5.4.2 Comparative results: time series estimations of all-wave net radiation

Monthly values of the complete time series of R_N and its principal components, R_S and L^*, for Canberra airport are presented in Figure 5.5 to determine whether or not there were any major errors or disparities evident in the data from 1951 to 2007.

Values of R_N and R_S show a highly regular annual cycle with only minor variations evident in intra-annual variability driven by the sinusoidal changes in the values of extra terrestrial irradiance (R_A) over the annual cycle. In contrast, the values of L^* show much higher variability reflecting the continual daily variation in air vapour pressure and cloud cover.

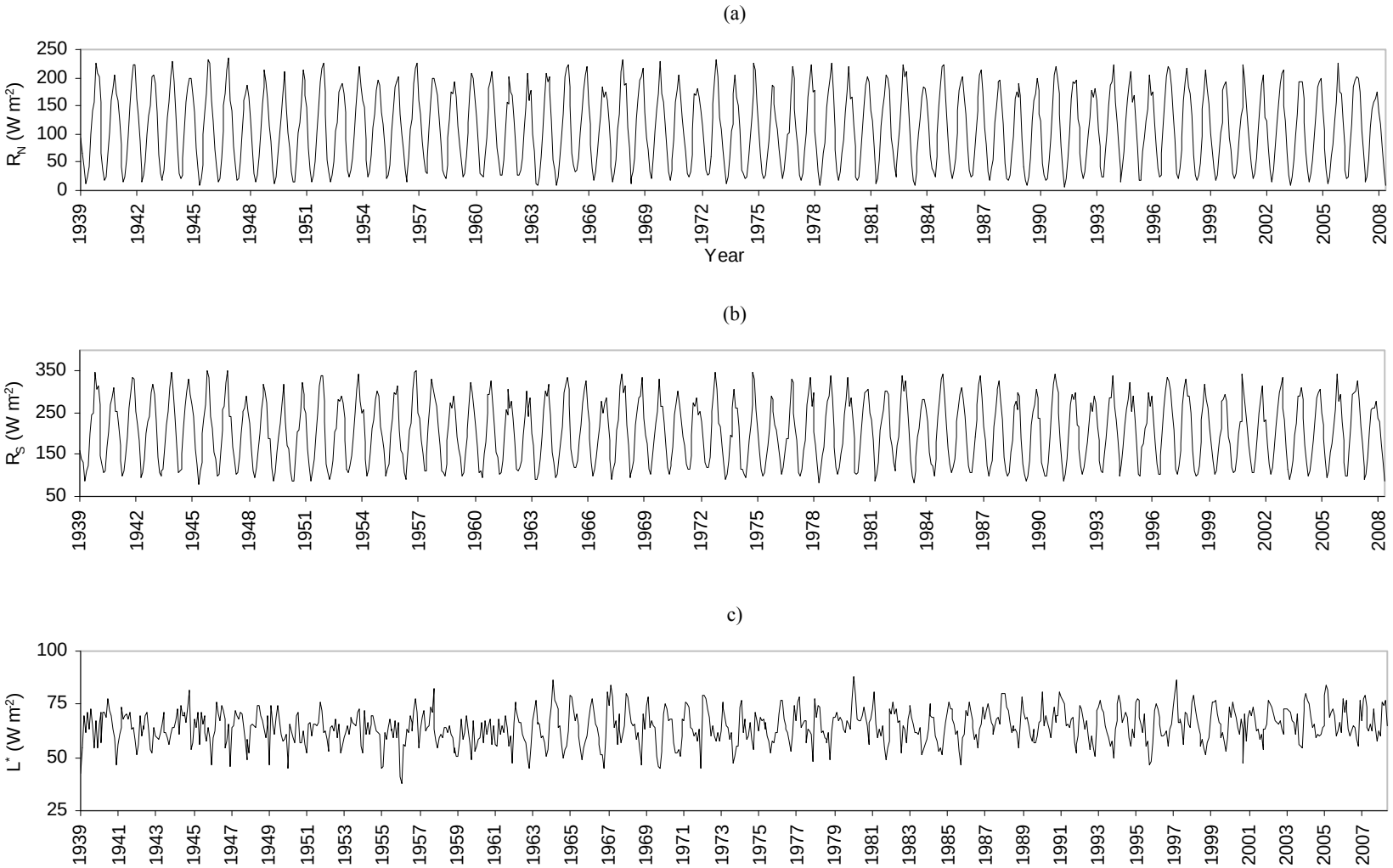

Figure 5.5 Summary of (a) R_N and its components (b) R_S and (c) L^* from weather data at Canberra Airport (1939-2007)

The results presented in Figure 5.4 (c) indicate the importance of estimating L^* accurately using the best available models and data available. From July 1951, L^* is estimated from three-hourly records of vapour pressure and cloud cover. Prior to 1 July 1951, L^* was estimated from mean daily vapour pressure using daily T_{MIN} and T_{MAX}, together with the same three-hourly of cloud cover data. Earlier estimations of L^* will therefore have greater errors and bias because of the coarser method used to estimate daily mean e_A. Indeed L^* values are highly variable prior to 1962 and appear to mask the sinusoidal pattern observed in the more contemporary record.

Comparisons were then made with results recorded from other studies on a monthly basis (Tables 5.9 and 5.10) for the two sites at Canberra Airport and Corin Dam in the upper Cotter River catchment. Predicted R_S at Canberra Airport summarised from 65 years of estimated daily R_S are in close agreement with that predicted by a study in the vicinity of Canberra undertaken by Paltridge and Proctor (1976), bearing in mind that the length of the studies are different. The values of monthly L^* were also relatively close in agreement. The values of L^*/R_S obtained from this study, however, do differ markedly from those calculated by Berry and Roderick (2004). Their approximation of L^* does not take into account the effects of daily variation in atmospheric water vapour pressure and cloud cover:

$$L^* \approx \sigma T_{MAX}{}^4 - \sigma T_{MIN}{}^4 \qquad (\text{W m}^{-2}) \qquad \text{Equation 5.32}$$

The present study findings are predicated on selecting the best empirical formula for estimating L^* under clear and cloudy skies (Brunt, 1932; Linacre, 1992; Iziomon, 2003). The greatest disparities between estimated L^* of this study and those from other studies were observed during the cooler months of the year.

The monthly mean values of R_N obtained for Canberra Airport in this study are comparable with those obtained by Paltridge (1975) for autumn, winter, and spring, but lower in summer. Paltridge' 1975 study was a comparably much shorter study than the current one, suggesting that the values in his study did not cover the full inter- and intra-annual variation in R_N values, as does this study.

In another radiation study, conducted in Bushrangers Creek in the middle Cotter River catchment by Moore *et al.* (1993), estimates of R_S for sloping surfaces were 5% lower than those found in the present study. Monthly estimates of L^* were also found to be very similar than those produced in Moore *et al.*'s study. Finally, he monthly estimates of R_N from this study are surprisingly comparable to those derived in the study by Moore *et al.* (Table 5.8).

Table 5.8 Estimated values of R_S, L^* and R_N (W m^{-2}) from this study and comparable studies at Canberra Airport

Month	R_A	R_S	R_S	R_S/R_A (%)	R_S/R_A (%)	L^*	L^*	L^*/R_S (%)	L^*/R_S (%)	R_N	R_N
	This study	Paltridge and Proctor (1976)	This study	Paltridge and Proctor (1976)	This study	This study	Paltridge (1975) see note 3	This study	(Berry and Roderick, 2004)	This study	Paltridge (1975)
Jan	501	305	306	61	61	61	36	20	15	196	224
Feb	450	268	266	59	59	59		22	16	168	
Mar	372	219	222	59	60	62		28	18	127	
Apr	284	164	175	58	61	65	79	40	21	79	70
May	214	116	128	54	60	65		56	26	39	
Jun	181	92	111	51	61	65		71	30	19	
Jul	194	100	118	52	61	67	75	67	27	26	25
Aug	250	133	145	53	58	69		52	22	54	
Sep	330	186	193	56	59	68		37	18	98	
Oct	415	238	231	57	56	65	62	27	16	139	135
Nov	481	283	272	59	57	63		22	14	176	
Dec	512	312	289	61	56	64		20	15	199	
Annual	**349**	**201**	**205**	**57**	**59**	**65**	**63**	**39**	**20**	**110**	**114**

Notes: (1) The estimations of R_N and its components are based on monthly averages of daily estimates (1939-2007).

(2) In the Paltridge (1975) study, the estimation of R_N and its components was presumably based on monthly averages taken over an unspecified number of years.

(3) Using Paltridge's data, L^* was based on an inversion of Equation 3.9, substituting L^* using the equation $L^* = L_{\uparrow} - L_{\downarrow}$ in Equation 3.9, and setting L^* as the dependent variable.

Table 5.9 Estimated values of R_S, L^* and R_N (W m^{-2}) from this study and published findings for the Cotter River catchment

Month	R_A	R_S	R_S	R_S	R_S (%)	L^*	L^*	L^*/R_S (%)	L^*/R_S (%)	R_N	R_N
	This study	Flat surface This study	Flat surface (Moore *et al.*, 1993)	Sloping surfaces (Moore et al., 1993)	Difference between this study and that of Moore (1993)	This study	Sloping surfaces (Moore *et al.*, 1993)	Flat surface This study	Sloping surface (Moore *et al.*, 1993)	This study	Sloping surfaces (Moore *et al.*, 1993)
Jan	501	297	311	292	5	61	53	21	17	187	195
Feb	450	263	252	238	25	66	44	25	17	154	158
Mar	372	215	215	205	10	70	51	33	23	112	123
Apr	284	159	143	138	21	70	45	44	28	67	72
May	214	109	106	103	6	68	49	62	42	30	39
Jun	181	85	101	98	-13	65	62	76	68	14	21
Jul	194	94	96	93	1	64	43	68	43	23	36
Aug	250	123	136	130	-7	62	48	50	36	53	63
Sep	330	172	185	176	-4	62	51	36	27	94	99
Oct	415	224	211	200	24	59	40	26	17	135	130
Nov	481	273	272	256	17	57	48	21	17	173	170
Dec	512	302	288	271	31	57	47	19	15	194	183
Annual	**349**	**193**	**193**	**183**	**10**	**63**	**48**	**33**	**29**	**103**	**107**

Notes: (1) The estimation of R_N and its components are based on monthly averages between 1962 and 2004.

(2) The period of records for estimation of R_N and its components from the Moore *et al.* (1993) study was not specified. The figures presented in their paper are presumed to correspond to the period of streamflow records (1968-1978) recorded in the Bushrangers Creek sub-catchment in the central western part of the Cotter River catchment. Their estimations of R_N and its components were based on monthly averaged climate data were obtained over a very short time span.

This is a good result given that R_N and its components are point-based rather than spatio-temporal. However, the monthly R_N values estimated from this study are 5-15% higher in late spring, early summer, and autumn than the values obtained for sloping surfaces in the study by Moore *et al*. However, the annual mean value of R_N estimated from this study is only slightly lower (3.7%) than that estimated by Moore *et al*. Because there are no on-site measurements of R_N in the upper Cotter River catchment, it is difficult to assess which of the two studies have produced the closest estimates to true monthly R_N values.

The comparison of R_N and its components from this study with the Canberra and middle Cotter studies, together other more recent R_S observations, confirms that the estimates of R_N and its principal components, R_S and $L_{\downarrow}$ can be used beyond the immediate weather station of Canberra Airport. Given that this study is a temporal study, the estimates of R_N are as accurate and reliable as the models of R_S and $L_{\downarrow}$ permit, employing the best available weather datasets. Figure 5.5 depicts how net radiation levels are relatively consistent in terms of the values of R_N, R_S and L^* over the full period of record since 1951, despite some anomalous L^* records between 1939 and 1964. In conclusion, the model of R_N can be used with some level of confidence to estimate $E_{\mathbf{P}}$ and its components, $E_{\mathbf{S}}$ and $E_{\mathbf{T}}$, to derive Soil Water Deficit (SWD) from the Soil Dryness Index (RSDI) model. This is also contingent upon other sub-models within the RSDI model not producing any substantial errors or biases, an issue that will be dealt with in the next chapter.

5.5 Findings in relation to estimation of all-wave net radiation

The results in section 5.1 clearly demonstrated that daily R_S, estimated from Canberra Airport weather station data and employing the best empirical equations, has a high R^2 (>90%), has minimal bias and has a low root mean square error. The best daily empirical estimates of R_S for Canberra Airport were obtained employing Equation 5.13 (Supit and van Kappel, 1998) especially where detailed cloud cover records exist. Since daily cloud cover data for the upper Cotter River catchment is not available, Equation 5.18 (Liu and Scott (2001) is the most appropriate model to estimate daily R_S for that area. However, the reliability of the estimate of daily R_S for the upper Cotter River catchment turned out to be fractionally lower than using the Supit van Kappel model to estimate daily R_S for Canberra Airport.

The results in section 5.2 demonstrated that values of surface albedo for the dominant vegetation types within the study area derived using equations described in Berry (2004) were closely comparable with those published in the literature. For the purposes of this study, the surface albedos estimated on an annual basis were considered adequate for estimating R_N even though surface albedos vary seasonally throughout the year. The values obtained for eucalypt forests and grasslands were consistent with published values for broad-leaved forests and grasslands.

In section 5.3, the Brunt equation was found to be the most accurate and reliable empirical equation for estimating daily $L_{\downarrow}$ for both clear and cloudy sky conditions, marginally outperforming the Brutseart and Prata $L_{\downarrow}$ formulas. However, the root mean square error associated with estimating daily $L_{\downarrow}$, employing the Brunt or any of the other equations, was still much higher than that associated with R_S, typically > 48 W m^{-2}. This is due to the highly variable nature of the vertical column of atmospheric water vapour during the day in the lower part of the atmosphere. The error may also be attributable to variable atmospheric amounts of dusts and aerosols in the atmosphere over time. The less than accurate estimation of daily $L_{\downarrow}$ can lead to variability in the estimate of R_N and hence E_P at any given location. The errors associated with estimating average cloud cover and e_A also contribute to errors in estimating $L_{\downarrow}$. Given the importance of $L_{\downarrow}$ in the estimation of R_N and E_P, the absence of data for reliably computing daily values restricts the potential application of the RSDI to weather stations near towns and cities, rather than to the more remote forested regions.

Finally, the comparisons of estimates of R_N and its components in section 5.4 indicate that they are broadly similar to estimates from published studies. Average monthly values of R_N are equivalent to, or slightly less than, those published, that is, for Canberra Airport (1.2% less) and in the upper Cotter River catchment (2.8% more). This is surprising given that the point-based values from this study do not take into account the variable shading effects of topography on R_N as the earlier spatio- temporal study of Moore *et al.*(1993) did. Estimation of all-wave net radiation (R_N) based on a montane or sub-alpine weather station in the upper Cotter River catchment would have been preferable, but a new automatic weather station has only been established at Mt Ginini in the last five years. However, it was recognised early in planning the modelling framework that the lack of medium-term weather data precluded that option. Values of R_N derived from Canberra Airport are used to estimate potential evaporation (E_P), soil evaporation (E_S) and plant transpiration (E_T) both for around Canberra and for the upper Cotter River catchment. The values of E_S, and $E_{T,}$, as well as E_A, obtained from the RSDI model, will be verified in Chapter 6 to ascertain whether or not the evaporation estimates are realistic and accurate, based on comparisons with other comparable field studies. Run-off data will also be used to see if the run-off obtained by the RSDI, MSDI, and Fowler daily soil water balance models model is in keeping with measured run-off.

The results and findings presented here therefore satisfactorily answer the fifth research question posed in the Introduction (Table 1.1): 'Can R_N and its components be estimated to sufficient levels of accuracy as a precursor to estimating potential evaporation (E_P)?'

Chapter 6: Calculation, Verification and Testing of Landscape Dryness Models

So far it has been shown that all-wave net radiation levels (R_N) can be estimated adequately for Canberra Airport (Cfa climate zone) and that these estimates can be extrapolated to the Canberra sub-montane plains and middle elevations of the upper Cotter River catchment in the Brindabella Ranges (Cfb climate zone). However, all-wave net radiation levels could not be estimated satisfactorily for the wetter and cooler Csc climate zone encompassing the high country of the north eastern extent of the Snowy Mountains and the higher peaks of the Brindabella Ranges because of the lack of suitable models and continuous weather data (see Chapter 4).

Estimation of R_N of Corin Dam in the upper Cotter River catchment (Cfb climate zone) can be extrapolated directly from Canberra Airport R_N records. Based on this extrapolation, soil water deficit (SWD) can now be estimated for all of the DSWBMs in the two climate zones outlined previously (Chapter 4). The soil water balance models (DSWBMs) are now tested against evaporation estimates from other studies and run-off measurements, the objective being to select those models that best simulate medium and long-term SWD.

The key objectives in this chapter are:

(1) to outline the methodology for estimating medium and long-term SWD from the Mount Soil Dryness (MSDI), the all-wave net radiation version of it (RSDI), and the Fowler daily soil water balance model (F-DSWBM);

(2) to compare the estimated values of the various evaporative components (E_S, E_T, E_{T+S}, E_I, and E_A) and modelled run-off with the findings of other studies in the region and elsewhere in Australia;

(3) to evaluate the trends in the SWD time series from the three DSWBMS; and lastly,

(4) to select the DSWBMS best suited to the analysis of the medium and long-term time SWD series.

6.1 Derivation of the landscape dryness time series

Methods used to produce landscape dryness (SWD) time series from each of the DSWBMs (MSDI, RSDI, and F-DSWBM) are outlined and the background parameters used to set up these DSWBMS are described. A spreadsheet was set up to calculate the SWD medium-term time series from the MSDI and RSDI models (see detailed EXCEL spreadsheets written to CD ROM in Appendix 2). The method of calculating the long-term SWD time series, based on the F-DSWBM, is documented by Fowler (1994; 2002).

6.1.1 Medium-term soil water deficit based on the MSDI model

A spreadsheet for the MSDI model was used to estimate daily SWD from T_{MAX} and P_{0900} for Canberra Airport (1939-2007) and for Cabramurra and the upper Cotter River catchment (1955-2007). Date, year, month, day, year-month and fire season temporal fields were incorporated into the spreadsheet to facilitate tracking of data and to summarise and manipulate fire season records.

The date and time fields, as well as the model input fields, were placed first in the spreadsheet. The algorithms for the MSDI were then placed in order after the date and time fields (Figure 6.1(a)). Algorithms are sequentially arrayed: starting with SWD at the start of the day (SDI_PM_1) transferred from the previous day, interception (E_I), flash run-off (Q_O), effective rainfall (P_{EFF}), soil capacity overflow(Q_T), evapotranspiration on a given day (E_{T+S}), and the SWD at the end of the day (SDI_PM_2). The algorithms correspond to those developed by Mount (1972) and outlined previously in section 3.1.

The key parameters for setting the level of interception and flash-run-off are based on a set of constant coefficients related to values of forest overstorey and understorey cover. A look-up table relates the values of forest overstorey and understorey cover to the Mount interception flash-run-off classes (Table 6.1). These cover values are based on those estimated for a dominant vegetation type close to the weather station or are estimated from an area-weighted set of canopy values representative of that catchment. The interception and flash run-off class is based on a dry sclerophyll forest type close to the weather station of Canberra and an area weighted overstorey and understorey cover in the case of the upper Cotter River catchment (Table 6.1). The values of intercepted water by evaporation and flash run-off are estimated from an interception and flash run-off class for that vegetation type and the amount of rainfall falling on a dry or a wet day. The details of these calculations are documented in Mount (1972).

Table 6.1 Representative vegetation cover at the locations surrounding the weather stations

Climate zone	Dominant vegetation types	Overstorey cover (%)	Understorey cover (%)	Mount interception and flash run-off class
Cfa - Sub-montane plains (Canberra Airport)	Lower montane dry sclerophyll forest	50	25-40	C
Cfb - Montane and sub-alpine upper Cotter River catchment (Corin Dam)	Sub-alpine grassy low forest, Alpine Ash tall forest, Higher montane sclerophyll forest, Montane Grassland	65	35-50	D

Note: The interception and run-off classes are based on Table 12 in Mount (1972:19). Vegetation cover is estimated in terms of percent canopy cover. Figures for the upper Cotter River catchment are based on a weighted area mean of the respective overstorey and understorey vegetation cover.

Evapotranspiration (E_{T+S}) is calculated from a lookup table based on the SWD at the start of the day and the T_{MAX} reached later on the same day. The daily T_{MAX} is adjusted for two periods of the year: between February and May T_{MAX} is adjusted downwards by 2°C but between July and January it is left unchanged. This is done because of the lag of the earth's temperature following warming in the second half of the calendar year (July – January) and cooling in the first part of the year (February-May) (Mount, 1980) which results in thermal hysteresis.

The soil water deficit (SWD) is calculated for each day using the variables depicted in Figure 6.1 (a); the value of SWD at the end of each day is transferred to the next row in the corresponding column for SWD at the start of the next day.

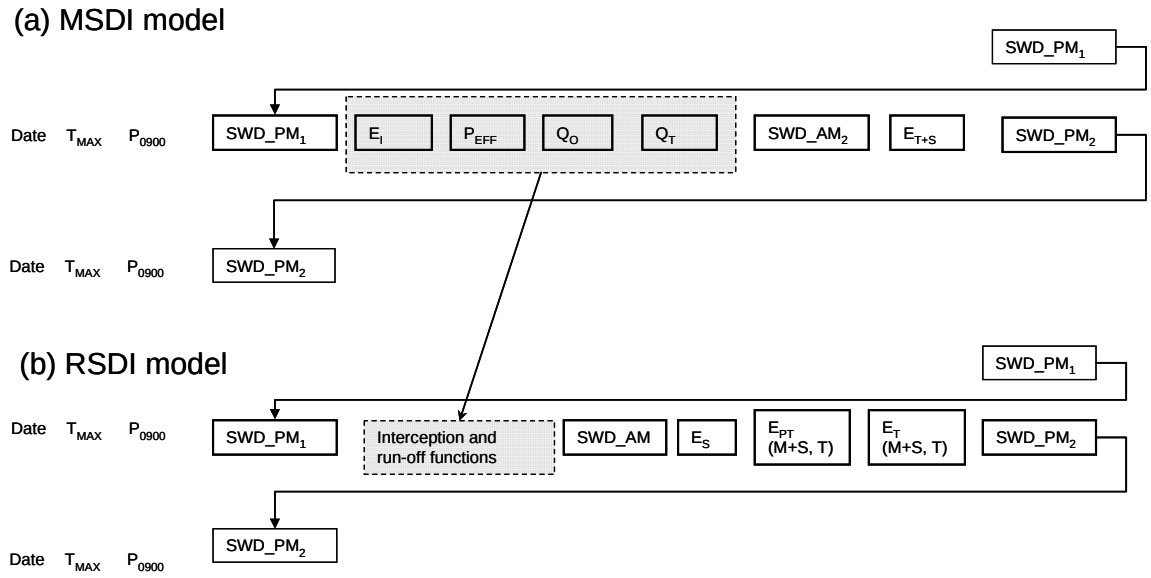

Figure 6.1 Daily calculation method in MSDI and RSDI spreadsheet

Note: The grey-shaded box in the above diagram refers to the combined processes of canopy interception (E_I), overland flow (Q_O) and the estimation of effective rainfall (P_{EFF}) and through-flow (Q_T). The algorithm used in the MSDI model is exactly the same as that used in the RSDI model.

6.1.2 Medium-term soil water deficit based on the RSDI model

Calculations of SWD from the RSDI is performed in the same spreadsheet as the MSDI model, with one exception: two separate algorithms for E_S and E_T replace the Mount E_{T+S} algorithm (see Figure 6.1 (b)). This enables SWD to be calculated for both the MSDI and the RSDI in one spreadsheet, reducing the possibility for errors. The spreadsheet used in these calculations is in Appendix 1 on the attached CD-ROM.

The additional parameters used in algorithms for E_S and E_T are shown in Table 6.2. In addition to the background interception and flash run-off parameters set in the MSDI model, the

Leaf Area Indices (LAIs) of the forest overstorey and understorey, as well as the proportion of projective foliage cover (PFC) of the TMS leaf types are needed as background vegetation parameters. Leaf Area Index (LAI) is defined as the one sided green leaf area per unit ground area (Anderson, 1981). The higher LAI and PFC values in the upper Cotter River catchment reflect the denser overstorey of the vegetation types in the catchment. Leuning *et al.* (2005) obtained an LAI value of 1.4 in Sub-alpine Ash Forest at Bago State Forest to the west of the study area. Higher leaf area index values, between 2.0 and 3.5, were obtained in moister Spotted Gum forest on the South Coast of New South Wales (Coops *et al.*, 1997). The value of LAI in the upper Cotter River Catchment was set to 1.6 and to 1.0 for dry sclerophyll forest near Canberra. The latter value corresponds to the mid-range of LAI values found by Anderson (1981) in drier Spotted Gum forest on the South Coast. At the soil surface, the LAI was adjusted upwards to take into account understorey shrub and grass cover. Values of LAI were difficult to estimate for representative vegetation in the two climate zones because of the paucity of studies measuring leaf area index for comparable Australian forests similar to those found in the study area and also because of the heterogeneity of vegetation, particularly in the montane and sub-alpine zones.

Table 6.2 Additional background parameters to be set in the RSDI model

Climate zone (Weather Station)	Dominant vegetation types	LAI of forest canopy	LAI of all forest layers	T PFC (%)	M PFC (%)	S PFC (%)
Sub-montane plains: Cfa (Canberra Airport)	Southern Tablelands dry sclerophyll forest	1.0	1.4	0.25	0.40	0.25
Montane and sub-alpine: Cfb (upper Cotter River catchment - Corin Dam)	Weighted average of vegetation types (see Table 6.1)	1.6	2.2	0.35	0.55	0.25

Note: The estimates of LAI at the canopy surface at either location represent iterative simulation values. These are close to those estimated in other studies in similar forest types within and adjacent to the study area (Anderson, 1981; Coops *et al*., 1997; Leuning *et al*., 2005).

6.1.3 Long-term soil water deficit based on the Fowler daily soil water balance model

The methods used to calibrate and derive a long-term soil water deficit from the inception of rainfall records at the Queanbeyan weather station are now described. A calibrated Fowler daily soil water balance model (F-DSWBM) is required to produce a long-term SWD time series for this study (See Table 4.1; section 4.1.1). The calibration relies on the soil water deficit estimated from the RSDI based on Canberra Airport precipitation records.

The Fowler daily soil water balance model (F-DSWBM) requires two simple inputs: mean daily evaporation (E_P) and rainfall (P_{0900}). Mean daily E_P was estimated from the Priestley-Taylor equation using the full length of record, that is, 1951-2007 (Figure 6.2). The Budyko estimate of mean daily evaporation is shown for comparison. Daily E_P calculated using the Priestley-Taylor equation is 0.3-0.5 mm lower than that estimated by the Budyko equation in the cooler months but becomes 0.5-0.7 mm higher for the January-February period. Estimates are comparable for November-December. The annual trend estimated from the Priestley-Taylor equation indicates a lower estimate of mean daily EP in winter and spring than that using the Budyko equation, amounting to a 0.2-0.5 mm per day difference. This would equate to slower evaporation rates being estimated in the F-DSWBM during these periods. This could result in slightly higher values of soil dryness in the lead up to the summer peak period in a fire season.

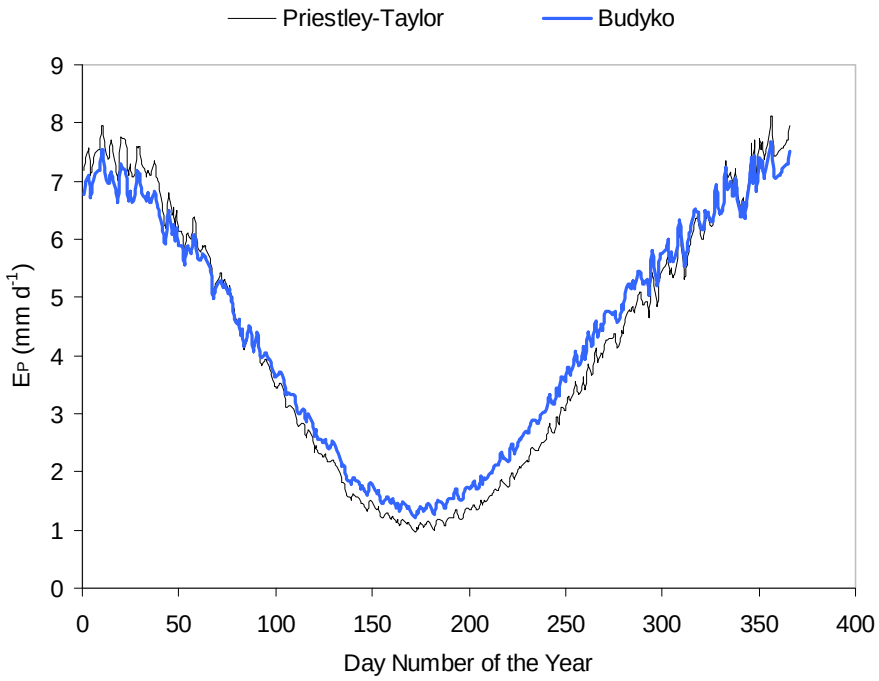

Figure 6.2 Mean daily E_P estimated using Budyko and Priestley-Taylor equations

Source: Daily E_P is estimated from the Priestley-Taylor equation (α=1.26) based on 56 years of BOM weather records at Canberra Airport (1951-2007). Daily E_P from The Budyko equation $E_P = \frac{R_N}{\lambda}$ is based on exactly the same records.

Given that the rainfall records at Canberra Airport only extend back to 1939, the nearby Queanbeyan rainfall station was used to extend the rainfall record in the sub-montane climate zone (Cfa) back to 1871. On a monthly basis, Queanbeyan weather station precipitation is well correlated with that of Canberra Airport (Slope=0.978, R^2=0.918) (Figure 6.3). Missing Queanbeyan rainfall records were estimated from neighbouring long-term rainfall stations of

Fairlight Station and Gidleigh using a parallel estimation method applied previously to other rainfall stations (see section 4.3.2).

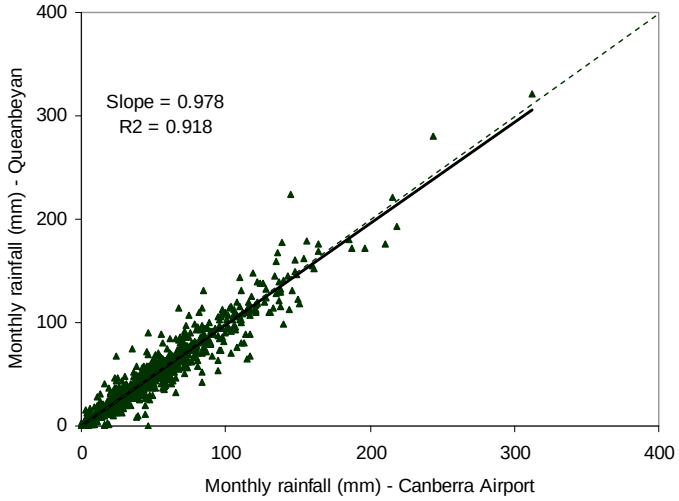

Figure 6.3 Correlation between monthly rainfall at Canberra Airport and Queanbeyan (1939-2007)

Source: Monthly rainfall data is derived from daily rainfall data recorded at the two weather stations (Bureau of Meteorology, 2007a)

Modelled soil water deficit (SWD) was first calculated from the Fowler daily soil water balance model for the sub-climate zone (Cfa) using Queanbeyan precipitation records and for the montane climate zone using Corin Dam precipitation records. Calibration of the two SWD datasets was conducted using the modelled estimates from the RSDI model using the same two weather stations (See Appendix 3).

In the case of Canberra Airport, the final version of the Fowler and the RSDI daily soil water balance models yielded comparable annual values for E_I and E_{T+S} between 1940 and 2007 (Figure 6.4 and Figure 6.5). For annual interception (E_I) losses, the relationship was relatively close lying close to the 1:1 line ($R^2 = 0.762$). Annual evapotranspiration (E_{T+S}) losses were similarly well correlated ($R^2 = 0.841$) with the greatest disparity in the annual values of E_{T+S} occurring in the wetter years.

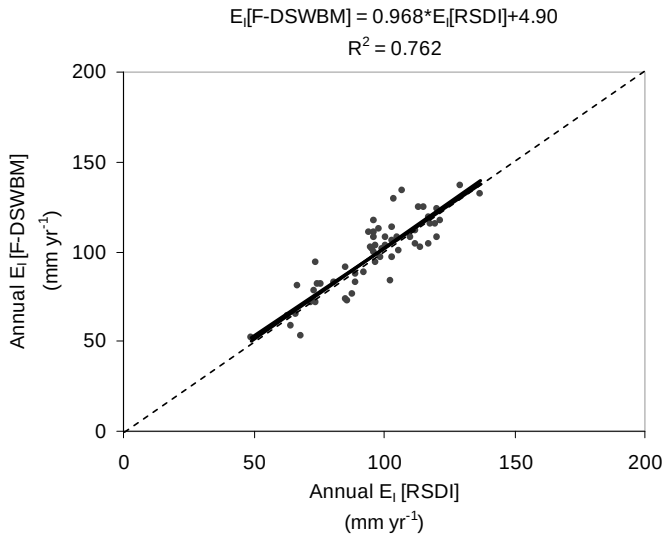

Figure 6.4 Correlation between annual canopy interception values from the SDI and F-DSWBM models (Canberra Airport - 1940 to 2007)

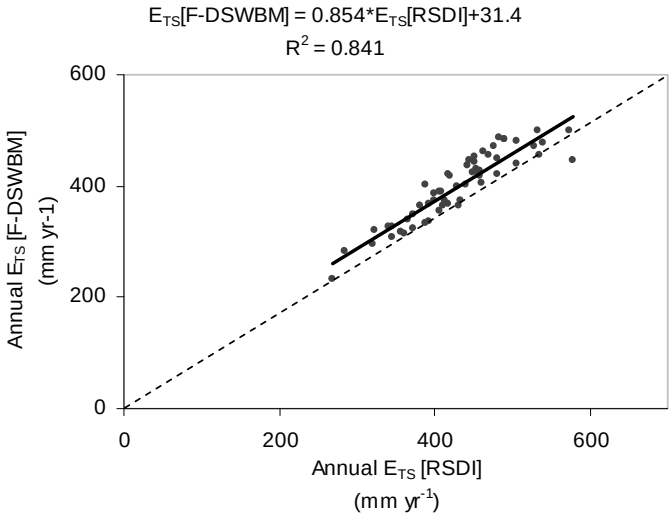

Figure 6.5 Correlation between evapotranspiration values from the RSDI and F-DSWBM models (Canberra Airport - 1940 to 2007)

Note: The values of evapotranspiration (E_{T+S}) estimated from the RSDI Model are based on the sum of the separate components, soil evaporation (E_s) and plant transpiration (E_T).

In the upper Cotter River catchment, the final version of the Fowler model produced comparable annual values for E_I and E_{T+S} between 1952 and 2007 (Figure 6.6 and Figure 6.7). For annual interception losses, the values of modelled E_I estimated from the F-DSWBM were 11% higher than those estimated from the RSDI model (R^2=0.846). The best fit achieved for annual evapotranspiration losses saw the E_{T+S} values from the F-DSWBM being overall 93% of those from the MSDI model (R^2=0.885).

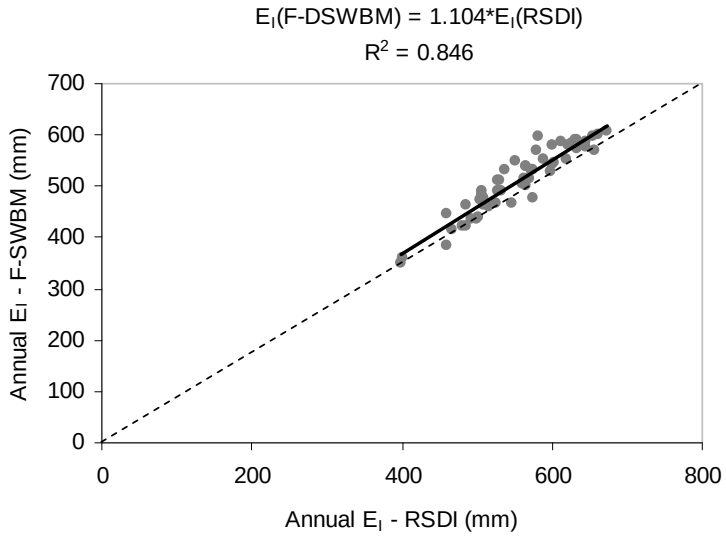

Figure 6.6 Correlation between annual canopy interception values from the SDI and F-DSWBM models (Corin Dam - 1952 to 2007)

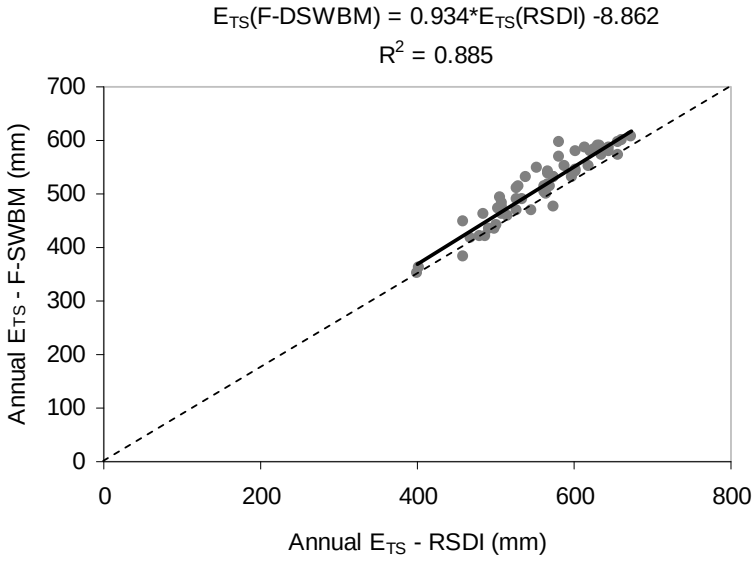

Figure 6.7 Correlation between evapotranspiration values from the RSDI and F-DSWBM models (Corin Dam - 1952 to 2007)

Having now completed the calibration of E_I and E_{TS} components of the F-DSWBM, based on two weather stations located in two separate climate zones, the long-term soil water deficit series for the sub-montane climate zone (Cfa) can be used with some confidence, recognising also the assumptions in the methodology up to this point. Some further verification of the E_I, E_{TS} and Q components of the F-DSWBM will still be conducted in section 6.4, before a final selection of daily soil water balance models is done in section 6.5 for later temporal analyses of landscape susceptibility to large fires in Chapters 8 and 9.

The next step is to check the validity of the estimates of actual evaporation (E_A) components of the RSDI (E_S and E_T) against comparable studies done in Australian forests.

6.2 Validity of the estimated values of evaporation components from the RSDI model

The question now arises as to whether the estimates of E_A and its components (E_S, E_T, E_{T+S}) are reasonably consistent and comparable with results from other studies. This is necessary to show that the RSDI model and input data yield valid estimates of SWD. A valid SWD will increase confidence in the results obtained by analysing and classifying the fire seasonal profiles of SWD (Chapters 8 and 9).

6.2.1 Validity of soil evaporation estimates

The validity of estimates of soil evaporative losses (E_S) produced by the RSDI model was verified by comparing the monthly and yearly values with those published in the literature for comparable climate and vegetation. Comparable estimates of E_S were obtained: by (1) Silberstein *et al.* (2001), in a short-term study of water and energy fluxes in dry sclerophyll Jarrah forests in Western Australia in October 1993 and March 1994; and (2) Vertessy *et al.* (2001), from a longer term water balance study of Mountain Ash forests in Victoria.

Annual and monthly estimates of soil evaporation (E_S) were summarised from daily E_S model estimates. The annual values of E_S for dry sclerophyll forest near Canberra Airport and for montane damp forest in the upper Cotter River catchment are shown in Figure 6.8.

Overall, annual soil evaporation (E_S) from dry sclerophyll forest near Canberra Airport was found to range from 74 to 197 mm per annum and average 125 mm per annum. For the upper Cotter River catchment, modelled loss was found to range between 79 and 165 mm per annum and average 118 mm. In both instances, annual E_S is estimated to be between 11 and 19% of the annual average rainfall, very slightly higher than that reported recently in other studies (Silberstein *et al.*, 2001; Vertessy *et al.*, 2001). Unlike these short-term studies, daily E_S in this study was estimated for 67 years (1940 to 2007).

Annual soil evaporation figures at the two weather station sites parallel each other over the times series. Higher annual values of E_S are found in the upper Cotter River catchment (annual average=130 mm a^{-1}) compared to those estimated for Canberra Airport (annual average = 105 mm a^{-1}), reflecting the higher rainfall under identical all-wave net radiation regimes (See section 5.4.2). The low annual values of E_S at both stations reflect the dry years (1944, 1957, 1967, 1982, 1985, 1997, 2002, and 2006) while the high values reflect moist individual or sequences of years (1956, early 1960s, early 1990s). Since 2000, there has been a noticeable decline in E_S and its year-to-year variability in annual E_S, which is comparable to that found in the early to mid 1940s.

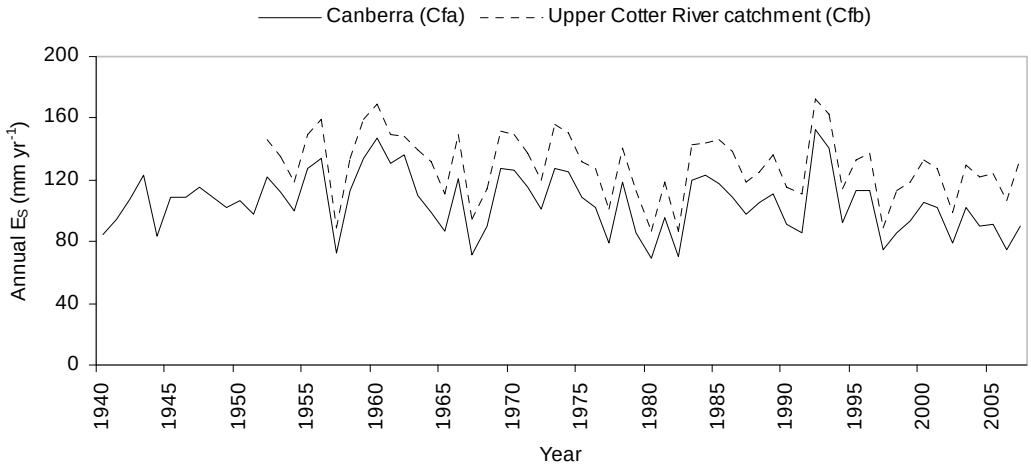

Figure 6.8 Annual soil evaporation estimated at the two weather stations (Canberra Airport, Corin Dam) representative of the two climate zones: Cfa and Cfb

Source: Modelled by RSDI daily soil water balance model using data from Canberra Airport and Corin dam in the upper Cotter River catchment.

Estimates of mean daily values of soil evaporation (E_S), for each month for forests adjacent to the weather stations for 67 years (1940-2007) are shown in Table 6.3. The table includes comparisons with soil evaporation observed in two other comparable studies. The lowest values of E_S were obtained in dry sclerophyll forest near Canberra airport with an annual mean of 0.29 mm d^{-1} with daily means ranging between 0.10 and 0.53 during the course of the year. These results are consistent with those found by Silberstein *et al.* (2001) who obtained values of 0.27 and 0.48 for the months of October 1993 and March 1994.

Average modelled annual evaporative losses from soil (E_S) of 0.35 mm d^{-1} in montane and sub-alpine forests in the upper Cotter River catchment over a period of 67 years (1951-2007) were similar to those from soils near Canberra Airport for the same period. The monthly range is wider in the upper Cotter River catchment, between 0.03 and 0.88, and with higher soil evaporation occurring in the moister spring months.

Both Figure 6.8 and Table 6.3 illustrate that there is not much difference between the values of E_S for the two sites in the Canberra region. This can be attributed to the fact that montane sub-alpine forests have a high leaf area index leading to less all-wave net radiation reaching the forest floor. This reduced all-wave net radiation compensates for the higher relative humidity regimes in the cooler environment found in the upper Cotter River catchment, and so lowers E_S. The more open conditions found in the dry sclerophyll forests around Canberra Airport enhance the potential for higher E_S but lower levels of surface soil moisture mean that soil losses are actually lower there.

On the Canberra plains and in the montane region to the west of Canberra, daily soil evaporation is highest in both dry and wet sclerophyll forests in spring. At this time, soil water availability is at its highest and net radiation levels (R_N) are in the moderate to high range. In contrast, the lowest mean daily E_S occurs in the winter months, when R_N is at its lowest. Soil moisture loss (E_S) rapidly falls off at both sites during summer despite the high daily R_N, reflecting drier soil conditions.

Table 6.3 Mean daily values of soil evaporation produced by the RSDI model compared with data from other studies

Forest Type	Dry sclerophyll forest near Canberra, ACT (585 m) This study	Jarrah forest in Western Australia Silberstein *et al.*, 2001	Upper Cotter River catchment forest (1250 m) This study	Old Mountain Ash forest in Victoria Vertessy *et al.*, 2001
Month	Soil evaporation ($mm\ d^{-1}$)			
Jan	0.27		0.18	
Feb	0.26		0.16	0.47
Mar	0.21	0.27	0.11	0.35
Apr	0.21		0.45	
May	0.11		0.33	0.15
Jun	0.10		0.03	
Jul	0.17		0.08	0.21
Aug	0.35		0.23	
Sep	0.43		0.77	
Oct	0.53	0.48	0.88	0.24
Nov	0.50		0.82	
Dec	0.31		0.21	
Annual average	**0.29**	**-**	**0.35**	**0.28**

Notes: (1) Mean daily E_S for Canberra Airport and the upper Cotter River catchment is estimated from Equation 3.17. Estimates of relative humidity for the Cotter River catchment are based on R_N and DP_{1500} values from Canberra Airport weather station records. The e_A values are derived by simply adjusting DP_{1500} using the dry adiabatic lapse rate of -6.7 ^{0}C per 1000 m: the estimation of relative humidity at the Corin Dam weather station from the relative humidity data recorded at Canberra Airport is reasonable (see section Figure 4.5, section 4.3.3).

(2) The daily E_S values are summarised for the period from 1951 to 2007 for both the Canberra and the upper Cotter River catchment localities.

(3) No other published comparable values for E_S could be found.

Annual average estimated values of E_S are comparable with those from at least two other short-term recent studies (Silberstein *et al.*, 2001; Vertessy *et al.*, 2001). These are not

contemporaneous studies with the present study so the comparisons are not strictly comparable. There are only two short-term measurements for the Jarrah forest study taken in the summer of 1993/94. The estimated values for dry sclerophyll forest near Canberra are similar to those measured in Silberstein *et al.*'s 2001 study for these two months. However, there are significant differences in monthly values estimated in this study for upper Cotter River catchment forest compared with those for the old Mountain Ash forest in Victoria. The differences are particularly evident in the October and February months. Annual soil moisture loss (E_S) is approximately 17% of modelled actual evaporation (E_A) in montane damp sclerophyll forests and 19% in dry sclerophyll forests in the study area. This initial comparison suggests that more on-ground studies of soil evaporation are required before one can be confident in the estimates obtained in this or other previous studies. In the absence of such studies, the derived values of E_S have sufficient integrity and accuracy for estimating E_S as part of total evaporative losses (E_A).

6.3 Validity of plant transpiration estimates

The other component in total evaporation is plant transpiration (E_T) estimated according to the methods outlined earlier (section 3.3.3). Estimates of transpiration losses (E_T sub-model) using the RSDI model are reviewed against the findings of a limited number of comparable studies in order to demonstrate that temporally-based estimates of E_T from the RSDI model are a good representation of transpiration losses for Canberra Airport and the upper Cotter River catchment. ET could not be modelled for the sub-alpine climate zone (Csc) (See 4.1.1) because of the lack of weather data and suitable models to estimate all-wave net radiation.

6.3.1 Comparison of annual and monthly values of plant transpiration

The E_T time series was computed using a pivot table within the RSDI spreadsheet for Canberra Airport and the upper Cotter River catchment and then plotted as a line graph (Figure 6.9). The inter-annual variation in E_T generally follows those of E_S (Figure 6.7) with maximum transpiration losses in wet years and less in the dry years. Annual E_T is minimal in the very dry years, 1944, 1957, 1982, 1994, and 2004.

Annual transpiration losses (E_T) for dry sclerophyll forests near Canberra Airport range between 153 to 441 mm and average 333 mm per annum. Transpiration in the upper Cotter River catchment is much higher at an average of 409 mm per annum with marginally less variability (299 and 488 mm per annum). High transpiration losses in the upper Cotter River catchment are explained by (1) a deeper regolith, with a significantly higher soil water holding capacity (AWC) supporting more productive montane forests, and (2) higher rainfall.

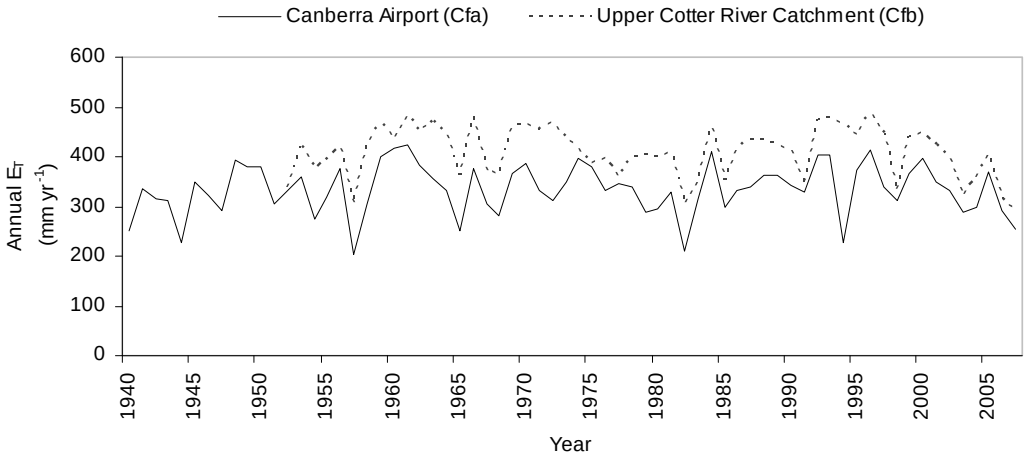

Figure 6.9 Estimates of annual plant transpiration in two climate zones, Cfa and Cfb

Notes: (1) Upper Cotter River catchment records from July 1951 to Jun 2008.

(2) The dash dotted line represents the mean annual E_T for Canberra Airport.

Table 6.4 illustrates the monthly E_T record. The Canberra Airport values of E_T range from 6 to 47 mm per month. The range is higher, between 12 to 63 mm per month in the cooler montane upper Cotter River catchment.

Table 6.4 Mean monthly values of plant transpiration calculated using the RSDI model at Canberra Airport and in the upper Cotter River catchment

	Monthly plant transpiration flux (mm)												
Site	**Jan**	**Feb**	**Mar**	**Apr**	**May**	**Jun**	**Jul**	**Aug**	**Sep**	**Oct**	**Nov**	**Dec**	**Average**
Canberra	45	34	28	18	10	6	10	21	33	45	50	51	**29**
Upper Cotter River catchment	55	44	37	25	17	12	15	23	37	52	59	63	**37**

Note: The values of mean monthly E_T were estimated from Canberra Airport data (1951-2007) and upper Cotter River catchment data (1962-2007).

To verify the modelled estimates of E_T produced by the RSDI model, a comparison was made of monthly transpiration flux data for the upper Cotter river catchment. The comparative dataset was derived from monthly gross primary productivity (GPP) data derived from remotely sensed bi-monthly MODIS data (Berry, 2007). The data for the upper Cotter River catchment was first extracted from a continental-wide time series (May 2001-July 2007). The extraction process used limited the GPP data to dry sclerophyll forests around Canberra Airport and to the watershed of the upper Cotter River catchment. The monthly GPP data were converted into monthly E_T data from an equation developed by Berry (2004), based on a simple water efficiency equation (Hari *et al.,* quoted in Berry, 2004).

The relationship is based on the annual CO_2 concentration in the atmosphere and its relationship to average water use efficiency at a CO_2 concentration of 360 μmol mol^{-1}:

$$E_T \approx \left(\frac{360}{[CO_2]} \right) \times 0.316 \times GPP \quad \text{(mm)} \qquad \text{Equation 6.1}$$

where GPP is the gross primary productivity (mol CO_2 m^{-2} a^{-1}, the constants 360 and 0.316 define the average plant water use efficiency at 360 μmol mol^{-1}, $[CO_2]$ is the average annual atmospheric carbon dioxide concentration (μmol mol^{-1}) measured at Cape Grim in Tasmania.

Comparison of estimates of monthly transpiration fluxes from dry sclerophyll forests near Canberra Airport between the two models is presented in Figure 6.10. Figure 6.10 (a) shows that the total monthly E_T calculated by the RSDI model shows greater variability than the MODIS estimates, with higher estimates of E_T in the warmer months and lower estimates of E_T in the cooler months. See also Figure 6.10 (b) which shows that, despite an apparent seasonal bias, the results nevertheless are reasonably correlated with those estimated by the MODIS study (R^2=0.624). The monthly average E_T calculated from both studies was close to 25 mm when averaged between May 2000 and November 2005.

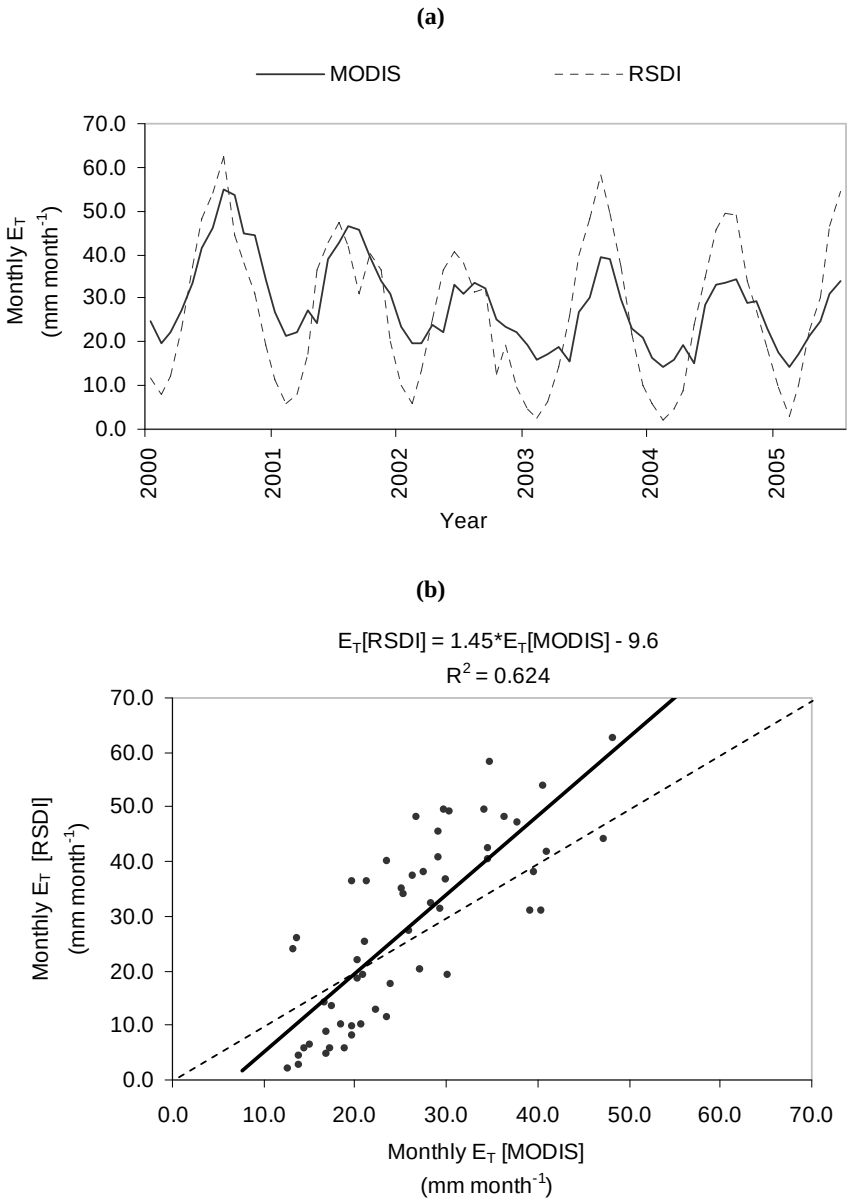

Figure 6.10 Comparison between estimated plant transpiration (E_T) from MODIS and RSDI models close to Canberra Airport: (a) serial trend and (b) correlation plot

Source: The MODIS ET data from Berry (2007) derived from MODIS data for the period May 2001 to November 2005. [CO2] data are from Earth System Research Laboratory (2007).

The results for transpiration for the upper Cotter River catchment derived using MODIS and the RSDI model are presented in Figure 6.11 (a) and (b). In the period prior to the January 2003 bushfires, the peak transpiration fluxes from the current study were 20 mm per month higher during the summer months than the MODIS data. In contrast, they were 10 mm per month lower during winter than the MODIS data. The high severity of the bushfires resulted in lower canopy cover values after the bushfires. The MODIS model takes into account reduced

canopy cover whereas the RSDI model does not. The MODIS model thus produced lower estimated monthly transpiration fluxes, by up to 20-25 mm per month.

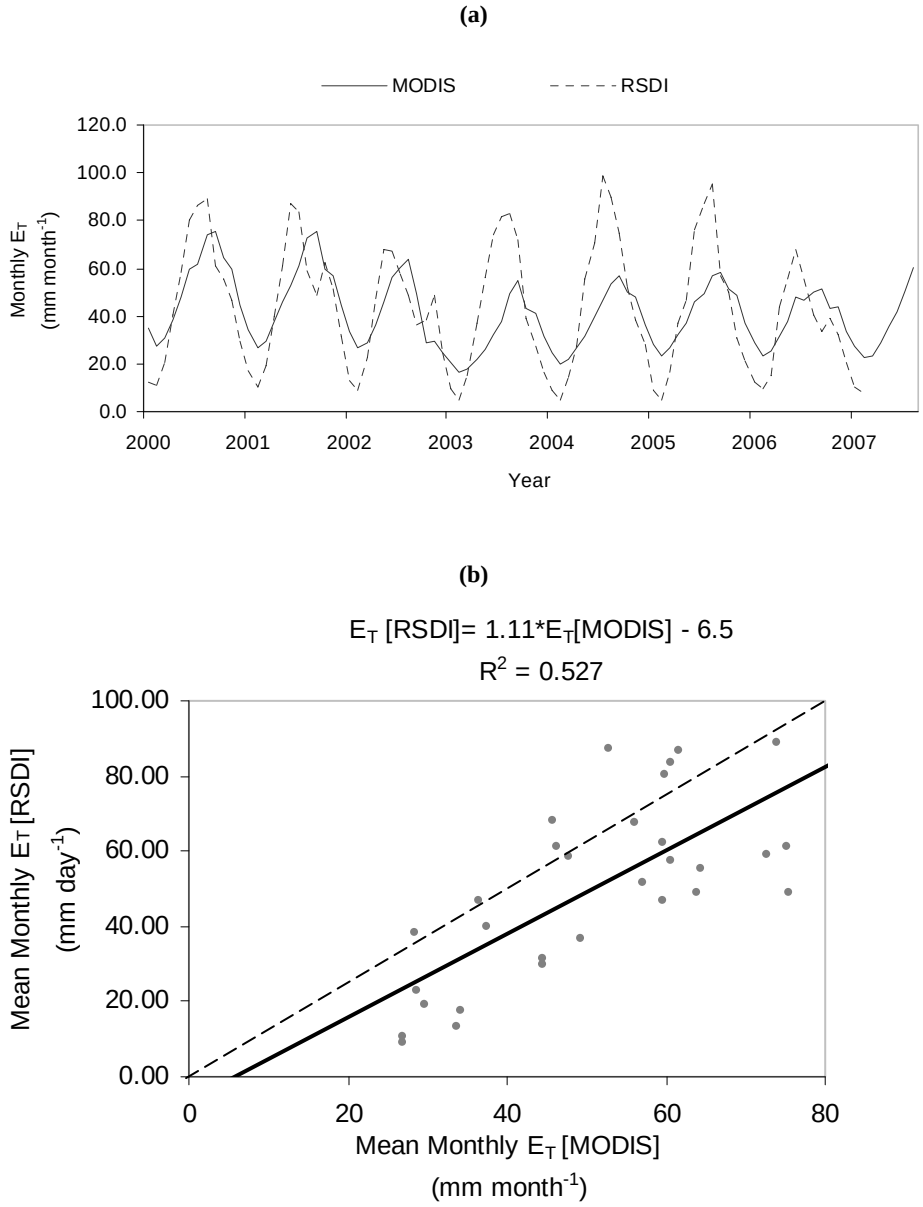

Figure 6.11 Comparison between plant transpiration from MODIS study and RSDI model, within the upper Cotter River catchment: (a) serial view and (b) correlation plot

Source: MODIS transpiration flux data from Berry (2007) derived from MODIS data (May 2001 to July 2007).

Note: The period of comparison is May 2000 to December 2002 in (b). Post January 2003 data were excluded to avoid the confounding effect of fire on vegetation transpiration after that date.

Figure 6.11 (b) shows that prior to the 2003 fire there is a moderately good correlation (R^2=0.527) between this study's estimates and those produced from the MODIS study of Berry (2007). However, the differences after the fires in part can be explained in part by the difference between time-scales used to derive the estimates in the two studies. The MODIS

study of Berry (2007) was based on monthly estimates of FPAR and GPP, which are derived from bi-monthly MODIS images across the Australian continent. The MODIS model estimates variable fractions of TMS for vegetation to estimate the values for these variables whereas the RSDI uses an average fixed value for projective foliage cover. The estimation of E_P, E_A and its components (E_S, E_T) in this study are thus estimated using a fixed area-weighted value of projective foliage cover (PFC). The other significant factor is that the values of GPP using MODIS satellite and FPAR algorithms may be underestimated in moderate to highly productive forests. Turner *et al.* (2006) in their study of FPAR and GPP across nine different biomes discovered that FPAR underestimates GPP and hence transpiration flux in high productive sites, such as forests. Both the dry sclerophyll site near Canberra and the moist sclerophyll site in the upper Cotter River catchment would be classified as high productive sites, relative to low productive sites, such as desert steppe or grasslands. These reasons therefore explain how the two methods yield different monthly estimates of potential and actual transpiration.

These findings provide confidence that the transpiration loss (E_T) model works satisfactorily even given the constraints of using a fixed projective foliage cover (PFC) for each of the TMS leaf types over time and the fact that estimates are point-based rather than being estimated from a detailed spatio-temporal daily soil water balance models. With the knowledge that transpiration losses do not vary significantly across a catchment, modelling or evaporation can be conducted using a single point representative of catchment conditions. Thus, it is essential to determine beforehand the initial vegetation parameters that are representative of average conditions in a catchment and to determine if these parameters change through time.

What now remains is to demonstrate the general applicability of these DSWBMs to model evaporation and run-off and to model water balance at both point and catchment scales.

6.4 Validity of the estimates of the components of the water balance

It is now important to demonstrate that the selected daily soil water balance models can predict accurately principal water balance components, evaporation and run-off in a field setting. The best field location identified in the modelling framework (section 4.1) is the upper Cotter River catchment because of the availability of stream flow records, whereas there are no records available closer to the site of Canberra Airport. If the components of the water balance are predicted well by the daily soil water balance models, then estimates of daily SWD can be applied with confidence.

In section 6.4.1 the validity of the E_I and E_{T+S} components of total evaporation (E_A) modelled by the three daily soil water balance models is compared. Seasonal levels of E_{T+S} were produced by combining combined E_S and E_T modelled outputs from the RSDI model; E_{T+S} is produced as a standard output from the MSDI and F-DSWBM models. Monthly rather than

daily results from each of the models for the upper Cotter River catchment were used for evaluating the three models.

In section 6.4.2, comparison of modelled with observed run-off from the upper Cotter River catchment demonstrates the ability of the three DSWBMs to predict annual runoff.

6.4.1 Validity of evaporation components

Annualised trends in E_I, E_{T+S} and E_A are presented for the upper Cotter River catchment from 1952to 2007 in Figure 6.12 (a), (b) and (c).

Figure 6.12 (a) shows that the Fowler daily soil water balance produces a higher modelled estimate of water intercepted and evaporated by the vegetation canopy. The greater disparity evident between the E_I values prior to 1976 calculated by the F-DSWBM and the algorithm used by the MSDI and RSDI Models is difficult to explain.

Figure 6.12 (b) shows that the modelled values of annual E_{T+S} produced by the RSDI model lie somewhere between those of the MSDI and F-DSWBM. The MSDI model produces higher E_{T+S} values compared with the two other DSWBMs throughout the time series, based on the representative average elevation of 1330 m within the catchment.

The total evaporation (E_A) produced by all the DSWBMs shows similar levels of agreement throughout the time series, fluctuating according to the amount of precipitation and net radiation received annually. The RSDI produces estimates of E_A closer to the F-DSWBM until 1985 (Figure 6.12 (c)). Thereafter, the RSDI produces higher values of E_A than the F-DSWBM. The change in estimates of E_A after 1985 cannot be explained.

The mean annual estimate of E_A (E_{T+S}+ $E_{I)}$ lies between 700 and 7790 mm per annum depending on which DSWBM is used. This estimate is close to that estimated from carbon flux studies at Bago State Forest 30 km to the west of the catchment at a similar elevation. There, Leuning *et al.* (2005) obtained an average value of 725 mm per annum over two years between 2001 and 2002. The average annual estimate from the RSDI model is 723 mm per annum, which is very close to the annual estimate produced by Leuning *et al.* Therefore the separate values of E_I, E_{T+S} and E_A are within realistic estimates based on very limited short-term data obtainable elsewhere in south eastern Australia.

Based on the evaluation of the three daily soil water balance models up to this point, none of the three daily soil water balance models is seen as the preferred models to be used in this study. Further evaluation of the three models will be conducted in section 6.4 to determine which of these should be used for interpreting landscape susceptibility to LLFs.

(a)

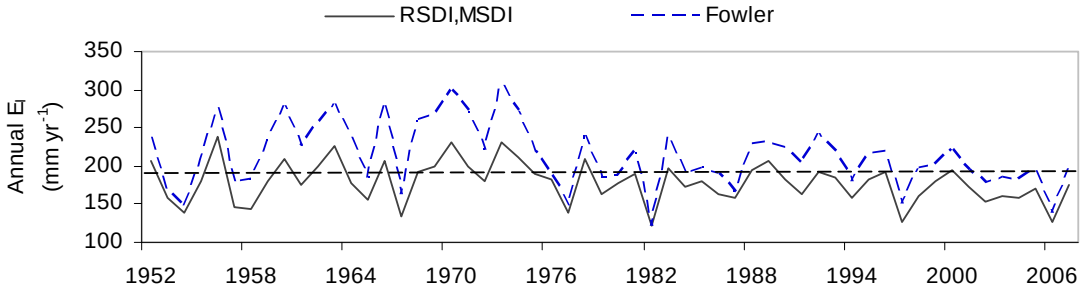

(b)

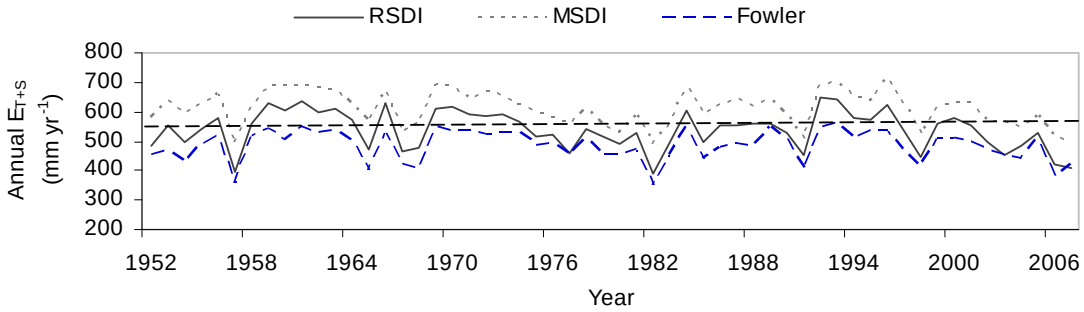

(c)

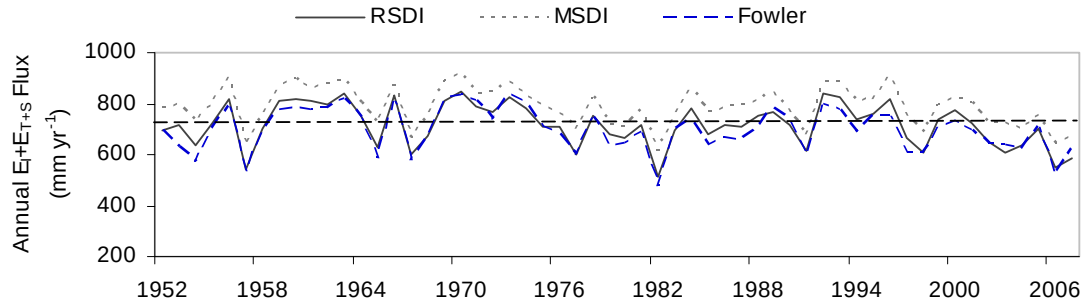

Figure 6.12 Annual trends in (a) evaporation of intercepted water (b) evapotranspiration and (c) total evaporation for 1952-2007 in the upper Cotter River catchment

Note: The E_I and E_{T+S} data are summarised from daily calculations in all models applied after 1952. The horizontal dashed lines indicate mean annual estimates of E_{T+S}, E_I and E_A obtained from the RSDI model.

The seasonal trends in monthly E_{T+S} are presented in Figure 6.13 (a) and (b) from modelled outputs from each of the three daily soil water balance models at Canberra Airport and the upper Cotter River catchment.

(a)

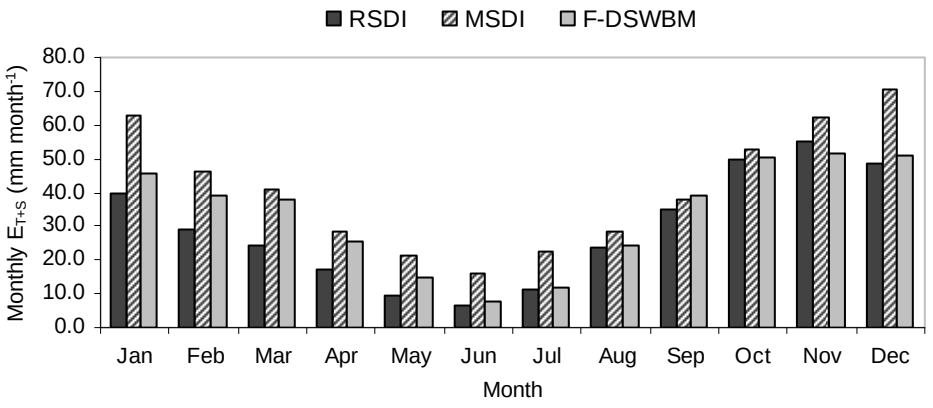

(b)

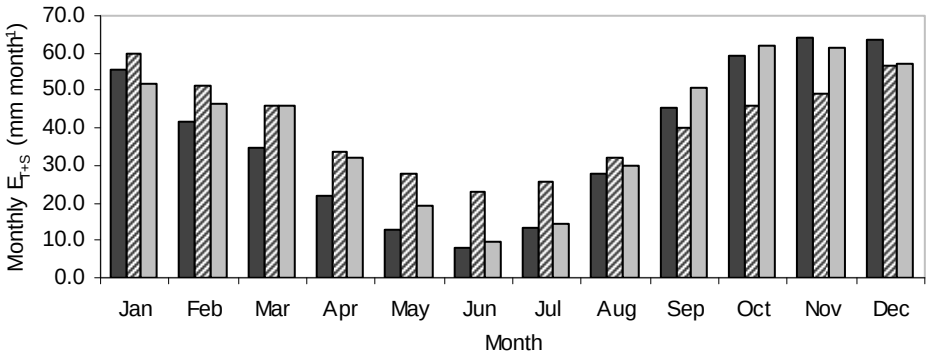

Figure 6.13 Average monthly evapotranspiration (E_{T+S}) compared for the three daily soil water balance models at two locations (a) Canberra Airport and (b) upper Cotter River catchment

Note: Period of comparison for (a) Canberra Airport and (b) upper Cotter River catchment is 1951-2007.

Inspection of Figure 6.13 (a) reveals that the monthly E_{T+S} for the RSDI model has comparable E_{T+S} values in the spring months and lower E_{T+S} in the autumn months to those estimated by the F-DSWBM. The congruence of the RSDI and the Fowler model could be improved with better estimation of values of R_N using locally derived cloud cover and relative humidity data and with further adjustments made to the Fowler coefficients (see Table 6.3). While the MSDI produces similar E_{T+S} values in the spring months, it along with the F-DSWBM produces higher estimates of E_{T+S} in the drier part of the year on average, during late summer and autumn.

Figure 6.13 (b) shows that both the RSDI and the calibrated F-DSWBM predict higher monthly moisture losses (E_{T+S}), up to 8-10 mm more in late summer and autumn than those produced by the MSDI model. Evapotranspiration predicted by the MSDI model is 10-15 mm higher in winter than those predicted by either the RSDI or the F-DSWBM models. By late

spring the RSDI and the F-DSWBM is predicting the values of E_{T+S} to be 10-20 mm than the MSDI model. The seasonal differences in values of E_{T+S} produced by the different models would result in different annual profiles of soil water deficit. The higher E_{T+S} fluxes estimated by the RSDI or F-DSWBM models in the upper Cotter River catchment in spring would result in higher values of soil water deficit earlier than those produced by the MSDI model. In addition, the higher E_{T+S} values in winter would result in an overestimation of soil water deficit during winter. Hence the importance of selecting the right daily soil water balance model for later analysis of landscape susceptibility to large fires.

6.4.2 Validity of annual runoff estimates

Is modelled run-off predicted by the three DSWBMS highly correlated with observed stream flow? Mount (1972) compared modelled and observed run-off first for Lidsdale State Forest, which along with soil moisture blocks, he calibrated his MSDI model. Following the success of his study there, he applied the model to catchments in northern and eastern Tasmania containing both wet and dry sclerophyll forest. He found that the MSDI modelled run-off satisfactorily in the wetter forests in Central Tasmania but performed worse in the drier forests in eastern Tasmania.

Run-off data in comparable dry sclerophyll forests in the lower Cotter River catchment were limited in the extent or were for modified landscapes containing mixed pine and eucalypt forests. Data from the Bushrangers Creek experiment (O'Loughlin *et al.*, 1986) could not be located nor could run-off data be found for catchments of mixed pine and eucalypt forests in the Lower Cotter catchment collected in the 1970s. Long-term records of run-off were, however, available for the upper Cotter River catchment in the western montane part of the study area from measurements taken since 1937 (Ecowise, 2007). The modelled daily run-off data were summarized into annualised data as used by Mount. An annual time scale was adopted because the MSDI and RSDI models do not contain parameters for attenuating run-off after a rain event nor take account of the delayed melt of snow in the higher parts of the catchment. Therefore, annual correlations between observed and modelled run-off provide a better basis for evaluating the DSWBMs.

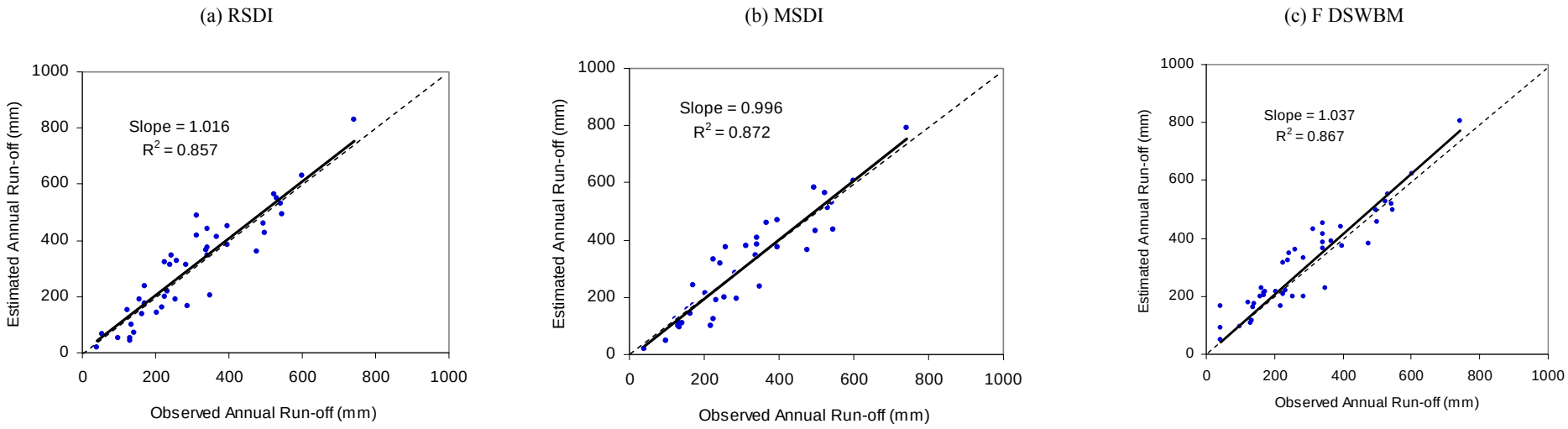

Figure 6.14 Comparison of modelled with observed runoff based on (a) RSDI, (b) MSDI, and (c) F-DSWBM models

Source: Observed runoff data from ActewAGL (1964-2007). The observed annual run-off data were from daily flow records taken at the Gingera gauging station in the upper Cotter River catchment.

Note: The dotted line indicates a 1:1 relationship between the independent variable on the x-axis and the dependent variable on the y-axis.

Predicted and observed run-off for the upper Cotter River catchment is presented for all three models in Figure 6.14 (a), (b) and (c). Closely comparable R-squared values were obtained for all three models (R^2=0.857 for RSDI R^2=0.872 for MSDI, R^2=0.867 for F-DSWBM). The slope of the regression line is also not that dissimilar for all three models. The only difference apparent between the models is that there is wider scatter of points apparent in the observed versus expected values in the MSDI plot (Figure 6.14 (b)), compared with the other two models. This comparison therefore does not identify which of the daily soil water balance models should be used for assessing the landscape dryness component of landscape susceptibility to large landscape fires in the medium or the longer-term. The selection of the preferred daily soil water balance models is deferred until the next section of this chapter.

6.5 Selection of preferred daily soil water balance models

The daily soil water balance models most suited to later adoption are selected based on the characteristics of the annual profiles through the time series. The modelled estimates of soil water deficit from the three models were compared using records gathered since 1951, at the two weather station sites: Canberra Airport and Corin Dam in the upper Cotter River catchment (Figure 6.15 and Figure 6.16). The comparison was made by scrutinizing the SWD produced by each of the three daily soil water balance models for the two weather station sites.

In relation to the simulations of SWD at Canberra Airport (Figure 6.15), the MSDI model does not differentiate the dry from the wet years as well as the RSDI and F-DSWBM models. These two models produce more similar annual profiles than the one calculated by the MSDI. However, in the upper Cotter River catchment, the annual profiles derived from the MSDI lies produces closer profiles to the RSDI model. The Fowler (F-DSWBM) model in turn is more similar to the RSDI model but not by much (Figure 6.16). When comparing the time series of the MSDI derived from weather data gathered within two different climate zones, the MSDI produces higher estimates of SWD at Canberra Airport (Cfa climate zone) but similar estimates to the RSDI model at Corin Dam in the upper Cotter River catchment (Cfb climate zone). Given that the all-wave net regime is similar at the two weather stations (see section 5.4.2), the results produced by the MSDI model indicate some further slight improvement to its evapotranspiration table may be all that is needed.

The principal reason for selecting the RSDI model over the MSDI model is because the former model is based on modelling evaporation as a biophysical process. A forest is a much more buffered and sheltered environment than a grassland, resulting in lower evaporation rates on the forest floor. It is difficult to conceptualise forest systems, especially dry vegetation and soil surfaces in a forest, as being in any way comparable to a standard evaporation pan placed in an open grassland environment, except when intercepted water is freely evaporated off the overstorey and understorey, and soil surfaces in forests.

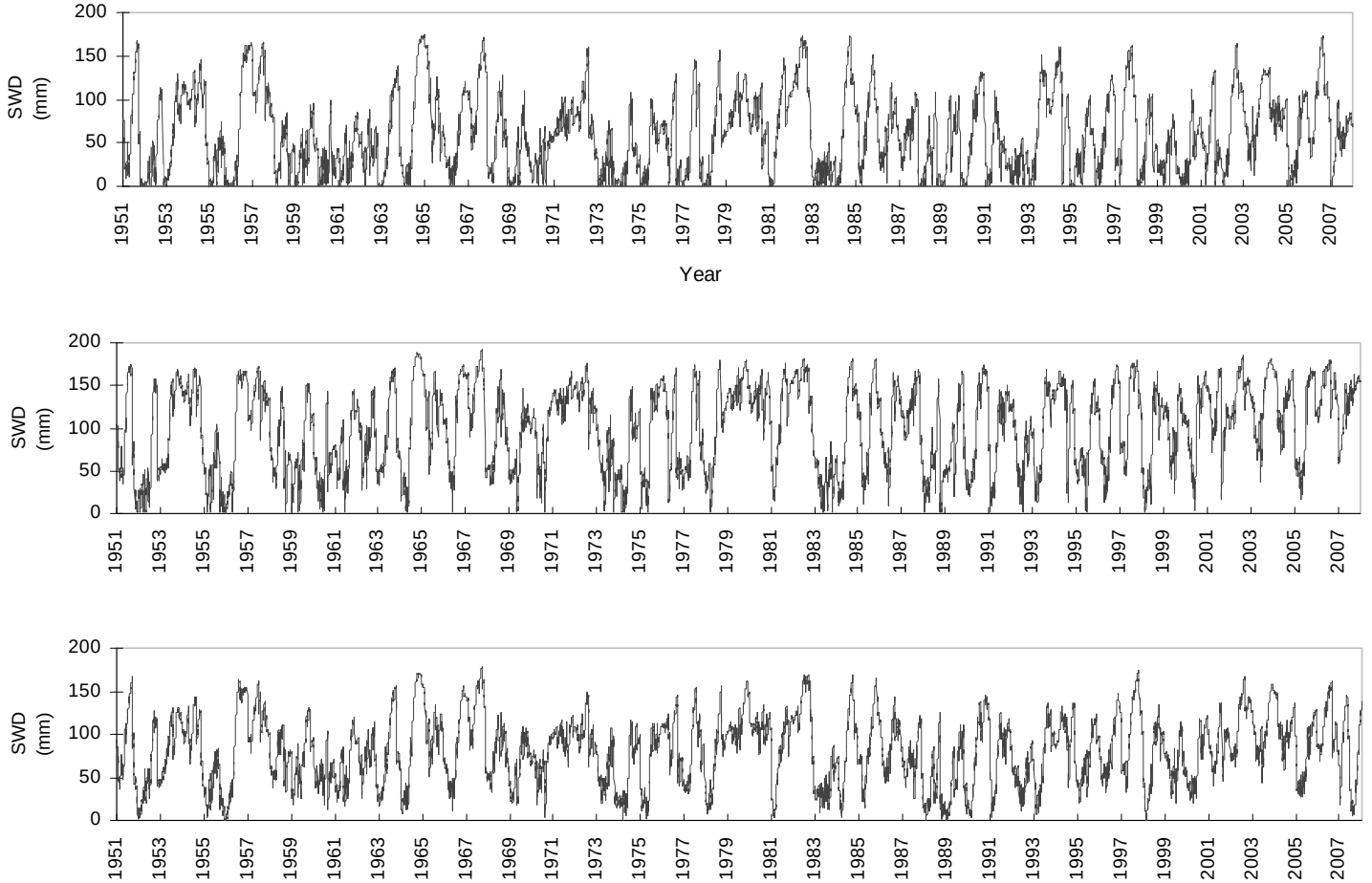

Figure 6.15 Comparison of SWD produced by RSDI (a), MSDI (b), and F-DSWBM (c) models using Canberra Airport data

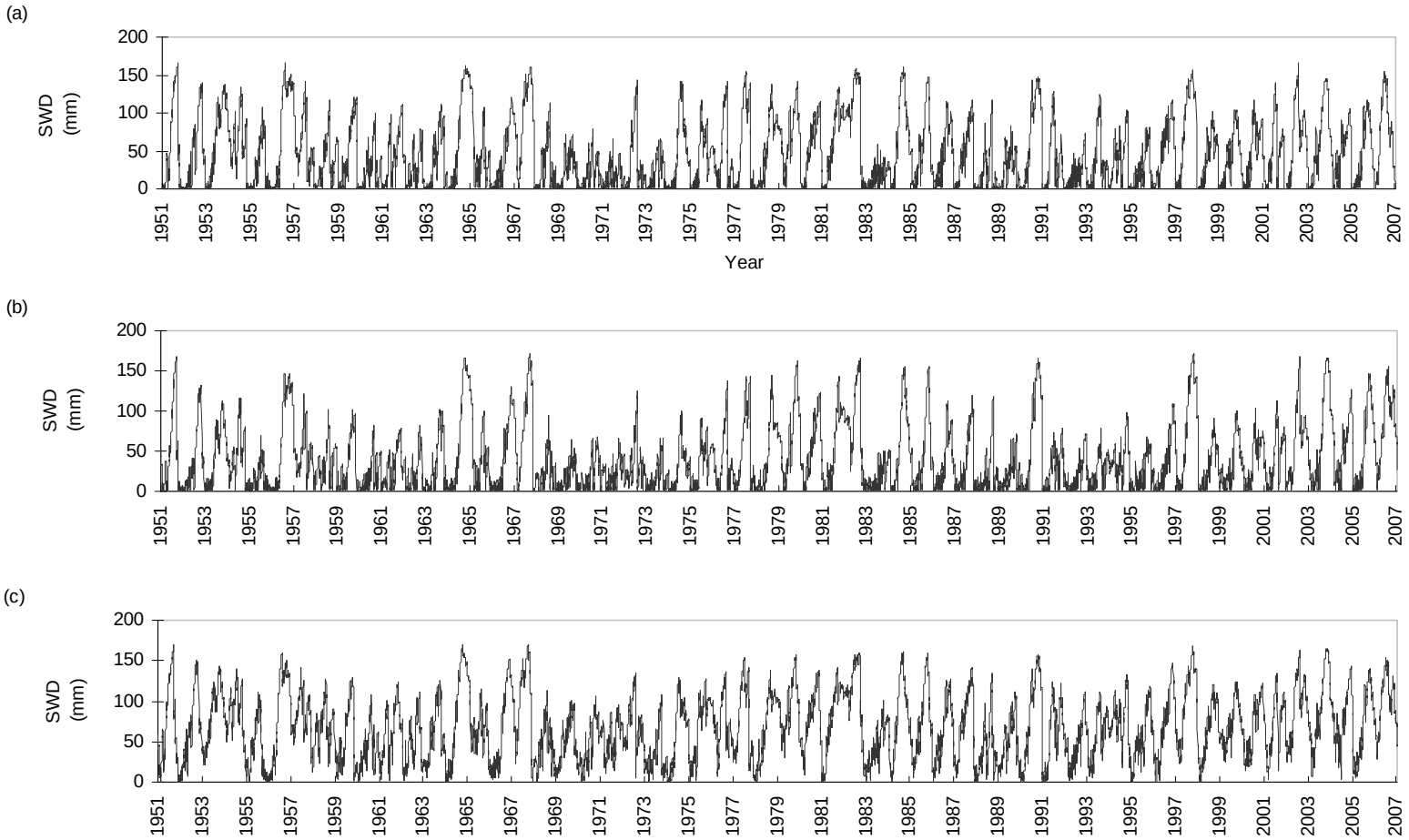

Figure 6.16 Comparison of SWD produced by the RSDI (a), MSDI (b), and F-DSWBM (c) models for the upper Cotter River catchment

The process of transpiration, on the other hand, is controlled by the factors of radiation, available soil moisture, humidity deficit, soil temperature, and the plant's physiological response to these factors. The process of soil evaporation is similarly controlled by the amount and proportion of net radiation (R_N) reaching the soil surface, the extent of ground cover, the available soil moisture and diffusivity below the soil surface. These forest processes are more complex than the process of free water evaporation from an open surface. Hence the MSDI evaporation sub-model lacks the subtleties and nuances needed to take account of these biophysical processes yet does a fine job modelling evapotranspiration using the Mount (1980).

The RSDI and F-DSWBM daily soil water balance models will therefore be used to model landscape dryness as anticipated earlier (Chapter 4).

6.6 Findings in relation to daily soil water balance models

This chapter set out to:

(1) verify the estimates of the principal components of the water balance: evaporation (E_A) and total run-off (Q); and

(2) determine which of the daily soil water balance models were the most applicable for developing realistic annual historical profiles of SWD (Chapters 8 and 9).

While total evaporation (E_A) is difficult to estimate with absolute certainty, the estimates from the RSDI model were comparable to those obtained from a comparable study undertaken by Berry (2007). The paucity of medium to long-term time series studies of evaporative losses (both E_S and E_T) in Australian forests signals the need for further studies, especially if models of landscape dryness and susceptibility to fire reflect field conditions. This results in models having to be tested against other models, not against field-based measurements of E_A and its components. Field-based heat and water measurements are both expensive and laborious to carry out, so tend to be of very limited duration as the Western Australian Silberstein *et al.* (2001) two month-study clearly demonstrated. Absence of medium or long-term measurements is a major shortcoming in producing accurate and reliable models of the components of evaporation.

The three daily soil water balance models evaluated in this chapter can adequately model total evaporation (E_A) and its components (E_S and E_T). As a result the daily soil water balance has been shown to be reasonably representative of field conditions in either a representative forest type (dry sclerophyll forests, Cfa climate zone) or for an averaged set of forest conditions in a complex catchment (upper Cotter River catchment, Cfb climate zone). For example, the estimated runoff in section 6.4.1 is in close agreement with gauged flow in the upper Cotter River catchment when conducted on an annualised basis. This is a remarkably good result

given that all DSWBMs are point-based models without complex spatial interpolation of rainfall and evaporation in the Cotter River catchment.

There are two main limitations of the MSDI model. The first limitation is that it relies on maximum daily temperature to estimate daily actual evaporation. Daily maximum temperature lags behind daily all-wave net radiation in the annual cycle by 27 days in the summer part of the fire season cycle at the study area's latitude of 35.5^{o}. The trends in average monthly evapotranspiration of the radiation-driven (RSDI, F-DSWBM) and daily maximum temperature-driven (MSDI) models reflect this (see Figure 6.13 (a) and (b)). This means that the peak in potential soil water deficit is likely to have a similar time-lag. The second limitation is its use of a single lookup table for E_{T+S} that is constant across vegetation canopy classes and are used to estimate vegetation canopy interception and flash runoff. Thus, it is surprising how well the MSDI model performs when applied to dry sclerophyll forest, especially given its overly simple approach to the estimation of E_P and the limited amount of model validation (Mount, 1972). For wetter forests, modelling of total soil and transpiration losses (E_{T+S}) by the RSDI model may need some further refinement to take account of reduced evaporation during winter.

The RSDI model can be better tailored to on-ground vegetation cover where LAI can be specified and calibrated to known vegetation conditions. Transpiration losses (E_T) in this study were based on average vegetation conditions, point-based precipitation and net radiation (R_N) to estimate evaporation in two localities, which have different climatic regimes (section 6.3.1). Additionally, the RSDI and F-DSWBM models are formulated on firmer thermodynamic and hydrological principles.

The RSDI and F-DSWBM models will thus be employed to produce annual profiles of the proxy of landscape dryness, SWD (see Chapters 8 and 9). As proposed in Chapter 4, the RSDI model will be used to produce a medium-term series of SWD at Canberra Airport. Its close counterpart, the F-DSWBM, will be used to produce a long-term time series of SWD, based on the calibration of this model with the RSDI model, at Canberra Airport.

Based on the calibration procedure (see Appendix 3) , the two daily soil water balance models have been shown to produce comparable estimates of evaporation, soil water deficit, and run-off and so seem suited for medium and long-term analysis of landscape dryness. This therefore has answered the two research questions posed in section 1.4: 'Which daily soil water balance models best approximate the hydrological processes of evaporation, run-off, and soil water deficit? Which of these models should be used for further analysis of landscape susceptibility to large fires?' (Table 1.1).

Chapter 7: Potential Fire Spread Indices and Thresholds of Landscape Dryness

The all-wave net radiation version of the Mount Soil Dryness Index and Fowler daily soil water balance models were found to best model medium- and long-term landscape dryness. Understanding the seasonal temporal nature of landscape dryness is the key to understanding the potential for fire spread in a landscape. Landscape dryness, a key factor in a potential fire spread index (PFSI), is further explored here to see how it is currently employed as a proxy of fuel availability and vegetation flammability. A well-correlated index of landscape dryness is required so that a critical threshold value of landscape dryness can be selected for warning of the imminent danger of a small fire rapidly escalating into a large landscape scale fire (LLF). In addition, a PFSI is required to anticipate the potential spread of a fire once the conditions have been reached.

This chapter undertakes to:

(1) highlight the role that landscape dryness plays in estimating fuel availability and vegetation flammability;

(2) identify literature-based SWD thresholds for heightened vegetation flammability; and

(3) identify which PFSI model is best suited to determine landscape susceptibility to LLFs.

The analysis commences with a review of the role that a daily soil water balance model plays in determining fuel availability and vegetation flammability in a landscape, followed by an exploration of the relationships between Live Leaf Moisture Content (LLMC), drought indices, vegetation flammability, and the potential for LLFs. A review of two widely used potential fire spread indices, the Canadian FWI and the Australian FFDI, is then undertaken. Finally, a preferred potential fire spread index is selected based on its suitability for predicting potential fire spread. The main findings are summarised in section 7.4.

7.1 The relationship between soil water deficit and fuel availability in potential fire spread models

Because it is impossible to measure or reconstruct the availability of the dead fuel components in a forest over a long period, soil water deficit (SWD) is used as an indirect measure of the amount of available dead fuels in forest vegetation, including the larger fuel components. Here soil water deficit is considered as having the same meaning as the term 'drought index'. In studying the relationship between fuel availability and the KBDI drought index, McArthur (1962a) showed that fire intensity increased linearly with drought index from 300 to 1200 BTU ft^{-1} s^{-1} (1000 to 4100 kW m^{-1}) when the KBDI increased from 25 to 100 mm in

a scale from 0 to 200 mm. Because his study was limited to the wetter end of the scale, he did not have the data to establish the possible relationship between SWD and fire intensity under drier conditions (100-200 mm). Therefore, there is no evidence for the type of relationship at extreme end of the scale of SWD and its relationship to potential spread and fire intensity in an index of potential fire spread.

Van Wagner (1987) determined from his studies in boreal forests that the amount of available fuel followed more of a sigmoid curve (Figure 7.1). This relationship is more likely to mimic the observed pattern of soil moisture loss as soils dry out as the seasons move from the cooler and wetter months in winter and early spring and approach a depleted soil moisture condition in summer to early autumn. The fuel availability model used in the Canadian Fire Weather Index shows a slower build-up in fuel availability until a value of SWD equal to 70 mm. Availability of fuels then accelerates rapidly up to a value of SWD equal to 100 mm. Thereafter it increases linearly until 80-90 % of the fuels become available, approaching the peak fuel availability at a value of SWD between 120 and 140 mm. This threshold value would of course vary between vegetation types.

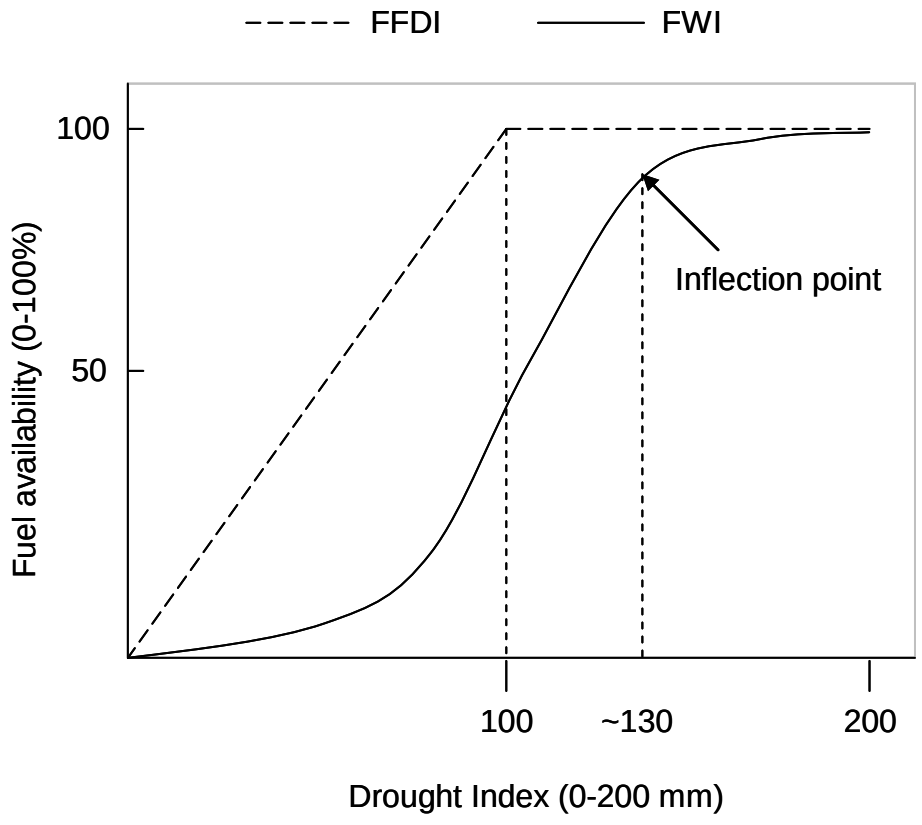

Figure 7.1 Relationship between fuel availability and a theoretical drought index expressed by FFDI and FWI

In contrast, the fuel availability curve in the FFDI model follows a straight line up to a value of a drought index of around 100 mm and thereafter the drought factor stays constant even

though landscape dryness conditions are becoming more severe in their effects on soil, vegetation, and fuel moistures. The MacArthur FFDI model therefore predicts that fuel availability increases more rapidly, and at a much earlier time, than that predicted by the FWI model.

The fuel availability relationship used in the Fire Weather Index model better explains the apparent sudden change in fire behaviour after soil and vegetation moisture fall to a critical threshold around the inflexion point. This sudden change in fuel availability, that is, availability of more combustible fuel, may partly explain the rapid escalation of small fire into a large landscape fire if fire weather conditions deteriorate. The contribution of vegetation flammability as another factor in increasing the potential for large landscape fires is explored next.

7.2 Live vegetation flammability and potential fire spread

As outlined in the previous section, availability of fuel in a forest is modelled indirectly using a drought or soil dryness index. This does not take into account the relative ease at which live vegetation can catch fire. This is termed live vegetation flammability and refers to its:

(1) ignitability, that is how easy it is for fuel to catch fire,

(2) sustainability or how well it continues to burn, and

(3) combustibility, how fast dead and live forest fuels burn (Anderson, 1970; Dimitrakopoulos and Papaioannou, 2001).

Flammability of live vegetation relates primarily to the moisture, ash, and flammable oil content in live leaves. Moisture content of dead or live fuels is expressed as the percentage of oven-dry weight, The moisture content of live leaf fuels can be anywhere between about 50 and 250%, depending on their phenology and their degree of water stress. Once the moisture content of live leaves falls below 100%, vegetation flammability increases significantly. Once live leaf moisture content falls below 70% (close to the wilting point in most plants), vegetation can become highly flammable.

By comparison, the moisture content of litter fuels is generally much lower (varying between vary between 2% and 30% moisture content) once the effects of recent rain have evaporated. Because of the much lower moisture content of dead fuel, dead rather than live fuels have been widely presumed to be the principal driver of fire spread over the full range of fire behaviour (Rothermel, 1972; Brown and Davis, 1973; Chandler *et al.*, 1983). Nevertheless, dead and live fine fuel moisture contents are incorporated into the denominator heat energy of pre-ignition (Q_{IG}) term of the Rothermel fire spread equation (Rothermel, 1972):

$$ROS = \frac{I_R \xi (1 + \phi_W + \phi_S)}{\sigma_B Q_{IG}} \text{ (m s}^{-1}\text{)} \qquad \text{Equation 7.1}$$

where ROS is the rate of spread of a fire (m sec^{-1}), I_R is the reaction intensity (kW m^{-2}), ξ is a dimensionless propagating flux ratio constant, σ_B is the bulk density of the fuel complex (kg m^{-3}), Q_{IG} is the heat energy of pre-ignition (kj kg^{-1}), ϕ_W is the wind coefficient and ϕ_S is the slope coefficient.

This equation expresses the rate of spread of a fire in terms of the ratio of the propagating heat flux of the dead fuels to the heat required for pre-ignition of unburnt live and dead forest fuels (denominator). The higher the propagating flux, the greater is the energy available to ignite and rapidly combust all fine fuels ahead of a fire front. The lower the heat energy of pre-ignition (Q_{IG}), the faster forests fuels combust, the faster the rate of spread of fire, and the higher the fire intensity, all other factors being held constant. The term Q_{IG} has been defined as 'the energy required to bring a fuel from its current temperature to ignition temperature' (Dasgupta *et al.*, 2006:141) and is applicable to both dead and live forest fuels.

Implicit in the estimation of potential rate of spread and fire intensity is the moisture content of live fuels as well as dry ground and aerial fuels. Therefore, any potential fire spread index (PFSI) will be greatly influenced by how dry both the dead and live fuels are. In essence, fuel moisture levels will determine whether a particular forest fire will progress rapidly to a LLF under very dry landscape and severe fire weather conditions. Associated with this rapid escalation is the potential for crown fires in forests. Rate of fire spread is much faster in crown rather than surface fires (Van Wagner, 1977). The added energy release from crown fires also promotes the development of convection columns over a fire, which can exacerbate its severity, and thus its controllability, particularly under very dry landscape and extreme fire weather conditions.

A PFSI should therefore incorporate the factors of dead fuel availability and live vegetation flammability that are embodied in Equation 7.2. At the present time, there is no relationship established between SWD and live vegetation flammability in the McArthur FFDI although vegetation flammability is taken into account in the Canadian Fire Behaviour System, using live leaf moisture content (LLMC) of the tree canopy when estimating crown fire behaviour (Van Wagner, 1977). The live vegetation flammability component is impractical and

difficult to model through time using a biophysical model. The only practical alternative is to establish an indirect relationship between the level of landscape dryness based on a soil dryness index and live vegetation flammability. Possible relationships between soil dryness, live leaf moisture content, vegetation flammability, and the potential for LLFs are explored next.

7.3 Relationship between live leaf moisture content, vegetation flammability, and the potential for LLFs

Moisture content of live leaves responds much more slowly to changes in ambient conditions than dead fuels, but is dependent on plant physiology, soil water regime and seasonal weather conditions (Castro *et al.*, 2003; Chuvieco *et al.*, 2004). In contrast, fine dead fuels respond to changes in ambient weather conditions (Viney, 1991b) with a time lag between one and ten hours depending on fuel thickness (Rothermel, 1972).

Based on a limited set of studies of the seasonal changes in live fine fuel, live leaf moisture content of understorey shrubs and herbaceous species can vary significantly while that of deeper-rooted plant species, such as *Pinus brutia*, do not (Dimitrakopoulos and Bemmerzouk, 2003; Pellizzaro *et al.*, 2007). The LLMC of herbaceous and grass species studied fell to below 30% in the middle of summer when the soil water deficit estimated by the Keetch-Byram Drought Index (KBDI) had reached 140 on a scale of 0 to 200 mm. Pellizzaro *et al.* (2007) found a lower value of soil water deficit (SWD =107 mm) based on the KBDI that was related to LLMC values below 50% in *Cistus monspeliensis* in pine forests and *Rosmarinus officinalis* in heathland in Spain. Again the values of LLMC for both shrub species was well below the wilting point for most herbs, shrubs, and grasses (LLMC<= 70%). On a theoretical basis, more extreme levels of soil water deficit, more highly combustible near-surface dead fuels and highly flammable live fuels in the shrub and tree canopy layers lead to a lower level of heat for pre-ignition being required and hence faster potential rates of spread (see Equation 7.1).

In another study in Greece, Dimitrakopoulos and Papaioannou (2001) found that low LLMCs were linked to higher flammability of Mediterranean shrubs and herbaceous species. The findings from this study supports earlier studies that increased vegetation flammability can be linked to a greater potential for the outbreak and spread of fires (Chandler *et al.*, 1983; Castro *et al.*, 2003). On a theoretical basis, more extreme levels of soil water deficit, more highly combustible near-surface dead fuels and highly flammable live fuels in the shrub and tree canopy layers lead to lower level of heat for pre-ignition and hence faster potential rates of spread (see Equation 7.1).

Critical levels for the initiation and spread of Chaparral fires in southern California were found to be below a Live Leaf Moisture Content (LLMC) of 77% (Dennison *et al.*, 2008) although there was no reported relationship with a drought index. The significant result for this study was that the largest landscape fires occurred when the estimated LLMC was between 61 and 77%. In the study of the effects of the late summer drought of 1965 in the ACT, Pook *et al.*

(1966) reported LLMCs of between 40 and 75% in overstorey eucalypts on rocky soils and LLMCs between 80 and 90% in open *Eucalyptus melliodora* (Yellow Box) woodlands with a deep regolith. The measurements were taken during March and April – the estimated soil water deficit during those months was estimated using the RSDI model as being between 140 mm and 165 mm. At the same time, there were large fires burning in east Gippsland, the Tumut area in the Snowy Mountains and on the coastal escarpment between Nowra and Ulladulla on the South Coast of New South Wales. The limited number of these studies allude to high levels of soil water deficit contributing to low values of LLMC playing a role in the spread of LLFs. These results agree with the findings of Chandler (1983), that a LLMC of 75% was a critical level for the propagation of LLFs in Mediterranean ecosystems.

Rothermel (1972) supports the notion that large fires are more likely to occur in late summer in the Rocky Mountains in United States and Canada because of the combination of low dead and live fuel moisture contents. Pompe and Vines (1966) also contend that fire intensities are exacerbated during drought conditions because of low dead and live fuel moisture content in vegetation.

Based on the relationships between KBDI and LLMC, vegetation flammability and the risk of LLFs, a critical threshold of flammability and fuel availability must be placed somewhere in the range of 100 to 140 mm. The threshold set may be dependent on the daily soil water balance model employed, the type of vegetation and soils, and climate. This threshold is critical for anticipating the potential of LLFs, independent of potential fire spread conditions. This threshold in a landscape dryness index will be investigated further in Chapters 8 and 9 to identify (1) fire seasons with high to very high landscape susceptibility to fire and (2) the likelihood of lightning ignition.

7.4 Evaluation of potential fire spread models

The factors of fuel availability and live vegetation flammability and their relationship to landscape dryness indices and potential fire spread indices (PFSIs) were explored in the previous section. The findings in the previous two sections suggest that landscape dryness has the potential to indicate both fuel availability and vegetation flammability changes in forest fuels. It is thus important to use a PFSI model that contains explicit and transparent components of landscape dryness and potential for fire spread in the landscape if it is to be applied to anticipating severe fire conditions in a landscape.

Two potential fire spread indices are evaluated for this study: (1) the Forest Fire Danger Index (FFDI) and (2) the Canadian Fire Weather Index (FWI). Both models embody: (1) a landscape dryness component; (2) an index of fine fuel moisture, and (3) wind speed estimated or measured at 10 m above the ground in the open.

7.4.1 Forest Fire Danger Index

The Forest Fire Danger Index (FFDI) was first developed to predict fire behaviour in eucalypt forest fires in south eastern Australia (McArthur, 1967). Noble *et al.* (1980) converted the FFDI into a series of equations that related the indices to: (1) drought-determining variables, and (2) hourly or daily fire weather variables: temperature, relative humidity and wind speed (Equation 7.2).

$$FFDI = 2.0 \times \exp(-0.450 + 0.987 \times \ln(DF) - 0.0345 \times RH + 0.0338 \times T + 0.0234 \times V \quad \text{Equation 7.2}$$

where DF is the Drought Factor estimated from either the KBDI or MSDI and days since rain and amount of rainfall, RH is the relative humidity, T is the temperature (^{o}C) and V is the wind speed (km hr^{-1}).

The Drought Factor is estimated from Equation 7.3:

$$DF = 0.191*(KBDI + 104) \times (D_{SR} + 1)^{1.5} \Big/ \left(3.52 \times (D_{SR} + 1)^{1.5} + P_{0900} - 1\right) \quad \text{Equation 7.3}$$

where KBDI is the Keetch-Byram Drought Index, D_{SR} is the number of days since last rainfall event, and P_{0900} is the amount of rainfall to 9am in the previous 24 hours (mm).

7.4.2 Canadian Fire Weather Index

The Canadian Forest Fire Weather Index (FWI), a key component of the Canadian Forest Fire danger Rating System (CFFDRS), was developed from a set of empirical relationships between fire spread and intensity and three key variables: available surface fuel, fuel moisture content and wind speed (Van Wagner, 1987). According to Van Wagner, the index was developed from the fire intensity equation for a headfire (Byram, 1959) whose equation combined the heat of combustion per unit of fuel, the rate of spread of a fire and the amount of fuel consumed (Equation 7.4).

$$I = HWR \quad \text{Equation 7.4}$$

where I is the fire intensity (W m^{-2}), H is the calorific heat content of fuel (J g^{-1}), W is the available fuels (kg m^{-2}) and R is the rate spread of the fire (m s^{-1}).

In the FWI system, fuel moisture content is derived for three classes of fuel: the fine fuel moisture (fine fuel moisture content (FFMC)), duff (duff moisture code (DMC)) and a drought code (moisture content of large logs and branches (DC)) (Van Wagner, 1972). The FFMC responds quickly to hourly changes in temperature, relative humidity and wind speed, whereas the DMC and DC have much slower response times of between 12 and 52 days, being responsive to factors such as day length, temperature, relative humidity, and rainfall. Notice that the DMC represents the drying and wetting of the duff layer in boreal pine forests in

Canada (Van Wagner, 1972) while DC represents a recoded soil water index of between 0 and 800 points similar to that used in the Keetch-Byram Drought Index.

The initial spread index (ISI) in the FWI system is estimated from the FFMC and the wind speed and represents fire spread on an even surface, without taking into account the deeper surface or larger fuels (Equation 7.5) (Van Wagner, 1987):

$$ISI = 91.9 \times \exp(-0.1936 \times m)) \times \left[1 + m^{5.31} \Big/ \left(4.93 \times 10^{-7}\right)^{+}\right] \times \exp(0.05039 \times WS) \quad \text{Equation 7.5}$$

where m is moisture content in %, estimated from FFMC; and WS is the wind speed measured at 10 m in the open

The second index, termed the build-up index (BUI), represents potential fuel availability and is estimated using a harmonic mean of the two longer-term variables, duff moisture code (DMC) and drought code (DC).

$$BUI = 0.8 \times \frac{DMC \times DC}{DMC + 0.4 \times DC} \quad \text{Equation 7.6}$$

Finally, the Canadian FWI uses a combined index of the ISI and the BUI, on an algorithmic scale to estimate severity of potential fire spread and intensity.

$$FWI = 2.72 \times (0.434 \times (0.1 \times ISI \times BUI)^{0.647} \quad \text{Equation 7.7}$$

Additionally, a daily severity rating (DSR) can be estimated from the FWI, using a weighting factor to express the degree of difficulty of fire control as FWI increases. The relationship between the FWI and the DSR is based on:

$$DSR = 0.0272 \times FWI^{1.77} \quad \text{Equation 7.8}$$

A monthly (MSR) or a seasonal severity rating (SSR) can also be estimated from DSR averaged or accumulated over the length of a month or a fire season (Van Wagner, 1987).

7.4.3 Comparison of PFSI models

The Canadian FWI is significantly more utilitarian than McArthur's FFDI. The Canadian FWI model makes no presumption about the worst set of fire weather conditions. In McArthur's FFDI, the upper boundary is set to 100, equivalent to the fire weather conditions experienced in the 1939 Black Friday fires in Victoria, when there was a maximum temperature of 40^{o}C, relative humidity of 15%, and a mean wind speed of 55 km hr^{-1} (15 m s^{-1}) (McArthur and Cheney, 1972). These conditions have been occasionally exceeded, for example during the worst fire weather experienced in the 1983 Ash Wednesday fires in Victoria and South Australia (FFDI=110) (Rawson *et al.*, 1986). Additionally, the FWI is an explicit and well documented system (Van Wagner, 1987) that explains in simple and logical terms the structure of the fuel moisture and wind effects on potential fire behaviour. In contrast, the McArthur FFDI supplies

little supporting documentation or evidence to support the type of models used in the index (McArthur, 1967; McArthur and Cheney, 1972).

The FFDI does not contain an explicit fuel moisture model nor does it have an explicit fuel availability factor. Instead, the variables, temperature and relative humidity, are implicitly imbedded in the FFDI model to estimate dead fine fuel moisture. To obtain an explicit value of dead fine fuel moisture, an algorithm from the Grassland Fire Danger Index (GFDI) or the fuel moisture algorithms in Leaflet 80 (McArthur, 1962b) can be used instead to approximate values of dead fuel moisture. The Drought Factor is a rudimentary algorithm for estimating fuel availability in forests. It should be regarded only as a first approximation of seasonal fuel availability in eucalypt forests.

One significant limitation in applying the Canadian FWI model to the study is calibrating the duff moisture code (DMC) and the drought code (DC). The fuel moisture algorithms, which calculate DMC and DC, were developed in the boreal coniferous forests of Canada. These forests are situated at much higher latitudes, between 50 and 55^{o}, in the northern hemisphere, than the latitudes of the study area (34^{o} 50' and 36^{o} 40'). Day length and monthly maximum and minimum temperatures are therefore likely to be markedly different between the more temperate latitude of the study area and the sub-polar regions in Canada, which may limit the potential applicability of these slower drying litter models used in this study.

The DMC is based on a logarithmic drying rate that also takes into account effective rainfall and a monthly day-length factor. These two latter factors are used, together with daily maximum temperature and day length, to estimate potential evaporation. The range in fuel moisture content in the DMC model is between 0 and 300% of oven-dried weight of fuel. The minimum equilibrium moisture content in the DMC is assumed to be 20%, which may be higher than that under very dry seasonal conditions in the ACT region.

The duff moisture content (DMC) is the moisture content of the semi-decomposed fraction of a deep litter bed with an average fuel loading of 4.9 kg m^{-2} and a fuel depth of 0.07-0.12 m (Van Wagner, 1987). By comparison, the fuel loading in a dry sclerophyll forest near Canberra is between 1.25 – 1.75 kg m^{-2} with an average fuel depth between 0.02 and 0.03 m (Author's own measurements in 2004). It is unusual for a duff layer to develop in dry sclerophyll forests although it does develop in wet sclerophyll forests in Victoria and Tasmania and in pine plantations in south eastern Australia. Litter beds in Australian forests tend to be more porous and decompose more slowly in the lower parts of the litter bed because of increased lignin and oils in the leaves. The differences in bulk density and fuel depth would affect the log dry rate and the DMC would need to be adjusted to take account of the above differences between a Boreal pine forest in Canada and a eucalypt forest in south eastern Australia. As a result, the DMC code used in the FWI system may not reflect a fast enough drying in the semi-decomposed and decomposed parts of the litter layer in Eucalypt forests. The only calibration

of the DMC attempted in this study is to adjust the average day length hours of each month of the year; however, further detailed field studies to calibrate this model for south eastern Australia was not possible in the time-frame set by this study.

The algorithm for estimation of drought code (DC) in the FWI employs a negative exponential algorithm to relate the value of DC to the moisture content of the duff layer. Daily drying is related to the potential evaporation rate and to effective rainfall, which is adjusted by a day length factor. It assumes a 200 mm soil water storage, equivalent to that used in the KBDI (Keetch and Byram, 1968). If these factors can be calibrated for Australian conditions, by adjusting the key input factors, then the FWI can be applied in this study. A similar adaptation was done when the Canadian FWI system was converted for use in New Zealand climatic conditions (Fogarty *et al.*, 1998b). An alternative approach is to substitute the MSDI model for the DC model, as long as there is a satisfactory correlation between the two drought indices. This approach therefore removed the problem of adapting the DC to Australian conditions, which is beyond the scope of this study.

Of the two potential fire spread indices explored, the FFDI and FWI, the FWI has the necessary features, such as integration with a DSWBM, explicit sub-indices and more realistic approximation of the range of potential fire spread, even though it was developed in the Boreal forests in Canada. Viegas *et al.* (1999) concluded that the Canadian FWI was one of the best suited potential fire spread indices to assess fire risk and potential in Europe.

7.5 Derivation: potential fire spread time and landscape dryness datasets

Based on a spreadsheet provided by the Canadian Forest Service, the fire weather dataset for Canberra Airport was expanded to calculate the FFDI and FWI concurrently (Appendix 4). SWD estimated from the now calibrated all-wave net radiation SDI model (RSDI) was transferred across to this spreadsheet from the spreadsheet in Appendix 2. In order for the SDI to have parity with the DC variable, it was scaled up from 165 to 200 mm and then converted from mm to points to be consistent within the imperial scale used in the calculation of DC in the FWI model. The assumption being made is that there is a general linear relationship between the two variables.

Values of SWD and FWI were then extracted from the principal spreadsheet and placed into a separate worksheet that estimated dummy values for the additional day required in non-leap years to create a consistent 366-day length year throughout the duration of the time series. A uniform day length year eliminates a shift in time of the days after the month of February. This is especially important in a 100-year time series of any variable.

7.6 Findings

The potential fire spread indices explored in this chapter rely on drought indices to estimate the availability of dead fine and coarse fuels, which is a critical factor in the estimation of potential fire spread across a landscape. The FFDI and FWI use slightly different modelling approaches to allow for the contribution that availability of fuels make toward potential fire behaviour. For the FFDI, the Drought Factor sub-model uses a constant linear relationship between SWD and available fuel up to a maximum value of SWD equal to about 100 mm for a constant D_{SR} and P_{0900}. Above this SWD value, the FFDI is insensitive to any further increase in fuel availability. Vegetation flammability becomes critical once live leaf moisture contents approach the wilting point, approximately when the KBDI exceeds 100-120 mm. Heightened vegetation flammability at live leaf moisture contents below wilting point (LLMC<70%) were shown to contribute to LLFs in Californian chaparral vegetation. As no critical LLMC threshold value has been established for Australian conditions, a tentative SWD threshold of 100-120 mm is proposed to indicate the critical point for live vegetation flammability. Beyond this point, available fuel can be considered to include live vegetation and adds to the potential for LLFs.

The Canadian FWI model is a more suitable PFSI than the FFDI because it integrates the sub-indices of fuel moisture (FFMC, DMC, and DC), fuel availability (BUI), and potential spread of fire (ISI) and FWI in a simple and transparent manner. To apply the FWI in an Australian forest setting, the DMC and DC codes first need further calibration to reflect the different drying and wetting conditions. This is achieved by substituting the DC model by the Mount SDI model matching the DMC to the monthly day length conditions for the local latitude. A problem remains in that the FFMC sub-model has not been tested and calibrated for eucalypt forests. Viney (1991a) found that the rates of eucalypt leaf litter and pine needle moisture absorption and desorption differ. This limits the applicability of the FFMC model to Australian eucalypt forests and its use could produce type I or II errors.

In answer to the seventh research question, 'Can a threshold of soil water deficit (SWD) indicate a realistic threshold in fuel availability and vegetation flammability in a forested landscape that, once exceeded, can lead to large landscape fires (LLFs)?' there is a suggested SWD threshold in the literature (100<SWD<120), indicating increased fuel availability and vegetation flammability that leads to LLFs. This threshold value requires further field studies to confirm it in different climate zones and vegetation types. In answer to the eighth research question: 'Which of the PFSI models is the most transparent and explicit, and best integrates the factors involved in estimating potential fire spread?' the Canadian FWI model appears more suitable than McArthur's FFFDI model. However, the ultimate choice of a PFSI will be held over until the next chapter using detailed seasonal analysis of daily potential fire spread.

Chapter 8: Interpreting Medium-term Landscape Susceptibility to Large Fires

The fundamental concept of this chapter is that of the time in the annual profile of fire susceptibility indexes when fire is likely in a fire season. The annual profile is defined from the daily pattern of variation of either of the susceptibility indexes, landscape dryness or potential fire spread. Being primarily driven by the rise and fall in solar radiation in the annual solar cycle, the annual profile is from July to June. The analysis starts from the profile of a normal fire season and its variation, leading to the identification of the profiles of all the fire seasons for which data is available. Examining the sequence of these fire seasons from year to year provides an understanding of the potential for LLFs and how this potential develops within and across fire seasons.

Earlier chapters focussed on the data and models requirements to deliver quantifiable indicators of fire susceptibility: landscape dryness and potential fire spread. Hierarchical classification is applied to these indices to identify annual profiles and form descriptive typologies of the sets of landscape dryness and potential fire spread. Cluster analysis identifies groups of fire seasons with similar annual profiles (Romesberg, 1984). The basis of hierarchical classification is to apply a clustering strategy that compares each pair of fire seasons using some form of similarity or dissimilarity, in this case Euclidian distance based on the root sums of squares differences (Mathsoft, 2005). First, the closest pair of fire seasons are clustered together. Then these are compared to the next closest matching fire season until there are recognisable clusters distinguished by recognisable differences in Euclidian distance values. A classification tree is then produced which links all the clusters together in the form of a hierarchically nested set of clusters (Gordon, 1987).

Hierarchical classification by cluster analysis is seen as the best technique to distinguish the different types of fire seasons and is based on the daily variation of each fire susceptibility indicator through a fire season. Romesberg (1984:90) summarises the use of cluster analysis:

> 'Cluster analysis is a method for describing the similarities among objects in a *sample*. It is a mathematical microscope for looking at the relations of similarity among a *given set* of objects. It cannot be used for making statistical inferences about these relations to a larger population. Any inferences a researcher makes by studying a hierarchical tree are made by using reasoned analogy rather than by formal statistical methods.'

Cluster analysis is a tool that classifies the seasonal profiles by comparing the similarity of each fire season with the rest of the fire seasons until a hierarchical classification tree or dendrogram is produced (Romesberg, 1984). The resultant classification can then be used to discern differing fire susceptibility patterns found in past fire seasons.

To that end, the approach adopted in this chapter is as follows:

(1) to examine and then define the natural seasonal periods for an average fire season;

(2) to identify broad groups and sub-groups of fire seasons using a hierarchical classification of annual profiles of SWD and FWI based on Canberra Airport daily weather data;

(3) to examine the year-to-year variation in fire seasons based on an index of FWI (SFWI) standardised to a scale from 0 to 100;

(4) to determine the thresholds of SWD and FWI at which landscapes have been highly susceptible to LLFs in the past and then apply those thresholds to identify the critical months in fire seasons based on the potential fire spread index (FWI); and

(5) to investigate the landscape and potential fire spread conditions under which dry thunderstorms and lightning ignition have occurred in the past 65 years.

8.1 The fire season calendar

It is important to define what a typical fire season calendar is like in the study region as this forms an important reference point in the analysis of landscape susceptibility to large fires within and between fire seasons. The intent is to create a more detailed view based on analysis undertaken at the daily time scale and to understand why the season is like it is based on the daily data from landscape dryness and potential fire spread models selected in earlier chapters.

Thus, it is important first to see how well contemporary definitions line up with the historical patterns of all-wave net radiation, temperature, and then with combinations of fire susceptibility indices already outlined (sections 8.1.1 and 8.1.2). According to Luke and McArthur (1978:15), the south eastern Australian fire season is classified as summer-dominant, commencing in September and ending in March. No start or finish dates are defined in their broad definition but in the absence of more detailed analysis, it has served a useful purpose. More pragmatically, durations of fire seasons have been varied to meet perceived variations in landscape and weather conditions, but the underlying basis for the fire season calendar has not been seriously challenged. A clear opportunity exists to redefine their broad definition and to establish recognisable intra-fire seasons within which to identify risk periods.

A season of the year can be defined in several ways. The first definition is based on an astronomer's definition. A season refers to:

> 'Any of the four periods into which the year is divided: spring, summer, autumn and winter. The seasons arise from the Earth's axis being tilted, so that different latitudes receive varying amounts of sunlight over the course of the year as the Earth orbits the Sun. Astronomically, the seasons are taken to begin at the equinoxes (spring and autumn) and the solstices (summer and winter)(Oxford, 2007).'

A pure calendar definition simply divides seasons into four three-monthly periods. The meteorological definition conforms exactly to the calendar definition (Dec-Feb, Mar-May, Jun-Aug, and Sep-Nov), starting or ending on the first and last day of each three monthly period. This is a matter of convenience; it enables climate and weather information to be summarised by calendar months. It is worth noting that the modern European (and North American) tradition is to recognise the equinoxes and solstices in defining their seasons.

In practice, the start and finish date of each fire season will vary from year to year, and is mainly dependent on the prevailing regional weather patterns. Weather patterns are known to be influenced by climate processes operating at both sub-global and sub-continental scales (Horel and Wallace, 1981; McBride and Nicholls, 1983; Hessl *et al.*, 2004; Coulibaly, 2006; Schoennagel *et al.*, 2005). The temporal and spatial variation of the factors operating at these scales drives the subtle seasonal variation in their values that occurs from year to year.

A more flexible definition of fire season would encompass a consideration of temperature, radiation and dominant synoptic weather patterns (Alpert *et al.*, 2004), The Alpert and co-workers study showed that seasons in the eastern Mediterranean can be defined by dominant synoptic features derived from long-term NCEP pressure data. Their idea presents a new approach to defining the natural breaks in seasons. The intention in this chapter is to define rigorous fire susceptibility criteria and present new definitions of the seasons to better define fire, and intra-fire, seasons.

8.1.1 The seasons in relation to temperature and all-wave net radiation

Records of mean daily net radiation and daily temperature are examined to identify possible periods for a typical fire season in the Canberra region. The critical factors are the timing, magnitude and seasonal variation of these climatic factors throughout the year.

Mean daily all-wave net radiation (R_N) and temperature (T_A) each follow a sinusoidal curve rising rapidly from a minimum in winter to a maximum at the peak of summer (Figure 8.1). At the latitude of 35.5^o S, the mean daily temperature lags behind mean daily R_N by about 27 days. This is because the land is heated by the absorption of radiation and the land in turn heats the atmosphere, which is why the maximum and air temperature lags behind the radiation maximum both on a daily and seasonal basis. Mean daily R_N shows more week-to-week variability in the spring and early summer period than at other times of the year, with peak variability occurring between the end of September (day 93) and early February (day 230) due to the passage of alternating weather systems and associated clouds. There are marked irregular rises and falls of mean daily R_N either side of the summer solstice (day 175 to day 205), attributable at least in part to highly variable spring weather. Thereafter the daily average variability in R_N reduces in late summer and stabilises in autumn.

Figure 8.1 shows the pattern of seasonal rise and fall in mean daily R_N. There is much less week-to-week variation in T_A values compared with daily R_N values over the annual cycle. Thus temperature is not a useful criterion for establishing natural breaks in the seasons within a fire season.

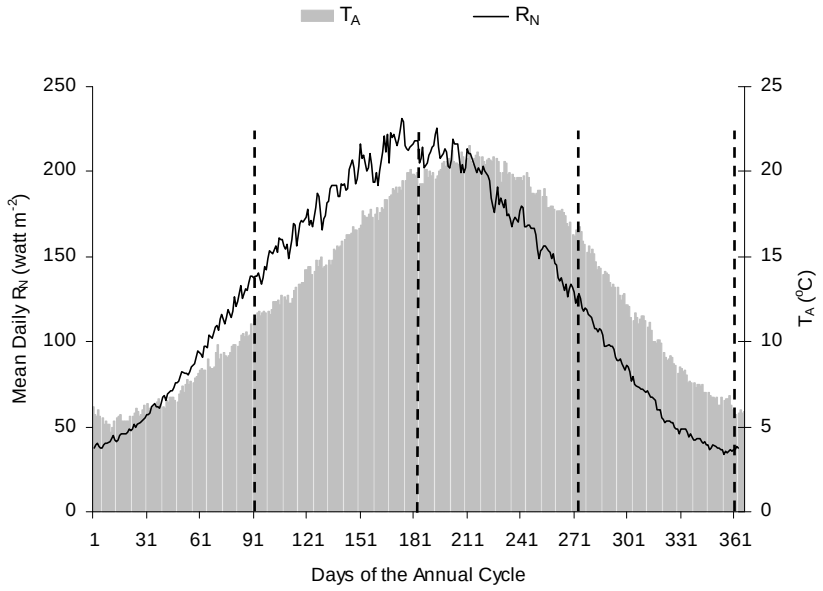

Figure 8.1 Astronomical breaks in the annual cycle in relation to daily all-wave net radiation (R_N) and mean daily temperature (T_A) for Canberra Airport

Source: Data extracted from meteorological records in the case of mean daily temperature; mean daily R_N estimated from net radiation equations shown in Chapter 5. Period of analysis is July 1951 - June 2007 based on daily weather data recorded at Canberra Airport.

The patterns for both mean daily R_N and T_A throughout a year are shown in Figure 8.2, suggesting an earlier start to all seasons in the annual cycle, about 22 days earlier than astronomical seasons. Mean daily R_N levels indicate a start of spring on 10 September (day 72) with the onset of higher variability in radiation levels, far earlier than the astronomical definition of 22 September (day 91). The onset of summer on 1 December (day 163) coincides with a marked observed levelling off in mean daily R_N. Based on mean daily R_N, the onset of autumn would occur on or about 1 March (day 253) but the onset occurs much later in fact a whole 27 days lag when the factor of landscape heat storage is taken into account. The average daily temperature pattern is ill-defined but suggests that autumn could start close to 1 April (day 283).

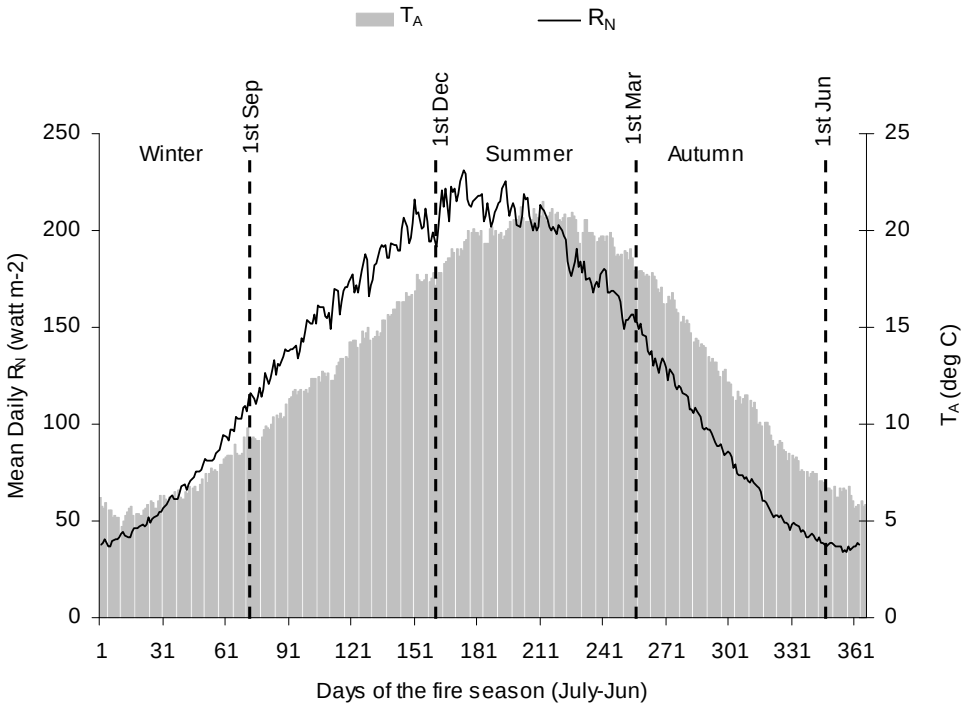

Figure 8.2 Meteorological breaks in the annual cycle in relation to daily all-wave net radiation (R_N) and mean daily temperature (T_A) for Canberra Airport

For all practical purposes, the astronomical definition of the spring equinox best defines the start of spring on 22 September, while a combination of meteorological and the astronomical considerations would define the onset of summer between 13 and 15 December and the end of the summer somewhere between 1 March and 1 April. Thus, the definitions of the start and finish of each fire season are not clearly defined using mean daily R_N or daily T_N.

8.1.2 The fire season calendar defined by fire susceptibility indices

A natural question to ask is how much do fire seasons differ from those predicated on astronomical or meteorological definitions. The criteria used in fire season definition were the longer-term seasonal index of landscape dryness (SWD) and two short-term daily potential fire spread indices, FFMC and FWI using records from 1951 to 2007 to be consistent with the length of the time series used in the medium-term analyses in this chapter. The FWI was scaled to that of the FFDI to facilitate comparison and was designated SFWI to distinguish it from FWI. Mean daily SWD and mean daily SFWI were plotted separately in Figure 8.3 (a) to delineate their influences on seasonality. Comparisons can be made between seasonal breaks delineated by soil dryness and by potential fire spread indices as shown in Figure 8.3 (a), with seasonal changes indicated by overlaying mean daily FFMC and mean daily SWD, as shown in Figure 8.3 (b). Figure 8.3 allows a simple comparison to be made between the seasonal positioning of these three key indices. Vertical grey dotted lines indicate the astronomical

seasonal boundaries, while vertical dashed lines demarcate seasons defined by fire susceptibility criteria. The breaks in the fire seasons are principally related to significant changes in the average SFWI, indicated by the horizontal dashed lines in Figure 8.3 (a). For instance, the start of the peak period in the fire season is marked by a sudden increase in FWI on 8 December and a sudden decrease on 10 February. From a fire perspective, there are clearly five distinctive seasons, not the four familiar seasons defined by consideration of astronomical and meteorological conditions alone (Table 8.1).

The main inference drawn from this analysis is that the 'typical' or 'average' fire season falls between 22 September and 28 April. The peak period of landscape susceptibility to large fires occurs between 8 December and 6 February, followed by a period when landscape scale fires may still occur, termed here 'late summer' that ends on, or about, 28 April. The definition of the fire season provided by Luke and McArthur (1978:15) did not specify which months comprised the highest fire season risk and did not delineate the different seasons and their duration in the fire season year. Based on this study, the fire season can be much more clearly defined and is presented here as a 'fire season calendar' (Table 8.1) applicable to the ACT region.

Table 8.1 Fire season calendar based on long-term seasonal dryness and potential fire spread criteria

Season	Start date	Finish date	Levels of landscape susceptibility to large fires
Winter	27 June	21 September	Low
Spring	22 September	7 December	Moderate, but sometimes high and rising towards the end of this period
High summer	8 December	6 February	High to very high and occasionally extreme
Late summer	7 February	28 April	High to very high and moderating gradually towards the end of this period
Autumn	29 April	26 June	Low to moderate and occasionally high

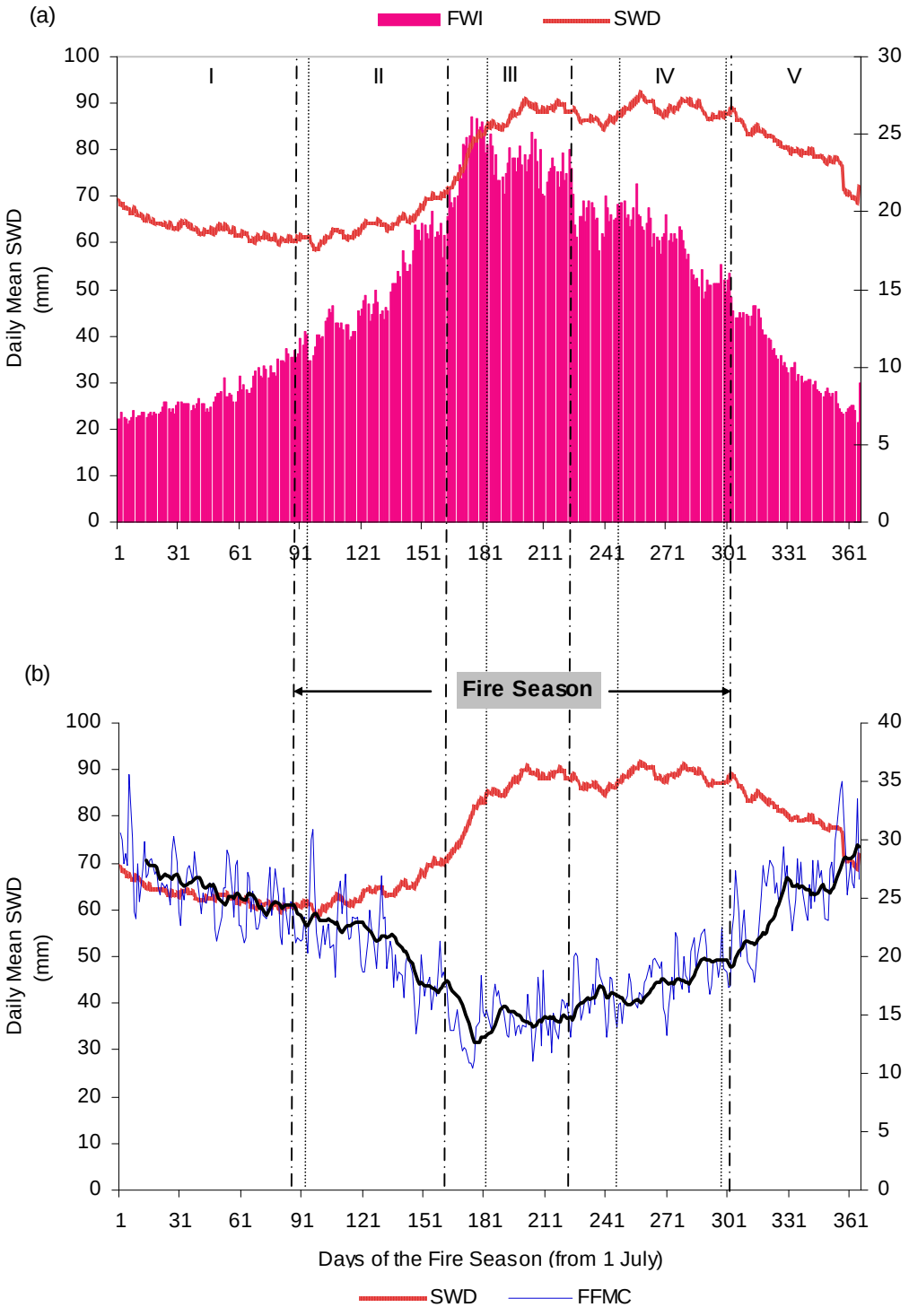

Figure 8.3 Seasonal markers in the fire season, based on fire susceptibility criteria (mean daily SWD, FFMC, and SFWI) with seasonal breaks previously derived in section 8.1.1

Source: Mean values of indices derived from spreadsheets of landscape dryness and potential fire spread in Appendix 1. Period of analysis is July 1951 - June 2007.

Notes: (1) Vertical dashed lines indicate seasonal breaks based SWD, SFWI and FFMC; while vertical dotted line show breaks based on mean daily R_N and temperature. The horizontal dashed lines indicate key values of mean daily FWI or FFMC.

(2) The Roman numerals refer to the seasons as follows: I-winter, II-spring, III-high summer, IV-late summer, and V-winter.

8.2 Classification: medium-term landscape dryness

The purpose of this section is to examine first the natural range of variation in daily landscape dryness in a fire season and second to classify the annual profiles of landscape dryness based on the medium-term SWD index into discernible types and sub-types. The medium-term SWD index is derived from the RSDI (section 6.1.2) from weather data at Canberra (Chapter 4) and models of all-wave net radiation and potential evaporation (Chapter 5).

8.2.1 Average seasonal variation in medium-term landscape dryness

A general seasonal pattern of soil water deficit is discernible from the individual profiles of all the years from 1951 to 2007. The first aim of this analysis is to illustrate both the average and the full range of variation in the annual profiles of SWD from the start of the time series. The second aim is to ensure that the intra-fire seasons defined earlier (section 8.1.2) are consistent with the breaks evident in the box plot-daily cycle routine based on the full range of potential variation rather than just on the mean daily SWD used in the analysis in section 8.1.2. The intra-annual variation of SWD is examined using a box plot diagram that produces (i) the daily median value of SWD throughout the year, (ii) the daily statistical variation from the median, in terms of quartiles and outliers for each day of the year in the annual cycle, and (iii) the daily extreme outliers. The box plot routine summarises the complete variation in the fire seasonal profiles of SWD in the medium-term time series. The next view of the seasonality of SWD is presented using an image plot of the seasonal variation in SWD for every fire season since 1951.

The daily SWD anomaly through the fire season (Figure 8.4) shows a wave-like pattern of the median daily SWD anomaly rising from a low in July-August to a high between the start of January and the middle of April. The sawtooth pattern represents the maximum and minimum values of daily SWD over the full course of the time series. The black areas represent the inter-quartile range that shows least variation in spring and early summer and most variation in the late summer period. There are recognisable variations in the daily median values of SWD that are mirrored in the extreme values. Outliers are most apparent in early to-mid-January, and in early February and mid-March. In early October, December and late January there are few outliers.

The ‘typical’ season starts in winter with a flat response until the winter/spring breakpoint, occurring around 13th September (day 84), nine days before the breakpoint established earlier (Table 8.1). Thereafter there is a rapid rise in SWD through spring until the 6th December.

Again, this is about nine days earlier than previously estimated. The high summer season corresponds to the period of driest soils; high median levels of SWD peak on the 31st January (days 215-216), six days earlier than the previously established break between high summer and late summer. From this point, there is a stepped flat decline in the SWD. This stepped decline relates directly to the onset of change in sub-tropical air masses that bring with it more stable synoptic patterns. This pattern persists until 17th April (day 309), which is nine days before that established earlier. The SWD thereafter declines rapidly until 30th June. The median SWD declines more gradually until the 31st July when the cycle finishes and starts again.

The first conclusion drawn from this analysis is that the mean annual profile of landscape dryness exhibits a distinctive pattern (Figure 8.4), despite the considerable variation evident in the 56 annual profiles (Figure 6.15: section 6.5). Figure 8.4 encompasses all of this variation in one graph and identifies the times of the year when weather and radiation patterns combine to produce drying out of soils in spring and earlier, followed by a relatively flat period in late summer, leading into a gradual decline of dryness during autumn. The peak in soil water deficit lies between mid December and mid April, indicating mainly dry autumns. Soil water recharge occurs mainly in winter (see Figure 6.15 and Figure 6.16, section 6.5), while spring is a period of soil evaporation, and plant transpiration and plant growth, when the soils generally have more soil moisture.

The second conclusion reached is that the breakpoints in the winter-spring, spring-high summer, high summer-late summer occur about six to nine days earlier than those previously derived in section 8.1.2, but overall are consistent with dates in the fire season calendar (Table 8.1). In addition, two notable breaks in the season are identifiable. The first is the spring-summer change that occurs on 6th December. The second is the late summer-autumn change that occurs towards the end of April. These start and finish dates form the principal part of the study region's susceptibility to LLFs. The high median values occur from mid to late January, which may mark the start of the period of the highest likelihood of LLFs. Large landscape fires may then occur anytime after that up until the end of April, depending on seasonal patterns of rainfall.

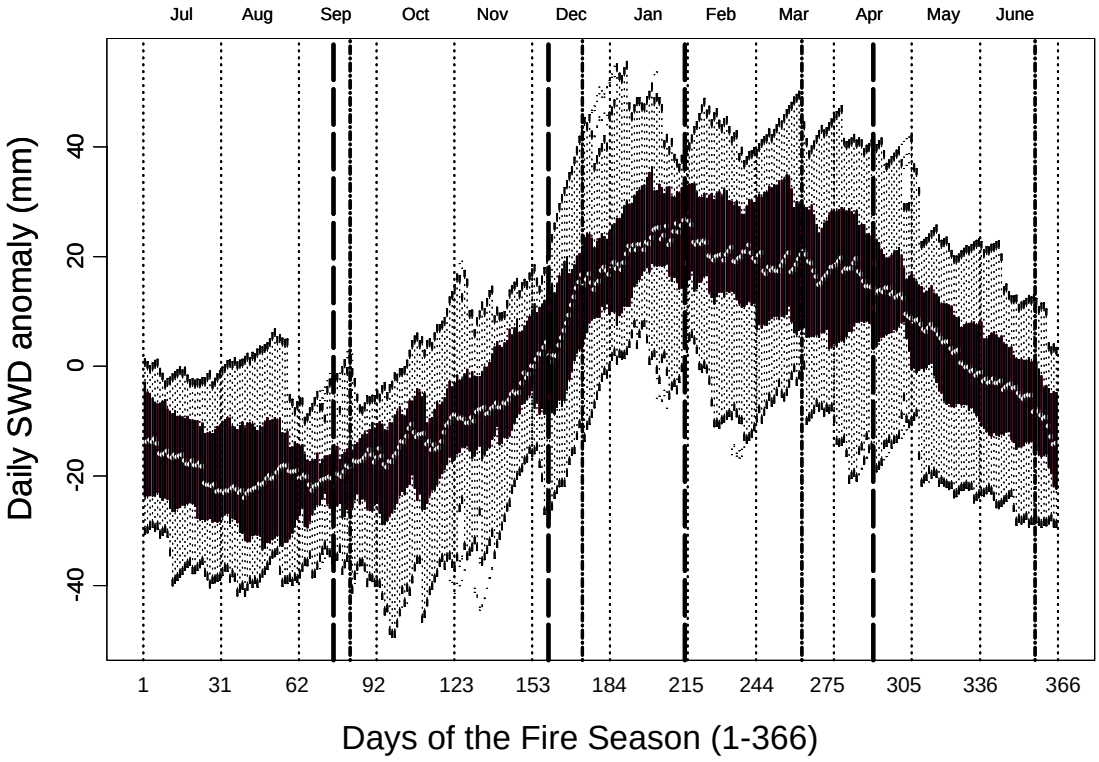

Figure 8.4 Daily SWD anomaly through the fire season (1951-2007)

Notes: (1) The strong vertical dashed lines represent seasonal markers indicated by SWD. The lines with dots and dashes indicate the seasonal markers defined by SWD, FWI, and FFMC (section 8.1.1). For context, the fine dotted lines represent the monthly periods in the annual cycle, starting in July and ending in June.

(2) The number of days in non-leap years is extended by one day to make a consistent 366 day annual fire season cycle for in the SWD time series.

8.2.2 Results: classification of landscape dryness by cluster analysis

The purpose in this section is to classify the fire seasons in the medium-term record of landscape dryness into recognisable types and sub-types using hierarchical classification. The intention is to classify fire seasonal profiles into sets that reflect different seasonal patterns of rainfall and levels of landscape dryness in the fire season calendar (Table 8.1; section 8.1.2). In addition, the extreme landscape dryness profiles should cluster into readily identifiable branches in the classification tree.

The results shown in this section were based on a classification of fire seasons 1951-2007. The period studied corresponds with the period of complete and homogenous weather data at Canberra Airport commencing on 1 July 1951 (see section 4.2.3).

A classification tree was produced using a hierarchical clustering method (Figure 8.5). Based on a detailed inspection of the classification tree, five major groups were discerned. Groups I and II are mainly moist fire seasons, although there are a few unusual years within Group II that have occasional very dry short peaks in either early or mid-summer. Groups III,

IV and V are the somewhat dry, periodically dry, and prolonged dry years in the SWD time series. The classification tree is ordered to show a gradual shift from moist to dry, from the left hand to the right hand side of the tree. The range in colours in Figure 8.5 is designed to represent the degree of and seasonality of landscape dryness in each of the types of fire seasons. However, in the middle of the classification tree two fire seasons do not follow this trend: the fire seasons in 1956/57 and 1964/65 were very dry.

The prolonged and severe dry years cluster into a set in Group V on the right hand side of the tree. These seasons experienced a dry period at the start of the season, becoming rapidly drier in spring, with the peak period occurring anywhere between the middle of December through to late January. The SWD peaks in early summer in two fire seasons (1957/58 and 1982/83) whereas the SWD peaks in the middle and late summer period between late January and early March (1967/68, 1997/98, 2002/03, 2006/07). All these fire seasons are characterised by a stepped decline in landscape dryness in late summer with an abrupt fall in late autumn. These severe fire seasons represent 2% of fire seasons since 1951.

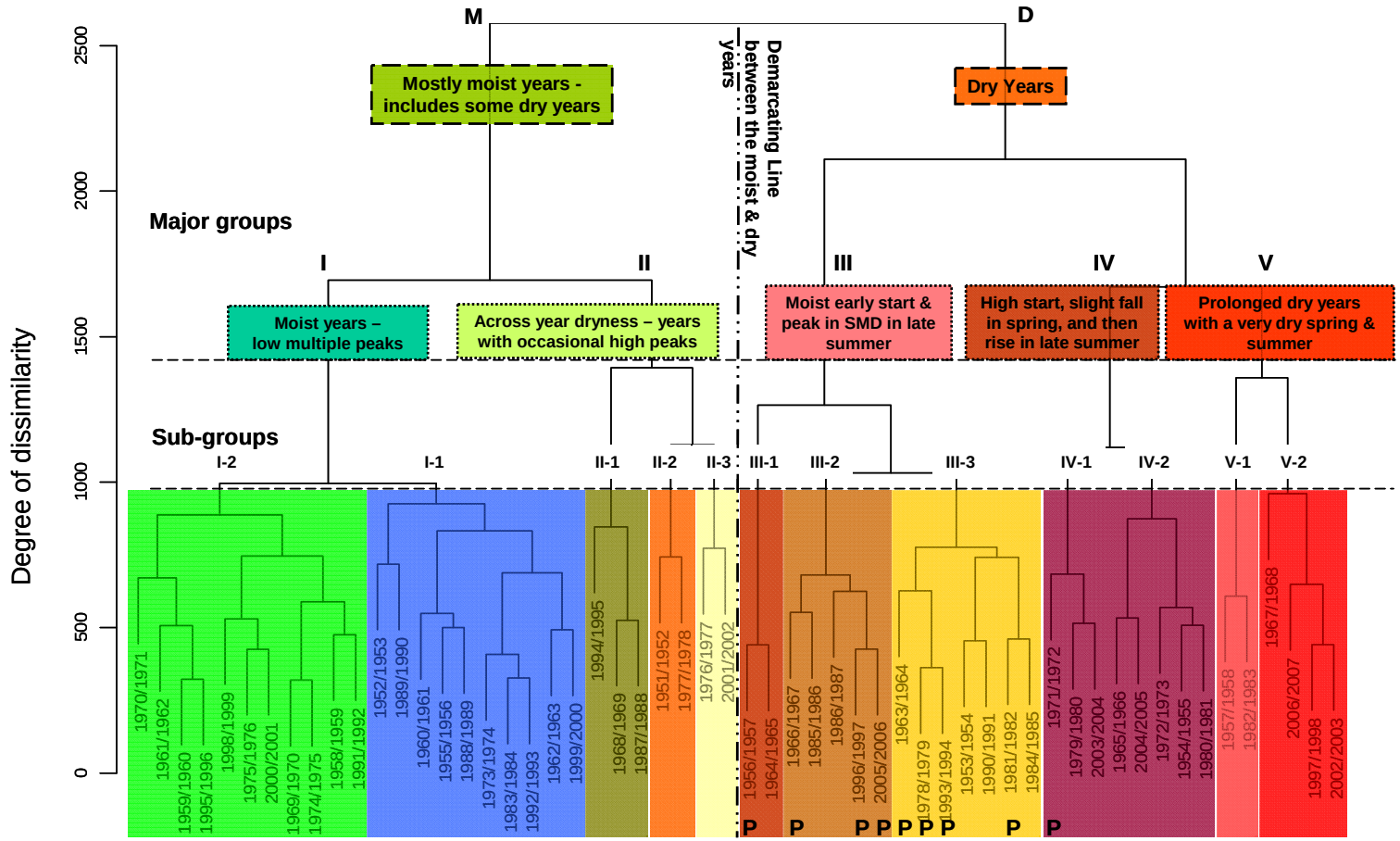

Figure 8.5 Hierarchical classification of fire seasons by annual profiles of soil water deficit (1951-2007)

Notes: (1) Soil water deficit is estimated by the RSDI model based on medium-term weather records recorded at Canberra Airport.

(2) The symbol P denotes fire seasons preceding a season with extreme values of soil water deficit, on most occasions indicated by a period of autumn dryness. This is a possible indicator of an approaching fire season with very high levels of landscape dryness.

Table 8.2 Fire season groups, based on daily SWD through solar year

Major group	Major group description	Sub-group	Sub-group description
I	Moist years with low multiple SWD peaks	I-1	Moist most of the year — values of SWD mainly below 75mm
		I-2	Moderate SWD values in early spring and then moderate to high values of SWD values in autumn
II	Single major seasons, culminating in peak dryness in early or mid-summer	II-1	Moderately dry SWD values across years in this class
		II-2	Dry spring and summer, major drop in SWD values in February
III	Preceding years in a dry sequence, with dry or very dry autumns (P)	III-1	Moist early start to season, finishing with a dry to very dry autumn
		III-2	Dry start in winter, build-up to peak in mid-summer and plateaus in autumn
		III-3	Moist at end of winter, grading into moderately dry in autumn – some high SWD values in mid summer within this sub-group
IV	High start, SWD usually maintained at moderate to high levels throughout year	IV-1	SWD values gradually decline from a high base at the start of the year to a moist end in autumn
		IV-2	SWD values usually stay at high levels throughout year, all the way into winter
V	Prolonged periods of high to very SWD	V-1	As above, but SWD values peak in middle of summer, abruptly ends in late autumn
		V-2	Very dry SWD values in spring and early summer, which then gradually tail off in autumn

Note: The majority of fire seasons that precede a major dry fire season classify into Group III.

The classification of the annual profiles of daily SWD values in the medium-term is listed in typology from moist years through to very dry years. The classes of groups and sub-groups relate closely to the sequences and levels of seasonal dryness or moistness during a fire season. The timing, relative number, and levels of the peaks of SWD characterise these groups, which have a meaningful typology that can be used to describe the current, and possibly anticipate the next, type of fire season. An example of this is the dry period in autumn and winter preceding a very dry fire season that causes a low level of recharge of soil water and hence a dry sub-soil in the lead-up to the dry summer period. In terms of the SWD groups, a group IV fire season presages a group V fire season. There are some very dry fire seasons though, such as 1951/52 and1984/85 that cannot be identified using the above method.

8.2.3 Classification: medium-term potential fire spread

This section deals with the hierarchical classification trees of potential fire spread based on the Standardised Fire Weather Index (SFWI), computed in a spreadsheet in Appendix 1 on the CD-ROM (section 7.4.2) and daily weather data at Canberra Airport (section 4.2.3). As in the previous section, the aim is to generalise the complex patterns in daily potential fire spread from year to year into recognisable and meaningful groups and sub-groups. Before undertaking this, a final choice had to be made as to which PFSI should be used (section 8.4.1) based on two criteria: a summarised seasonal comparison and an overview of the classification trees.

8.2.4 Selection of the preferred potential fire spread model

A Forest Fire Danger Rating System is recognised as the most useful and principal tool for assessing likely forest fire risk because it provides information about the temporal and spatial susceptibility of forests to fire in the short term (Taylor and Alexander, 2006). However, the short-term use of this tool is limited in its capability in anticipating landscape susceptibility to large fires. First, it combines the variable conditions of landscape dryness and fire weather into a single index for a constant set of landscape, vegetation, and fuel conditions. Second, its application relies on a forecasted daily or hourly component of fire weather that can only be predicted from a few days to one week in advance, so focussing on the immediate rather than the longer-term perspective. Third, in Australia, the understanding of the longer-term perspective of landscape dryness and potential fire spread in past fire seasons is not as highly developed as it is in other countries, such as North America, Canada, New Zealand, Portugal, Spain, France, Italy and Greece. Thus, this study takes the longer-term view of the potential risk and size of fires occurring in potentially flammable landscapes under worst-case fire weather conditions.

The preferred potential fire spread index was selected based on two comparisons:

(1) seasonal variation in the annual profiles,

(2) the structure of the classification trees of the two indices.

A LOESS filter of 51 days in length was first applied to both the SFWI and FFDI time series before undertaking a seasonal comparison of the two potential fire spread indices. LOESS is defined as locally weighted smoothing of values in a time series. The length of filter was based on a comparison of the effects of the 11, 21, 31, and 51-day smoothing filters on the standardised SFWI data. The 51-day filter was found to smooth the daily SFWI to best effect. Essentially, this filter retained the broad character of the annual profiles while removing finer shorter-term variation of less than one week.

Placing the annual profiles of daily potential fire spread anomaly of the two indices one above the other proved to be the best method of comparison (Figure 8.6 (a) and (b)). The two figures show the median (50^{th}), 25^{th} and 75^{th} percentiles as well as outliers for each day of the

year in the annual profile. The median FFDI, as well as 25th and 75th percentiles peaks up to one month earlier than those of the SFWI, which lies outside the peak fire season period defined earlier in section 8.1.1 and Table 8.1. Figure 8.6 (b) shows the highest values of potential fire spread of the FFDI generally occurring in spring and early summer. During the late summer period, the median FFDI also declines more quickly than the SFWI. The SFWI has a cumulative function in the availability of fuel, termed the BUI, which is a negative exponential function (Van Wagner, 1987) whereas the FFDI has a drought factor linearly scaled from 0-10, based on SWD and a days-since-rain function (Noble *et al.*, 1980). The different box plot profile produced by each PFSI suggests that the fuel availability functions in these potential fire spread indices exert a significant influence on the seasonal variation in the annual profiles. Hence, the different PFSI indicate significantly different timing of peak severity and a possible type I error in spring and a type II error in the late summer period, as shown in Figure 8.6.

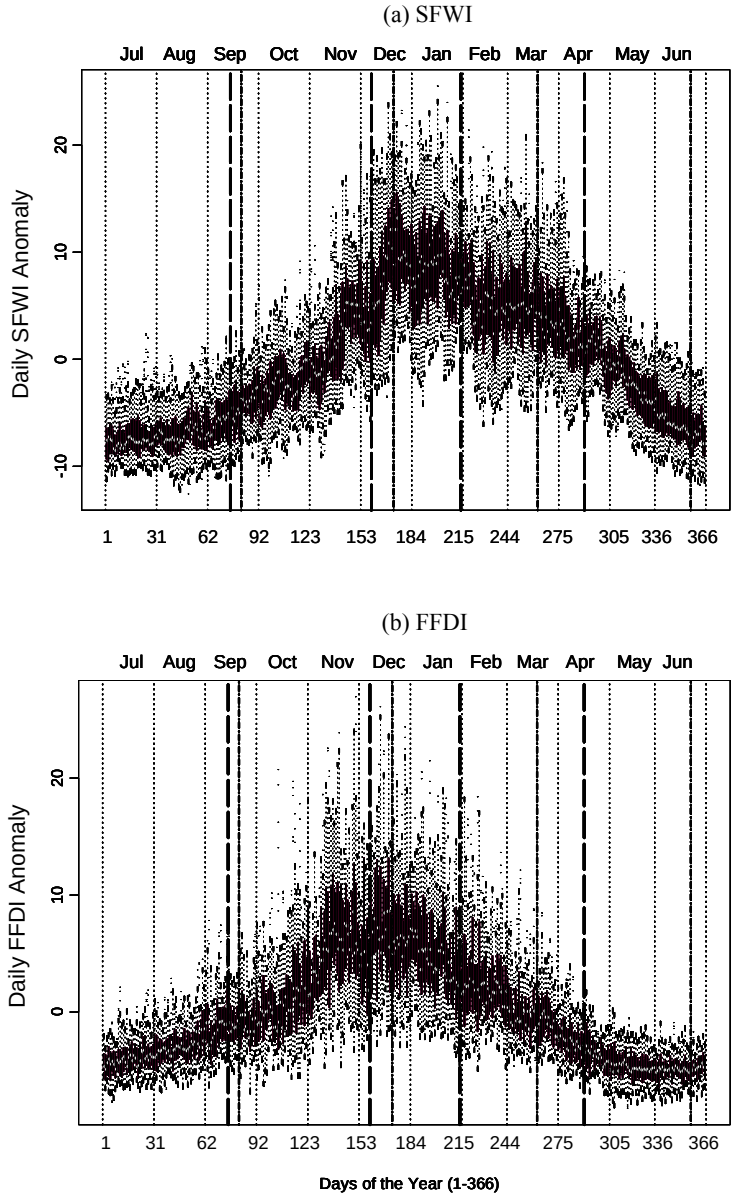

Figure 8.6 Annual profile of (a) SFWI and (b) FFDI daily anomalies

Note: Comparison of the intra-annual variation in fire spread potential is based on daily data from 1951 to 2007.

The next comparison of the two potential fire spread indices is based on the branching pattern of the clusters in the classification trees of the two indices (Figure 8.7). The standardised Fire Weather Index is chosen over the FFDI for three reasons. First, some of the fire seasons with extremes of potential fire spread, such as 1957/58, 1982/83 and 1997/98, appear in a separate sub-tree at a very high level in the FFDI classification tree. This cluster is distinctly separate from the other similar fire seasons with high and sustained values of FFDI, in the first cluster on the left hand side of the classification tree (Figure 8.7 (b)). In the case of the SFWI, these fire seasons cluster in with the rest of the fire seasons at a lower level in the classification tree. Second, some of the fire seasons do not appear to group in a logical way. For instance, two very different seasons in terms of SWD grouping classify together in the FFDI: 1974/75 belongs to SWD group V whereas 1993/94 belongs to group III.

In contrast, the classification of SFWI produces a more balanced and hierarchical classification tree. The more severe fire seasons are found in one branch of the classification tree, which includes the three severe seasons that grouped together separately in the FFDI classification tree.

Based on these findings, the classification of annual profiles of potential fire spread will be based on the SFWI, which appears to better model the seasonality of potential fire spread and hence potential fire spread in the peak and late summer periods in the fire season calendar. This is in contrast to the FFDI's modelled potential fire spread that occurs earlier in late spring and early summer. This conclusion is in agreement with an earlier finding, reported in section 7.1, that the linear model embedded in the Drought Factor within the FFDI may produce an earlier occurrence in the peak of seasonal potential fire spread severity. In this case, once the SWD exceeds 100 mm, there is no further increase in the landscape dryness factor. Interestingly, this value corresponds to the threshold at which fuel availability and flammability were also found to change (see section 7.3). Hence, the modelling of landscape dryness over that threshold may not indicate any further changes to fuel connectivity, availability and flammability, which may be key factors in the predisposition of a landscape to larger and more severe LLFs. This is an issue for future research into the possible effect of the embedded Drought Factor (DF) on fuel availability and potential combustibility.

(a) SFWI

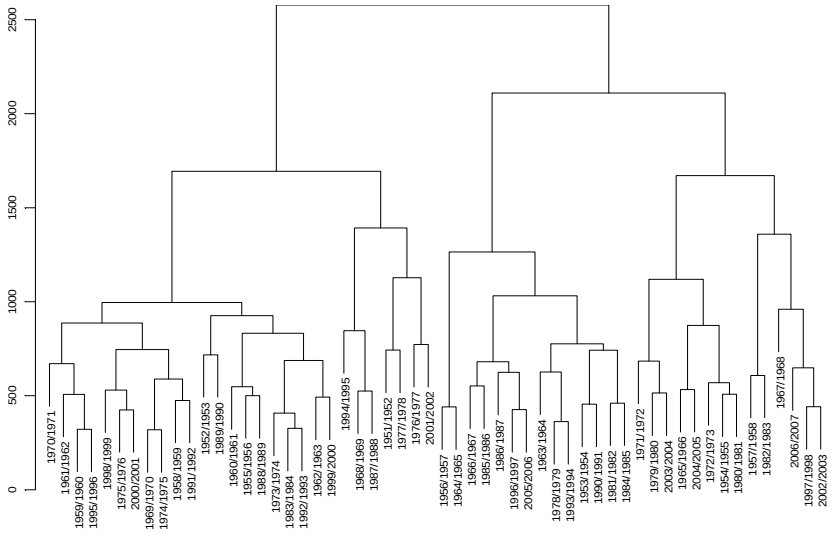

(b) FFDI

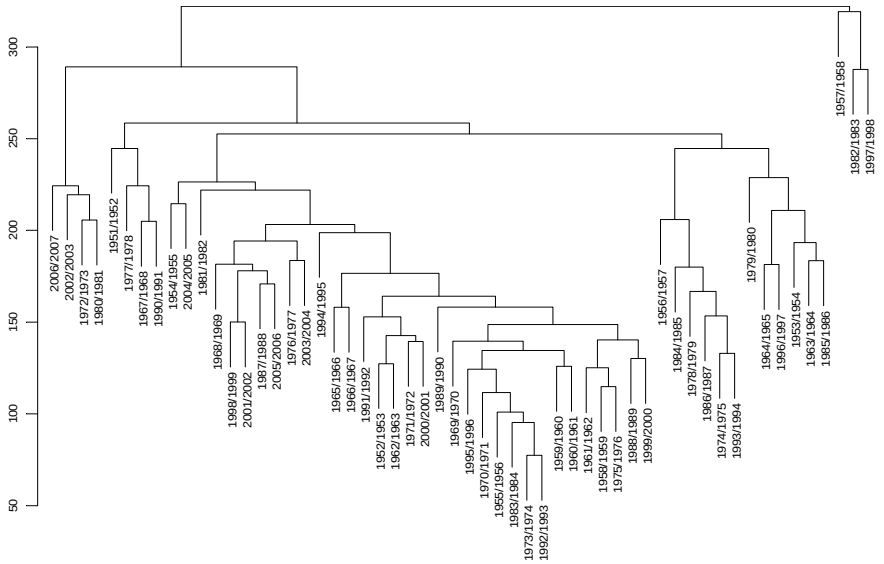

Figure 8.7 Comparison of classification trees of (a) SFWI and (b) FFDI

8.2.5 Classification: annual profiles of medium-term potential fire spread index

This section deals with the classification of the annual profiles of potential fire spread, using the standardised fire weather index (SFWI) to identify fire seasons that could have had a high landscape susceptibility to large fires.

The classification of the annual profiles of SFWI was based on a smoothed standardised SFWI, minimising variability in the daily SFWI and responding quickly to changes in fine fuel moisture, wind speed, and slope for any given level of fuel availability (BUI).

In the classification tree of potential fire spread (Figure 8.8), SFWI is broadly divided into two classes: an ‘S’, seasons with severe potential fire spread, and an ‘M’, seasons with low to

high potential fire spread. Employing a value of ~290, on a scale of 100 – 400, the cutting of the SFWI classification tree at that level, produces seven distinct SFWI fire season categories (I to VII). SFWI groups VI and VII are more similar to each other than the other SFWI groups.

Class S -- severe fire season class -- represents years when the SFWI was extremely high and where soils (high SWD) were extremely dry (groups I to III). This class contains five out of the seven years classified into SWD group V, suggesting close correspondence between the two classifications. The fire seasons in this class with the greatest potential for large landscape fires were: 1957/58, 1977/78, 1982/83, 2002/03 and 2006/07.

The 'M' class contains low to moderate fire seasons with high values of SFWI occurring in short periods in either late spring, early summer, or autumn, or a combination of all three (groups IV to VII) without the sustained levels of potential fire spread found in the 'S' class of fire seasons.

Interestingly, group IV contains some very dry years belonging also to SWD groups III and IV. This group contains seasons with moderate to high potential for large landscape fires. Group V fire seasons are characterised by low values of SFWI for most of the year, with some occasional short periods of moderate to high SFWI. Most of the fire seasons in this group are located in SWD group 1 (20 out of 22). The dampening effect of low to moderate SWD likely decreased the potential for large landscape fires in most of these fire seasons. Group VI contains three significant fire seasons (1951/52, 1978/79, 1984/85), which had very high to extreme SFWI values in the later half of the peak fire summer period following a rapid build-up of landscape dryness from spring into summer. Group VII is a highly heterogeneous group of eleven fire seasons that do not readily classify into recognisable patterns of SFWI during the year.

The different groups can be distinguished on the following criteria:

- frequency and amplitude of the pulses of SFWI values through the season;
- the timing and duration of the more extreme periods of SFWI, and
- the timing and relative power of the peak potential fire spread days.

A description of the fire season SFWI groups is presented in Table 8.3.

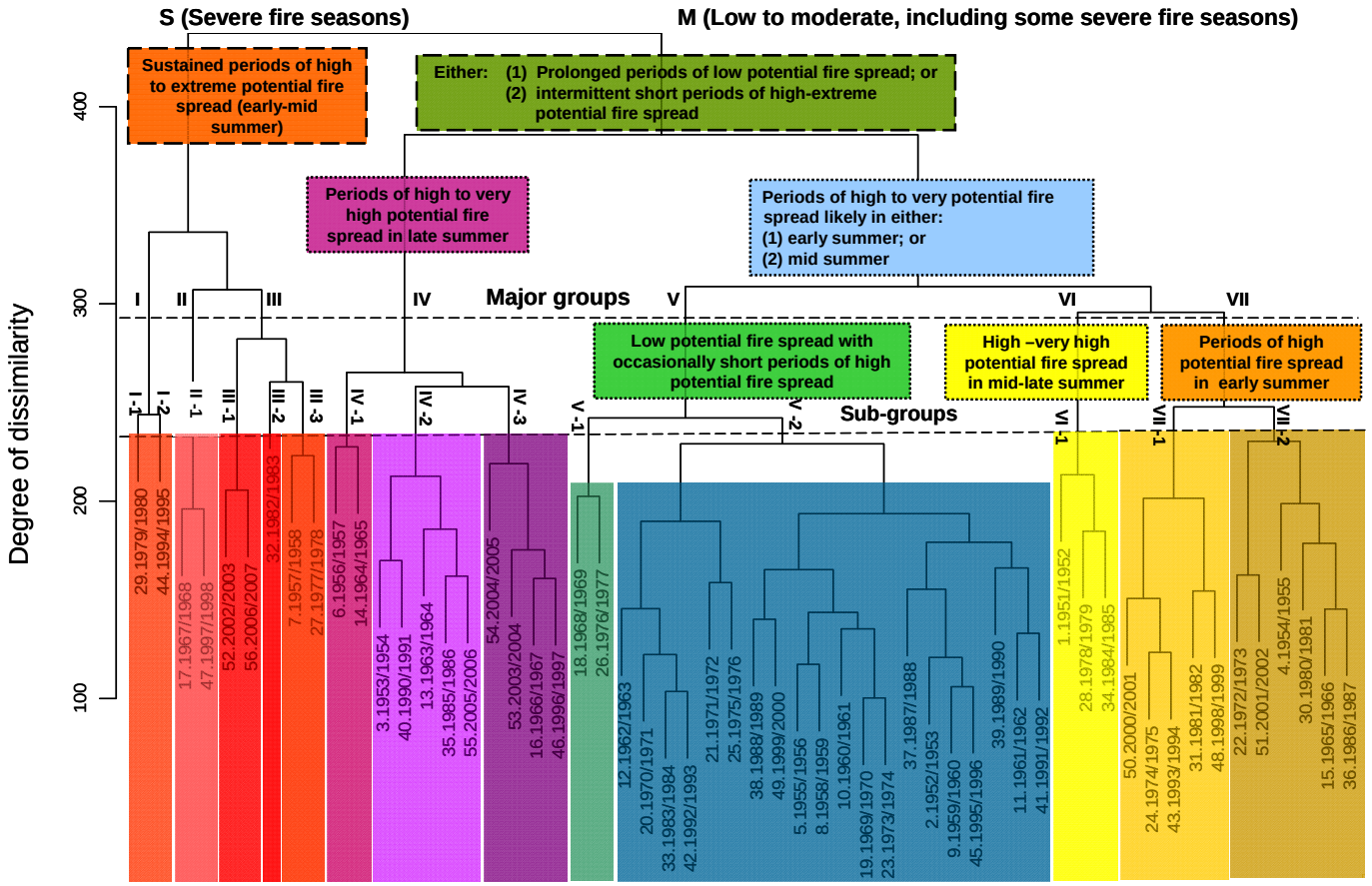

Figure 8.8 Fire season classification based on SFWI index of potential fire spread (1951-2007)

Notes: (1) The time series of SFWI was smoothed using a LOESS smoother of 51 days to enhance the differences in the PFSI annual profiles.

(2) The colours are designed to reflect fire seasons with differing potential for large landscape fires in early to late summer. For instance, shades of red indicate groups and sub-groups of fire seasons with the highest potential for LLFs. At the other end of the scale, shades of blue indicate groups and sub-groups of fire seasons with the lowest potential for LLFs.

Table 8.3 Groups of Fire Seasons, based on annual SFWI profiles

Class	Major group	Major group description	Sub-group	Sub-group description	Fire seasons
Mainly severe fire seasons (S)	I	Dry years with sustained high SFWI values – sometimes severe to extreme	I-1	Very high SFWI values between late spring and early summer. Periodic high values of SFWI values from high summer through to early autumn	1979/80
			I-2	Fortnightly episodes of high to very high SFWI from spring to mid summer with high to very high SFWI values between late March and early May	1994/1995
	II	Very dry years with frequent peaks in SFWI up to very extreme, likely to occur in either early or late summer	II-1	Gradual build-up of SFWI values from early spring to mid-December in a series of fortnightly to three weekly high spikes in SFWI values. Lull in early January followed by another late summer period of very high to extreme SFWI until April	1967/68, 1997/98
	III	Very dry years with much broader periods of very high to extreme SFWI, based on the early or middle summer period	III-1	Sustained values of SFWI occur across most of the fire season with monthly spikes of very high SFWI values from September onwards. Near-extreme and extreme SFWI values are found in spring and high summer. Major decline in SFWI values in autumn	2002/03, 2006/07
			IIII-2	Later start to very high SFWI values than in subgroup III-1, starting in early November and peaking in late December. Frequent spikes in SFWI values until late March	1982/83
			III-3	A set of heterogeneous years — mainly characterised by extreme SFWI values from mid October until the end of December. Some occasional spikes of very high SFWI values from late January onwards, gradually receding by early April	1957/58, 1977/78

Table 8.3 continued

Class	Major group	Major group description	Sub-group	Sub-group description	Fire seasons
Low to moderate potential fire spread (M) with some occasionally severe fire seasons	IV	Late summer and early autumn periods of very high SFWI, occurring in short frequent blocks	IV-1	Low SFWI values in winter and spring. SFWI values are high to very high from high summer onwards, with occasional short periods of very high to severe SFWI values in late summer, either breaking early in late February or April. Moderate to high SFWI values occur until the end of autumn	1956/57, 1964/65
			IV-2	High to very high SFWI values usually from early to mid December until mid-late May, with some occasional severe SFWI days in the frequent moderate to high SFWI peaks in values characteristic of this group	1953/54, 1963/64, 1985/86, 1990/91, 2005/06
			IV-3	High to very high SFWI days from late November occur until the end of May. SFWI values increase slightly into autumn in some cases	1966/67, 1996/97, 2003/04, 2004/05
	V	Low SFWI usually throughout season with some occasional bursts in either early or mid-summer	V-1	Low to moderate SFWI values in both autumn and spring with some very high SFWI levels in high summer	1968/69, 1976/77
		Low power in season over most of the year, with a few exceptions	V-2	Low to moderate SFWI values throughout the year but with some occasional short spikes up to very high SFWI levels in high or late summer	1952/53, 1955/56, 1958/59, 1959/60, 1960/61, 1961/62, 1962/63, 1969/70, 1970/71, 1971/72, 1973/74, 1975/76, 1983/84, 1987/88, 1988/89, 1989/90: 1989/90; 1991/92, 1992/93, 1995/96, 1999/2000
	VI	Years with very high power in mid summer, usually between late January and mid February	VI-1	Low SFWI values are found in winter, early spring and autumn periods. Some very high SFWI values on occasional days in the high and late summer periods of the fire calendar	1951/52, 1978/79, 1984/85
	VII	Highly heterogeneous group of years, with a low to moderate SFWI until mid November	VII-1	Usually a broad spike of SFWI values in early to mid summer, with occasional sporadic high SFWI days in late summer	1974/75, 1981/82, 1993/94, 1998/99, 2000/2001
			VII-2	A heterogeneous group that has some significant SFWI days in mid-summer in some seasons, otherwise difficult to characterise	1954/55, 1965/66, 1972/73, 1980/81, 1986/87, 2001/02

8.3 Temporal variability of potential fire spread

Sections 8.2 and 8.2.3 of this chapter have shown how SWD and SFWI can be used to identify which fire seasons have had the highest potential for Large Landscape Fires (LLFs) on an annual basis. In this section, the inter-annual variability of fire seasons is explored in more detail (section 8.4.1) using the classification based on potential fire spread (section 8.2.5). The index of potential fire spread is further analysed in section 8.4.2.

8.3.1 Year-to-year variation in the potential for LLFs based on potential fire spread index

The purpose of this section is to examine and illustrate the year-to-year variation in potential for LLFs based on an annualised index of the FWI that is termed the annual severity rating (TDSR). TDSR is based on the sum of daily severity rating (DSR) summed for each year in the time series to indicate the past severity of fire seasons. The year-to-year variation is best illustrated using the recommended TDSR index to assess the potential for LLFs on either a monthly or a yearly basis.

To put the classification into a time sequence, two adjacent diagrams are required (Figure 8.9):

(1) the classification of the SFWI fire season groups developed in section 8.2.5 and rated according to their TDSR (Figure 8.9 (b)); and

(2) the chronological sequence of the SFWI fire season groups showing the variation in TDSR through time (Figure 8.9 (a)).

TDSR is rated from very high-to-extreme (shades of red), to very high (shades of purple), through to moderate-to-high (orange, yellow, and green). The measure of annual TDSR is used to distinguish the different SFWI groups in terms of the landscape potential for large fires.

SFWI groups I, II and III represent fire seasons far more severe than groups IV, V, VI, and VII (Figure 8.9 (b)).

The reordering of the classification, as is presented in Figure 8.9 (a), shows that the annual severity rating (TDSR) for each SFWI group closely reflects landscape dryness and potential fire spread conditions that give rise to varying potential for LLFs. Severe fire seasons where TDSR exceeded >15000 also line up with the strong El Niño years of 1951/52, 1957/58, 1964/65, 1979/80, 1982/83, 1997/98, 2002/03 and 2006/07. These fire seasons were presaged by mainly SFWI group IV fire seasons in the preceding year, indicated by open circles in Figure 8.9 (a).

Fire seasons giving rise to the highest potential for LLFs have occurred eight times in the past 56 years at intervals between three and ten years apart. The sequence shown in Figure 8.9 (a) also suggests that these severe fire seasons can follow one another at relatively short

intervals, and be followed by a significant gap thereafter. Generally, the more severe fire seasons in the ACT region are generally associated with El Niño events (see Figure 9.4 (a)). However, on occasions (for example 1951/52, 1984/85) a narrow subset of fire seasons can have short bouts of severe conditions of landscape dryness and potential fire spread that are not linked to El Niño. This would imply that continental scale interactions of climate and weather might play a role. For further discussion on the synoptic scale climatic factors on landscape susceptibility to large fires, see Chapter 9 (section 9.4.2).

8.4 Defining the thresholds and timing of extremes of fire susceptibility

The previous sections have revealed that there has been a strong temporal structure of timing and severity of fire seasons since 1951, based on two susceptibility indices, SWD and SFWI. This section examines two aspects of fire susceptibility by combining these two susceptibility factors. The first aspect is the thresholds at which a changed state in landscape conditions might be associated with a high to extreme risk of severe fire weather, leading to very high to extreme conditions of potential fire spread. This threshold (SWD>100mm) has also been identified in the literature (section 7.3). The second aspect is confirming that highest potential for LLFs did indeed occur in the most severe fire season groups in the high summer months.

The first step involved deriving the thresholds for monthly mean SWD and monthly total DSR (MDSR) (section 8.5.1). In section 8.6.2, the thresholds defined in section 8.5.1 are then used to determine the monthly occurrence of combinations of above the threshold values for landscape dryness and potential fire spread for each of the SFWI groups. Lastly, the timing of the extremes of potential fire spread is examined on a daily rather than a monthly basis (section 8.5.3).

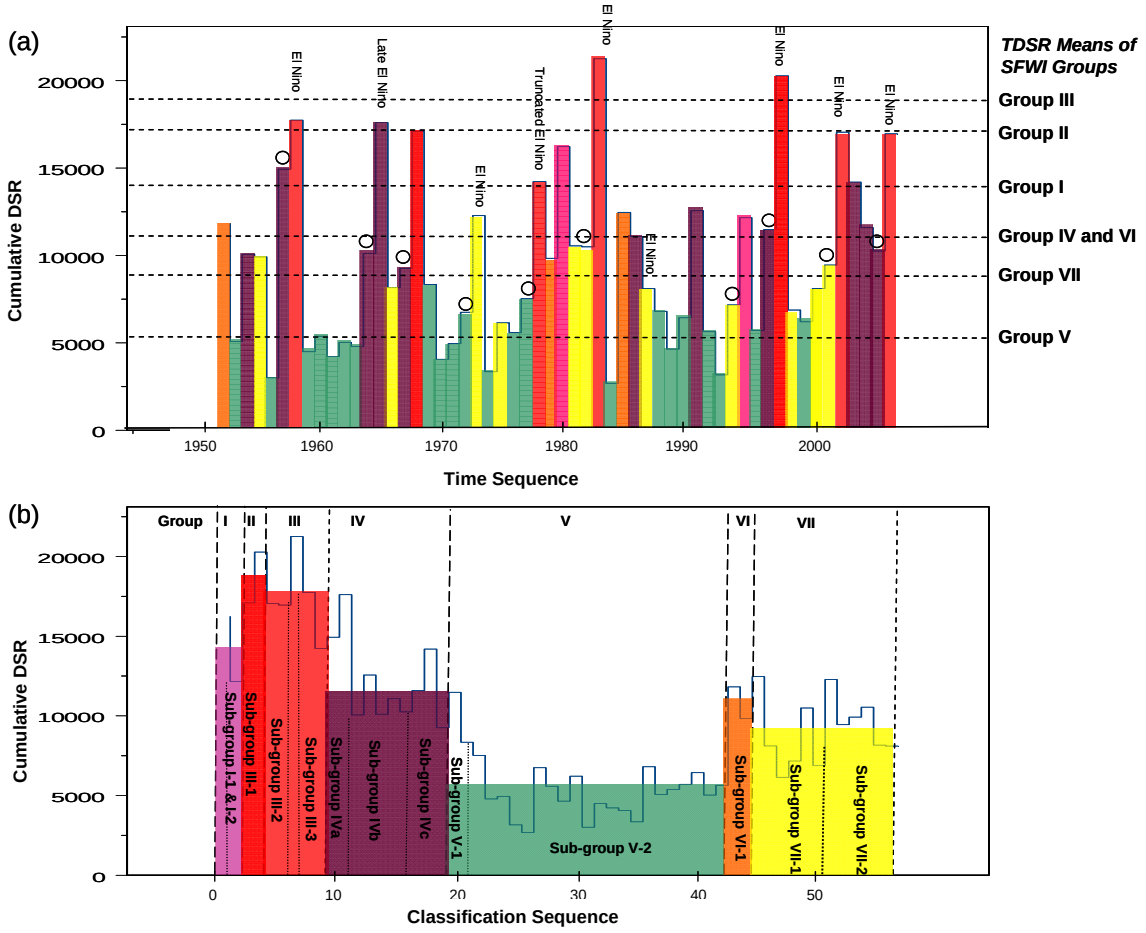

Figure 8.9 Temporal sequence (a) and classification (b) view of fire seasons (1951-2007).

Notes: (1) Open circles represent fire seasons antecedent to more severe fire seasons. The horizontal lines in (a) relate average values of TDSR in each of the SFWI groups to the individual values for each fire season.

(2) For further information on El Nino years, refer to section 9.1.2, and in particular the seasonal patterns of Southern Oscillation Index (SOI) revealed in Figure 9.4 (a).

8.4.1 Seasonal monthly extremes of fire susceptibility

The purpose of this section is to determine the likelihood of the combination of extremes of landscape dryness and potential fire spread in any given month of an ACT fire season, based on the setting of threshold values for each of these factors.

The first stage in examining seasonal monthly extremes of fire susceptibility involved determining the thresholds of monthly mean SWD (MSWD) and monthly total DSR (MDSR). This involved two steps. The first step was to set a threshold for MDSR based on difficulty of control. The second step involved setting a threshold of MSWD based on a visual inspection of these two indices by months in the fire season. Once these thresholds were determined, the second stage involved examining the frequency of the combination of extremes in each month of the fire season. The final step in this stage involved assessing the frequency of the extreme combinations of landscape dryness and potential fire spread in each of the months within each of the SFWI groups.

To identify the threshold of MDSR which best represented the division between the more and less extreme values of FWI, MDSR values equal to 600 and 1200 were marked onto a graph of mean monthly values of MDSR for 1951-2007 (Figure 8.10). A MDSR equal to 600 -- equivalent to a value of mean monthly FWI value equal to 42 – is therefore used as a threshold between potentially unmanageable fires and those that might be controlled. An FWI equal to 40 is considered in other studies to be the threshold at which fires can become highly uncontrollable, usually associated with sustained crown fires (Van Wagner, 1977; Good *et al.*, 2008).

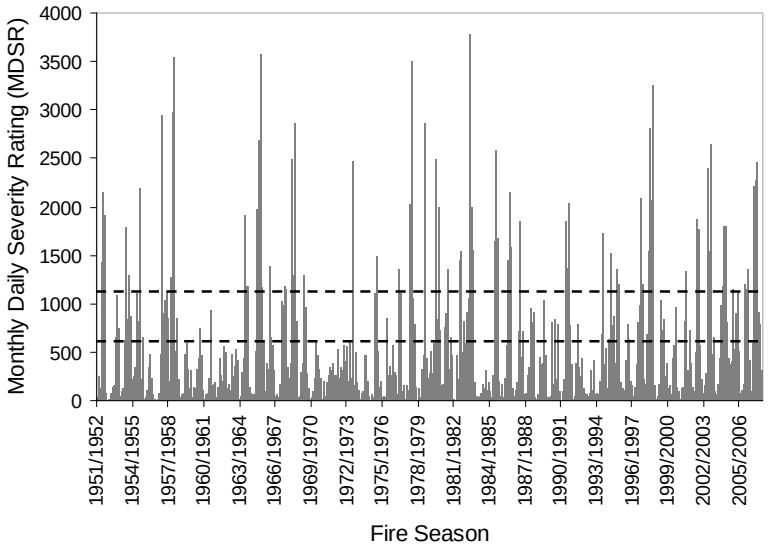

Figure 8.10 Thresholds of Monthly Daily Severity Rating juxtaposed against monthly severity rating values (1951/52-2006/07)

Note: The two horizontal lines indicate possible threshold values for the potential risk of large landscape fires in a given fire season.

Earlier in section 7.3, a SWD of 100 mm was found from the literature to be a possible critical threshold at which there is a sudden change to higher fuel availability and more flammable fuel and vegetation conditions. To confirm this threshold, matched monthly values of MSWD and MDSR were plotted against each other (Figure 8.10). The thresholds of SWD=100 and MDSR=600 were used to define those months when landscapes were most susceptible to severe fires.

Three distinct groups of months can be identified from the twelve panel plots. The first group of months, the traditional winter months of June, July, August, show an almost flat response of MDSR to changes in MSWD. The next group of months, April, May, September, and October, exhibit a slightly stronger response of MDSR to MSWD, particularly above the MSWD threshold value of 100 mm. A higher fire spread potential exists in April than in the other three months in this group. November, December, January, February, and March comprise the months that have had the highest landscape susceptibility to large fires. With the exception of November, these months comprise the high summer and late summer periods in the ACT's fire season. Note also that the late summer period also comprises April, which can have occasional months with a high potential for large fires if the landscape dryness is well above 100 mm (SWD >120mm).

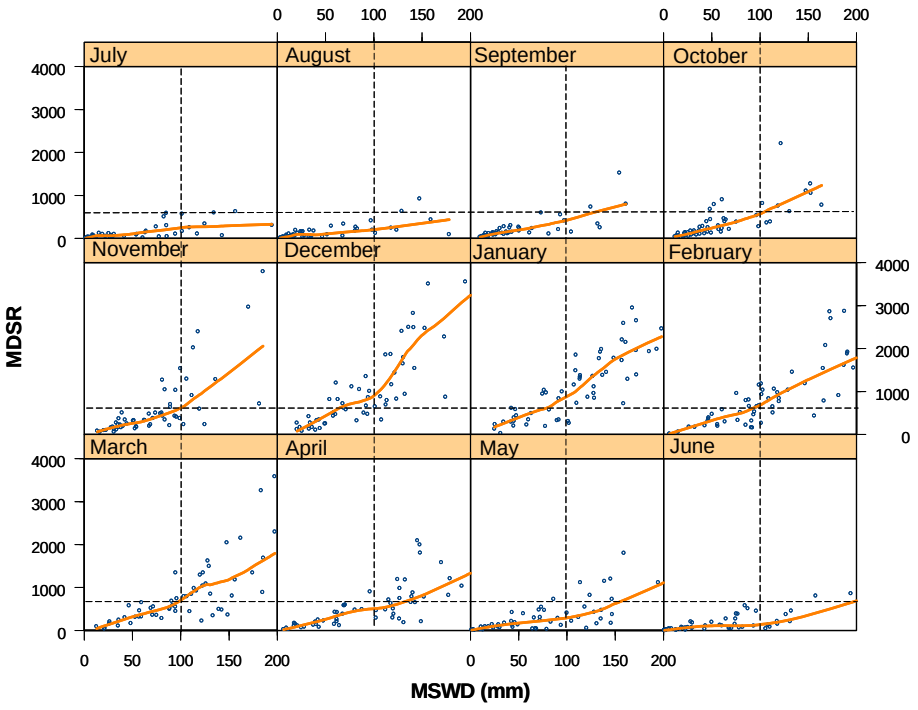

Figure 8.11 Thresholds of fire susceptibility based on mean monthly values of landscape dryness and potential fire spread

Note: (1) Thresholds of MSWD>=100 mm and MDSR>-600 was set respectively for critical landscape dryness and potential fire spread, respectively, to capture the more extreme monthly potential for large fires.

Based on this visual interpretation of the spread of the extreme months (November-March), a threshold of MSWD greater than 100 and MDSR greater than 600 encompasses most of the monthly records of landscape susceptibility to large fires. The month of January stands out as having the highest number of months (24 occasions) when the combined thresholds of landscape dryness and potential fire spread have been exceeded (Figure 8.12). The month of December is the next most frequent (15 occasions) followed by February and March (10 and 11 occasions respectively). This finding supports the earlier finding that LLFs are more likely to occur in the high summer and late summer between early December and early April (Table 8.1 ; section 8.1.2) with a peak in January. Outside of these high-risk periods, there have been on six occasions when very high to extreme potential for LLFs existed in either April or November.

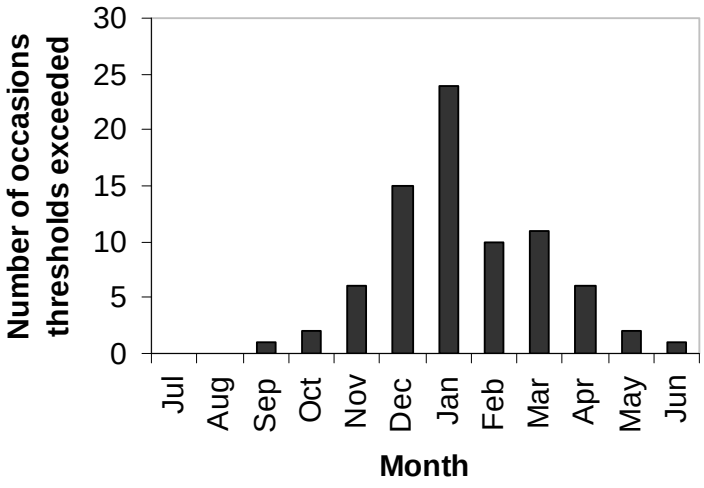

Figure 8.12 Frequency of occasions when thresholds of landscape dryness and potential fire spread have been exceeded (1951-2007)

To find out more specifically in which fire season group there is the highest potential for LLFs, extreme combinations of MSWD and MDSR were extracted from the monthly time series, using threshold values of MSWD≥100 mm and MDSR≥1200 (Table 8.4). An MDSR of 1200 corresponds to an average value of FWI equal to 60. This threshold value corresponds approximately to an FFDI value of 50, which defines the start of the extreme part of the FFDI scale between 0 and 100.

SFWI groups II and III have the highest monthly means of MSWD and MDSR (SWD = 170,166; MDSR = 2251, 2253 respectively) of the SFWI groups. SFWI Groups II and IV has equivalent values of MSWD but slightly lower MDSR (SWD=170,160, MDSR=1902, 1991) but spans a longer period of the year. The month of January stands out as most frequently

exceeding the selected values of landscape susceptibility thresholds in all these groups (24 months) followed by December (15 months).

Occurrences of above threshold values of MSWD and MDSR can occur in any SFWI group but the indices are highest for groups II and III when landscapes are highly predisposed to high susceptibility to LLFs, with some potential for LLFs in groups VI and VII. In all of these groups, a very high landscape susceptibility to LLFs has occurred relatively infrequently (~12% of months between 1951 and 2007). Additionally, landscape susceptibility to LLFs in the ACT region has occurred during the high summer period between December and February on a total of 38 months in the same period (~6.0% of all months between 1951 and 2007).

Table 8.4 MSWD and MDSR values corresponding to months exceeding threshold values by SFWI groups

SFWI Group	Months	Number of Months	MSWD value (mm)	MDSR value
I	September	1	154	1527
	December	1	136	2496
	March	1	129	1498
	April	1	148	1995
		4	**142**	**1879**
II	December	2	141	2656
	January	2	167	1621
	February	2	178	2471
	March	2	191	2777
	April	1	179	1211
		9	**170**	**2251**
III	October	2	137	1739
	November	5	145	2490
	December	5	174	2777
	January	4	184	2122
	February	2	192	1580
	March	1	174	1345
		19	**166**	**2253**

Table 8.4 continued

SFWI Group	Months	Number of Months	MSWD value	MDSR value
V	November	1	106	1294
		1	**106**	**1294**
VI	December	2	126	1540
	January	3	151	2167
	February	3	184	2217
	March	1	186	1684
		9	**160**	**1991**
VII	December	2	135	2168
	January	10	138	1649
	February	1	165	1539
		13	**140**	**1721**
All SFWI Groups		**77**	**154**	**2000**

Note: The bold-faced numbers in column 3 correspond to the total number of months, which have potential exposure to LLFs in each of the SFWI groups I-VII. The boldfaced numbers in columns 4 and 5 correspond to the mean values of MSWD and MDSR respectively for each of the SFWI groups.

8.4.2 Seasonal variability of daily potential fire spread

The annual index of potential fire spread (TDSR) has been shown to fluctuate significantly between years (section 8.3.1). In section 8.5.1, it was demonstrated that December to January period in the SFWI time series have the highest occurrence of combinations of extreme landscape dryness and potential for high fire spread corresponding to the high summer period of a fire season. To investigate this further, daily SFWI since 1951 was plotted to show the seasonal patterns of SFWI within and across years (Figure 8.13). The horizontal dotted lines show the breaks in the fire season calendar identified in section 8.1.1. The vertical dotted lines indicate the major seasonal shifts in of high SFWI, usually following a fire season with very high to extreme landscape dryness and very high potential fire spread (for example, 1957/58, 1967/68, 1982/83, and 1997/98).

In the 1950s, the peak period of high SFWI, indicated by the dark blue, occurred in the late spring and in the early part of high summer. By the 1960s, the peak period of high potential fire spread had moved to the high summer and late summer period. Highest SFWI reverted in the mid 1970s to the spring-early peak with a gap in high summer, followed by a short period at the start of late summer. The peak in SFWI then drifted further into high summer-late summer during the mid 1980s. It again shifted in the mid 1980s to the late summer period. Between the late 1980s and the mid 1990s, the fire season extended from spring to the summer-autumn

shoulder. Then the late 1990s saw a return to a late summer peak in SFWI that was short-lived. In the early and mid 2000s the peak SFWI had returned to the high summer period.

Based on this analysis, an increased likelihood of LLFs sets in for periods up to 5 or 6 years in the late 1950s, the early to mid 1980s and the early 2000s. This is denoted by the darker blue shades of colour, appearing as horizontal streaks in the peak summer period (Figure 8.13). The highest potential for LLFs is likely at this time (see Figure 8.12). This is not to say that high levels of landscape susceptibility to fire have not occurred outside of this period, for instance in late spring, or the summer-autumn shoulder. These are shown as dark blue streaks in the spring and late summer period (Figure 8.13).

During periods of low potential for fire spread, severe fire seasons in early summer can emerge very quickly on occasions without warning. Two instances of this appear in the SFWI time series; 1972/73 between 1968/69 and 1976/77; and 1990/91 between 1986/87 and 1992/93. The peak potential for high fire spread emerged suddenly following a previous wet winter (Figure 8.9).

In summary, the sequences of varying susceptibility to LLFs, illustrated on an annual time scale in Figure 8.9 and on a daily time scale Figure 8.13 clearly illustrate the changes in the season and magnitude of potential high fire spread. This usually follows a fire season with a very high potential for landscape fires (S class of fire seasons, and particularly SFWI group III). Up until 1982/83, SFWI group V fire seasons with a low potential for LLFs came after a severe fire season (Table 8.3). Thereafter, the years immediately after a fire season with very high potential for LLFs (1997/98, 2002/03, and 2006/07) reverted to either SFWI group IV, showing a strong autumn trend or to a SFWI group VII, and not SFWI group V.

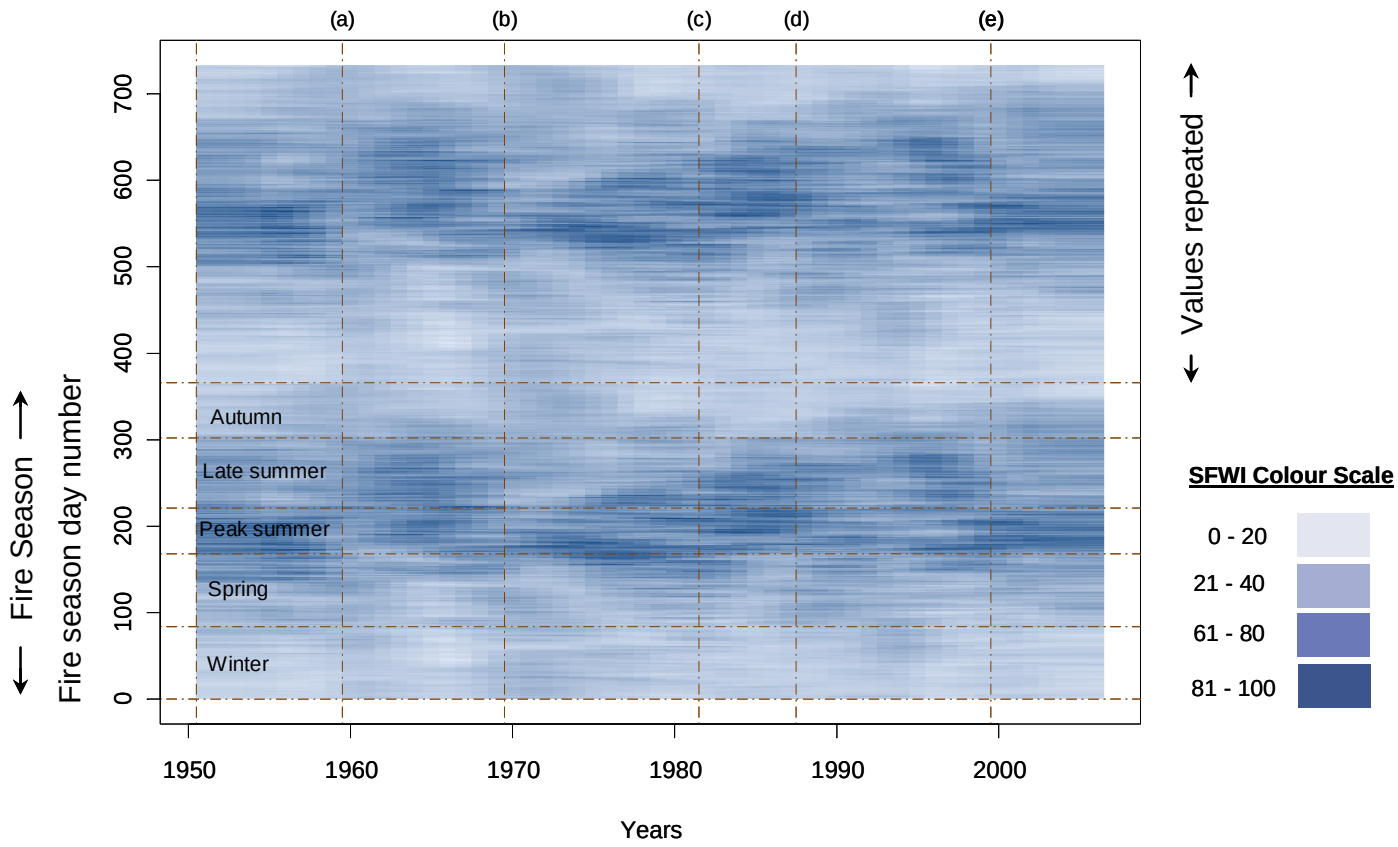

Figure 8.13 Smoothed seasonality of daily potential fire spread (SFWI) (1951-2007)

Notes: (1) Vertical red dash-dotted lines indicate significant shifts in seasonality of potential fire spread through time. The labels at the top of the diagram refer to fire seasons (a) to (e) that are related to significant La Niña events. Horizontal red dash-dotted lines refer to the breaks in the fire season defined in section 8.1.2.

(2) The values of SWD in each fire season are repeated twice in the figure in order to see the seasonal changes in patterns of landscape dryness within and between fire seasons in the diagram.

(3) The darker the blue shade in the diagram, the greater is the value of potential fire spread. The colours shown in the colour scale are approximate to those in the diagram.

The final comment about the seasons of potential high fire spread is that they do not stay fixed; there is an apparent drift in and out of the high summer period, depending on the seasonal landscape dryness conditions and the climatic influences directing hot, dry and windy weather at any time during spring to autumn.

8.5 Potential lightning ignition

The potential for lightning ignition is a consequent factor of conditions of very dry landscapes and particular sets of daily weather. The coincidence of a dry atmosphere, combined with surface atmospheric instability and turbulence over mountainous regions can initiate dry thunderstorms associated with lightning ignition and limited potential for rain. Multiple lightning ignitions from dry thunderstorms are a significant factor in the initiation of LLFs in the mountainous forested regions in south eastern Australia. These lightning ignitions are often coincident with very dry fire seasons that recur on a 20 to 30 year cycle. These factors, together with periods of dry and hot weather, resulted in LLFs occurring in the following regions:

- East Gippsland in 1964/65;
- the Victorian Alps in 1984/85, 2002/03, and 2006/07;
- the Snowy Mountains in 1964/65, 1982/83, and 2002/03;and
- the Sydney Basin in 1984/85, 1993/94, 1997/98, 2002/03, and 2006/07.

In all these cases, multiple lightning ignitions occurred when the landscape was very dry just prior to the onset of dry, hot, and windy weather conditions.

In the ACT Region, 6% of the months across all fire seasons from 1951 to 2007 have experienced extreme combinations of landscape dryness and potential fire spread. The extreme combinations are more likely to occur in the months of December and January, particularly in SFWI groups III and VI. There is a question of how likely is it that lightning ignition could precede or coincide with these highly fire-susceptible conditions of extreme landscape dryness and potential for high fire spread?

On occasions during the summer period, dry thunderstorms can produce dry lightning that start fires, while producing little if any rain to douse the resulting flames. On other occasions ‘wet’ thunderstorms produce much more rain, sometimes as much as 25 to 100 mm, depending on land temperature, atmospheric instability, and the vertical air temperature and moisture profile of the lower atmosphere. Thus, the purpose of this section is to investigate the conditions of landscape dryness and weather that are most likely to lead to the ignition and spread of fire.

8.5.1 Temporal model of potential lightning ignition

A plethora of spatio-temporal models of potential lightning exists in the literature. Out of all these, only one has a strong temporal aspect to it, which is based on the probability of lightning ignition in given months of a fire season (Cary, 1998). So far in this study the other two factors, landscape dryness and potential fire spread, affecting the potential for LLFs, have been examined on a daily time scale, it was apt to develop a daily temporal model of lightning ignition that spanned the full range of accurate and reliable records of lightning ignition in the ACT.

A decision tree modelling procedure in S-PLUS was selected as the preferred method for predicting potential lightning ignition on a daily basis. A range of variables characterising the development of dry afternoon thunderstorms and lightning ignition is tabulated in Table 8.5. These variables were selected to see if landscape dryness and fire weather conditions could explain the likelihood of lightning ignition with a decision-tree model. The only available dataset that could be used for this purpose are weather variables recorded daily at 1500 hours at Canberra Airport (see Table 4.7, Chapter 4).

Incidence of lightning-started fires was extracted from the records of Environment ACT: 80 lightning-started fires have been recorded since July 1951. The timing of lightning fires was matched with the detailed fire weather records from Canberra airport between 1951 and 2003. Included in the fire weather record is a variable called 'thunderstorm days' which is defined as: 'days on which thunder is heard within earshot from a weather station' (Bureau of Meteorology, 2007b). Thunderstorms can be heard at some distance from the weather station, up to 20 km away in some cases. There is no differentiation between 'wet' and 'dry' thunderstorms in the record.

Table 8.5 Modelling variables used in potential lightning ignition model

Type of variable	Surrogate variable	Comment
Landscape dryness	SWD	Indicates degree of landscape dryness
Thunderstorm type	Thunder-storm day, P_{0900}, and RH_{1500}	Differentiates between wet and dry thunderstorms
Convective instability	T_{1500}	Atmospheric instability has only been recently recorded at Canberra Airport
Fuel moisture and wind conditions	SFWI	Combined Index of landscape dryness (SWD), fuel moisture (FFMC) and wind speed (W_{1500})

Source: Weather data is taken from records of afternoon weather records at Canberra Airport from July 1951 to June 2003.

At the start of the modelling, the minimum deviance allowed for each possible branch in the tree model was set at 0.1. The final model, after several iterations, is shown in Figure 8.14. The sub-tree on the left hand side of this diagram provides the weather conditions associated with lightning from a dry thunderstorm, which is likely to start a fire on the ground. This sub-model combines the presence of a thunderstorm (Thunder-day=1), a very dry air stream (RH_{1500}<28.7%), the absence of rain (Precip.9am<0.1) and a high PFSI rating (SFWI>=27.8) to predict ignition. Based on the level of deviance explained in this part of the lightning ignition model, 72% of the occurrences of historical dry lightning-started fires can be explained. The sub-tree on the right hand side of the model predicts the remaining historical ignitions by combining the presence of a thunderstorm (Thunder-day=1), a moderately dry airstream (RH_{1500} between 30.5 and 43.5%) at a time when the landscape exceeds moderate dryness (SWD ≥ 64.6 mm). This sub-model has less predictive power than the first sub-model.

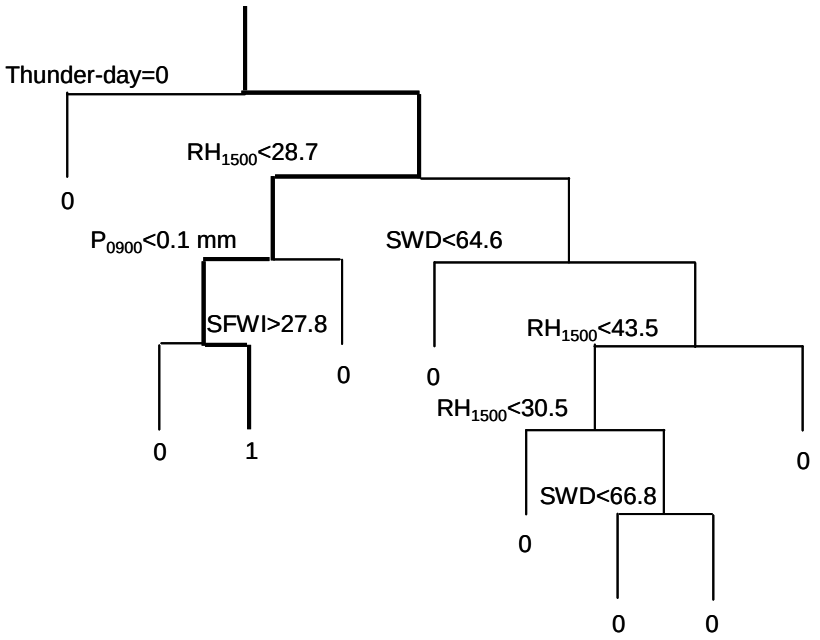

Figure 8.14 Best performing potential lightning ignition model

Note: Each branch represents how much deviance is explained by the explanatory variable at that point. The right hand fork in the first branch in the tree uses the variable thunder-day to distinguish thunderstorm-days from non-thunderstorm days. At the second branch, RH1500 <28.7 the left hand fork separates the very dry thunderstorms from the rest. At the third branch, if very little precipitation (Precip.9am<0.1) results from a dry thunderstorm, then if the SFWI is very high (SFWI ≥ 27.8, there is a high likelihood of a lightning ignition (right-hand branch with a 1 below it).

When the first sub-model is applied to the afternoon weather records at 1500 hours, it captures most of the lightning-started fires associated with hot and dry days in peak fire season conditions between early December and early February. Almost 50% of the lightning starts are associated with a SWD greater than 100 mm. In one of the model iterations, a SWD threshold

of 160 mm and above was found to be associated with 30% of lightning-started fires. This model therefore complements the original lightning-started fires model developed by Cary (1998), in which he used thunderstorm days, as well as precipitation and months of the year as predictive variables. The model characterises better the conditions under which lightning might start a fire and therefore provides a significant new aid in forecasting days on which dry thunderstorms might cause lightning ignitions in the ACT region.

8.5.2 Atmospheric conditions relating to dry thunderstorms

To understand better the atmospheric conditions that characterise dry thunderstorms that cause lightning ignition, daily morning samples of the atmospheric moisture and temperature conditions were extracted from aerosonde data taken at Wagga Wagga airport. Four examples were selected from the record that had definitely known single or multiple ignitions from lightning arising from dry thunderstorms in the ACT region and nearby in the Byadbo area of Kosciuzko National Park. The four significant dates were 13th^{h} January 1983, 12th January 1988, 3rd December, 2002 and 8th January 2003. The vertical atmospheric profiles are based on skew-T curves extracted from the archives of the (University of Wyoming, Department of Atmospheric Science, 2008). Wagga Wagga airport lies 100 km to the west of the ACT region and therefore is representative of easterly moving dry and unstable air masses that are likely to pass over the ACT region later in the same day during the peak fire-risk period from December to February.

A common vertical profile of atmospheric temperature and moisture was observed (Figure 8.15). The curves illustrate conditional instability in the lower atmosphere. Dry air in the lower 3000-4000 m is overlain by a shallow layer of moist layer, with dry air above it. This is the trigger that is needed for thunderstorms to develop under such conditions of atmospheric instability. In all these cases, the lifting condensation level lies between 2000 and 3000 m. A significant uplift mechanism is required for clouds to form on each of these days, and the orographic uplift of air over the Snowy Mountain Ranges provides this. The Cumulus clouds rise up to over 2000 m in elevation to the west and south west of Canberra. Conditional instability exists in the next layer above the moist layer so that cumulonimbus clouds can form, with less likelihood of rain falling and a higher likelihood of lightning ignition.

Based on the decision-tree model, lightning ignition risk is therefore based on a narrow range of atmospheric conditions, usually associated with relatively dry air ($RH_{1500} < 30\%$), a hot day during the peak of the summer period ($T_{1500} > 32\ ^{o}C$), and convective uplift over the mountain ranges to the west of Canberra under conditions of conditional atmospheric instability. Lightning ignition can occur across all the SFWI groups, with a higher likelihood of ignition within the drier SFWI fire season groups. The characteristic dry thunderstorms that could have produced lightning-started fires is relatively rare in the 56 years of weather records, amounting to 104 days in all, of which 80 had lightning-started fires recorded. There have been three fire

seasons in the last 56 years in which potential for high fire spread coincided with an actual lightning ignition: 1951/52 (SFWI group V), 1982/83 and 2002/03 (SFWI group III). These lightning ignitions occurred in the months of January and February at a time when the potential for high spread coincided with extreme landscape dryness conditions. Thus, the coincidence of the likelihood of the extremes of landscape dryness, potential fire spread, and ignition from dry thunderstorms has been relatively rare from 1951 to 2007.

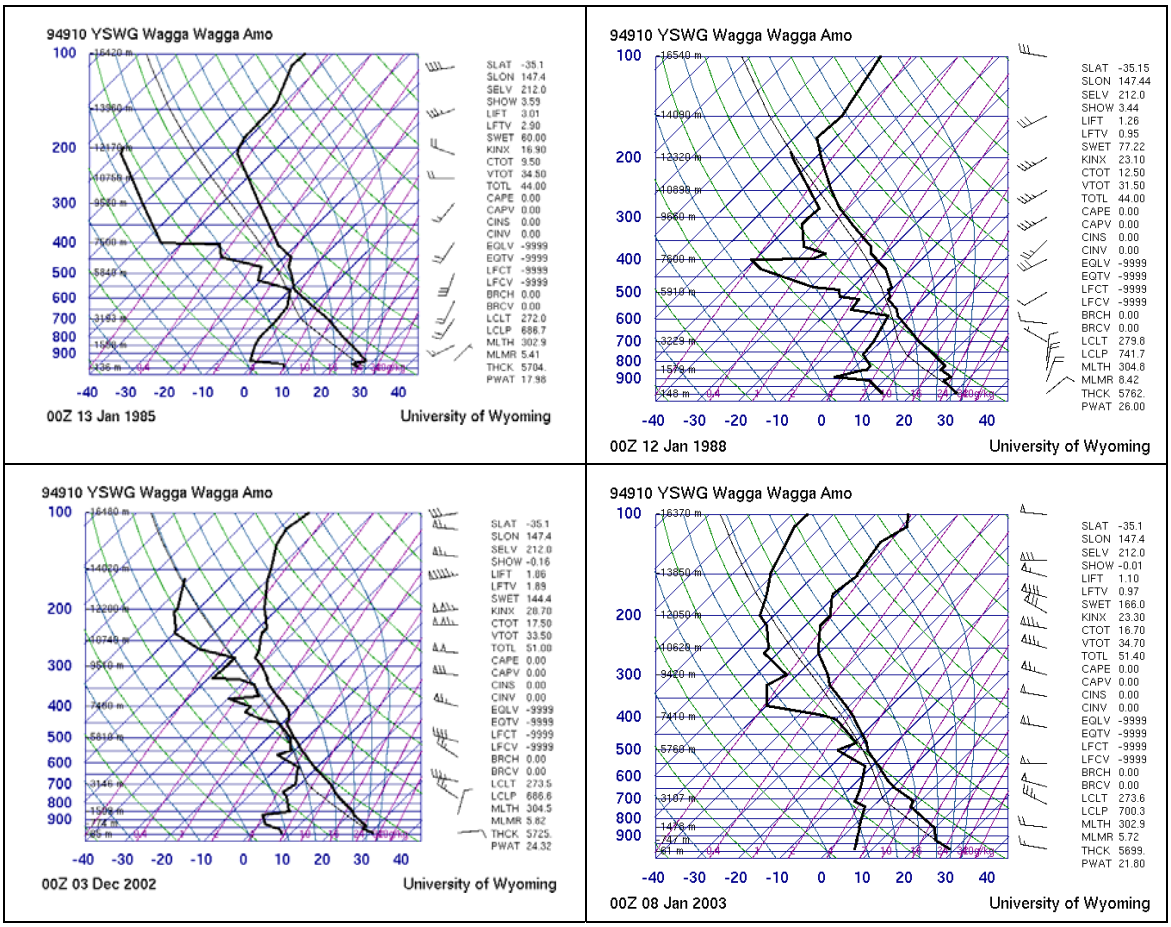

Figure 8.15 Aerosonde profiles taken at Wagga Wagga airport for days on which significant LLFs were started by lightning

Source: Daily aerosonde records are from the archives of the University of Wyoming (Department of Atmospheric Science, 2008).

Note: Source of ignition data for 1985, 1988, 2002, and 2003 fires selected from ACT fire history data between 1940 and 2003. Source of ignition data for the 1988 lightning fire at Byadbo is extracted from a research report undertaken on wildfires in the southern part of Kozciusko National Park (Bartlett (1993).

8.6 Findings in relation to medium-term susceptibility to large landscape fires

Three research questions dealing with the analysis of medium-term susceptibility to LLFs were posed in section 1.4 of the Introduction (Table 1.1). A summary of the findings for each research question follow.

8.6.1 Derivation of a new fire season calendar

The first part of this chapter investigated the traditional divisions of the year into seasons in relation to climatic and fire weather variables. Instead of the traditional four seasons, five seasons were derived using fire susceptibility indices of SWD, FWI, and FFMC. The five seasons have been classified as winter, spring, high summer, late summer, and autumn. The days on which the breaks in the seasons occur differ from the more conventional definitions that use astronomical and meteorological parameters. The breaks in the season were later found to be useful for interpreting the drift in the potential high fire season risk over time. Figure 8.13 illustrates that the peak potential fire spread drifts in a recognisable structured pattern across the breaks in the seasons in the annual cycle (see section 8.1.1).

This therefore addresses the ninth research question in section 1.4 of the Introduction (Table 1.1): 'Does redefining the season and the periods within a fire season using fire susceptibility criteria, such as landscape dryness, fine fuel moisture, and potential fire spread, produces a more meaningful definition than previous definitions?'

8.6.2 Classification of fire seasons using indices of landscape dryness and potential fire spread

Classification of the fire seasonal profiles of landscape dryness and potential fire spread has produced distinct groups and sub-groups of fire seasons, ranked from the highest to lowest in terms of landscape susceptibility to large fires. The groups and sub-groups identified using hierarchical classification have recognisable and interpretable seasonal patterns in landscape dryness and potential fire spread.

Most of the severe fire seasons, with regard to potential fire spread, were found in the S fire potential class. The S class contains two of the most significant SFWI groups: groups II and III. The major differences between these groups were found to be due to three factors:

(1) the build-up and timing of SWD in the spring months. In this case the more severe fire seasons were found in SFWI groups I, II, III, and V – all of which had a rapid build-up of dryness in the spring months;

(2) the level and duration of SWD reached in the peak and/or the late summer period. In this case, SFWI group fire seasons did not high levels of landscape dryness during the year and only reached sub-critical levels of potential for a LLF; and

(3) the timing and pattern of the decline of SWD from the late summer period to the cooler months of the year. In the case of SFWI group III, landscape dryness declined abruptly whereas in the case of SFWI group II it lasted well into late summer.

The one SFWI group that is very hard to anticipate is SFWI group V. This group shows very few anticipatory signs that are recognisable in the sequence of annual profiles. These fire seasons emerge suddenly during the wetter times in the SWD time series.

Two possible indicators of a severe fire season were identified in this chapter. The first indicator is a dry autumn and winter in the preceding fire season, leading to a high-risk fire season. In that respect a SFWI group IV fire season was found to be a very good indicator of a more severe fire season to come (SFWI groups II, III, and V). Eight out of nine fire seasons in SWD group IV indicated a possible extreme fire season with a high landscape susceptibility to fire.

The second more obvious indication is the onset of a dry spring prior to extreme conditions of landscape dryness in the following summer. However, 'green' droughts sometimes mask the level of soil water deficit present in forest soils. After a hot dry spell the remaining water in the soil profile is used up and extreme conditions in landscape dryness can result.

In the earlier part of the SFWI time series there were more distinct contrasts between the severe fire seasons and the less active ones (1951-1984). Usually after a major fire season, there followed a sequence of fire seasons with reduced potential for LLFs for a period of up to five to nine years, with an occasional fire season of somewhat less power and duration than a severe one. Since 1985, there has been a trend for fire seasons that follow severe ones to have dry autumns rather than the traditional break into fire seasons with wet autumns and winters. Since 2000, the alternating wet and dry fire season pattern found prior to 1984 has been replaced with a pattern of more prolonged dry fire seasons following a severe fire season without a substantial period of wet fire seasons.

The earlier landscape dryness threshold (SWD $\geq$ 100) determined from the literature in Chapter 7 was confirmed in this chapter as being a significant threshold above which landscapes become more highly susceptible to LLFs. The analysis presented showed that a mean monthly SWD greater than 100 mm on a scale of 0 to 200 mm did indeed encompass the periods with potentially very high to extreme potential fire spread (MDSR $\geq$ 2000), mostly during the high summer period between December and March. This analysis therefore confirmed the high-risk period as defined earlier in the fire season calendar (see section 8.1.2).

In summary, the methods of classifying the fire seasons in the historical time series at Canberra Airport are robust and tractable, using the methods devised in this study. This is indicated by the cross comparison of fire seasons in the more extreme groups of SWD that are mostly found in the very high to extreme SFWI groups. There are some exceptions to this general rule, with some of the fire seasons in a very high SWD group appearing in other

SWFWI groups (for instance the 1956/57 and 1964/65 fire seasons). The interesting difference with these fire seasons is that the timing of potential fire spread occurs outside of the normal high summer period. In these instances, the higher potential for LLFs occurred later in the fire season, in late summer.

This therefore substantially addresses the tenth research question in section 1.4 of the Introduction (Table 1.1): 'What can classification and time series analysis of landscape dryness and potential for high fire spread reveal about landscape susceptibility to LLFs in the medium-term?'

8.6.3 Potential for lightning ignition

The model presented in this study builds on Cary's model (Cary, 1998) but in this case provides more about the type of weather which is associated with dry lightning ignitions on any given day in a fire seasons. The accuracy in forecasting dry lightning fires was relatively high for dry thunderstorms (more than 70% of actual occurrences were predicted by the model). Further testing of the model could be done in other lightning-prone forest regions in south eastern Australia if fire weather datasets are available.

The model based on a decision-tree modelling approach showed that lightning ignition is more likely to occur under severe conditions of potential fire spread during the passage of a dry thunderstorm. The characteristic conditions were: (1) conditional atmospheric instability, (2) high temperatures at the land surface and associated low atmospheric vapour pressure (e_A), and (3) moderately severe potential fire spread conditions. Historically, these conditions have occurred on 104 days in the last 56 years. On three separate occasions in three separate fire seasons severe potential fire spread followed lightning ignition: in 1951/52 (SFWI group VI), in 1982/83 and in 2002/03 (SFWI group III). Generally, the highest risk of a LLF started by lightning ignition has occurred in the critical fire-susceptible period between early December and early February in the fire season calendar (defined in section 8.1.2). In terms of seasonal landscape dryness, the critical conditions for LLFs have generally occurred when SWD has exceeded 140 mm, which is higher than the values of SWD equal to 100, revealed in section 7.3.

The results and findings have therefore addressed the eleventh research question posed in section 1.4 (Table 1.1): 'Can a model based on particular combinations of landscape dryness and weather predicts the potential for lightning ignition in the ACT region'.

Chapter 9: Interpreting Longer-term Landscape Susceptibility to Large Fires and Contributing Climatic Factors

The issue of fire susceptibility is placed into a broader temporal and spatial context in this chapter.

In terms of the broader temporal context, time series analysis is used to break down the trend and seasonal components of the medium and long-term landscape dryness to illustrate the underlying trends at time scales longer than one or two fire seasons (section 9.1). A classification of the long-term SWD dataset is then undertaken to identify groups and sub-groups of fire seasons with varying seasonal landscape dryness (section 9.2). Fire seasons since 1871 are identified based on the thresholds of landscape dryness identified in Chapters 7 and 8 section 9.3 and the seasons within a fire calendar in section 8.1.2.

In section 9.4, the role of possible sub-global and synoptic climatic factors in setting up conditions of landscape dryness are canvassed, along with the potential for high fire spread and lightning ignition.

9.1 Time series analysis of medium and long term landscape dryness

This section examines the inter-decadal, decadal, and sub-decadal trends in fire susceptibility of a landscape to large fires using time series analysis of medium and long-term SWD data (sections 9.1.1-9.14). This section looks at the full variation in seasonal build-up and decline of SWD over the time series.

Time series analysis is the analysis of a 'series of values of a particular quantity or rate of change in a variable at successive times, often at equal intervals' (AOED, 2004:1351). Methods range from Fourier and harmonic analysis, to moving averages, filtering, stochastic and Markov modelling of temporal data (Klein, 1997). These methods make assumptions about the data, such as having a normal distribution or data independence. Traditional techniques render the data 'stationary' by taking means or differences of the original dataset.

More modern and less conventional statistical tools employed in time series analysis make fewer assumptions about the nature and distribution of the data in the time series. Strongly seasonal and non-linear data can be better handled with time series analysis tools that decompose the long, medium and short-term patterns using a flexible set of trend filters (Mathsoft, 2005).

The time series decomposition function (STL) within S-PLUS decomposes a time series into three components: the trend component, the seasonal component and the remainder (Cleveland *et al.*, 1990). The remainder contains random or real components of variation not

picked up by the trend or the seasonal component. A set of LOESS smoothers acts on the original time series to uncover the underlying temporal patterns in the data. At the end of this process, trend, seasonal and residual values are extracted. LOESS blends least squares regression with non-linear estimation (Cleveland and Devlin, 1988) and uses a small subset of points, either side of a point in time, to define the position of the curve at that point. LOESS then progressively moves through the sequence of points to estimate a line of best fit (Johnson, 2003). The advantages of LOESS are threefold. First, it is suited to analysing complex patterns in data. Second, LOESS does not produce a displaced set of values such as in moving averages. Third, the number and length of the various smoothers can be varied to match known cycles in nature. Fourth, LOESS is a robust smoothing algorithm that is not affected by outliers in the data. However, while the LOESS algorithm does require a high number of data points to run effectively, this does not present a problem because even the more constrained medium-term time series of SWD or FWI have over 24,000 values in the time series.

9.1.1 Longer-term trends in medium-term landscape dryness

The analysis in this section now turns to deciphering the variability of the time series of landscape dryness (SWD) from a longer-term serial rather than a seasonal perspective (Chapter 8). This is done to understand the sequencing of the landscape dryness factor at different time scales: inter-decadal, decadal, and sub-decadal. In order to break down of the complexity of the medium-term SWD time series into its component parts, trend filters approximating inter-decadal, decadal, and sub-decadal time scales were applied. The choice of these trend filters was based on likely factors or processes influencing rainfall and hence SWD in the ACT region: the Pacific Decadal Oscillation (PDO) between 20 and 40 years in length (inter-decadal); sunspot cycles (decadal), and ENSO (El Nino-Southern Oscillation) operating between 3 and 5 years (sub-decadal).

Based on the average cycles of the PDO since 1900, the inter-decadal trend filter was set to 27 years. At this time scale, the smoothing of the time series is not that sensitive to the length of the filter which can be varied up or down by five years without affecting the general trend greatly. A slightly shorter length trend filter of 20 years picks up more of the detail where as a 35 year length filter will show a much smoother long-term trend in the data. This equates to an approximate average length in the PDO cycle, which amounts to about half the length of the apparent long-term rainfall cycle in the ACT region of 40-55 years (Figure 9.1). A long-term cycle of 50 years is also apparent in the long-term rainfall record at Queanbeyan. A general decline in rainfall from the late 1890s until the mid 1940s is one evident trend. Since then, the cumulative deviation from the mean monthly rainfall rose until the mid 1990s while a decline in the past 10 years signals a significant downward trend, which, on the past limited record, may persist for another 40 years even in the absence of a global trend towards a much warmer and potentially drier climate. The instrumented rainfall record in the region only goes back to the

mid 1870s so some caution is required in predicting future rainfall patterns based on limited data less than one hundred and fifty years in length.

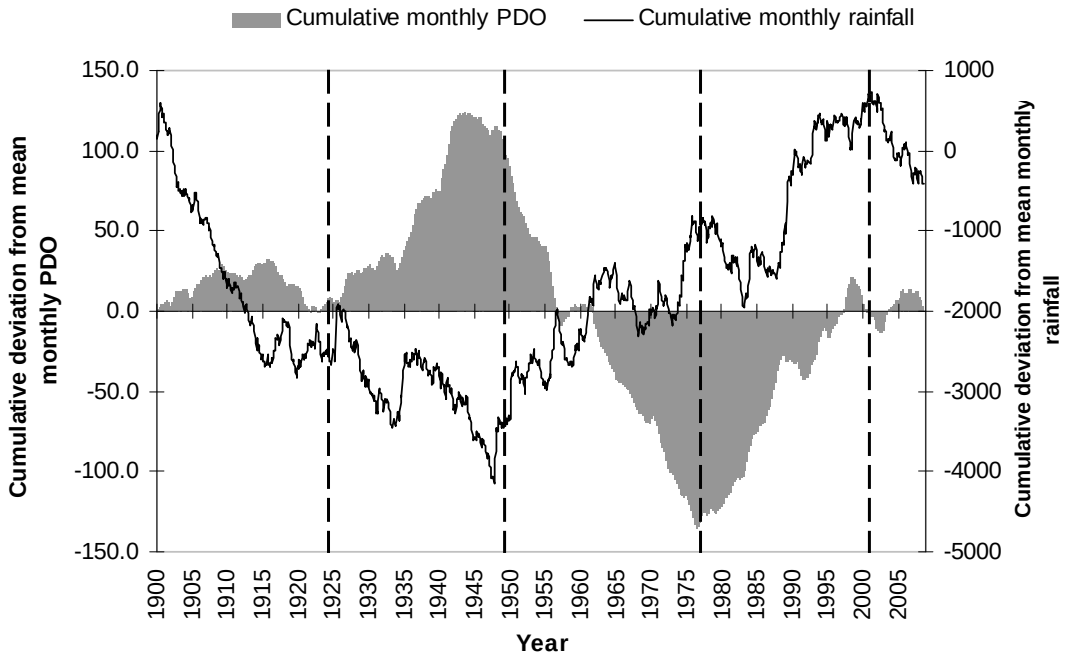

Figure 9.1 Trends in deviations of PDO and rainfall at Queanbeyan from their respective means

Note: The vertical bars indicate when there has been a major reversal in the PDO index. Note that the cumulative deviation from mean rainfall at Queanbeyan appears to run at roughly double the length of the PDO cycle (between 40 and 50 years).

A trend filter of thirteen years was chosen to accommodate the sunspot cycle of eleven years and conjectured bushfire cycles of thirteen years in south eastern Australia (Vines, 1974; Burroughs, 2003). This trend filter was designed to detect approximately decadal cycles in the SWD time series. Sensitivity testing showed that varying the trend filter from 10 to 15 years had little effect on the resultant decadal trends.

A sub-decadal trend filter of approximately five years was then chosen as it equates to double the average length between definitive switches in the Southern Oscillation Index (SOI), ~2.7 years, since 1876. This length of trend filter is consistent with the 2-4 inter-decadal interval determined by Jiang *et al.* (1995). Changes in polarity in the cumulative deviation from the mean SOI during this period are depicted in Figure 9.2, the SOI being the relative difference in surface atmospheric pressure between Darwin and Tahiti. The negative cumulative trend since 1974 represents an increased frequency of El Niños and perhaps fewer and shorter La Niña events in the Pacific Ocean.

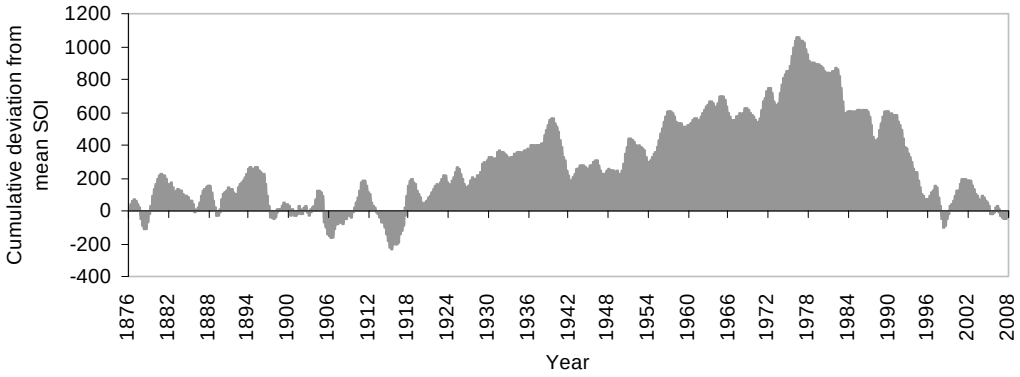

Figure 9.2 Cumulative deviation from mean Southern Oscillation Index 1876-2008

Note: The sub-decadal LOESS filter is based on major changes in direction in the cumulative deviation from the mean.

Based on the inter-decadal (27 years), decadal (11 years), and sub-decadal (~5 years) LOESS filters, the trends in the SWD since 1 July 1939 were examined with STL time series decomposition (Figure 9.3). There is marked complexity in the structure of the annual profiles of the SWD, with considerable variation inter-annually and from decade to decade (Figure 9.3).

A particularly significant feature of the SWD record, which is shown in panel 1, is the number of pairs of dry years, indicated by grey bars: 1956/57-1957/58, 1966/67-1967/68, 1981/82-1982-83, 1993/94-1994/95, and 2005/06- 2006/07. This indicates pairs of years in which soil water recharge did not occur in late autumn or winter before the next fire season. This feature was also picked up in the classification of medium-term SFWI (see Figure 8.8). This means that the lower part of the soil profile is dry in the lead-up to the fire season. This in turn affects the vegetation flammability and fuel availability when the soils become very dry during the peak of the fire season. This lack of soil water recharge in the over-wintering period is therefore a major indicator for the potential of LLFs in the subsequent summer. In terms of planning for a LLF, this then becomes the first sign of an impending fire season.

Another characteristic of the trend is the sudden reversal of SWD from low to high soil moisture values following these extended dry spells. The sixth panel in Figure 9.3 shows a strong positive residual value in the drought year and a strong negative residual value in the year after the drought years. The 2001/02-2002/03 sequence was a notable exception to this general rule – soil conditions were dryer than anticipated and there was a smaller negative residual value for two years after 2002/03. This suggests that the usual pattern of recovery of soil moisture in a wet year following a sequence of dry years was unusually delayed until the spring of 2005/06. A similar delay in recovery of soil moisture was observed in a wet year that followed the drought years between 1939/40 and 1942/43.

A single severe fire season following a sequence of wet-to-moderately dry years (hatched grey bars), was observed in 1942/43, 1951/52, 1984/85, and1985/86). These years were characterised by a summer seasonal pattern of extremely dry (near zero soil moisture) soils. Presaging the LLF events, the SWD rose very rapidly during late spring and early summer and dropped in late summer, after fires and following good rains. The residuals (sixth panel of Figure 9.3) found in these fire seasons suggest that the seasonal drivers of rainfall were operating differently to the ones evident in the first panel of Figure 9.3.

Broad long-term trend in SWD at the sub-centennial timescale is indicated by a gradual decline in SWD until the 1990s (second panel of Figure 9.3) when there has been a general trend upwards in SWD, resulting from a sequence of relatively dry years. The decadal trend (panel 3) suggests an almost regular cycle of 10-15 years. The shorter sub-decadal trend (panel 4) indicates a somewhat irregular cycle between four and six years until the 1980s. Subsequently, a pattern of greater regularity has arisen.

The analysis now moves onto the long-term time series of SWD to see if there are consistent trends between it and the medium-term time series of SWD revealed in this section.

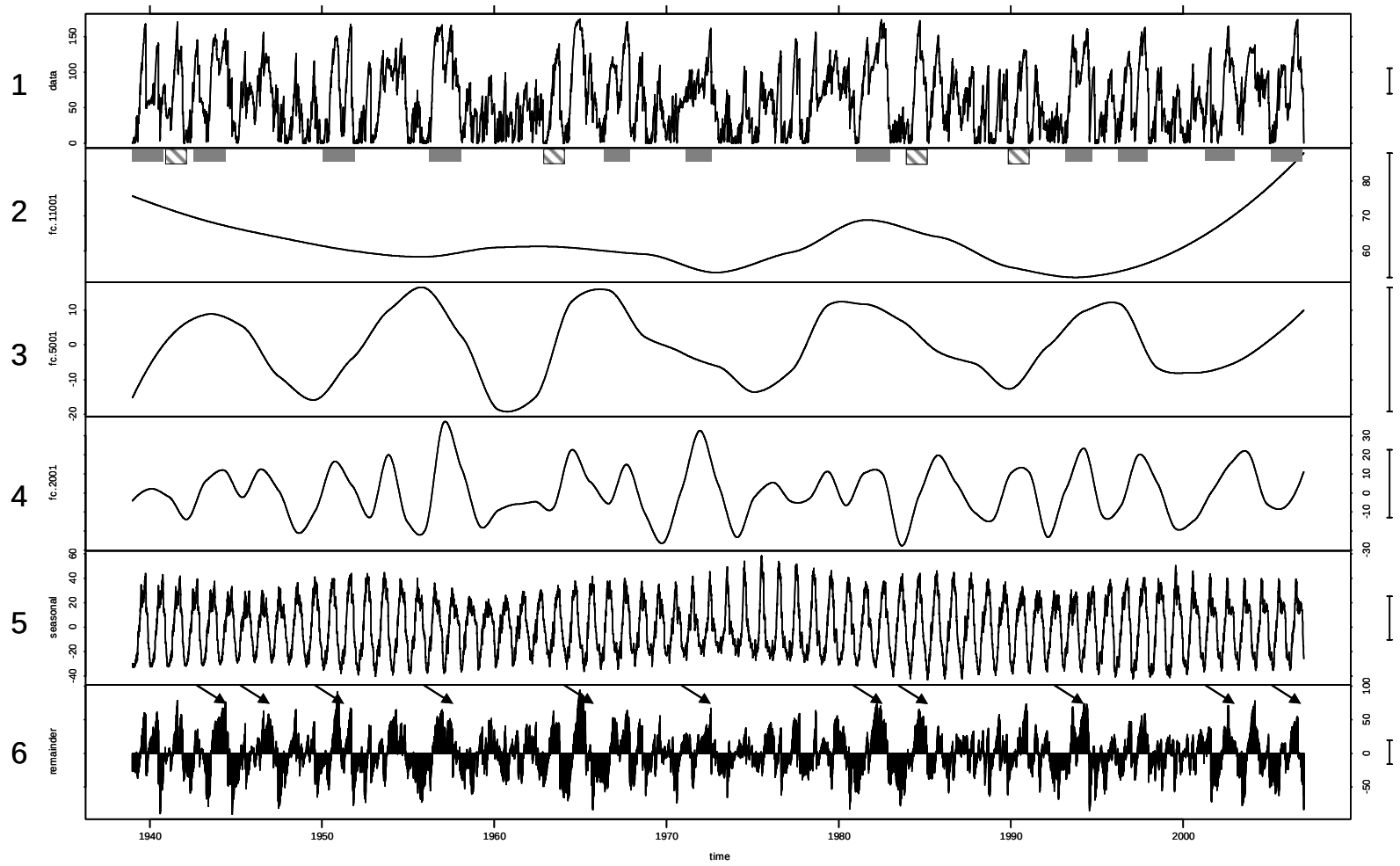

Figure 9.3 Simplification of medium-term trends in soil water deficit (Canberra Airport 1939-2007)

Notes: (1) Original SWD data (panel 1), Inter-decadal trend (panel 2), decadal trend (panel 3), sub-decadal trend (panel 4), seasonality (panel 5) and residual values (panel 6).

(2) The grey horizontal bars in panel 1 indicate pairs of dry years while the hatched bar indicates sudden dry years emerging from a previous wet autumn and winter.

9.1.2 Underlying trends revealed: medium-term time series of landscape dryness

The method discussed in section 9.1.1 revealed some definite quasi-periodic cycles at the decadal and sub-decadal time scales, but less definite at the inter-decadal time scale. The question is: if the trend filters were combined, would any predictable underlying trends in the fluctuations of landscape dryness over time be revealed? To achieve a simplified view of the complex variability in SWD (first panel of Figure 9.3), the trends in panels 2, 3 and 4 in Figure 9.3 were added together in different combinations to reveal composite trends. The individual and composite trends are presented in Figure 9.4 (b) and (c), shown against the trends in the Southern Oscillation Index (SOI) in Figure 9.4 (a) for the period between 1939 and 2007.

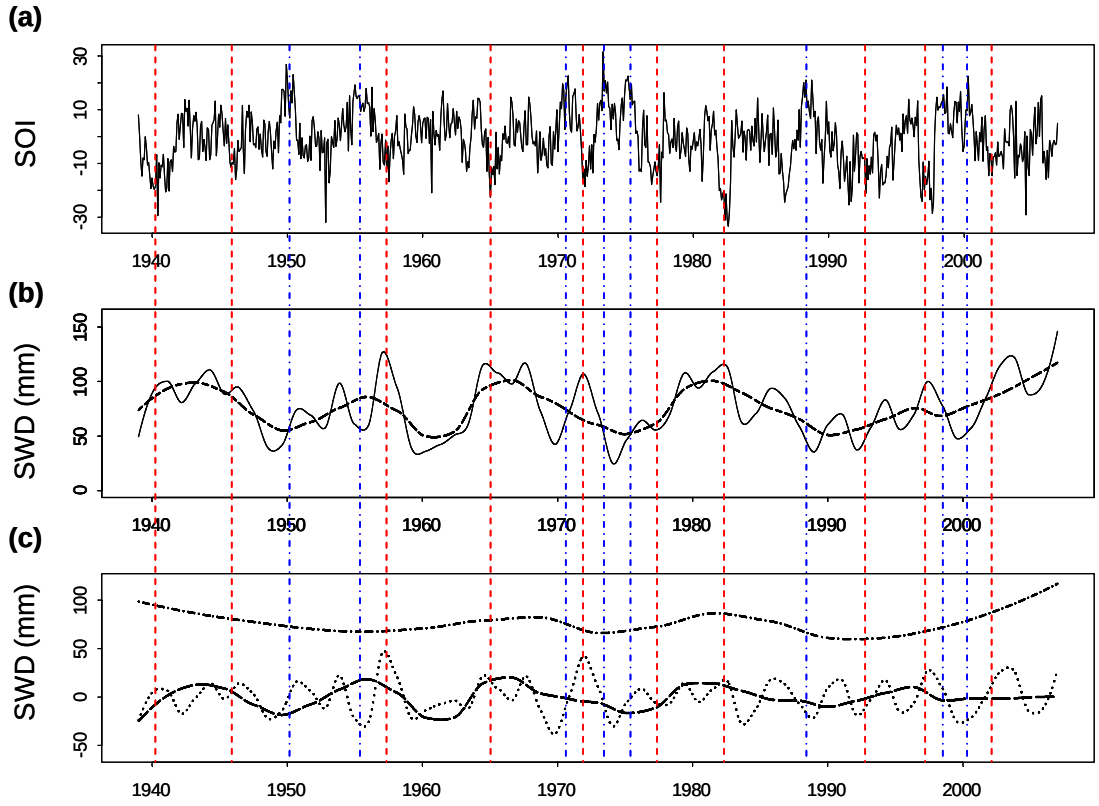

Figure 9.4 Trends in Southern Oscillation Index (a) compared with composite (b) and individual (c) sub-decadal, decadal, and inter-decadal individual trends in SWD from 1939 to 2007

Source: Monthly SOI values come from Bureau of Meteorology records and daily SWD values are for dry sclerophyll forest near Canberra Airport, produced by the RSDI model.

Notes: (1) The separate trends revealed by the LOESS trend filters (sub-decadal — 5 years, decadal — 13 years, and inter-decadal — 27 years) are shown in Figure 9.4 (c). Composite trends by combining the values from decadal and inter-decadal (dashed line) and all three LOESS filters (solid line) are shown in Figure 9.4 (b). (2) The blue dotted and dashed vertical lines indicate fire seasons with sustained positive SOI values associated with La Nina fire seasons whereas the vertical dotted red lines indicate negative SOI values.

Individual trends in SWD at the inter-decadal, decadal, and sub-decadal time scales are presented in Figure 9.4 (c). Underlying the complexity in landscape dryness is first, a four to five year cycle (dotted line) and second, a quasi-periodic cycle between twelve and fourteen years between 1940 and 1990, which then disappears after 1990 (dashed line). There is no detectable trend in SWD apparent at the inter-decadal time scale (dashed dotted line above the two other lines).

The solid line in Figure 9.4 (b) is based on the combined ~27, ~13, and ~5 year LOESS trend filters. High levels of landscape dryness are evident in the fire seasons of 1939/40, 1944/45, 1946/47, 1951/52, 1954/55, 1957/58, 1964/65, 1967/68, 1972/73, 1979/80, 1982/83, 1985/86, 1991/95, 1994/95, 1997/98, and 2002/03. The troughs in the composite trend using the combined ~27, and ~13 year LOESS trend filters (dashed line) indicate only short periods of moist seasonal profile, that is to say, 1949/50, 1955/56, 1970/71, 1973/74, 1974/75, 1983/84, 1988/89, 1998/99 and 1999/2000 (solid line in Figure 9.4 (b)). These shorter periods mainly correspond to 'La Niña events', whose effects appear short-lived, except for the period 1959-63. The breakdown in trends using the different length of LOESS trend filters suggests some form relationship between SOI and SWD, when SOI values are either strongly positive or negative for at least four months. Outside of these conditions, other continental scale climatic factors affecting rainfall at the synoptic scale may be involved, thus affecting the seasonal patterns of landscape dryness.

The seasonal trends within and between fire seasons is now examined using a combination of a serial and a seasonal view of SWD since 1939 (Figure 9.5). Despite there being noticeable late summer blocks of landscape dryness, only occasionally do the peak levels of dryness move into the high summer period (for example, in the mid 1950s, the late 1970s, and early 1980s, and in early 2000s). The vertical lines with the corresponding fire seasons indicate marked shifts in season of landscape dryness, associated with major La Niña events from 1939 to 2007. These are short periods of three to four years of moderately wet years before the landscape is again dry in spring (for example, early 1950s, mid-late 1970s, or early 2000s), or to late summer/autumn dryness) (for example, mid 1960s, mid to late 1980s, or late 1990s). The conclusion from this is that there have been only short periods when extremes of landscape dryness has occurred in the high summer period in the past 65 years, despite having regular dry periods at intervals between three and five years for most of the time series.

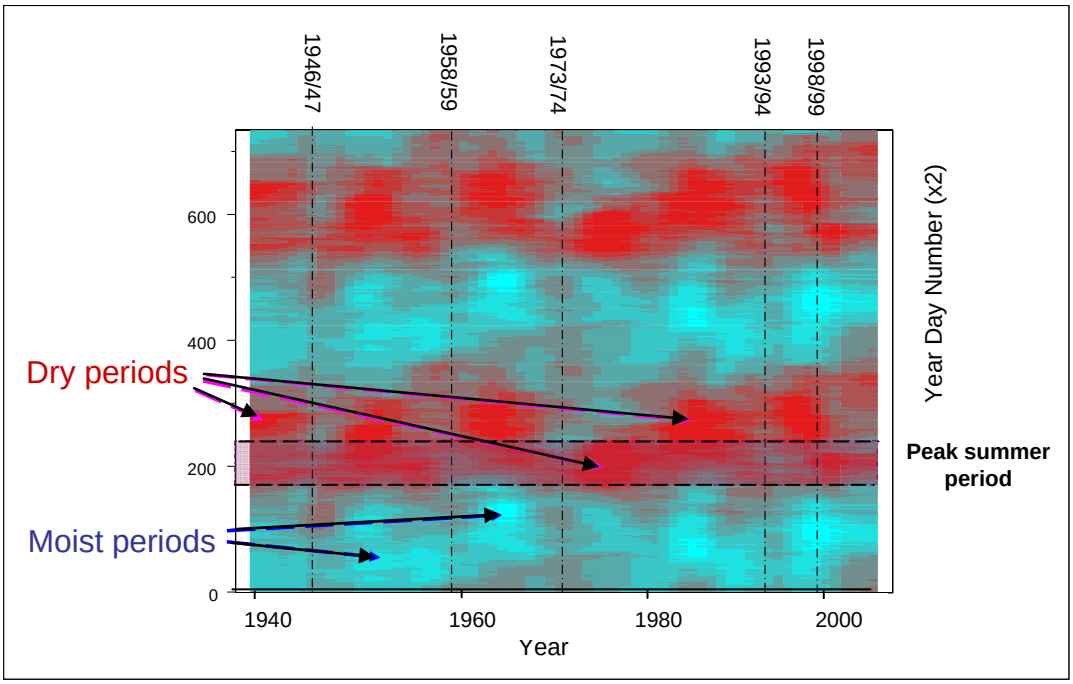

Figure 9.5 Shifting season of landscape dryness 1939-2007

Note: Vertical lines show fire seasons after which major shifts in the season of peak landscape dryness have occurred.

The general conclusion is that soil dryness in combination reveals marked variation in amplitude and periodicity throughout the time series, reflecting the highly variable nature of the sequence of wet and dry fire seasons in this region. Broad periods of much drier landscapes were evident in the early to mid 1940s, mid 1960s, late 1970s and early 1980s, and then in the late 1990s and early 2000s. In between these broad periods, there were short wet periods: in the late 1940s, the late 1950s, the early 1970s, and the mid 1980s. The composite trend analysis previously revealed a lack of regular periodicity of fire seasons with severe landscape dryness, using the index of SWD. The extended seasonal view as shown in Figure 9.5 does not reveal any predictable rhythms in the cycles of wet and dry fire seasons. The next section presents the patterns evident in the long-term time series of SWD to determine whether there is any periodicities evident using similar time scales applied in this section.

9.1.3 Long-term time series analysis of landscape dryness

As proposed in the modelling framework (Table 4.1), the Queanbeyan rainfall, which is closely correlated with Canberra Airport (section 4.3.2), was used to generate a long-term time series using the F-DSWBM model (section 6.1.3).

One feature of the long-term pattern of soil water deficit was found to be its relative unevenness and irregularity through time, despite the essentially invariate inter-annual net radiation (R_N) cycle being firmly embedded in the index. For the most part SWD oscillates annually between 30 and 170 mm although deep groundwater recharge occurs intermittently.

Irregularity in the soil moisture regime is governed almost entirely by the changing quantity, frequency, and seasonality of rainfall. Viewing the original long-term time series of SWD in this manner does not reveal any regular cyclical or quasi-periodic patterns.

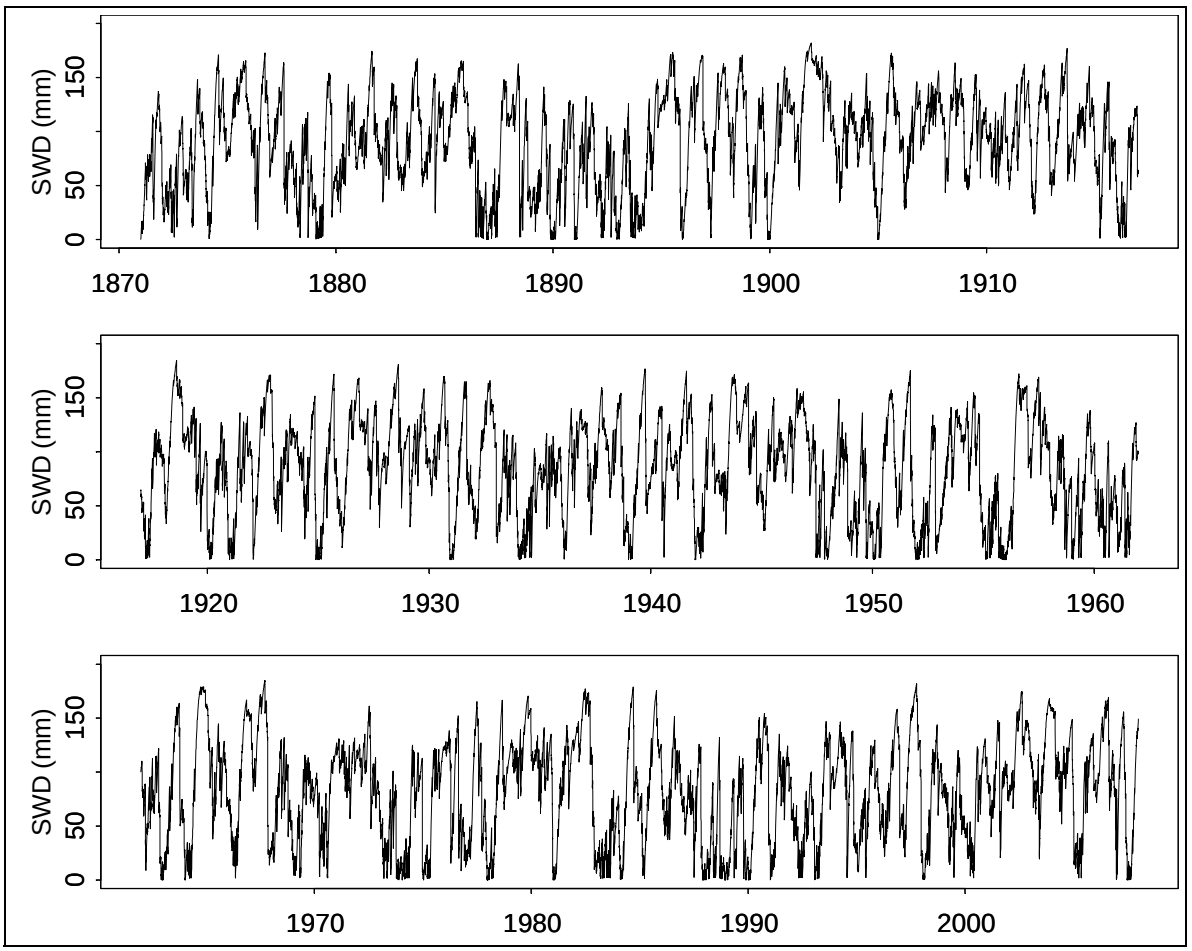

Figure 9.6 Long-term time series of soil water deficit for a hypothetical dry sclerophyll forest near Canberra Airport weather station (July 1871 to June 2007)

A significant feature of the intrinsically noisy SWD cycles is the intermittent pattern of complete recharge of the soil profile, when the modelled SWD falls to zero.

The longest interval between full recharge was between 1905 and 1917 at the end of the Federation drought. In the driest periods on record, 1880-1886, 1925-32, 1943-47, 1977-1983 and 2000-2005, there was little variation in soil moisture levels signalling minimal soil water recharge in winter and spring.

Sub-decadal, decadal, and inter-decadal rhythms in SWD are now examined.

9.1.4 Sub-decadal, decadal, and inter-decadal variability in the long-term landscape dryness time series

The first step taken to account for the variability of SWD over the past 136 years was to select trend filters that picked up trends at sub-decadal, decadal, and inter-decadal time scales. Based on the analysis of results of using the trend filters applied in the time series analysis of the medium-term SWD time series, fractionally shorter trend filters of 25, 13 and 4 years were applied in the current time series analysis. This was done to see if any discernible differences in trends between the medium- and long-term SWD time series could be identified.

The result of applying the inter-decadal trend filter of 25 years shows a small but significant rise in SWD in the late 1870s and early 1880s, and an obvious perturbation between the late 1880s until almost 1920 reflecting lower than average rainfall during those periods (Figure 9.7, panel 2). The next 60 years show a steady net decline (30-40 mm) in soil water deficit reflecting a slight increase in annual rainfall. On a rather shorter time scale, small rises in SWD are evident in the mid 1920s, the early 1940s, the mid 1960s, the late 1970s, and the early 1980s, all of which correspond to droughts. The sharp rise from the mid 1990s reflects the dry years but more recent excursions, at the end of the time series, is simply be an aberration caused by the LOESS smoothing algorithm (Cleveland and Devlin, 1988). The LOESS algorithm is otherwise very stable in the central part of the time series.

A thirteen-year trend filter revealed a twelve-to-fifteen year cyclical pattern in landscape dryness from the mid 1920s until the early 2000s (Figure 9.7, panel 3). While the cyclical pattern was also evident from the 1870s until the mid 1890s, an irregular cycle became established between 1890 and 1920.

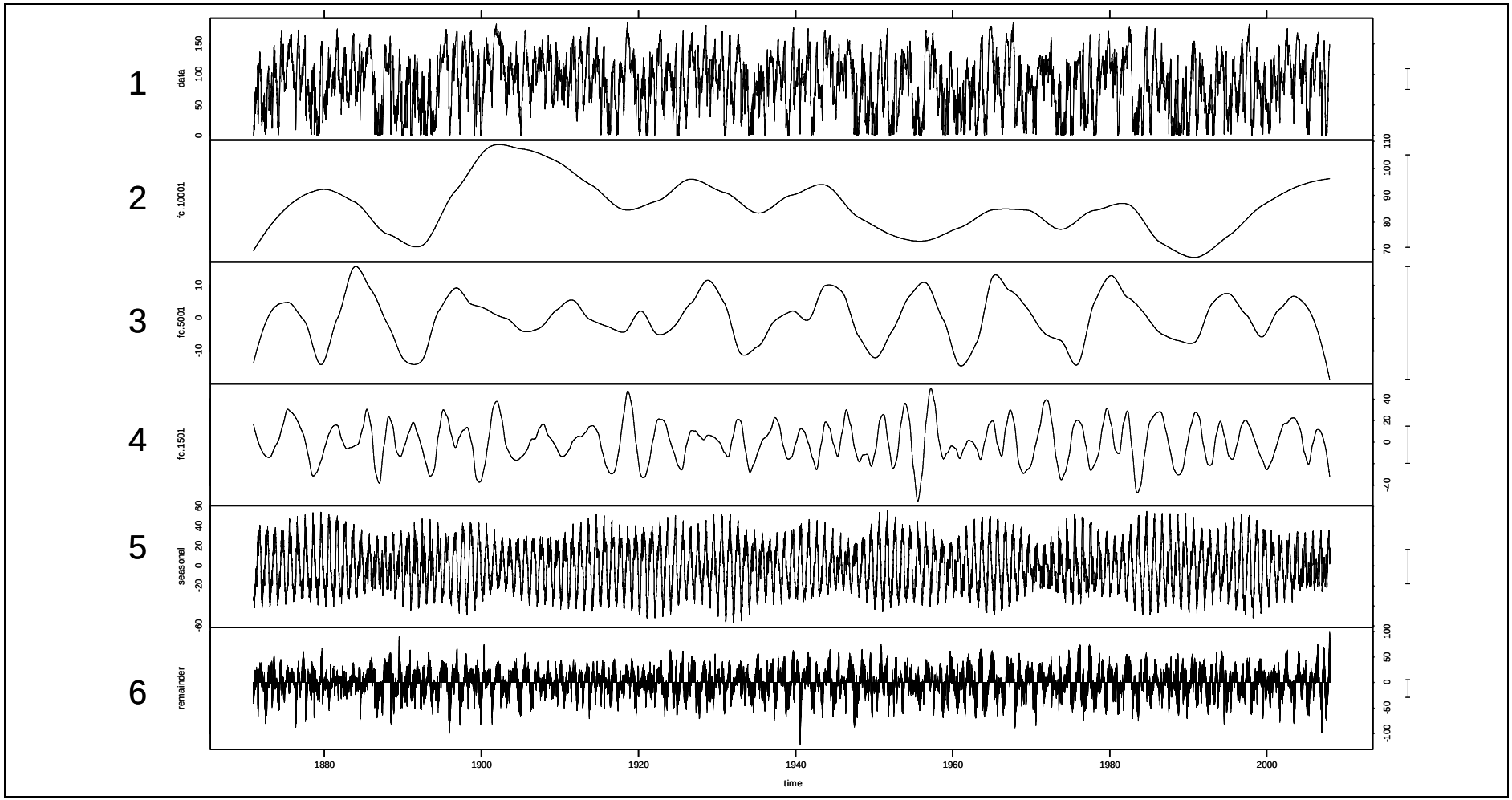

Figure 9.7 Simplification of inter-decadal, decadal, and sub-decadal trends in long-term soil water deficit at Canberra Airport (1871-2008)

Note: Original SWD data (panel 1), Inter-decadal trend (panel 2), decadal trend (panel 3), sub-decadal trend (panel 4), seasonality (panel 5) and residual values (panel 6).

The seasonal signals in the fourth and fifth panel in Figure 9.7 are too complex to interpret fully at the scale of the diagram. The obvious patterns evident are twofold. The first is that the seasonal amplitude (between the peak and trough of SWD) became contracted when there was either:

(1) no significant recharge during winter and spring (from the 1900s to the 1920s) or

(2) above average rainfall throughout the year to keep the SWD low (for example, the late 1880s, the mid 1930s, the early 1960s, and the early 1970s).

The second is that is that the seasonal amplitude of SWD increased during periods of very dry summers preceded by wet winters and early springs. For instance, this happened in the early 1930s, the mid 1960s, the mid 1980s, and the late 1990s.

The residual values in the sixth panel show an alternating pattern of positive and negative values, reflecting the difference between the original SWD series and the values removed by the three smoothers and the seasonal factors in the four panels above (Figure 9.7). Like the residual values of Figure 9.3 (sixth panel), there is a an irregular see-saw oscillation between wet and dry fire seasons corresponding to a 2-4 year cycle from the 1900s onwards. The patterns revealed are complex to interpret and would require significantly more time to determine any underlying pattern, which is beyond the scope of this study.

The seasonal patterns are best interpreted by plotting the seasonal signal as an image plot (Figure 9.8). The darker blue patches represent drier periods (high SWD) while the whiter shades represent wetter periods (low SWD). The arrows indicate general trends in seasonal extremes of soil water deficit. Before the 1920s, the smoothed seasonal signal displays an alternation of wet and dry sequences with: (1) an average interval of 10 years in the wetter periods, and (2) an interval of about 5-6 years in more normal and drier years. Thereafter, and for about 25 years, there appears to be a seasonal drift of dry conditions, followed by an extended period, between the mid 1940s and the mid 1970s, of unseasonably good rains. For the whole of the record pre-1970, and about once every 10 to 12 years, there are intervening wet years breaking the summer dryness pattern. More recently, that is post 1970, there has been a seasonal shift of dryness towards autumn and an overall pattern of fewer extended wet periods. The emerging pattern is therefore one of exceptionally dry landscape conditions during a high summer fire season.

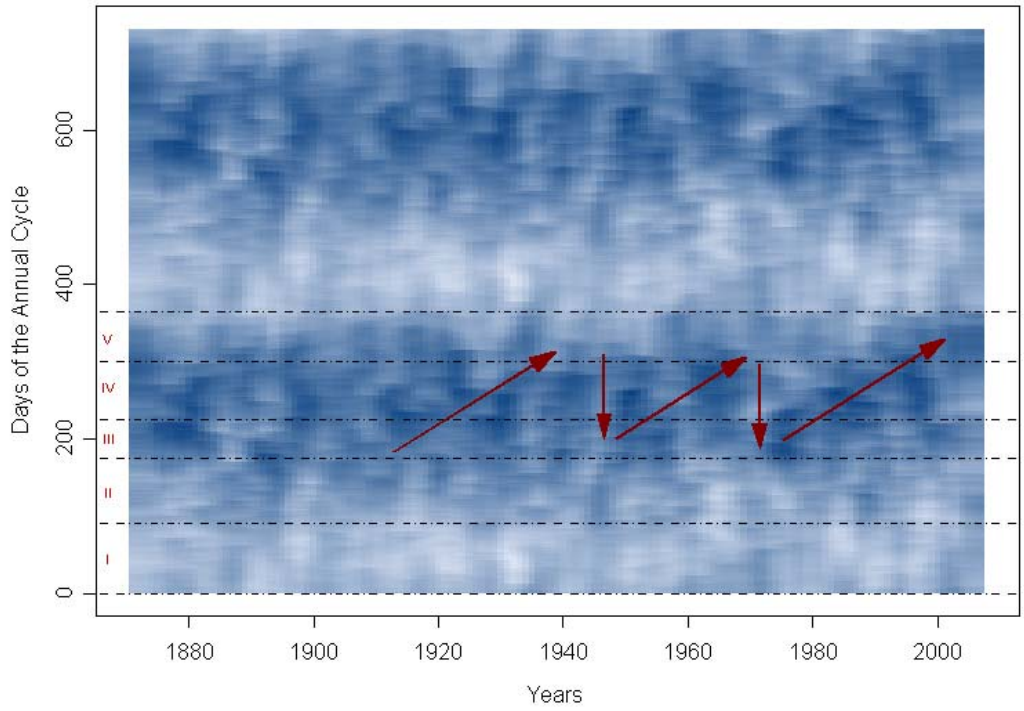

Figure 9.8 Variation in annual seasonal profiles of Soil Water Deficit (1871-2007)

Notes: (1) Red arrows indicate generalised trends in the season of extreme soil water deficit.

(2) The roman numerals within the horizontal dashed-dotted lines refer to the seasons in an average fire season, previously defined in Table 8.1.

9.2 Classification: long-term landscape dryness

To complement the earlier classifications of medium-term landscape dryness and potential fire spread, a hierarchical classification of the long-term SWD time series was performed. This classification employed a smoothing 21-day filter as presented in Figure 9.9. Since the daily evaporation values in the F-DSWBM are based on averaged daily figures over the past 30 years (see section 6.1.3), there is already some inherent smoothing of the SWD time series. A LOESS smoother of 21 days filters the SWD signal less than the longer-term 31 or 51-day smoothers. This is because the fire seasonal profiles produced by the Fowler daily soil water balance model are much smoother than those produced by either the MSDI or RSDI models.

The classification tree first branches at a value close to 1900 (Figure 9.9). The upper left hand fork (M) comprises the wettest 86 fire seasons on record. Despite being in the wetter classification, some fire seasons were very dry for short periods until late summer; other fire seasons may have had dry autumns; and a few fire seasons experienced incidences of dry spring leading into very dry summers and autumns for short periods in the middle of summer.

The classification of fire seasons based on long-term SWD was primarily delineated by a value of 1400 in the classification tree, and otherwise sorted by similarity of seasonal patterns of SWD (Table 9.1). Of these, the majority of the fire seasons, 47, are classified as a moist group (SWD group 2) and 38 in a very dry group (SWD group 6). What distinguishes the groups are two factors: (1) the seasonal amount and frequency of rainfall; and (2) the commencement and persistence of extended spells of dry weather.

Table 9.1 General description of the six SWD groups in the long-term landscape dryness record

General Class	Group number	Seasonal dryness characteristics	Significant breaks in either wet or dry spells	Number of fire seasons	Percentage of fire seasons
Moist earlier in the annual cycle, occasionally leading to some very dry years in the middle of the annual cycle (M)	1	Dry to very dry spring leading into high summer period-moist autumns	Dry spell usually ends between day 160 and day 230	19	14
	2	Generally moist or somewhat dry springs, leading into a dry summer and a dry autumn	Start and finish of dry spells highly variable between years. Breaks in seasonal dryness more evident in sub-groups	47	35
	3	Moist winter and spring lead into a damp summer and then either in two of three years a damp or a dry autumn. Dry spells usually last less than 70 days	Tendency for breaks in dry spells to occur between day 270 and day 300	20	15
Dry to very dry late in the annual cycle, leading to very dry extended periods later in the annual cycle (D)	4	Very dry throughout the major part of the year	Dry spell breaks between day 225 and day 260 and ends for the most part by day 310	4	3
	5	Moist in spring and early summer, tending to very dry in autumn	Dry spell starts on between days 170 and day 225 and becomes drier into the following winter	8	6
	6	First pattern is dry winter and spring, followed by a moist summer and then finally by a dry autumn. Second pattern is a dry spring, followed by a dry summer and autumn, breaking very late	Highly heterogeneous patterns in starts and finishes of dry spells but very dry spell starts between day 90 and day 140	38	28

Note: Moist conditions refers to a SWD value from 0 to80 mm. Dry conditions refers to a SWD value from 80 to 140 mm. Very dry conditions exist above a SWD value of 140 mm.

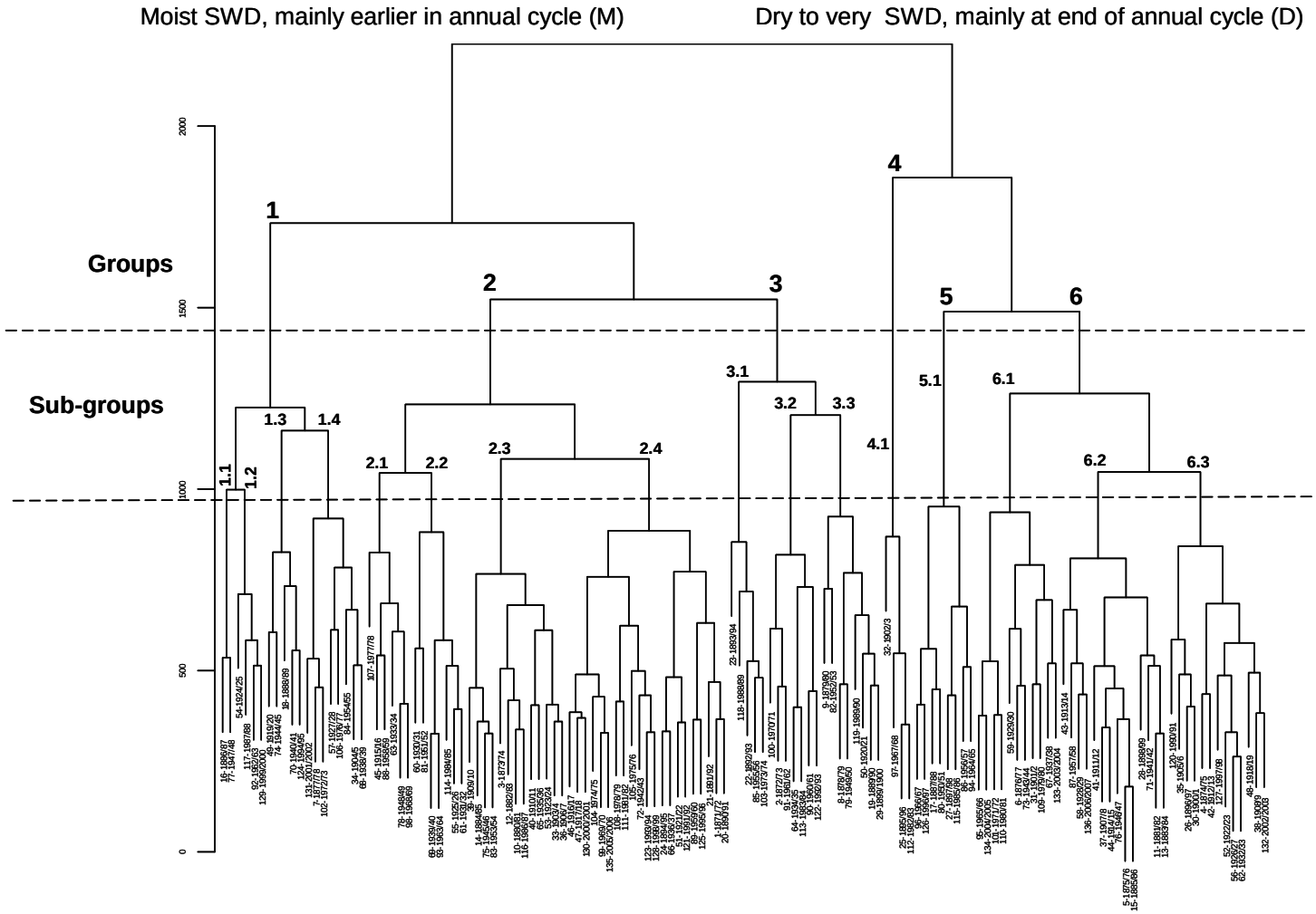

Figure 9.9 Hierarchical classification tree of soil water deficit (1971-2007)

Note: The horizontal dashed lines indicate where the classification tree was cut to produce the SWD groups and sub-groups.

Some further division of the six seasonal soil dryness groups into sub-groups was undertaken (Figure 9.9) giving sixteen labelled sub-groups in all.

Detailed descriptions of each of the sub-groups are presented in Table 9.2. For each of the sub-groups the general descriptions of the season of wet or dry spells, and the timing of the significant breaks within each fire season have been determined from the individual fire seasonal profiles.

While the less dry years appear more prominent in the hierarchical classification, the focus remains on years with seasons dominated particularly by dry mid or late summers (sub-groups 1.4, 2.2, 4.1, 6.2, and 6.3). These sub-groups represent some 31% of all fire seasons, in which the study region has been most exposed historically to LLFs.

Table 9.2 Description of the sixteen SWD subgroups in the long-term landscape dryness record

Sub-group	General description	Significant breaks	Number of fire seasons	Percentage of fire seasons in the time series
1.1	Dry spring , moist summer and autumn	Dry spring break between day 150 and day 160	2	1
1.2	Dry winter start, damper in spring and high summer, grading to dry in late summer and moist in autumn	Dry spell breaks about day 80 to 130. Late summer dry spell ends between days 300 and 310	4	3
1.3	Very dry winter and spring, moist early summer, mildly dry in late summer and autumn	Break in dry spring between days 150 and 175	5	4
1.4	Somewhat dry in winter, moist in spring and summer, fairly dry in late summer, but moist in autumn	Break in dry winter between days 80 and 130. Break in late summer dry spell at about day 300	8	6
2.1	Moist winter-dry spring and summer, moist late summer and autumn	Dry spring builds from a moist winter. Break in dry spring at about day 170	6	4
2.2	Moist winter, dry spring, very dry late summer, moist autumn	Dry spring starts from day 90 to day 110. Dry spell ends abruptly in middle of late summer between days 260 and 280	7	5
2.3	Somewhat dry throughout the year. Starts with a mildly dry winter and spring,-then a dry summer back-to-back with a mild dry autumn	Breaks in wet or dry spells were difficult to predict in this sub-group	13	10
2.4	Moist start to year usually up to the start of high summer period, becoming dry for the rest of the year. Some occasional years with dry years in late spring	Dry spell starts on or about day 180 – the start of summer. End of fire season variable, moving from day 225 to day 310	21	15

Table 9.2 continued

Sub-group	General description	Significant breaks	Number in sub-group	Percentage of total number in time series
3.1	Moist to occasionally dry from winter all the way through to the middle of late summer. Very moist after that	End of fire season between days 250 and days 275. Start of dry period indeterminate because of irregular timing and amount of rainfall	5	4
3.2	Damp or fairly dry winter grading into a damp summer and a fairly dry late summer and autumn	Moist summer starts between days 110 and 150. Short dry spells between day 250 and day 300 or occasionally to day 350.	7	5
3.3	Moist winter and spring grading into dry high summer and late summer conditions, and ending with a moist autumn	Dry spells generally occurs from day 170 to day 250 or 300.	8	6
4.1	Extremely dry throughout the year	Driest period ends between days 225 to 255. Abrupt end to dry spell about day 317	4	3
5.1	Moist winter and early spring grading into a dry summer and then a very dry late summer and autumn	Start of summer dry period between on or days 160 to 180. End of dry period usually as late as mid winter and possibly extending into the next fire season	8	6
6.1	Very dry winter grades into a very dry early spring. Some breaks in late spring reverting back to a dry late summer and autumn	End of very dry winter on or about day 50. Start of dry conditions in very late summer, on about day 225, then staying dry until mid winter	11	8
6.2	Dry winters lead into a progressively drier spring, occasionally becoming very severely dry in the high summer or late summer period. Autumns still dry after some rainfall	Highly variable start to summer dry period. Either starts early, between days 130 or 140, or starts much later around day 170. Intensely dry period ends between days 220 and 310	14	10
6.3	Somewhat dry to dry in the first part of winter and sometimes moist in early spring, becoming progressively drier in late spring. Extreme dryness in mid or late summer, extending into autumn	Summer dry period can start as early day 140-150 and ends by day 210. A later summer period is evident in some years starting as late as day 170 and finishing between day 310 and 330	13	10

Note: Grey shading indicates SWD fire season groups that have had the highest potential exposure to large landscape fires.

Moist conditions refer to a SWD value from zero to80 mm. Dry conditions refer to a SWD value from 80 to 140 mm. Very dry conditions exist above a SWD value of 140 mm.

To distinguish the dry season SWD groups better, an image plot of the fire seasons ordered by the classification sequence was created (Figure 9.10). Fire seasons are represented on the abscissa and the ordinate represents the days in the annual cycle starting on 1 July and ending on June 30. The values of SWD are plotted from lowest to highest SWD values with heavy orange dashed lines indicating the breaks between the SWD groups, and dotted orange lines the breaks between sub-groups. Outside of SWD groups 1 and 4 there is considerable variability within the other groups (2, 3, 5, and 6) in the timing of onset and level of landscape dryness. Displaying the fire seasonal profiles of SWD in this form confirms the breaks made in the classification tree to produce the groups and sub-groups of SWD (see Figure 9.9).

Figure 9.11 shows three diagrams on the one diagram: (a) the classification tree at the top of the diagram (Figure 9.9), (b) the long-term seasonal daily SWD anomaly (left hand side of diagram), and (c) the classified fire seasonal profiles reproduced from Figure 9.10 but reordered by the sequence of fire seasons in the classification tree (Figure 9.9). The long-term daily seasonal SWD anomaly diagram view reveals that the driest time of the year is normally between late summer and early autumn despite the fact that, in wetter years, the driest period occurs earlier, that is from spring to mid-summer. The sub-groups in which landscape dryness reaches its peak at this time are: SWD groups 1.4, 2.2, 4.1, and 6.3. These sub-groups are the only ones in the fire seasonal profiles of SWD having fire seasons with the values of peak landscape dryness sometimes occurring earlier than the pattern evident in the long-term daily SWD anomaly. This suggests a different combination of broader climatic influences in the development of landscape dryness in these SWD sub-groups.

Now that the fire seasons have been classified into readily identifiable groups and sub-groups, the next step is to examine the temporal sequence of the SWD groups and sub-groups over the long-term time series.

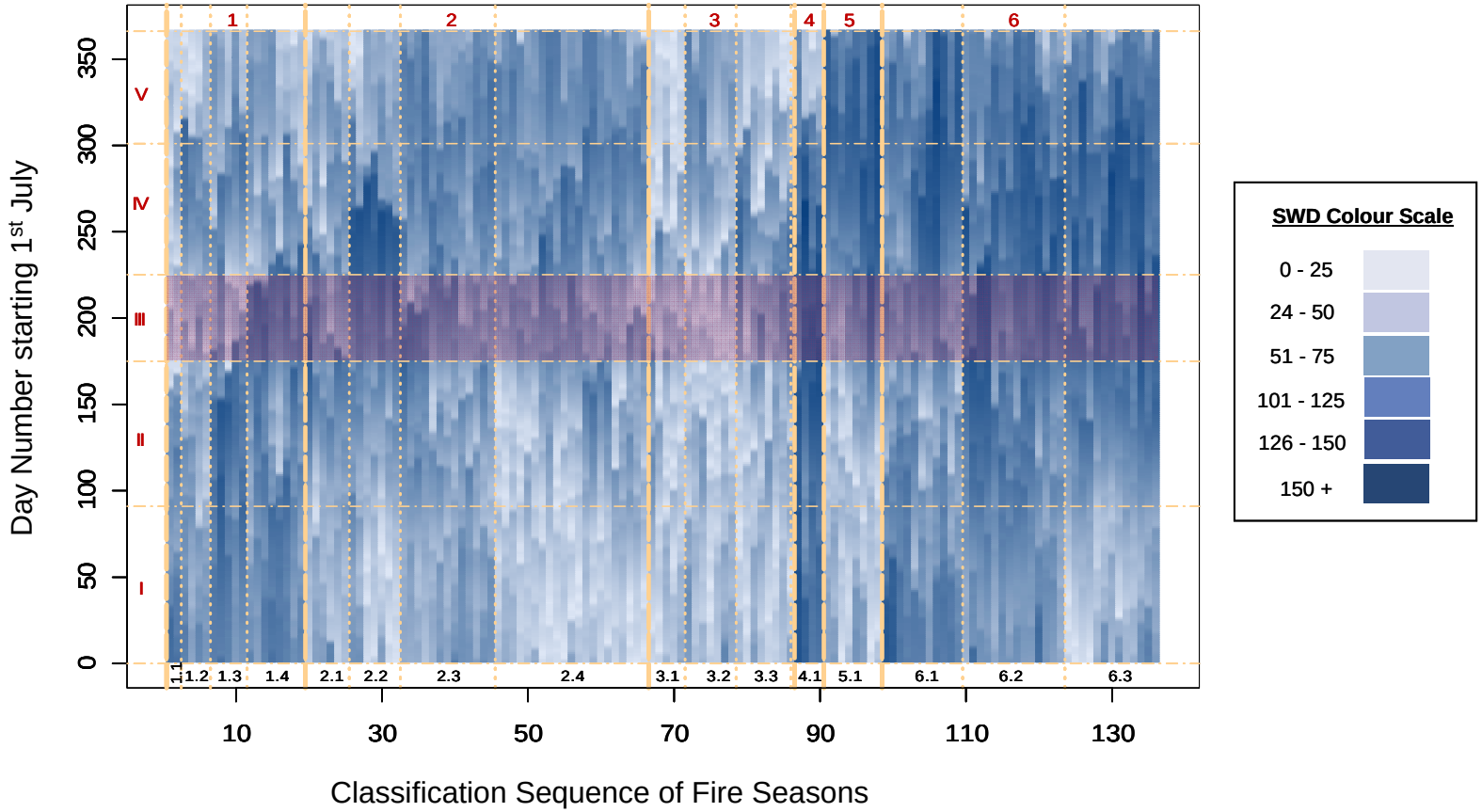

Figure 9.10 Hierarchical classification of Soil Water Deficit viewed from a seasonal (x-axis) classification sequence (Y-axis) (1971-2007)

Notes: (1) The orange vertical dashed and dotted lines indicate the boundaries between the groups and sub-groups, respectively. The numbers refer to those found in the classification tree in Figure 9.9.

(2) The darker the blue shade in the diagram, the greater is the value of Soil Water Deficit (SWD). The colours shown in the colour scale are approximate to those in the diagram.

(3) The reddish pink colour area in the middle of the figure represents the high summer fire risk period previously defined in the ACT's fire season calendar (see Table 8.1).

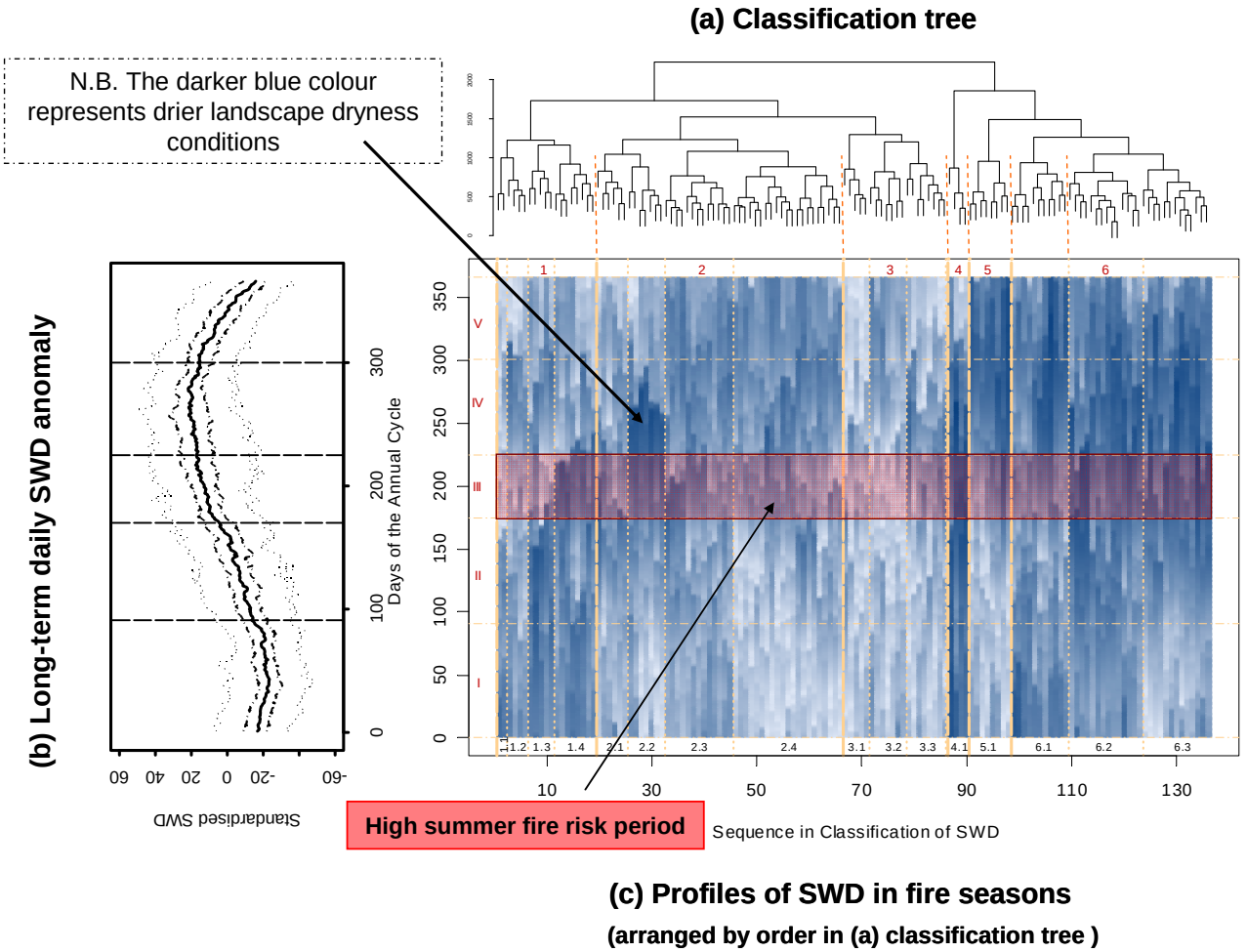

Figure 9.11 Combined view of (a) classification tree, (b) long-term daily SWD anomaly, and (c) profiles of SWD in fire seaso

9.2.1 Temporal sequence of fire seasons based on classification group and sub-groups

The previous section classified the years in the SWD time series into recognisable and interpretable groups and sub-groups of fire seasons. This section explores the temporal sequences of the original SWD time series juxtaposed against the SWD year groups and sub-groups (Figure 9.12). The colour codes represent different levels of landscape susceptibility to large fires based on the SWD groups developed earlier (Figure 9.9). Blue and green colours represent fire seasons with low susceptibility to large fires (SWD fire season groups 2 and 3). The yellow colour represents fire seasons with intermediate susceptibility to large fires, (SWD group 1); and the purple, deep orange and red colours represent fire seasons with high to very high susceptibility to large fires (SWD groups 4, 5, and 6). The top box represents the classified SWD group and the bottom box represents the SWD sub-group classified for that fire season.

The colour coding of fire seasons by the SWD groups and sub-groups helps to identify the sequences of wet and dry seasons, as well as the timing of acute dryness of that fire season. The blue coded SWD group 3 fire season, representing the very moist to moist fire seasons, occurs relatively infrequently and irregularly at a relatively low recurrence (~15%). Sometimes such seasons have occurred two years in a row, yet at other times, these fire seasons have occurred at much longer intervals, at 10, 15, or 20 years. The yellow coded sub-group 1.1 fire seasons represents the wetter end of the moist-dry fire seasons within the SWD group 1 fire season. At the drier end of this group, SWD sub-groups 1.3 and 1.4 contain some fire seasons with a very high potential for LLFs, such as those occurring in 1938/39. They are relatively sporadic in occurrence, becoming more frequent from the 1920s onwards, but occurring at relatively long and irregular intervals between seven and twelve years apart.

More often, the slightly drier SWD group 2 fire seasons (which constitutes 35% of the fire seasons) alternate with the very dry SWD group 6 fire seasons (28% of fire seasons) over the time series or have occurred in consecutive years during a drier cycle, such as in the 1910s or early 2000s. Unlike the SWD group 1 fire seasons, the green coded SWD group 2 fire seasons have generally had less complete soil water recharge at the end of the year, resulting in higher soil water deficits at the start of the next fire season. In a few fire seasons, near extreme levels of landscape dryness can occur towards the end of the high summer period.

The temporal sequencing of the fire seasons within their respective groups and sub-groups does not show a clear regular pattern but rather an irregular one. However, one feature of the time series does stand out: SWD group 6 fire seasons have recurred for up to three or four years in a row. SWD group 2 fire seasons can sometimes interweave amongst the SWD group 6 fire seasons for up to two years. On occasions, SWD group 6 fire seasons alternate with SWD groups 1 and 5 fire seasons. On rare occasions, a SWD group 5 fire season has signalled a very dry one to follow.

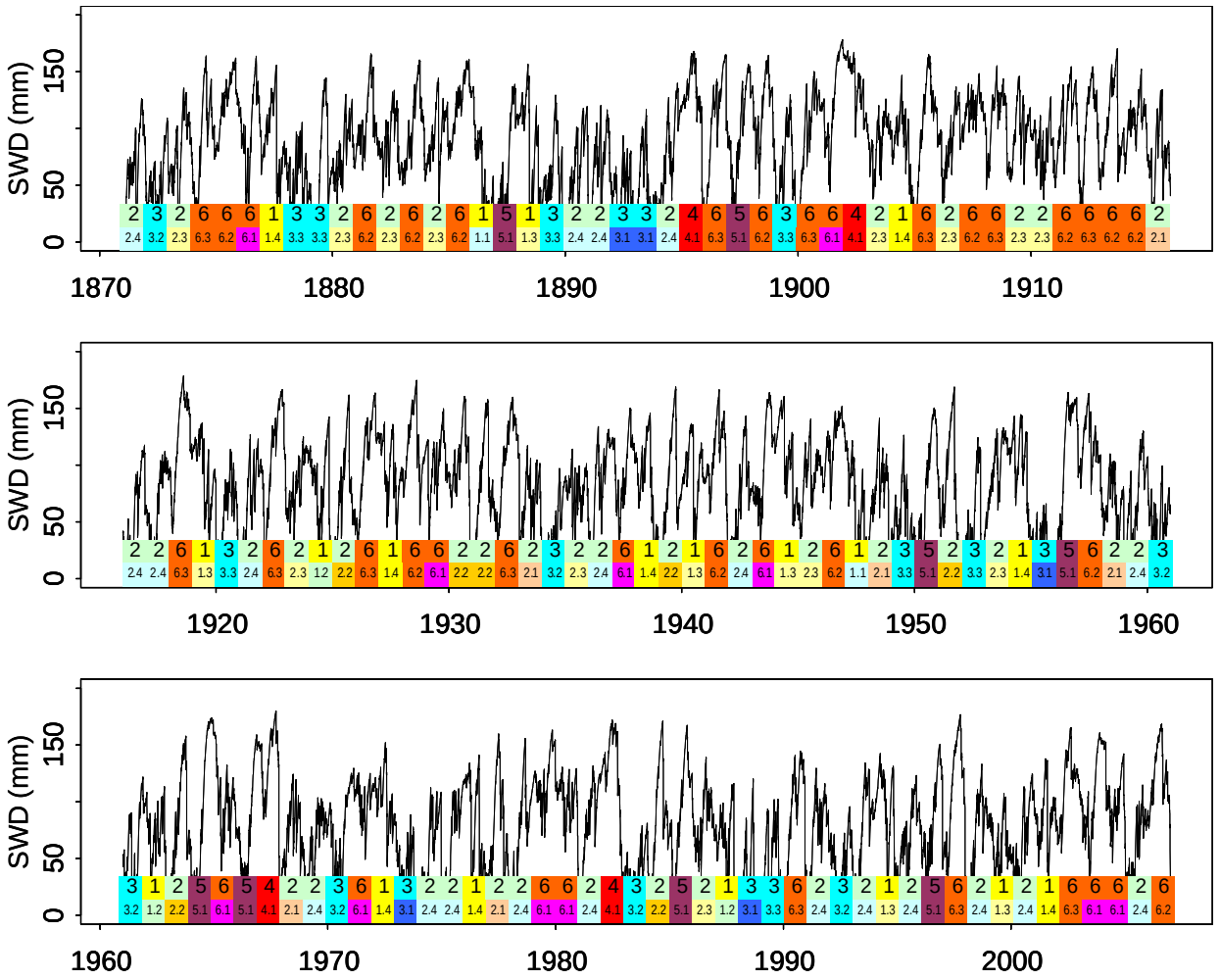

Figure 9.12 Temporal sequence of groups and sub-groups of annual profiles of landscape dryness juxtaposed with original time series

Note: The colour coding reflects the landscape susceptibility to large fires in a colour continuum from low (dark blue) to extreme levels (dark red).

The sequence of groups and sub-groups in Figure 9.12 reveals a more chaotic and irregular pattern than those revealed by the sub-decadal and decadal LOESS filters in the time series decomposition (section 9.1.4). The complex interactions among all the climatic and synoptic scale factors responsible for producing rainfall are responsible for this variability. This is discussed further in section 9.3.

9.2.2 Fire seasons leading to landscapes being highly susceptible to large landscape fires

The purpose of this section is to identify the fire seasons in landscapes most susceptible to LLFs since 1871. The idea behind this is that the period of highest susceptibility to LLFs occurs when extremes in landscape dryness conditions are aligned with high summer (Table 8.1; section 8.1.1). However, the periods either side of the high summer period still have some potential for LLFs. In addition, in the earlier or later parts of the fire season, the spells of potential fire spread are not as long or as severe as those occurring in the high summer period.

The first step in identifying the high risk fire seasons was to plot the long-term SWD data as two dimensional plot with years on the abscissa and days of a fire season on the ordinate (Figure 9.13 (a), first panel). The yearly profiles of SWD are plotted as a matrix of years by days of the year, the lighter areas indicating the moister times and the darker areas in the figure indicating the drier times in the year. Although some of the very dry fire seasons stand out, having extended darker blue colours, it is difficult to know which of these fell into the fire season periods of II, III, and IV, representing spring, high summer, and late summer respectively.

To discriminate the high-risk fire seasons to LLFs from the rest, an SWD of 120 mm was applied. At this threshold, near-surface and heavier ground fuels are fully dried out, there are high levels of curing of grasses, and live leaf moisture content (LLMC) is minimal with consequent high vegetation flammability and high to very potential for LLFs (section 7.3).

The results of applying this critical threshold show the fire seasons with critical periods of dryness in either peak or late summer (Figure 9.13 (b), second panel). Each SWD sub-group was given a unique line pattern and colour to help differentiate them from each other. The first SWD group 1.3 is shown as a blue vertical line. The purple vertical line represent SWD sub-group 4.1 while the red vertical lines represent SWD sub-groups 6.2 and 6.3. The green and orange lines represent the fire seasons with some potential for LLFs (for example, 1.4); or sub-groups of fire seasons (5.1, 6.1) whose peak SWD occurred very late in the annual cycle. This second panel illustrates the relative frequency of fires seasons with the highest potential for LLFs through the time series.

Prior to the 1940s, a higher frequency of fire seasons with the potential for LLFs is indicated. Since the 1940s, the frequency of peak SWD years, signifying potential risk to LLFs

has decreased, with some notable gaps being found in the late 1940s and early 1950s, 1970s and the 1990s.

The threshold of 120 mm was then applied to just those fire seasons whose peak period dryness overlapped with high summer (Figure 9.13 (c), third panel). This was designed to locate fire seasons that have had the landscape susceptibility to LLFs.

This analysis showed that there was a much higher likelihood of LLFs from the 1900s, until the mid 1940s, with intervals between high risk fire seasons, occurring at shorter intervals between five and ten years. This mirrors the higher frequency of LLFs found by earlier studies (Brackenreg, 1926; Pryor, 1939; Banks, 1982). Since the 1940s, the interval between fire seasons with very high potential for LLFs has widened to 12 to 20 years. A reverse trend has become evident since the early 2000s, with the intervals between high risk fire seasons shortening to four or five years. This final panel shows that the intervals between fire seasons with highest susceptibility to LLF have shortened or lengthened in the last 135 years in three recognisable periods: (1) from the 1900s to the 1940s; (2) from the 1940s to the 1990s; and (3) from the early 2000s to the present. If one presumes landscape dryness at the right time of the year predisposes landscapes to LLFs, then the likelihood of LLFs occurring has varied considerably in this long-term study (1871-2007). Since the incidence of lightning-started fires was found to be most likely in the high summer period (section 8.5), this leaves only the fire seasons of 1951/52, 1982/83, and 2002/03 as being likely to have the potential for LLFs. The rest of the potentially high risk fire seasons identified in Figure 9.13 (c) either did not have the potential for dry thunderstorms and multiple lightning ignitions or the peak landscape dryness did not fall within high summer. This longer-term study has therefore confirmed the original proposition that only in particular types of fire seasons have landscapes been susceptible to LLFs.

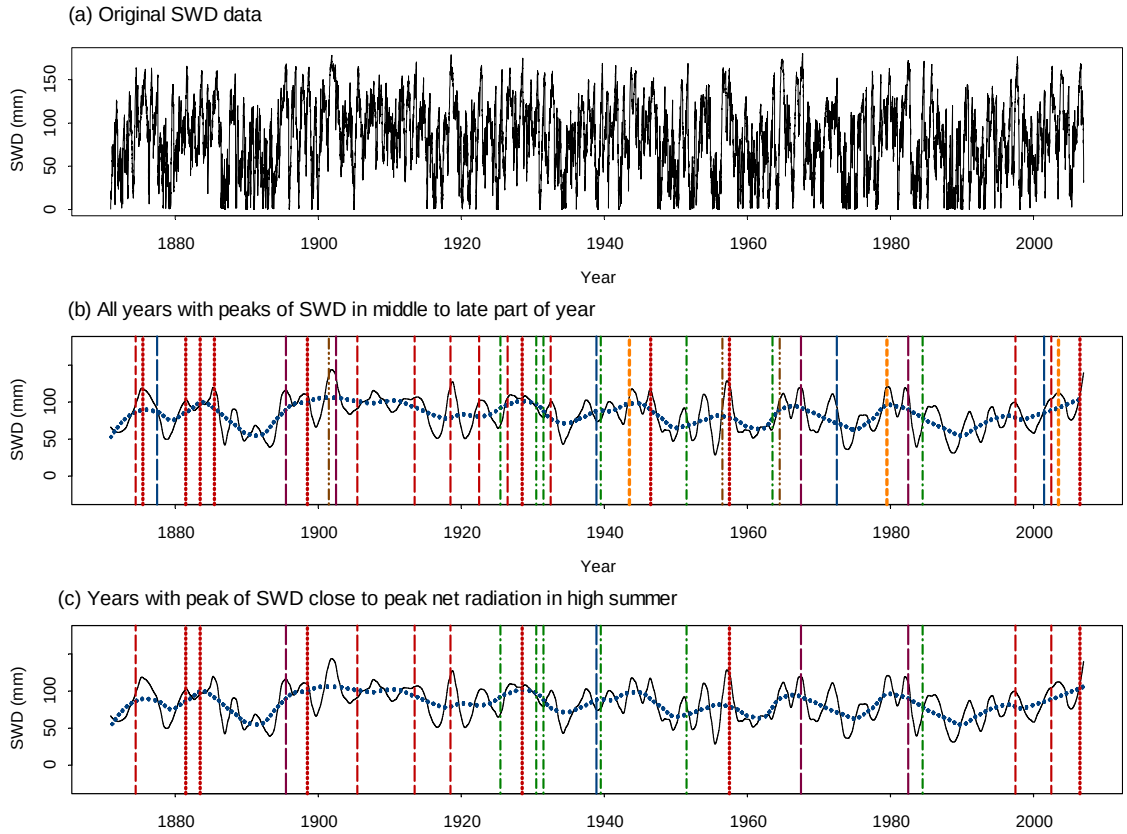

Figure 9.13 (a) Original SWD data (b) SWD >120 mm in peak and later summer periods, and (c) SWD >120 mm only in the high summer period

Note The vertical lines in the second and third panels represent the fire seasons that belong to the SWD groups 1.4, 2.2, 4.1, 5.1, 6.1, 6.2, and 6.3 identified as being the most likely to being predisposed to LLFs.

The blue hatched vertical lines correspond to fire seasons in SWD sub-group 1.3. The green dash and dotted lines represent fire seasons in SWD sub-group 2.2. The purple long dashed lines represent fire seasons in SWD sub-group 4.1. The orange heavy dotted lines represent fire seasons in SWD sub-group 6.1. Lastly, the red dotted and dashed lines, and dashed lines, represent fire seasons in SWD subgroups 6.2 and 6.3 respectively.

The fire seasons in which landscape dryness exceeded an SWD value of 120 mm in the high summer period are shown in Figure 9.14. By applying this filter, 43 high-risk fire seasons were extracted from the original 136 fire seasons in the long-term time series.

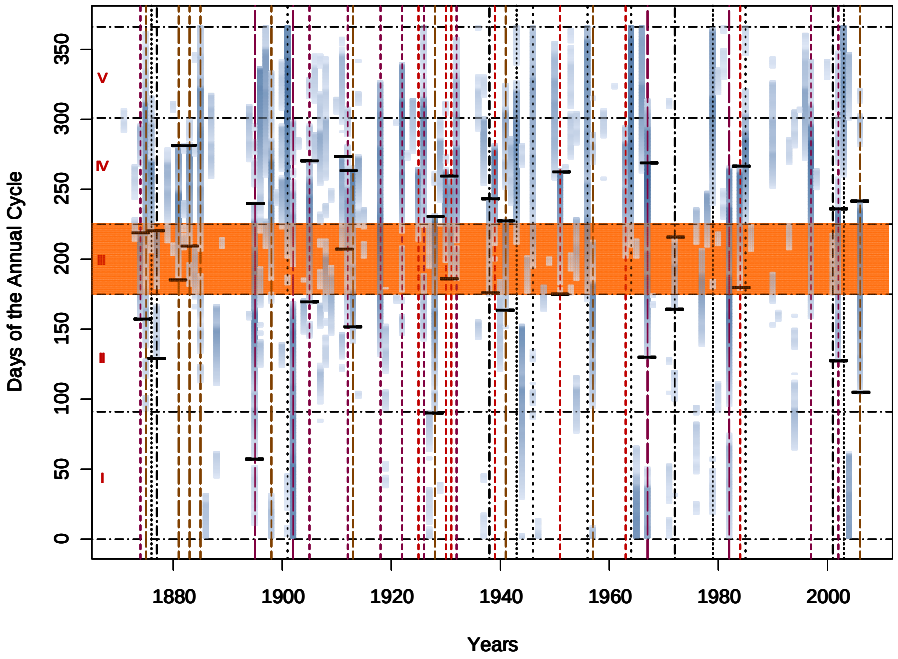

Figure 9.14 Fire seasons with peak landscape dryness (SWD>120) falling in the high summer period

The high-risk fire seasons identified in Figure 9.14 were cross-tabulated with those in the fire seasons' chronology in the study region (see section 2.5) to produce Table 9.3. Those that feature the most often in Table 9.3 are SWD sub-groups 2.2, 6.2 and 6.3. Sub-group 2.2 had the highest occurrence rate, with six out of seven of the fire seasons starting early in the peak period of SWD and ending in the middle of the late summer period. Although most of the fire seasons in sub-groups 6.2 and 6.3 ended at about the same time in the late summer period, there were six fire seasons in these two sub-groups that ended abruptly, either just in or just outside high summer (Table 9.3: boldfaced fire seasons in column 2). These included 1874/75, 1905/06, 1928/29, 2002/03 and 2006/07. Two other sub-groups that have very dry periods ending abruptly include 1895/96 (sub-group 4.1) and 1938/39 (sub-group 1.3). The fire season of 1938/39 features very much in the history of disastrous fire seasons in Australia. However, in the ACT region the 1938/39 the fire season was not as severe in terms of landscape dryness as some other fire seasons, such as 1902/03, 1918/19, 1964/65, 1982/83, and 2002/03.

Table 9.3 Fire seasons with landscapes highly susceptible to LLFs

Sub-group	Fire Seasons	Total number in sub-group	Filtered number	Proportion of number in sub-group	Proportion of LLFs in sub-group
1.3	1877/78, **1938/39**, 1972/73, **2001/02**	5	4	80%	50%
2.2	**1925/26**, 1930/31, **1931/32**, 1939/40, **1951/52, 1984/85**	7	6	86%	67%
4.1	1895/96, 1967/68, **1982/83**	4	3	75%	33%
6.2	**1875/76**, **1881/82**,**1898/99**, **1928/29**, 1943/44, 1957/58, **2006/07**	14	7	50%	71%
6.3	**1874/75**, **1905/06**, 1913/14, **1918/19**, 1997/98, **2002/03**	13	6	46%	67%
Total		**43**	**26**	**60%**	**58%**

Note: The fire seasons highlighted in bold are the ones that had known LLFs (Chapter 2: section 2.5).

Of all the SWD sub-groups, fire seasons classified as sub-groups 2.2, 6.2 and 6.3 have the highest proportion of fire seasons with known LLFs in the historical record (67, 71 and 67% respectively), followed by sub-group 1.3 (50%).

As well as the very high risk fire seasons (SWD sub-groups 1.3, 4.1, 6.1, and 6.2), landscape susceptibility to large fires in sub-group 2.2 almost reaches the same risk levels as these. For this reason, they are highlighted in bold italics, marking them as seasons with a very high potential for LLFs. The highlighted fire seasons identified in this fire susceptibility analysis are indeed those recognised in records as mostly having LLFs (see section 2.5). Therefore, this simple approach using only one indicator of fire susceptibility has the capability to identify past high-risk fire seasons with high to very high potential for LLFs.

The method used to identify seasons with a high potential for LLFs historically could also be used to identify the risk of LLFs in the lead-up to and during the high summer period, by matching the current fire seasonal profile to one of more of the SWD group or sub-groups. Other climatic factors and influences should be used in conjunction with this simple method and are discussed in the next section.

9.3 Climatic influences setting up LLF conditions

The tools currently used to forecast the type and severity of fire seasons have tended to focus on climatic indicators at sub-global and continental scales (Lindesay, 2003). These climatic indicators are rudimentary and sometimes limited in their ability to anticipate the evolution of a fire season at a regional scale. The most widely used indicator, the Southern

Oscillation Index (SOI), uses differences in surface pressure between Darwin and Tahiti. Examples of indicators of sea surface temperatures (SSTs) include the Indian Ocean Dipole (IOD), Niño3 in the central Pacific, and Niño4 in the western Pacific. Various combinations of these indicators have been used to explain or forecast the potential for wet and dry fire seasons across Australia and indeed for other countries or regions bordering the Pacific. The relationships between drought and these indicators are tenuous and have low levels of correlations in most parts of south eastern Australia (McBride and Nicholls, 1983) and in northern New Zealand (Fowler and Adams, 2004). For example, low levels of correlations (R^2=0.1-0.4, and up to a maximum of 0.6) between monthly rainfall and the SOI were found based on the spring quarter (McBride and Nicholls, 1983; Drosdowsky and Williams, 1991). The relationship between the SOI and rainfall is even more tenuous for the ACT region, given that it is not located in the central core of the regions where rainfall is more highly correlated with SOI.

The purpose of this study is to derive a temporal history of fire susceptibility factors SWD and FWI (section 1.3), using a classification approach that differentiated the general groups and sub-groups of fire seasons. The synoptic-scale weather patterns and rainfall processes are regarded as being more influential in the development of the most severe fire seasons than the broad scale indicators, such as the SOI, which is currently used to predict severe droughts and fire seasons with a high potential for LLFs. At this synoptic scale, these patterns and processes could serve as complementary indicators to the sub-global and continental climate indicators already mentioned. At one level, the groups of historical fire seasons examined in Chapter 8, and in this chapter, provide an insight into the ways in which synoptic and sub-global climatic factors have produced different types of fire seasons.

9.3.1 Australian climatic factors and influences

To this end, it is more appropriate to examine the climatic factors that produce daily and monthly weather patterns at the regional synoptic scale. A summary of the major synoptic and background influences on the weather patterns across the Australian continent is illustrated in Figure 9.15, from the Bureau of Meteorology's web site. This diagram summarises the key synoptic features that interact on a daily basis to produce the patterns of weather at any point on the continent.

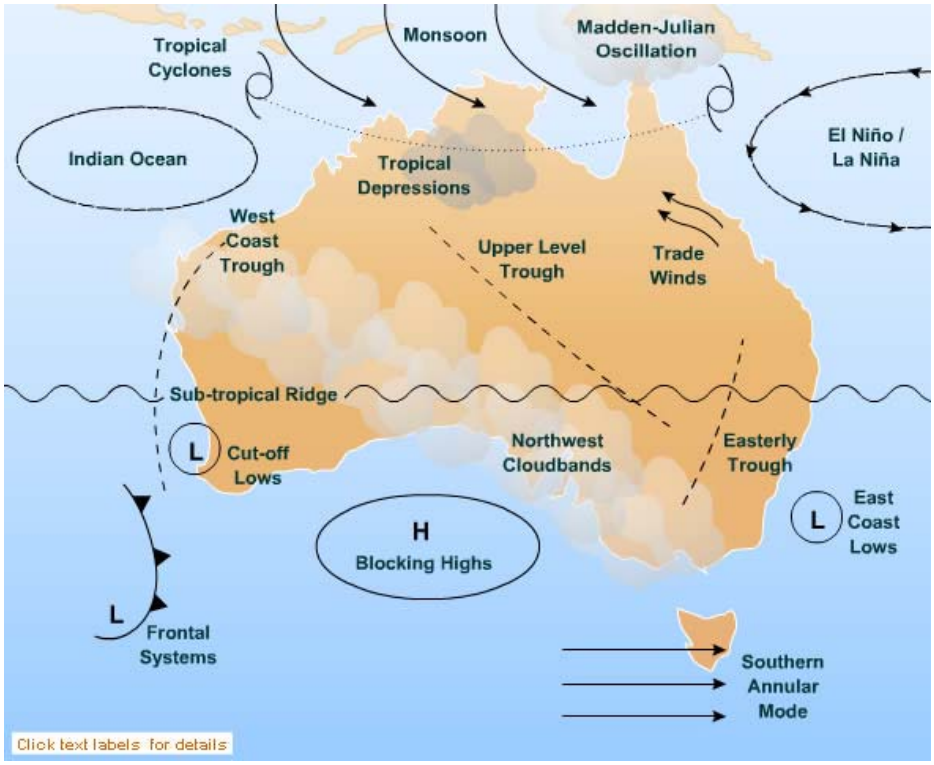

Figure 9.15 Significant climatic influences across the Australian continent

Source: Bureau of Meteorology, 2008.

At this scale, the study area lies within a belt of mid-latitudinal high pressure systems (anticyclones) that dominate the atmospheric circulation of Australia and New Zealand (Sturman and Tapper, 2006). These high-pressure systems are located in what is termed the sub-tropical ridge. The highs generally track further north in winter at about latitude 30-35^{o} whereas in summer they track further south at about latitude 40-45^{o} (Hobbs, 1998). The anticyclones travel more slowly than the faster-moving depressions and associated cold fronts (bottom left of diagram). The anticyclones therefore dominate the weather patterns with stable warm and dry weather for periods up to five or seven days, with a one or two day passage of the cyclonic systems. This sets up on average a seven to ten day cycle of the two alternating weather systems in the southern half of the Australian continent.

Because the study region and the southern part of the Australian continent are located within the belt of sub-tropical highs, the weather patterns tend to be dry under the influence of these stable high-pressure cells. Extended dry periods can result if these stable high-pressure cells dominate the weather patterns for weeks at a time. Therefore, the long dry patterns seen in the majority of fire seasons (see Figure 9.10) should be considered the normal pattern and the occasional days of rain as much less common and stochastic. A majority of the major rainfall events are made possible by the interaction of sub-tropical-temperate troughs with low-pressure cells to the south of the continent to produce rainfall in the study region and elsewhere in southern Australia (Murphy and Timbal, 2008). However, not all the sub-tropical-temperate

troughs come laden with atmospheric moisture. Those troughs bringing dry hot and unstable air from the continent can result in severe fire weather, and if combined with a dry landscape, can produce severe fire-risk conditions. This is discussed further in the following section.

9.3.2 The influence of the sub-tropical-temperate trough on landscape susceptibility to LLFs

Another feature which plays a major role in drawing moisture from the sub-tropical regions of Northern Australia is the westerly upper level troughs that develop in the central regions of the continent, particularly during the warmer times of the year (Hanstrum *et al.*, 1990; Sturman and Tapper, 2006). These should be more correctly termed tropical-temperate troughs (Harrison, 1986, cited in Lindesay 1998). These systems are involved with the flow of energy from the tropics across the continent into the cooler maritime area, the Southern Ocean, south of the Australian continent. These westerly tropical-temperate troughs are almost always associated with southern frontal systems passing through the Great Australian Bight (Hanstrum *et al.*, 1990). In some instances, these troughs assist in the formation of cut-off lows which are responsible for the major rainfall events in south eastern Australia, or the east coast lows which form in the Tasman Sea (Sturman and Tapper, 2006).

During the height of summer, tropical-temperate troughs carry little if any moisture and so can direct hot dry and windy weather into south eastern Australia, instead of rain. The upper levels of these troughs can carry very little air moisture. From inspection of many synoptic weather charts, the orientation of the line of the troughs affects how much air moisture, if any, is carried into this region. A tropical-temperate trough of air aligned longitudinally will generally draw more moisture into the region as it is more connected with the sub-tropical air masses further to the north. Hence, it is likely to result in higher rainfall more often than not.

A trough that is aligned meridionally transports very dry hot air into the region, prior to the arrival of a polar maritime cold front (Hanstrum *et al.*, 1990). The latter type is often associated with extreme fire spread potential days that have occurred historically on the 13th January 1939 (Foley, 1947), the 5th February 1952 (Luke and McArthur, 1978), 16th February 1982 (Hanstrum *et al.*, 1990), 18th, 26th and 30th January 2003 (Taylor and Webb, 2005), and most recently the 7th February 2009. On these days with extreme potential fire spread, tropical-temperate troughs draw hot, dry, and unstable air from the centre of the continent. As a result, hot and dry north-westerly winds are generated ahead of the trough and associated cold front, producing the extremes of fire weather witnessed in most of the severe fire seasons that resulted in the LLFs in south eastern Australia in 1938/39, 1982/83, 1997/98, 2002/03, 2006/07, and 2008/09. If the trough is aligned half way between the vertical and horizontal position during a dry fire season in the high summer period (III), it is most likely to be associated with dry thunderstorms and lightning-ignited fires (for example, 5th February 1952, 8th January 2003, and 1st December 2006).

The north-west cloud bands over the study region are often associated with deeper and moister westerly sub-tropical-temperate troughs, particularly when the monsoon is active in northern Australia or sea surface temperatures off the northwest coast of Western Australia are warmer than usual. These north-west cloud bands diminish in frequency and moisture during dry fire seasons when there is less moist sub-tropical air rising from the Eastern Indian Ocean and less upper air convergence associated with the jet stream moving south at these times. At the same time, less tropical moisture is also linked to Hadley cells that have moved further eastward over the central Pacific Ocean, during moderate to strong El Niño events (Lindesay, 2005). Thus, the tropical-temperate troughs are of critical importance in cooling or heating up the local climate of the region. A repeated sequence of dry and hot tropical-temperate troughs can therefore produce the dry lead-up conditions to a severe fire season, including lightning ignitions and severe fire weather that initiate and create LLFs. Follow-up studies of this critical synoptic-scale phenomenon may lead to better understanding of the factors that produce the switch from cool and moist to hot, dry, and windy conditions associated with the development of severe fire seasons.

As well as the tropical-temperate troughs, the easterly trough system separates the moist air mass arising from the Tasman Sea from the inland drier air, mainly along the Great Dividing Range that runs north-south 50-150 km inland from the eastern Australian coastline. This trough is largely responsible for the development of east coast lows that produce large rainfall events and the development of summer thunderstorms that move towards the eastern Australian coastline. Based on an analysis of thunder-day data from Canberra airport, the easterly trough has produced on average 22 thunderstorms a year in the area since 1939 (Figure 9.16 (a)).

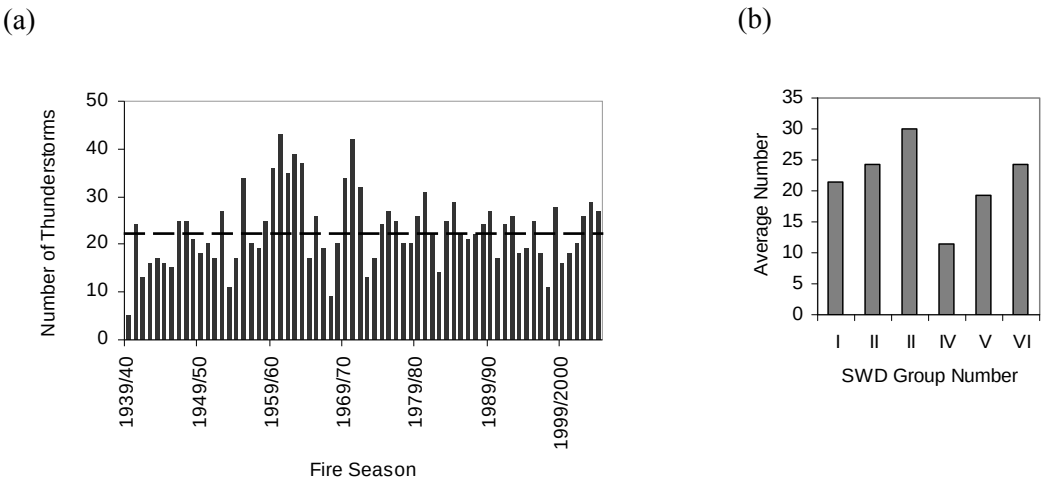

Figure 9.16 (a) Number of thunderstorms in each fire seasons since 1939/40 and (b) average number in each SWD group

Source: Extracted from weather data for Canberra (1940-2007).

Note: Number of thunderstorms is based on records of thunder-days in Canberra Airport's weather record.

During La Niña years (SWD group 3, long-term time series), thunderstorm activity is more pronounced, rising to an average of 29 thunderstorm days per year. Otherwise, thunderstorm days are close to the average in all other SWD fire season groups, with the exception of SWD group IV in the medium term series, when thunderstorm activity is well below the average, at twelve thunderstorm days (Figure 9.16 (b)). Thus, moist thunderstorms are crucial for the summer rains to abate the usual dry hot summer conditions associated with high levels of all-wave net radiation on clear sunny days. In the severe fire seasons clustered into group IV, fewer and drier thunderstorms occur and are more likely to ignite fires before severe fire weather days.

9.3.3 The effect of the sub-tropical ridge and other synoptic weather features on the potential for large landscape fires

The previous discussion focussed on synoptic processes operating in the sub-tropical ridge zone in which the study area lies. The interactions, or the lack thereof, between the sub-tropical highs and the tropical-temperate troughs with low pressure systems further to the south of the Australian continent are critical for understanding the sequences and type of fire weather found in the study area. The Southern Annular Mode (SAM) is one indicator of the influence of Southern Ocean lows on rainfall in south eastern Australia. SAM has been found recently to influence rainfall in the winter, spring and summer periods of the year in the southwest and southeast of Australia in a way that is mainly related to the latitudinal position and strength of the westerly winds over these southern areas of Australia (Kidson, 1988). When SAM is in a negative phase, the lows move northward and have a significant influence on rainfall and temperature in the southern parts of the continent. Conversely, when in a positive phase, SAM contributes to a lower and drier trend in the southern parts of the continent.

There is a current trend in SAM towards a higher, positive polarity in summer and a lesser, positive trend in autumn. Hence, the increased tendency towards a positive polarity could lead to fewer strong cold fronts and perhaps fewer high rainfall events during the critical lead-up period in spring and early summer. Reduction in rainfall would also occur because of reduced sub-tropical moisture in northern Australia when SAM is in a positive mode. At the sub-annual time scale, SAM is at its strongest in winter-spring and weakest in late summer-autumn. A positive SAM at the onset of a fire season would signify a lower potential for rainfall. This state, combined with other factors such as lower moisture over the north of the Australian continent (under El Nino conditions) would produce extended dry spells during spring and early summer. These combinations of conditions inevitably lead to very dry landscape conditions (high to very high SWDs) by the middle of summer as evidenced in the SWD groups and sub-groups in the medium-term (section 8.2.2) and long-term (section 9.2) series of landscape dryness.

Another way of looking at the influence of SAM is to use indices of mean sea level pressure (MSLP) within and adjoining the southern Australian continent to define the latitudinal position and strength of the Sub-Tropical Ridge (STR). Essentially the north and south latitudinal movement of the STR is highly correlated with the mid-latitude jet stream (MLJ) which is located on the poleward side of the STR (Williams and Stone, 2008). When the SAM is in a negative mode, the STR and the MLJ move northward, enhancing the potential for higher rainfall events over south eastern Australia. Conversely, when the SAM is positive, the STR moves south along with the MLJ, thus lowering the potential for rainfall, through the combined effects of higher than average pressure in both the lower and upper troposphere.

The sub-decadal and decadal movements of the STR are strongly correlated at 3-4 years and at 12 years respectively (Williams and Stone, 2008), which corresponds to the cycles found in the fluctuations of landscape dryness (SWD) in the time series analysis conducted at sub-decadal (Chapter 9; section 9.1.1) and decadal time scales (section 9.1.2). Although not statistically significant, Thresher (2002) found a relationship between sunspot cycles and the position of the STR at intervals between 10 and 12 years. These recent studies suggest that the earlier proposition put by Vines (1974) of a possible relationship between bushfire and sunspot cycles may have some basis to it, especially in relation to the strength of the STR during spring and summer during a severe fire season.

The establishment of very dry landscape conditions can therefore be related to the interactions of the key climatic factors and processes relative to the geographical location of the study area and to the continent at large (see Figure 9.15). The key factors and processes identified but not explored in this study, can be summarised as follows:

- the relative latitudinal and longitudinal position and strength of lows and highs in relation to the sub-tropical ridge (STR) traversing Australia and New Zealand, particularly the establishment of a blocking high pattern in the Tasman Sea, leading to low pressure systems migrating further south during extended spells of landscape dryness;
- the spatial configuration of, and anomalies in and between, land and sea surface temperatures during a fire season, particularly cooler temperatures in the eastern Indian Ocean and the Tasman Sea;
- the origin and amount of moisture in the lower, middle, and upper regions of the lower atmosphere from source regions, such as the northern Australian tropical zone, the Tasman Sea and the Southern Oceans immediately south of the Australian Bight. It appears that cooler sea surface temperatures result in less atmospheric moisture and cloud in the form of north west cloud bands reaching the region; and
- the origin and transfer of moisture into the region via low pressure troughs, cut-off lows and the passage of cold fronts weakens during periods of landscape dryness.

The particular conditions of dry thunderstorms and hence lightning-started fires can be related to a particular set of atmospheric conditions and with a westerly sub-tropical-temperate trough, associated with a weak frontal system to the south of the continent, more likely occurring in December and January during a dry spell when the landscape dryness is above 64 mm SWD. Multiple lightning ignitions resulting from dry thunderstorms may be more likely when index of the landscape dryness exceeds a critical threshold value of SWD somewhere between 100 and 140 mm. Note that the latter threshold of SWD corresponds to the suggested tipping point for increased fuel availability and flammability found in the literature (section 7.3) and empirically in this study (section 8.4.1).

9.3.4 Key synoptic factors influencing the potential for large landscape fires

Finally, the onset of severe fire weather appears to occur close to the peak of landscape dryness just before a reversal to moister and cooler conditions in the late part of the high summer or late summer period (see section 9.1.1). Drawing on experience in Canada and north western America, the timing and severity of fire weather appears to be related to the breaking down of the sub-tropical ridge over the North American continent (Simard, 1991; Johnson and Larsen, 1991). In particular, Johnson (1992) identified three main factors predisposing boreal forests in Canada to large fires:

(1) the position and strength of blocking highs centred over central Canada for long periods;

(2) a breakdown of this strong seasonal pattern with a possible shift in the position of the jet stream; and

(3) the advance of the Arctic airstream southwards.

Johnson contends that the severe fire weather associated with strong westerly airstreams usually coincides with deeper low-pressure systems finally displacing the stationary blocking highs at some critical point in the fire season. As can be seen from Chapter 8, the timing and severity of fire weather has been related to the high summer period between early December and early February, although the peak of fire weather can sometimes lag by one or two months, as in the case of the late summer category of fire seasons (SWD groups 5.1 and 6.1). The high summer fire risk period in south eastern Australia therefore corresponds to the possible change from the dominance of the sub-tropical high-pressure ridge in the lead-up and during the high summer period to more intense synoptic patterns conducive to severe fire weather that can drive LLFs. During the high summer period, the coincidence of a very dry sub-tropical temperate trough angled across central Australia combined with a very strong low pressure cell in the Southern Ocean below Australia can produce the hot dry and windy weather to propel LLFs over very dry landscapes in the ACT region and elsewhere in south eastern Australia.

The synoptic weather pattern associated with severe fires in Australia has affinities with that found in the Canadian studies, except that Australia is located in the heart of the Southern Ocean at sub-tropical and mid-latitudes. Blocking highs and westerly troughs, previously discussed in this section, are key features in the Australian context and have been associated with past severe LLFs in south eastern Australia (Luke and McArthur, 1978; Hanstrum *et al.*, 1990; Taylor and Webb, 2005). Significantly, it is the sub-set of years in the four principal SWD sub-groups 1.3, 2.2, 6.2, and 6.3 (Table 9.2; section 9.2) that has experienced the highest occurrence of LLFs, as a result of a warm dry spring followed by a hot and dry summer. The position and strength of the sub-tropical highs interrupt the usual synchronicity of the weather systems that produce rainfall. This pattern is consistent with findings in the Rocky Mountains in the USA (Morgan *et al.*, 2008). Morgan *et al.*'s study showed a significant relationship between spring and summer climate and fire incidence. As well, the PDO in their study was also shown to be the main driver of fire activity in its positive phase and a major dampener in its negative phase.

9.4 Findings

The main findings of this chapter relate to the twelfth question posed in the Introduction (Table 1.1): 'What does a broader temporal and spatial view of fire susceptibility tell us about its longer term history, climatic factors and influences contributing to it?'

Analysis of longer-term temporal variability of landscape dryness (SWD) revealed regular quasi-periodic cycles in medium and long-term landscape dryness at intervals of 10-15 years. Such regular trends were less apparent at the sub-decadal time scale (3-5 years), when the intervals between the major dry fire seasons have varied between 3 and 15 years. The composite LOESS filter was reasonably successful in identifying the major dry and wet fire seasons in the past but has no statistical power to infer the potential for LLFs in a future fire season. To do that, one has to use particular SWD groups in the preceding fire season to identify a fire season with potentially high indicators of landscape susceptibility to fire.

Despite some heterogeneity evident in both the groups and sub-groups of fire seasons, the fire seasons fit within six or seven groups. Based on the detailed analysis of the long-term time series of SWD in the ACT region (section 9.1), knowledge of the type, sequence, and chronology of the groups and sub-groups of fire seasons was confirmed in the documented fire chronology for the study region (see 0).

Finally, in section 9.3 the sub-tropical-temperate troughs, and their interaction with other synoptic scale weather systems, were shown to be significant in the development of high-risk fire seasons that lead to LLFs in south eastern Australia.

9.4.1 Putting the medium-term results into a longer-term temporal context

The Fowler daily soil water balance model (Fowler, 1992; Fowler, 2002; Fowler and Adams, 2004) was a valuable adjunct to the RSDI model developed previously in Chapters 3, 5 and 6. The former soil water balance was successfully calibrated with the other calibrated RSDI model in Chapter 6. While there were some apparent differences in values of the two models, particularly in the moister years, the results of the classification of SWD in this chapter proved to be relatively consistent with the medium-term SWD classification results (section 8.2). The classification techniques tested on three separate occasions in this and the previous chapter have proved to be robust, consistent, and reliable.

9.4.2 Influence of background climatic factors and processes

A summary of the key synoptic scale climatic factors and processes is presented in Table 9.4, which influence the onset and severity of LLF conditions of landscape dryness, potential lightning ignition, fire weather and moist break in the fire season. For instance, higher levels of landscape dryness are more likely to occur following a spring and early summer sequence of continual high pressure cells ridging west back over Australia from the Tasman Sea west of New Zealand. Late summer or autumn spells of landscape dryness similarly can result from blocking highs establishing in the southern Australian Bight. At the same time the Southern Ocean lows and associated fronts migrate southward, often associated with 'Rossby' wave patterns 1-3 (Sturman and Tapper, 2006), while SAM is in a positive mode. Drier than usual sub-tropical air masses over northern Australia and the eastern Indian Ocean can develop during these times, particularly when a moderate-strong ENSO event is in progress. This can lead to less moisture feeding into south eastern Australia from the sub-tropics to the weather processes that produce rainfall.

The study of the climatology of tropical-temperate troughs in relation to the types of fire seasons presented in this and the previous chapter could prove insightful into the type and frequency of westerly troughs that produce dry lightning storms and severe fire weather. The last two factors define the risk of a LLF occurring in a very dry landscape during the high summer period in this region and elsewhere in south eastern Australia.

Table 9.4 Factors influencing key factors in landscape susceptibility to large fires

LLF condition	Nature of high pressure systems	Nature of low pressure systems	Air mass stability	Source of moisture	Moisture transfer	Other factors
Dry spring and summer	Blocking highs establish over the Tasman Sea, centred over the NW of New Zealand, which strengthen progressively over Spring and summer	Low pressure systems weaken and move further south to lower latitudes south of the latitude of Tasmania	Upper atmospheric stability is higher for longer than in an average fire season. Jet stream weakens over region	Air masses from northern Australia become drier as a result of positive SOI and negative IDO	Continental heat troughs orientate more in a horizontal position, lessening transfer of sub-tropical air into the region	North-west cloud bands weaken are associated with thinner and less well developed cloud formations
Lightning ignition	High centred in the Tasman and another one ridging in from the west centred to the south of Adelaide in South Australia	Weak cold front to the south of the study area, associated with a moderately weak low pressure system	Unstable air associated with hot continental air, convective uplift over the mountains	Air mass drier than in a typical wet summer but sufficient to generate dry thunderstorms	Some sub-tropical moisture, but enough to trigger a dry thunderstorm	Alignment of westerly trough at about 325to 340 degrees compass direction
Severe fire weather	Blocking highs reach full strength and then break down with the onset of stronger low pressure systems , replaced by more settled summer weather patterns	Low pressure systems strengthen, often associated with multiple cold fronts	High instability associated with passage of severe fire weather, relatively stable as highs take over following passage of trough or front	Lack of any moisture in central and western Australia	Continental heat trough lie in a flatter horizontal position	Alignment of westerly trough 280 to 290^{o}
Moist break in fire Season	Highs move west from the blocking high position and weaken	Lows strengthen and move further northwards	Lower and upper atmosphere cooler, moister, and more unstable than average. Centre of jet stream positions itself over region	Sub-tropical air becomes moister and widespread in the sub-tropics	Continental heat troughs orientate in a more northerly direction and connect with sub-tropical moist air in northern Australia	North-west cloud band strengthen and connect with low pressure systems to the south ahead of cold fronts

Chapter 10: Summary and Conclusions

This chapter provides a general set of findings and conclusions based on the findings and conclusions presented in earlier chapters. The major findings are first outlined to show whether the study as outlined in the introduction achieved its general aims and objectives. This is then followed by a critical appraisal of the factors that limited the scope and accuracy of the models and data to model landscape dryness and potential fire spread in the three climate zones identified earlier. Areas for future research are then highlighted to strengthen the models formulated in this study. Finally, conclusions a re drawn as to the potential application of the methodology to other regions in south eastern Australia and how this study can help to anticipate extreme conditions of landscape dryness and potential fire spread, based on the classification and time series analysis techniques developed in this study.

10.1 Overview and major findings

The thesis set out to develop a methodology for identifying past seasons with the highest potential for LLFs, using the key indices based on already calibrated indices of landscape dryness and potential fire spread. Detailed calibrated landscape and potential fire spread models, using the best available historical weather data, were developed. Care was taken to ensure that the primary and intermediate input weather data were of the highest quality to avoid problems in later analysis. The effort expended in the preliminary chapters (Chapters 3-6) selecting models and data, and then verifying their outputs against other studies was crucial for classifying and analysing the fire seasonal profiles in the medium term (Chapters 8) and in the long-term (Chapter 9).

Chapter 2 outlined the climate, topography, vegetation, and soils of the ACT regional landscape. The long-term rainfall pattern showed that, for drier than average years, the landscape was consistently dry across all three climate zones (Cfa, Cfb, Csc) leading to a consistently dry regional landscape at these times. Despite the complexity of the regional landscape in terms of climate, topography, and vegetation, the data and models of landscape dryness developed in the later chapters could be applied in two out of the three climate zones (Cfa, Cfb). Summarising previous fire chronology studies indicated that three different categories of LLFs have occurred in very dry fire seasons in the past. The most critical ones have been in seasons where there is an absence of moisture barriers to retard the progress of fire across all three climate zones, enabling a LLF to traverse the full range of vegetation and topography in the ACT region. The results achieved in subsequent chapters did indeed show that indices of landscape dryness could be developed and calibrated for the dominant vegetation types in two out of the three climate zones. However, an index of potential fire spread could only be produced for the sub-montane plains (Cfa) based on weather data collected at Canberra Airport. This therefore partially answered the first research question posed in Section 1.3

(Table1.1): 'How feasible is it to apply a simple temporal model of landscape susceptibility to large fires to a region with wide ranging climate, topography, vegetation, soils, and fire history?'

The conceptual framework for a net radiation-based daily soil water balance model was successfully advanced in Chapter 3. An all-wave net radiation-based sub-model of soil evaporation (E_S) and plant transpiration (E_T) was developed from published relationships. These equations derived mainly from generalised sub-models sourced from the remote sensing literature and were not based on detailed site-specific ground studies. While both the soil evaporation and plant transpiration sub-models could be considered approximations of soil evaporation and plant transpiration processes, they were subsequently tested and evaluated in Chapters 5 and 6 and demonstrated to produce equivalent values to evaporation models published elsewhere. The development of such models facilitated a means for evaluating all-wave net radiation and net evaporation (R_N and E_A). This answered the third research question (Table 1.1) in the affirmative: 'Can simple and elegant sub-models of soil evaporation and plant transpiration replace evapotranspiration models?'

The modelling plan formulated in Chapter 4 was constrained by the lack of medium and long-term weather records for the high and remote country to the west of Canberra, particularly in the Csc climate zone at high elevations. Only Canberra Airport records could be used to model landscape dryness and potential fire spread in the sub-montane climate zone (Cfa). Thus, despite there being long-term records of precipitation at the key weather stations of Fairlight Station, Corin Dam, Queanbeyan, Kiandra-Cabramurra, and Canberra Airport, many of the key input variables for the estimation of potential fire spread were just not available. Since continuous daily, rather than monthly, records are required to model landscape dryness, only reference climate stations in the Bureau of Meteorology's weather station network are suitable for this analysis. Canberra Airport provided reliable, accurate, and consistent medium-term weather datasets to model soil water dryness over the long-term. As a result of careful calibration with the all-wave net radiation SDI model (RSDI), the Fowler daily soil water balance model was extended as far back as 1871 using rainfall data from the nearby Queanbeyan weather station. However, other two soil dryness indices, the Mount Soil Dryness Index and the all-wave net radiation version of it (RSDI), could only be extended back to 1939 using the Canberra Airport dataset. These latter two daily soil water balance models require additional weather variable inputs such as T_{MAX}, T_{MIN}, RH_{1500}, and e_A that were not recorded at Canberra Airport prior to 1939 or were missing from the Queanbeyan records. A landscape dryness dataset driving all three landscape dryness models was created for the upper Cotter River catchment, using in part proxy estimation of key variables for the MSDI and RSDI in the absence of on-site measurements at Corin Dam. Only one out of the three climate zones (Cfa) had representative weather stations for modelling the required indices of landscape dryness and potential fire spread. The fourth research question (Table 1.1) was therefore only partially

answered: 'As part of the ideal modelling framework for this study, what datasets for medium and long-term indices of landscape dryness and potential fire spread can be constructed in the three climate zones?'

The estimates of all-wave net radiation (R_N) were found to be highly dependent on the accuracy and bias of its principal components: surface irradiance (R_S) and net long-wave radiation (L^*). R_S can be estimated using the Supit and Von Kappel empirical R_S model (Supit and van Kappel, 1998). This model is entirely dependent on having three-hourly or half-daily records of cloud cover. It was shown in Chapter 5 that R_S from Canberra Airport could be used to model R_N for the upper Cotter River catchment successfully. Reasonably high correlations were obtained between R_S values for Canberra Airport with those observed at Googong Dam and Corin Dam in the upper Cotter River catchment (R^2 >0.834, 0.732). However, modelling of downwelling long-wave radiation ($L\downarrow$), the key variable input into L^*, was more problematic. The best empirical estimate for $L\downarrow$ was obtained using the Brunt model when it was combined with a slightly modified Iziomon cloud effect model. The values of monthly R_N and its components were found to be comparable with some earlier studies (Paltridge and Proctor, 1976; Moore *et al*., 1993). The values obtained for L^* in this study were at slight variance from those previously published mainly due to the different lengths of study. Anomalies in values obtained for L^* found in the time series may be attributed to the methods used for estimating ambient vapour pressure (e_A). Because the modelling of R_N and its components was only achieved in the Cfa and Cfb climate zones, and not the Csc climate zone, this has in partially answered the fifth research question (Table 1.1) in the affirmative: 'Can all-wave net radiation (R_N) and its components be estimated to sufficient levels of accuracy as a precursor to estimating potential evaporation (E_P)?'

In Chapter 6, the analyses of the components of evaporation, E_S and E_T, demonstrated that the modelled values produced by the RSDI model were consistent and comparable with short-term data produced by other Australian studies. The evapotranspiration estimates (E_T+E_S) from the RSDI and F-DSWBM were also found to simulate expected higher E_A values in late spring and early summer when there is generally higher soil water availability and moderate to high all-wave net radiation (R_N). In contrast, the MSDI model simulated higher E_A values in summer reflecting the later peak in seasonal maximum temperatures. Total evaporation (E_S+E_T+E_I) or E_A calculated from all the models was not that different at an annual time scale. The differences were much more apparent when evapotranspiration (E_{T+S}) was examined at a monthly time scale especially during spring when seasonal values of E_{T+S} from the RSDI and F-DSWBM were found to be higher than those in the MSDI model. This reflects a sensitive response to higher seasonal water availability and moderate to high all-wave net radiation levels (R_N) during spring and early summer.

Verification of the daily soil water balance models using run-off data failed to discriminate between them, which meant that the final selection had to be made on inter- and intra- annual

patterns of soil water deficit (SWD) over the full time series. The SWD profiles produced by RSDI and F-DSWBM were found to be more consistent than those produced by the MSDI model when the SWD time series from the two principal sites, Canberra Airport and the upper Cotter River catchment, were compared side by side. While DSWBMs based on pan evaporation data can simulate evaporation up to a point, the seasonal timing of evaporation from such models can affect the amplitude and frequency of SWD in moister fire seasons. As a result, it is difficult to distinguish the very dry years from the not so dry years with the MSDI model. The SWD time series produced by the RSDI and F-DSWBM models were chosen for further analysis because they appeared to simulate better the seasonal evaporation patterns better than the MSDI model. This has therefore satisfactorily answered the sixth research question (Table 1.1): 'Which daily soil water balance models best approximate the hydrological processes of evaporation, run-off, and soil water deficit and should be used for further analysis of landscape susceptibility to large fires?'

The first part of Chapter 7 presents evidence found in the literature that suggests that a threshold of landscape dryness above SWD=100 mm using the Keetch-Byram Drought Index directly affects increased fuel combustibility and vegetation flammability. The few relevant studies of flammability and live leaf moisture content conducted in Europe and California provide strong evidence that vegetation flammability increases markedly once live leaf moisture contents falls below 70%. The empirical evidence from the relationship of SWD to live leaf moisture content (LLMC) suggests that this occurs when the KBDI exceeds a SWD value of 100 mm. In California, large landscape fires were found to be associated with LLMCs below 70% in Chaparral shrublands. There is little empirical field evidence to substantiate this value of LLMC in south eastern Australia, with the possible exception of a study undertaken by Pook (1965) on the effects of drought on LLMC in the ACT region. However, the evidence from elsewhere suggests that very high levels of SWD are crucial in predisposing landscapes to LLFs. The altered flammability threshold lies somewhere between 100 and 140 mm, depending on the DSWBM and regional characteristics of topography, vegetation, and soil. This has therefore positively answered the seventh research question (Table 1.1): 'Can a threshold of soil water deficit (SWD) indicate a realistic threshold for fuel availability, combustibility, and vegetation flammability in a forested landscape?'

In the second part of Chapter 7, an argument for using the Canadian Fire Weather Index instead of McArthur's Forest Fire Danger Index was put. The principal reason given was that the Canadian FWI is much more explicit and transparent, permitting other components of potential fire spread to be estimated, such as the individual moisture components (Fine Fuel Moisture Content, Duff Moisture Code, and Drought Code), and the fuel availability and fire behaviour components (Build-up Index, Initial Spread Index, and Fire Weather Index). This enabled checking and validation of the intermediate as well as final outputs of fire weather and fire spread variables. The only issue with the FWI is that the longer-term fuel moisture

components such as DMC and DC have not been calibrated to Australian conditions. To counter this in part the all-wave net radiation SDI model replaced the Canadian DC model in the estimation of BUI within the FWI model. This has therefore satisfactorily answered the eighth research question (Table 1.1): 'Which of the PFSI models is the most transparent and explicit, and best integrates the factors involved in estimating potential fire spread?'

Conceptually, re-defining the start and end of fire seasons proved invaluable for benchmarking the different periods of landscape susceptibility to large landscape fires in the fire seasonal profiles of SWD and SFWI (Chapter 8). It also aided in identifying in which fire seasons the ACT region's landscapes had been most susceptible to large landscape fires (Chapter 9). Classifying annual profiles of SWD or FWI identified the types of fire seasons that have been the most susceptible to LLFs in the past. Using either index, a hierarchical classification approach revealed a heterogeneous but orderly set of groups and sub-groups of fire seasons that have occurred in the study region. Up to seven groups, or types, of fire seasons were apparent. Splitting groups further into sub-groups provided further meaning in terms of the timing and potential for fires using either index of fire susceptibility, landscape dryness or fire spread potential. Using the RSDI model as an index of landscape dryness, the fire seasons with early summer high landscape susceptibility to fire were 1957/58 and 1982/83. Similarly, the fire seasons with high landscape susceptibility to fire in high summer were 1967/68, 1997/98, 2002/03, 2006/07.

Using the SFWI as an index of potential fire spread, the seasons when landscapes were most susceptible to LLFs fell into three categories: (1) early high summer period —1957/58 and 1997/98; (2) middle of high summer period — 2002/03 and 2006/07; and (3) middle-late high summer period — 1967/68, 1982/83, and 1997/98. The latter fire seasons classified into SFWI groups II and III, having the highest fire spread potential of any of the 56 fire seasons since 1951. Only one other set of fire seasons (SFWI group V; sub group V-1) had similar fire spread potential: 1951/52, 1978/79, and 1984/85. These fire seasons had a peak fire spread potential from about mid January to early February, which is two to three weeks later than the category (2) fire seasons of 2002/03 and 2006/07 (SFWI Group III; subgroup III-1). The analyses and findings in Chapter 8 has therefore substantially answered the ninth and tenth research questions positively (Table 1.1): 'Does redefining the season and the periods within a fire season using fire susceptibility criteria, such as landscape dryness, fine fuel moisture, and potential fire spread produces a more meaningful definition than previous definitions? What can classification and time series analysis of landscape dryness and potential for high fire spread reveal about landscape susceptibility to LLFs in the medium-term?'

The analysis of potential fire ignition in Chapter 8 also showed that lightning-started fires could be anticipated using three sources of information:

(1) the lightning-fire decision tree model developed in this thesis;

(2) the 1000 hours aerosonde sampling of dewpoint and temperature profiles at Wagga Wagga; and

(3) the interpretation of the angle and position of the sub-tropical temperate troughs on a synoptic scale weather map.

The combination of dry landscape and fire weather conditions under which dry thunderstorms has occurred rarely: 42 days with these characteristic conditions were identified within 56 years of detailed weather data. Out of the 42 critical days, only three critical LLFs have resulted in the ACT region from the right sequencing of conditions as follows:

(1) extreme levels of landscape dryness during the months of January or February;

(2) lightning ignition just prior to the run of severe fire weather; and

(3) extreme periods of fire weather running for more than a day.

The combination of these conditions occurred historically in the following fire seasons of 1951/52, 1982/83, and 2002/03. This implies that the sequencing conditions have been relatively rare in the weather record but the resulting large fires have had devastating consequences on the landscape and/or adjoining people and their assets. Using the methods developed in this study, warning of the likelihood of future occurrences similar to these would allow authorities to take proactive fire management measures. This has therefore answered the eleventh research question in the affirmative: 'Can a model based on particular combinations of landscape dryness and weather predicts the potential for lightning ignition in the ACT region?'

In Chapter 9, the time series analysis revealed a complex sequence of fire seasons when using either medium or long-term soil water deficit (SWD) as an index. The inter-decadal trend in SWD showed a small but significant increase in landscape dryness in the last 10-20 years. The decadal trend showed regular fluctuations in SWD throughout the time series with a regular cycle running between 10 and 15 years. The sub-decadal trend revealed a near-regular pattern in SWD with irregular amplitude. Overall, the composite LOESS smoother, based on the intervals chosen for the sub-decadal, decadal, and inter-decadal time scales, enabled the major dry and wet years in the time series to be identified in the time series. This confirmed that the complex variability in SWD in the medium-term could be decomposed with de-trending smoothers. These reflected broader climatic processes occurring at 27, 13, and 5-year intervals, representing the inter-decadal, decadal, and sub-decadal time-scales, respectively.

The models for landscape dryness and potential fire spread selected in this study proved in the analysis chapters (Chapters 8 and 9) to be the most appropriate models (Chapters 6, 8 and 9). First, the RSDI and F-DSWBM models were found to better simulate the timing and severity of dryness of fire seasons than the MSDI. Second, the FWI, adapted as much as possible to local conditions, appeared to represent the seasonal timing of potential fire spread better than the FFDI (see section 8.2.4). In particular, the FWI model better incorporated the

build-up and development of dryness over a fire season, extending the period of potential fire spread potential well into late summer.

The longer-term study of SWD in Chapter 9, using the F-DSWBM, confirmed the patterns in the type and sequencing of the types of fire seasons discovered in Chapter 8. In the longer-term study of SWD, six types of fire seasons were recognised at a broad level in the hierarchical classification. A further sixteen sub-groups were identified that corresponded closely to the amount and timing of rainfall during the course of the fire season. Major fire seasons were recognised from the major dry years in the SWD time series that corresponded to the peak of landscape dryness overlapping with the peak fire potential period between early December and early February. These fire seasons corresponded well with the known chronology of major fire seasons in and surrounding the ACT since the 1900s (section 2.5). Some 31 percent of fire seasons were found to be have periods of high to extreme landscape susceptibility to LLFs, in high and late summer.

In the final part of Chapter 9 some broad inferences were drawn about synoptic-scale weather processes and conditions of sea surface temperature that are conducive to landscapes being highly susceptibility to LLFs in particular categories of fire seasons. There appears to be a relationship between blocking highs in the Tasman Sea in the spring and summer period of the fire season, conditions that lead to lower rainfall, hence higher levels of SWD and potential fire spread. The position and timing of the blocking highs, as well as the latitudinal position of the polar maritime cold fronts and low pressure cells, could relate directly to the general groups of fire seasons (Chapters 8 and 9). A further study of the relationship between the categories of fire seasons arising from this study and synoptic scale climatic and weather patterns could further deepen the knowledge of type of fire seasons based on fire susceptibility factors: landscape dryness and potential fire spread.

The two broad areas of research undertaken in Chapter 9 have therefore answered satisfactorily the twelfth and final answer research question (Table 1.1): 'What does a broader temporal and spatial view of fire susceptibility tell us about its long-term history, climatic factors and influences contributing to it?'

10.2 Limitations of the study

This study set out to model fire susceptibility in three climate zones (Chapter 4; Table 4.1). While medium-term high quality weather data are collected near towns and cities, more remote and rugged areas are not well covered in the Bureau of Meteorology's network of weather stations. The lack of suitable medium and long-term weather records in the more remote parts of the study area, including the upper Cotter River catchment, placed a severe limitation on applying the models of fire susceptibility within the higher, cooler and moister climate zones (Cfb and Csc). Within these zones, there are insufficient weather data to model directly all-

wave net radiation and fire weather, which are key inputs into the fire susceptibility indices of landscape dryness and potential fire spread. Instead, only the net radiation model for Canberra Airport was successfully transferred to the upper Cotter River catchment, using parallel estimation methods of the critical weather variables of T_{MAX}, T_{MIN}, and RH_{1500} (Chapter 4, sections 4.3.1 and 4.3.3). This data, together with P_{0900} data, were used to model Soil Water Deficit (SWD) in the upper Cotter River catchment with a modicum of success (Chapter 6, Section 0).

Rainfall records were also found to be inconsistent at one of the critical stations (Cabramurra) identified in the sub-alpine climate zone (Csc) as part of the modelling framework. The reduction in quality of rainfall records could be related to the changeover from manned to automatic weather stations in 1999. A correlation with rainfall records at the nearby station of Yarrangobilly suggests that the Cabramurra pluviometer/weather station may not be recording precipitation received as snow or ice accurately.

This study found that very few other independent, continuous studies of R_N, E_S and E_T, and catchment run-off that could be used for direct comparison with the modelled results. Fortunately, over 30 years of run-off data were available from the upper Cotter River catchment against which to compare modelled run-off predicted by the daily soil water balance models (DSWBMs). To develop a medium-term time series of SWD based on the RSDI model requires estimates of cloud cover, surface irradiance, and long-wave radiation to be collected at remote locations. These data are needed to estimate empirical equations for the components of R_N, based on daily and three-hourly weather collections of variables such as rainfall, maximum and minimum temperature, relative humidity, and cloud cover. The lack of such data may limit the application of the RSDI model to other regions in south eastern Australia.

One further limitation in this study relates to the index used to develop fire seasonal profiles of either landscape dryness or potential fire spread for classification of fire seasons into groups and sub-groups. For instance, the RSDI was selected rather than the MSDI in Chapter 6 on two grounds: (1) *a priori* the former model had closer relationships to biophysical processes, and (2) the model computed higher evaporation in spring and early summer followed by slower evaporation in late summer and autumn. The hypothesis that the two models would have produced similar results in the classification was not tested. Further research into the effect of the different models on fire season classification is recommended to validate the results presented here.

The results of this study relate to the general seasonal patterns of landscape dryness and potential fire spread in either the medium or long-term time series. The methods used here cannot identify exactly to the day when particular combinations of worst-case conditions may occur within a given fire season. However, these methods have revealed in what type of fire season and in what month and year the predisposing conditions for large landscape fires might recur at some future date.

10.3 Directions for future research

There is a great need to profile the development of future fire seasons as each unfolds, based on the philosophy and approach developed in this study but doubtless expanding it. This study is regarded as a significant first step in understanding the type and past incidence of fire seasons with peak fire susceptibility and the possible factors that cause them. The development and application of the models of landscape dryness and fire spread potential could be readily applied elsewhere by developing an integrated system of weather data, models, and analytical tools found within R or SPLUS. The tools developed here could be used in training fire management planners to understand the type and variability of past fire seasons. The training method could be based on the process diagram (Figure 1.2) and further developed into an interactive package. It is recommended that the initial research undertaken here into landscape susceptibility to LLFs be applied and improved to refine further the concepts, models, and analytical tools to understand and interpret fire seasons' susceptibility to LLFs.

Further testing of the soil evaporation and plant transpiration components of the RSDI model is needed to validate the results presented in this study. Testing could establish whether the modelling of the components of evaporation does apply in different regions and different vegetation types. In particular, the E_S modelling approach should be validated using detailed field studies. Similarly, further validation of the E_T (transpiration flux) estimated by the process-based RSDI model should be undertaken using an approach similar to that adopted in section 6.3.1.

A critical part of this study has been the investigation of heightened vegetation flammability above particular thresholds of landscape dryness based on the SWD index. Further research is required to validate the apparent threshold value (100>SWD <140) to determine whether this threshold applies to a wide range of vegetation or requires specific modification to suit particular vegetation types or climatic regions.

As for the applicability of potential fire spread models, both the FWI and the FFDI potential fire spread models require further testing and refinement. The FWI system needs further calibration studies before it can be applied more widely in Australia. The three fuel moisture codes (FFMC, DMC, and DC) embedded in the Canadian FFWI model also need further verification in field conditions in south eastern Australian forests. This could lead to a much improved potential fire spread model and fire danger rating system than the current FFDI model which has had very little rigorous scientific testing and calibration since its adoption in the mid 1960s.

There are two serious problems with the FFDI model: First, the inherent simplicity in the algorithms hides the estimation of fine fuel moisture. Second, the drought factor does not properly account for the changes in available fuel or vegetation flammability at the very dry end of the soil dryness scale. An improved fuel moisture function should take account of the

different time lags associated with different types of forest fuel, as does the FWI model. A revised drought factor function should incorporate the increasing levels in fuel availability and vegetation flammability across the full range of soil water deficit, rather than the function ceasing at a value of SWD equal to 100 mm. By having a better measure of these two factors' impacts on potential fire spread, the FFDI model could better model seasonality and severity of potential fire spread.

As well as improved calibrated models of landscape dryness and potential fire spread, the study of the day-to-day or week-to-week sequencing and coincidence of landscape dryness, lightning ignition, and extremes of potential fire spread will further add to the broader findings summarised here on a landscape's susceptibility to LLFs. This would represent another level of study that would aim to link the interactions of synoptic scale climate and weather processes to the development of landscape dryness, the potential for lightning ignition, and the onset of severe potential fire spread. From indications in this study, extremes of fire behaviour occur towards the end of extended dry spells at anytime during the fire season, and particularly in the high summer period identified in the fire calendar (sections 8.1.2 and 8.4). Lightning ignition potential also coincides on occasions with the more severe conditions of landscape dryness and potential fire spread during the high summer (section 8.5).

10.4 Conclusions

Models of seasonal dryness and fire spread potential were found to be sensitive to the model inputs and required careful calibration using independent data before applying these indices to the study of fire susceptibility at either medium or long-term time scales. Calibrated models of these two fire susceptibility indices were also needed to analyse and interpret patterns of historic fire susceptibility or for day-to-day use in forest fire management. The models of landscape dryness and fire spread potential (KBDI, FFDI) currently in use in south eastern Australia remain largely uncalibrated. Therefore, calibration and validation studies of such indices should be made mandatory before these or other replacement models are used in fire management applications.

The general approach relating fire seasonal profiles of landscape dryness (SWD) and fire spread potential (FWI) to the fire season calendar using hierarchical clustering methods, provided stable and robust groups of fire seasons with differing potential for LLFs. The classification of fire seasons proposed here could be used to anticipate landscape susceptibility to LLFs in future fire seasons, by looking at them in combination with:

- subdividing a fire season into its respective seasons using the indicators of landscape susceptibility to large fires (section 8.1.2);
- the general trends in the quasi-periodic cycles at the inter-decadal, decadal, and sub-decadal trend filters (section 9.1.4);

- the classification and hence typology of historical fire seasons (section 9.2);
- the long-term sequences of the groups developed from the classification (section 9.1.3), and the possible relationship of sub-decadal, decadal, and inter-decadal trends with SOI (section 9.1.4)
- their relationship of the SWD groups to a region's fire history (section 9.2.2); and
- the predisposing climate and weather factors at sub-global and synoptic scales (section 9.3).

The approach adopted could also be readily applied to other regions in south eastern Australia to determine whether the types of fire seasons are consistent with those found in this study. In particular, the study has produced a robust model of landscape dryness (RSDI), based on thermodynamic principles, and has been shown to produce more consistent seasonal comparable values of evaporation than the original MSDI model. The parsimonious F-DSWBM model calibrated to the RSDI model is most invaluable in unravelling the longer-term types of fire seasons and their associated potential for LLFs.

Analyses of longer-term, along with the medium-term study of landscape dryness, confirmed that the highest level of susceptibility of a landscape to LLFs is found in those fire seasons with landscape dryness (SWD) peaking in high summer. The usual tendency is for peak landscape dryness to occur later in the fire season in the majority of the dry to very dry fire seasons. The coincidence of landscape dryness with very high to extreme fire spread potential has been relatively rare in the high summer period. Thus, it can also be concluded that fire seasons with the highest susceptibility to LLFs appear to differ in their climate and weather history to those found in the rest of the less severe fire seasons.

The primary driver behind peak landscape susceptibility to fire is the continental heat trough that brings dry, hot and windy air masses to this region at regular and frequent intervals during summer. The passage of these heat troughs through the study area can trigger dry thunderstorms that are associated with limited air moisture aloft as well as very high to extreme conditions of fire weather. Multiple lightning ignitions are the result of very dry landscape conditions, the atmospheric conditions associated with the sub-tropical temperate trough, and the mountainous terrain that these systems pass over. If the sub-tropical temperate trough becomes even drier, severe fire weather can develop ahead of and within the trough system. If the two predisposing factors follow each other in short succession, the conditions for large landscape fires are inevitable. All these coincidences are most likely to occur during the period of peak fire susceptibility from early December to early February in the study region.

The underlying factor behind peak fire susceptibility is the seasonal landscape dryness factor. Once critical levels of low moisture in the vegetation and the underlying regolith have been surpassed (SWD>120 mm), increased fuel availability and heightened vegetation flammability create the precursory conditions for a LLF. This predisposing condition results

from the continual lack of air moisture and rain in the months preceding this critical summer period of fire susceptibility. At the synoptic scale, the dominance of the sub-tropical ridge in the preceding months over this part and elsewhere in south eastern Australia stifles the development of good seasonal rains. The establishment of such strong ridges of high pressure leads to particular types of fire seasons identified in the classification of fire seasons in both the medium and long-term analyses of landscape dryness. These high-risk fire seasons are remarkably distinct from the rest of the fire seasons in the classifications. The three fire seasons of 1951/52, 1982/83 and 2002/03 belong to particular groups of fire seasons with distinct seasonal profiles in landscape dryness and potential fire spread.

The knowledge gained in this study clearly shows that critical thresholds in landscape susceptibility do exist, and should be further verified in each region of south eastern Australia. Based on previous scientific knowledge and the results presented in this study, the fire seasons with the highest landscape susceptibility to large fires can be anticipated in advance by:

(1) determining the thresholds of landscape dryness; and

(2) simply monitoring the soil water deficit at a few representative points in a given region.

This study has demonstrated that the knowledge and understanding of landscape susceptibility to fire can be inferred from a single point in the landscape that is representative of an area or region out to the boundaries of the climate zone in which it is located. Finding these representative points and locating long-term weather stations at these points will further deepen and improve our understanding of the susceptibility of the more remote forested regions to large landscape fires in south eastern Australia. Having this knowledge, together with other supportive climate and weather forecasting tools, helps to understand what the present fire susceptibility is like in relation to the past.

The study fills a major gap in knowledge that can be applied as part of a pro-active fire watch system: this, and contrary to common wisdom, can be put in place in a timely manner. Measures and activities in this fire watch system might include:

(1) setting up weather stations at sites representative of the different climate zones in a region to collect the necessary data;

(2) routinely running the methods to analyse the trends in landscape dryness and potential fire spread models to determine the risk of LLFs;

(2) field checking of the levels of soil, fuel and vegetation dryness and potential flammability across the region, and

(3) enacting higher levels of fire-preparedness, increased fire suppression capability, and forewarning of rural and urban communities once critical thresholds in landscape dryness and potential fire spread are indicated.

A heightened sense of awareness based on the knowledge and understanding of historical fire susceptibility could lead to improved protection of natural, cultural, and social assets within a region. In an increasingly uncertain world of potential climate change, knowing what the fire susceptibility was like is like having an advanced fire warning map in a temporal sense. The history of landscape susceptibility to larger fires is therefore a crucial step in understanding when a large landscape fire might or could happen in the future.

References

Alexander, M. E. (1998) Crown fire thresholds in exotic pine plantations of Australasia, PhD Thesis, Forestry Department, The Australian National University, Canberra

Alpert, P., Osetinsky, I., Ziv, B. and Shafir, H., 2004. A new seasons definition based on classified daily synoptic systems: an example for the eastern Mediterranean, *International Journal of Climatology,* **24** (8): 1013-1021.

Anderson, H. E., 1970. Forest Fuel Ignitability, *Fire Technology,* **6**(4): 312–319.

Anderson, M., 1981. The geometry of leaf distribution in some south eastern Australian forests, *Agricultural Meteorology,* **25**: 195-205.

Oxford, 2007. *A Dictionary of Astronomy,* Oxford University Press, Australian National University. Available at: http://www.oxfordreference.com/views/ENTRY.html?subview=Main&entry=t80.e3304 (accessed 10/03/2008)

ANU Forestry Department, 1973. *A Resource and Management Survey of the Cotter River Catchment*, ACT Forests Branch, Department of the Capital Territory, ACT.

AOED, 2004. *The Australian Oxford Dictionary,* Oxford University Press, Melbourne.

Australian Bureau of Statistics, 2003. *Year book, Australia*, Issue 83, Australian Bureau of Statistics, Canberra.

Banks, J. C. G. 1982. The Use of Dendrochronology in the Interpretation of the Dynamics of the Snow Gum Forest, PhD Thesis, Forestry Department, Australian National University, Canberra.

Bartlett, A.G. 1993. *A case study of wildfire management in the Byadbo and Tingaringy wilderness areas*, Research Report No. 38, Department of Sustainability and Environment, Melbourne.

Berry, S. L. 2001. A study of the relationships between climate, carbon dioxide and the vegetation cover of the Australian continent at the present and the last glacial maximum, PhD thesis, The Australian National University, Canberra.

Berry, S. L. 2007. Unpublished data, Mean monthly estimates of Gross Primary Productivity (GPP) derived from MODIS imagery, Fenner School of Environment and Society, The Australian National University.

Berry, S. L., Farquhar, G. D. and Roderick, M. L., 2006. Co-evolution of Climate, Vegetation, Soil and Air, In *Encyclopedia of Hydrological Sciences*, Vol. 1 John Wiley and Sons, Chichester.

Berry, S. L. and Roderick, M. L., 2002. Estimating mixtures of leaf functional types using continental-scale satellite and climatic data, *Global Ecology and Management,* **11**: 23-29.

Berry, S. L. and Roderick, M. L., 2004. Gross primary productivity and transpiration flux of the Australian vegetation from 1788 to 1988 AD: effects of CO_2 and land use change, *Global Change Biology,* **10**: 1884-1898.

Bessell, R. 2006 Predictability of Fire Season Severity from Atmospheric Circulation Analysis, School of Resources, Environment and Society, The Australian National University, Canberra, pp. 81.

Brackenreg, J. G., 1926. Unpublished fire report, Federal Capital Commission, Commonwealth Government of Australia.

Bristow, K. and Campbell, G. S., 1984. On the relationship between incoming solar radiation and daily maximum and minimum temperatures, *Agricultural and Forest Meteorology,* **78**: 31-51.

Brown, A. A. and Davis, K. P., 1973. *Forest Fire Control and Use,* McGraw Hill, New York.

Brunt, D., 1932. Notes on radiation in the atmosphere, *Quarterly Journal of the Royal Meteorological Society,* **58**: 389-418.

Brutsaert, W., 1975. On a derivable formula for long-wave radiation from clear skies, *Water Resources Research,* **11**: 742-744.

Budyko, M. I., 1974. *Climate and Life,* Academic Press, New York.

Bureau of Meteorology, 1997. *Guidelines for the Siting and Exposure of Meteorological Instruments and Observing Facilities*, Melbourne, Bureau of Meteorology, Department of the Environment Sports and Territories.

Bureau of Meteorology, 2005. *Surface Irradiance Data from Australian weather stations*, Climate Services Division, Bureau of Meteorology. Melbourne.

Bureau of Meteorology, 2006, *List of current and disused weather stations*, Climate Services Division, Bureau of Meteorology, Melbourne.

Bureau of Meteorology, 2007a. *Australian Rainfall data,* Climate Services Division, Bureau of Meteorology, Melbourne.

Bureau of Meteorology, 2007b. *Daily weather data collected at Canberra and Cabramurra weather stations (1951-2007)*, Climate Services Division, Bureau of Meteorology, Melbourne.

Bureau of Meteorology, 2007c. *Three-hourly weather data collected at Canberra weather station (1951-2007)*, Climate Services Division, Bureau of Meteorology, Melbourne.

Bureau of Meteorology, 2008. *Australian Climatic Influences,* Bureau of Meteorology. Available at: http://www.bom.gov.au/watl/about-weather-and-climate/australian-climate-influences.html?bookmark=introduction (accessed 01/06/2008).

Burroughs, W. C., 2003. *Weather Cycles - Real or Imaginary,* Cambridge University Press, Cambridge.

Burrows, N. D., 1987. *The soil dryness index for use in forest fire control in Western Australia*, Technical Report No. 17, Department of Conservation and Land Management.

Byram, G. M., 1959. Combustion of forest fuels, In Brown A.A. and K.P. Davis (Eds). *Forest fires: control and use,* McGraw Hill, New York, pp. 61-80.

Byram, G. M. and Jemison, G. M., 1943. Solar radiation and fuel moisture, *Journal of Agricultural Research,* **67** (4): 149-175.

Cary, G., 1998. Predicting fire regimes and their ecological effects in spatially complex landscapes PhD Thesis, The Australian National University, Canberra.

Castro, F. X., Tudela, A. and Sebastià, M. T., 2003. Modeling moisture content in shrubs to predict fire risk in Catalonia (Spain), *Agricultural and Forest Meteorology,* **116** (1-2): 49-59.

Chandler, C., Cheney, P., Thomas, P., Trabaud, L. and Williams, D., 1983. *Forest Fire Behaviour and Effects,* Vol. 1, John Wiley and Sons.

Cheney, N. P., 1981. Fire Behaviour, In *Fire and the Australian Biota*, Eds A.M. Gill, R. H. Groves, & I.R. Noble Australian Academy of Science, Canberra.

Chuvieco, E., Aguado, I. and Dimitrikopoulos, A., 2004. Conversion of fuel moisture content values to ignition potential for integrated fire danger assessment, *Canadian Journal of Forest Research,* **34** (11): 2284-2293.

Cleveland, R. B., Cleveland, W. S., McRae, J. E. and Terpening, I., 1990. STL: A Seasonal-Trend Decomposition Procedure Based on Loess, *Journal of Official Statistics,* **6**: 3-73.

Cleveland, W. S. and Devlin, S. J., 1988. Locally Weighted Regression: An Approach to Regression Analysis by Local Fitting, *Journal of the American Statistical Association,* **83**: 596-610.

Coops, N., Delahaye, A. and Pook, E., 1997. Estimation of Eucalypt Forest Leaf Area Index on the South Coast of New South Wales using Landsat MSS Data, *Australian Journal of Botany,* **45**: 757-769.

Costin, A. B., 1954. *A Study of the Ecosystems of the Monaro Region with Special Reference to Soil Erosion,* Soil Conservation Service of New South Wales, Sydney.

Costin, A. B., Wimbush, D. J. and Cromer, R. N., 1964. Volume *V. Soil Moisture Characteristics and Evapotranspiration, Studies in catchment hydrology in the Australian Alps*, CSIRO, Melbourne.

Coulibaly, P., 2006. Spatial and temporal variability of Canadian seasonal precipitation (1900-2000), *Advances in Water Resources,* **29**(12): 1846-1865.

Council of Australian Governments 2003. *Natural Disasters in Australia: Reforming mitigation, relief, and recovery arrangements*, Australian Government, Canberra.

Dasgupta, S., Qu, J. J. and Hao, X., 2006. Design of a Susceptibility Index for Fire Risk Monitoring, *IEEE Geoscience and Remote Sensing Letters,* **3**(1): 140-144.

Davies, C., 1997. *Analysis of Fire Causes on or Threatening Public Land 1976/77-1995/96*, Research Report No. 49, Department of Natural Resources and the Environment, Melbourne.

Deeming, J. E., Burgan, R. E. and Cohen, D. E., 1978. *The National Fire Danger Rating System - 1978*, Intermountain Forest & Range Experiment Station, General Technical Report INT-39, USDA Forest Service, Ogden, Utah, USA.

Dennison, P. E., Moritz, M. A. and Taylor, R. S., 2008. Evaluating predictive models of critical live fuel moisture in the Santa Monica Mountains, California, *International Journal of Biometeorology,* **17**: 18-27.

Department of Environment and Climate Change, 2005. *Southern Comprehensive Regional Assessment GIS datasets,* New South Wales Government, Department of Environment and Climate Change, NSW.

Department of Sustainability and the Environment, 2009. Major Bushfires in Victoria, Department of Sustainability and the Environment, Melbourne. Available at: http://www.dse.vic.gov.au/DSE/nrenfoe.nsf/LinkView/E20ACF3A4A127CB04A25679300155B04358FFCDA5CA1F43FCA256DA6000942C9 (accessed 25/09/2009).

Dimitrakopoulos, A. P. and Bemmerzouk, A. M., 2003. Predicting live herbaceous moisture content from a seasonal drought index, *International Journal of Biometeorology,* **47**: 73-79.

Dimitrakopoulos, A. P. and Papaioannou, K. K., 2001. Flammability Assessment of Mediterranean Forest Fuels, *Fire Technology,* **37**: 143–152.

Donatelli, M. and Campbell, G. S. (Eds.)*,* 1998. *A simple model to estimate global solar radiation* 5th Congress of the European Society for Agronomy, II, Nitra, Slovakia.

Drosdowsky, W. and Williams, M., 1991. The Southern Oscillation in the Australian Region. Part I: Anomalies at the Extremes of the Oscillation, *Journal of Climate,* **4**(6): 619-638.

Duarte, H. F., Dias, N. L. and Maggiotto, S. R., 2006. Assessing daytime downward long-wave radiation estimates for clear and cloudy skies in Southern Brazil, *Agricultural and Forest Meteorology,* **139** (3-4): 171-181.

Dudley, M., 2003. Current Methods to Assess Fire Danger Potential, In *Wildland Fire Danger: Estimation and Mapping - The Role of Remote Sensing Data*, Ed, Chuvieco, E. World Scientific Publishing, Singapore.

EcoWISE, 2008. *Daily weather data from Corin Dam (1996-2008)*. EcoWISE Environmental Services, Canberra.

Environment ACT, 2004. *Map of Fire History (Wildfires and Prescribed Fires)*, Environment ACT, Department of Urban Services, ACT.

Fisher, J. B., Tu, K. P. and Baldocchi, D. D., 2008. Global estimates of the land–atmosphere water flux based on monthly AVHRR and ISLSCP-II data, validated at 16 FLUXNET sites, *Remote Sensing of Environment*: **112**: 901–919.

Flannigan, M. and Wotton, B., 2001. Climate, weather and area burned, In *Forest fires* Eds, Johnson, E. and Miyanishi, K. Academic Press, New York, pp. 351-373.

Fogarty, L. G., Pearce, H. G., Catchpole, W. R. and Alexander, M. E., 1998b. Adoption vs. adaptation: lessons from applying the Canadian Forest Fire Danger Rating System in New Zealand. *In Proceedings, 3rd International Conference on Forest Fire Research and 14th Fire and Forest Meteorology Conference*, Luso, Coimbra, Portugal, 16-20 November, 1998.

Foley, J. C., 1947. *A Study of Meteorological Conditions associated with Bush and Grass Fires and Fire Protection Strategy in Australia*, Bureau of Meteorology, Commonwealth of Australia. Melbourne.

Fowler, A.G. 1992. Climate change and water resources in the Auckland region, PhD, University of Auckland, Auckland.

Fowler, A. G. 1994. User Manual for DBMS92 software, University of Auckland, Auckland,

Fowler, A. G., 1999. Potential climate change impacts on water resources in the Auckland Region (New Zealand), *Climate Research,* **11** (3): 221-245. Available at: http://www.int-res.com/abstracts/cr/v11/n3/p221-245/ (accessed 10/04/2008).

Fowler, A.G. 2002. Assessment of the validity of using mean potential evaporation in the computation of the long-term water balance, *Journal of Hydrology,* **256**: 248-263.

Fowler, A.G. and Adams, K., 2004. Twentieth century droughts and wet periods in Auckland (New Zealand) and their relationship to ENSO, *International Journal of Climatology,* **24** (15): 1947-1961.

Gash, J. H. C. and Shuttleworth, W. J., 1991. Tropical Deforestation: Albedo and the Surface-Energy Balance, *Climatic Change,* **19**: 123-133.

Geerts, B., 2003. Empirical estimation of the monthly-mean daily temperature range, *Theoretical and Applied Climatology,* **74** (3-4): 145-165.

Gellie, N. J. H., 2005. The Vegetation of the Southern Forests: South-East Highlands, Australian Alps, South-west Slopes, and SE Corner bioregions, *Cunninghamia,* **6** (2): 219-253.

Geoscience Australia, 2003. *1:2.5 Million Topographic Data*, Geoscience Australia, Commonwealth of Australia, Canberra.

Gill, A. M., 2005. Landscape fires as social disasters: An overview of 'the bushfire problem', *Environmental Hazards,* **6**: 65-80.

Good, P., Moriondo, M., Giannakopoulos, C. and Bindi, M., 2008. The meteorological conditions associated with extreme fire risk in Italy and Greece: relevance to climate model studies, *International Journal of Wildland Fire,* **17**: 155-165.

Gordon, A. D., 1987. A Review of Hierarchical Classification, Journal of the Royal Statistical Society. Series A (General), **150** (2): 119-137.

Hanstrum, B. N., Wilson, K. J. and Barrell, S. L., 1990. Prefrontal Troughs over Southern Australia. Part II: A Case Study of Frontogenesis, *Weather and Forecasting,* **5** (1): 32-46.

Hargreaves, G. L., Hargreaves, G. H. and Riley, P., 1985. Irrigation water requirement for the Senegal Water Basin, *Journal of Irrigation Drainage Engineering ASCE,* **111**: 265-275.

Hari P., Mäkelä A., Berninger F. *et al.* (1999). Field evidence for the optimality hypothesis of gas exchange in plants. Australian Journal of Plant Physiology, 26, 239–244.

Harrison, M. S. J. 1986. A synoptic climatology of South African rainfall variations, PhD Thesis, University of Witswatersrand, Johannesburg.

Hessl, A. E., McKenzie, D. and Schellhaas, R., 2004. Drought and Pacific Decadal Oscillation linked to Fire Occurrence in the inland Pacific Northwest, *Ecological Applications,* **14** (2): 425-442.

Hobbs, J. E., 1998. Present Climates of Australia and New Zealand, In *Climates of the Southern Continents - Present, Past and Future* Eds, Hobbs, J. E., Lindesay, J. and Bridgman, H. A., John Wiley and Sons, Chichester.

Horel, J. D. and Wallace, J. M., 1981. Planetary-Scale Atmospheric Phenomena Associated with the Southern Oscillation, *Monthly Weather Review,* **109** (4): 813-829.

Idso, S. B., 1981. A set of equations for full spectrum and 8- to 14μm and 10- to 12.5μm thermal radiation from cloudless skies, *Water Resources Research,* **17**: 295-304.

Idso, S. B. and Jackson, R. D., 1969. Thermal radiation from the atmosphere. *Journal of Geophysics Research,* **74**: 3397-3403.

IPCC, 2007a. *Climate Change 2007 - The Physical Science Basis. Contribution of Working Group I to the Fourth Assessment Report of the IPCC,* Cambridge University Press.

Iqbal, M., 1983. *An introduction to solar radiation* Academic Press, Toronto.

Iziomon, M. G., Mayer, H. and Matzarakis, A., 2003. Downward atmospheric long-wave irradiance under clear and cloudy skies: measurement and parameterization, *Journal of Atmospheric and Solar-Terrestrial Physics,* **65**: 1107-1116.

Jarvis, P. G., James, G. B. and Landsberg, J. J., 1976. Coniferous Forest, In *Vegetation and the Atmosphere* Vol. 2, Ed, Monteith, J. L., Academic Press, New York.

Jiang, N., Neelin, J. D. and Ghil, M., 1995. Quasi-quadrennial and quasi-biennial variability in the equatorial Pacific, *Climate Dynamics,* **12** (2): 101-112. Available at: http://dx.doi.org/10.1007/BF00223723 (accessed 16/09/2008)

Jimenez, J. I., Alados-Arboledas L., Castro-Diez Y. and G, B., 1987. On the Estimation of Long-Wave Radiation Flux from Clear Skies, *Theoretical Applied Climatology,* **38**: 37-42.

Johnson, E. A., 1992. *Fire and Vegetation Dynamics: Studies from the North American Boreal Forest,* Cambridge University Press.

Johnson, E. A. and Larsen, C. P. S., 1991. Climatically Induced Change in Fire Frequency in the Southern Canadian Rockies *Ecology,* **72**: 194-201.

Keetch, J. J. and Byram, G. M., 1968. *A Drought Index for Forest Fire Control*, Research Paper SE-38, South-East Forest Experimental Station, USDA Forest Service, Asheville, NC, USA.

Kidson, J. W., 1988. Indices of the Southern Hemisphere zonal wind, *Journal of Climate,* **1**: 183-194.

Kimball, J. S., Running, S. W. and Nemani, R., 1997. An improved method for estimating surface humidity from daily minimum temperature, *Agricultural and Forest Meteorology,* **85** (1-2): 87-98.

Klein, J. L., 1997. *Statistical Visions in Time,* Cambridge University Press, Cambridge.

Kuczera, G. 1988. The Soil Dryness Index Streamflow Yield Model: An Overview of Its Development and Capabilities, In *18th Hydrology and Water Resources Symposium, Canberra, A.C.T,* Institution of Engineers, Australia, Barton, ACT.

Langford, K. J., Duncan, H. P. and Heeps, D. P., 1978. Evaluations and use of a water balance model., *Institute of Engineers of Australia Civil Engineering Transactions*: 48-53.

Leuning, R., Cleugh, H. A., Zegelin, S. J. and Hughes, D., 2005. Carbon and water fluxes over a temperate Eucalyptus forest and a tropical wet/dry savanna in Australia: measurements and comparison with MODIS remote sensing estimates, *Agricultural and Forest Meteorology,* **129** (3-4): 151-173.

Lhomme, J. P., 1997. Towards a rational definition of potential evaporation, *Hydrology and Earth System Sciences,* **1 (2)**: 257-264.

Linacre, E., 1992. *Climate Data and Resources - a reference and guide,* Routledge, London.

Linacre, E., 2004. Evaporation Trends, *Theoretical Applied Climatology,* **79**: 11-21.

Linacre, E. and Geartz, B., 1997. *Climates and Weather Explained,* Routledge, London.

Lindesay, J., 2003. Climate and Drought in Australia, In *Beyond Drought - People, Policy and Perspectives* Eds, Botterill, L. C. and Fisher, M., CSIRO Publishing, Collingwood.

Lindesay, J., 2005. Climate and Drought in the Sub-Tropics-The Australian Example, In *From Distaster Response to Risk Management - Australia's National Drought Policy* (Eds, Botterill, L. C. and Wilhite, D. A.) Springer, Dordrecht, The Netherlands.

Liu, D. L. and Scott, B. J., 2001. Estimation of Solar Radiation in Australia from rainfall and temperature observations, *Agricultural and Forest Meteorology,* **91**: 209-221.

Luke, R. H. and McArthur, A. G., 1978. *Bushfires in Australia,* Australian Government Publishing Service, Canberra.

Mathsoft 2005. *S-PLUS language Reference Guide*, Data Analysis Products Division, Mathsoft, Palo Alto.

McArthur, A. G., 1962. *The Application of a Drought Index to Australian Fire Control*, Forest Research Institute, Forestry and Timber Bureau, Canberra.

McArthur, A. G., 1962. *Control Burning in Eucalypt Forests*, Leaflet No. 80, Forest Research Institute, Forestry and Timber Bureau.

McArthur, A. G., 1966. *Weather and Grassland Behaviour*, Leaflet No. 100, Forest Research Institute, Forestry and Timber Bureau, Canberra.

McArthur, A. G., 1967. *Fire Behaviour in Eucalypt Forests*, Leaflet No. 107, Forest Research Institute, Forestry and Timber Bureau, Canberra.

McArthur, A. G. and Cheney, N. P., 1972. *Source Notes on Forest Fire Control*, Forest Research Institute, Forestry and Timber Bureau, Canberra.

McBride, J. L. and Nicholls, N., 1983. Seasonal Relationships between Australian Rainfall and the Southern Oscillation, *Monthly Weather Review,* **111** (10): 1998-2004.

McKenzie, N., Jacquier, D., Isbell, R. and Brown, K., 2004. *Australian Soils and Landscapes - an illustrated compendium* 2nd Edition*,* CSIRO, Collingwood.

McLeod, R., 2003. *Inquiry into the Operational Response to the January 2003 Bushfires in the ACT*, ACT Government, Department of Urban Services.

Monteith, J. L., 1965. Evaporation and the Environment, *Proceedings of Symposium on Experimental Biology,* **19**: 205-234.

Moore, C. J., 1976. A comparative study of the radiation balance above forest and grassland, *Quarterly Journal of the Royal Meteorological Society,* **102**: 889-899.

Moore, I. D., Norton, T. W. and Williams, J. E., 1993. Modelling environmental heterogeneity in forested landscapes, *Journal of Hydrology,* **150** (2-4): 717-747.

Morgan, P., Heyerdahl, E. K. and Gibson, C. E., 2008. Multi-season climate synchronised forest fires throughout the 20th century, Northern Rockies, USA, *Ecology,* **89** (3): 717–728.

Mount, A. B., 1972. *The derivation and testing of a soil dryness index using run-off data*, Forestry Commission of Tasmania, Hobart.

Mount, A. B. 1980. *Estimation of evaporative losses from forests; a proven simple model with wide applications*, Hydrology and Water Resources Symposium, Institute of Engineers of Australia, Adelaide.

Murphy, B. F. and Timbal, B., 2008. A review of recent climate variability and climate change in southeastern Australia, *International Journal of Climatology*, 28(7): 859-879.

Noble, I. R., Bary, G. A. V. and Gill, A. M., 1980. McArthur's fire-danger meters expressed as equations, *Australian Journal of Ecology* **5**: 201-203.

Oke, T. R., 1987. *Boundary Layer Climates,* Methuen, London.

O'Loughlin, E.M., Cheney, P. and Burns, J., 1986. The Bushranger's experiment: Hydrological response of a eucalypt catchment to fire, In *The First National Symposium on Forest Hydrology*, Eds, E.M. O'Loughlin and Bren, L. J., Institute of Engineers Australia, Canberra.

Palmer, W. C., 1965. *Meteorological drought*, US Department of Commerce Weather Bureau, Washington DC.

Paltridge, G. W., 1975. Net Radiation over Australia, Search, **6**: 37-39.

Paltridge, G. W. and Proctor, D., 1976. Monthly mean solar radiation statistics for Australia, *Solar Energy,* **18** (3): 235-243.

Pellizzaro, G., Cesaraccio, C., Duce P., Ventura, A. and Zara, P., 2007. Relationships between seasonal patterns of live fuel moisture and meteorological drought indices for Mediterranean shrubland species, *International Journal of Wildland Fire,* **2007**(16): 232-241.

Penman, H. L., 1948. Natural evaporation from open water, bare soil, and grass, *Proceedings of the Royal Society of London, Series A, Mathematical and Physical Sciences,* **193**: 120-145.

Pompe, A. and Vines, R. G., 1966. The influence of moisture on the combustion of leaves, *Australian Forestry,* **30**: 231-241.

Pook, E. W., Costin, A. B. and Moore, W. E., 1966. Water stress on native vegetation during the drought of 1965, *Australian Journal of Botany,* **14** (2): 257-267.

Prata, A. J., 1996. A new long-wave formula for estimating downward clear-sky radiation at the surface, *Quarterly Journal of the Royal Meteorological Society,* **122**: 1127-1151.

Prescott, J. A., 1940. Evaporation from a water surface in relation to evaporation, *Transcripts of the Royal Society of South Australia,* **54**: 114-118.

Priestley, C. H. B. and Taylor, R. J., 1972. On the assessment of surface heat flux and evaporation using large scale parameters, *Monthly Weather Review,* **100**: 81-92.

Pryor, L. D., 1939. The Bushfire Problem in the ACT, *Australian Forestry,* **4**: 33-38.

Raupach, M. R., Kirby, J. M., Barrett, D. J., Briggs, P. R., Lu, H. and Zhang, L., 2001. *Balances of Water, Carbon, Nitrogen, and Phosphorus in Australian Landscapes: (2) Model Formulation and Testing*, CSIRO Land and Water Technical Report 41/10, CSIRO, Canberra.

Rawson, R.P., Billing, P.R., & Duncan, S.F. 1983, The 1982/83 forest fires in Victoria, *Australian Forestry*, **46** (3): 163-172.

Reiff, J., Blaauboer, D., de Bruin, H. A. and van Ulden, A. P., 1984. An air mass transformation model for short-range weather forecasting, *Monthly Weather Review,* **112**:393-412.

Roderick, M. L., 1993. *Methods for Calculating Solar Position and Day Length Including Computer Programs and Subroutines*, Western Australian Department of Agriculture, Perth.

Roderick, M. L., 1999. Estimating the diffuse component from daily and monthly measurements of global radiation. *Agricultural and Forest Meteorology*, **95**: 169-185.

Romesberg, H. C., 1984. *Cluster Analysis for Researchers,* Lifetime Learning Publications, Belmont, California.

Rothermel, R. C., 1972. *A mathematical model for predicting the spread in wildland fuels*, US Department of Agriculture Forest Service, Intermountain Forest and Range Experimental Station, Ogden, Utah, USA.

RSBS (2008) Short and long-wave radiation measurements taken at Canberra Airport (2007-2008), Research School of Biological Sciences, Canberra.

Schoennagel, T., Veblen, T. T., Romme, W. H., Sibold, J. S. and Cook, E. R., 2005. ENSO and PDO variability affect drought-induced fire occurrence in rocky mountain subalpine forests, *Ecological Applications,* **15** (6): 2000-2014.

Sear, C. B., Kelly, P. M., Jones, P. D. and Goodess, C. M., 1987. Global surface-temperature responses to major volcanic eruptions, *Nature,* **330**: 365-367.

Silberstein, R., Held, A., Hatton, T., Viney, N. and Sivapalan, M., 2001. Energy balance of a natural jarrah (*Eucalyptus marginata*) forest in western Australia: measurements during the spring and summer, *Agricultural and Forest Meteorology,* **109**: 79-104.

Simard, A. J., 1991. Fire severity, changing scales, and how things hang together, *International Journal of Wildland Fire,* **1** (1): 23- 34.

Stewart, J. B., 1971. The albedo of a pine forest, *Quarterly Journal of the Royal Meteorological Society,* **97**: 561-564.

Stretton, L. E. B., 1939. *Report of the Royal Commission to Inquire into the Causes of and Measures Taken to Prevent the Bush Fires of January 1939, and to Protect Life and Property*, Government Printer, Melbourne.

Stull, R. R., 2000. *Meteorology for Scientists and Engineers,* Brooks Cole, California.

Sturman, A. and Tapper, N., 2006. *The Weather and Climate of Australia and New Zealand. 2nd edition,* Oxford University Press, Melbourne.

Supit, I. and van Kappel, R. R., 1998. A simple method to estimate global radiation, *Solar Energy,* **63** (3): 147-160.

Swinbank, W. C., 1963. Long-wave radiation from clear skies, *Quarterly Journal of the Royal Meteorological Society,* **89**: 330-348.

Talsma, T., 1983. Soil of the Cotter catchment, ACT: distribution, chemical and physical properties, *Australian Journal of Soil Research,* **21**: 241-255.

Taylor, J. and Webb, R., 2005. Meteorological aspects of the January 2003 southeastern Australia bushfire outbreak, *Australian Forestry,* **68** (2): 94-103.

Taylor, S. W. and Alexander, M. E., 2006. Science, technology, and human factors in fire danger rating: the Canadian experience, *International Journal of Wildland Fire,* **15**(1): 121-135.

Thresher, R. E., 2002. Solar correlates of Southern Hemisphere mid-latitude climate variability, *International Journal of Climatology,* **22**: 901-915.

Turner, D. P., Ritts, W. D., Cohen, W. B., Gower, S. T., Running, S. W., Zhao, M., Costa, M. H., Kirschbaum, A. A., Ham, J. M., Saleska, S. R. and Ahl, D. E., 2006. Evaluation of MODIS NPP and GPP products across multiple biomes, *Remote Sensing of Environmen*t, 102(3-4): 282-292.

Trevitt, A. C. F., 1989. Weather parameters and fuel moisture content: standards for fire model inputs, In *Proceedings - Conference on Bushfire Modelling and Fire Danger Rating Systems*, CSIRO Canberra.

Trnka, M., Zalud, Z., Eitzinger, J. and Dubrovsky, M., 2005. Global solar radiation in Central European lowlands estimated by various empirical formulae, *Agricultural and Forest Meteorology,* **131**: 54-76.

University of Wyoming , Department of Atmospheric Science, 2008. *Atmospheric Soundings,* College of Engineering, University of Wyoming. (acccessed online between 01/07/2006 and 04/04/2008).

Van Wagner, C. E., 1972. Heat of combustion, heat yield, and fire behavior, *Forestry Service Informational Report* PS-X-35, Environment Canada.

Van Wagner, C. E., 1987. *Development and Structure of the Canadian Forest Fire Weather Index System*, Petawawa National Forestry Institute, Canadian Forestry Service, Ottawa.

Vertessy, R. A., Watson, G. R. and O'Sullivan, S. K., 2001. Factors determining relations between stand age and catchment water balance in mountain ash forests, *Forest Ecology and Management,* **143**: 13-26.

Viegas, D. X., Bovio, G., Ferreira, A., Nosenzo, A. and Sol, B., 1999. Comparative study of various methods of fire danger evaluation in southern Europe, *International Journal of Wildland Fire,* **9**(4): 235-246.

Vines, R. G., 1974. *Weather patterns and bushfire cycles in southern Australia*, CSIRO Division of Chemical Technology Technical Paper No. 2, CSIRO, Melbourne.

Viney, N. R., 1991. A Review of Fine Fuel Moisture Modelling *International Journal of Wildland Fire*, 1 (4): 215-234.

Ward, R. C. and Robinson, M., 2000. *Principles of Hydrology* 4th Edition*,* McGraw Hill, London.

Westerling, A. L., Gershunov, A., Brown, T. J., Cayan, D. R. and Dettinger, M. D., 2003. Climate and Wildfire in the Western United States, *American Meteorological Society,* May 2003*:* 595-604.

Williams, A. J. and Stone, R. C., 2008. An assessment of relationships between the Australian subtropical ridge, rainfall variability, and high-latitude circulation patterns, *International Journal of Climatology,* **2008** (9999): 9999 (Early view).

Winslow, J. C., Hunt, E. R. and Piper, S. C., 2001. A globally applicable model of daily solar irradiance estimated from air temperature and precipitation data, *Ecological Modelling,* **143**: 227-243.

World Meteorological Organization, 1983. *Guide to Meteorological Instruments and Methods of Observation*, WMO.

World Meteorological Organization, 1988. *Technical Regulations, General Meteorological Standards and Recommended Practices*, WMO.

Wotton, B., 2008. Interpreting and using outputs from the Canadian Forest Fire Danger Rating System in research applications, *Environmental and Ecological Statistics*, accessed 20/06/2008).

Appendix 1: Calculations of All-wave Net Radiation, Evaporation, and their respective Components for Canberra Airport and the upper Cotter River catchment

Refer to CD-ROM

Appendix 2: Calculations of Soil Water Deficit (SWD) for Canberra Airport and the upper Cotter River catchment

Refer to CD-ROM.

Appendix 3: Method for Calibrating the Fowler daily soil water balance model

The rainfall and cumulative E_P data were combined to produce a single dataset for input to the Fowler daily soil water balance model supplied by Fowler (1994). This model requires a detailed set of parameters to run the model (Table A3.1). Acronyms for the model parameters are documented in Fowler's user manual that explains how these input variables can be used to calibrate the Fowler (F-DSWBM) model.

To calibrate the Fowler daily soil water balance model, the values of the key parameters for this model at Canberra Airport and in the upper Cotter River Catchment were adjusted in a series of model runs until a satisfactory fit between F-DSWBM and the RSDI model were achieved (R_2>0.80).

First, the interception values in the Fowler daily soil water balance model were matched with those used until a close fit was attained. Then the values of the key parameters to adjust values of evapotranspiration and runoff were PEtsPEg0, PEtsPEg5, AWC, D_{MAX}, Dc and SRF_RL. Available water capacity was increased from 165 to 200 mm to reflect the increase in soil water capacity in the deeper forest soils (see Table A3.1). At the start of simulations, PEtsPEg0 was set as equal to 1.0 and PEtsPEg5 as equal to 0.65.

For Canberra Airport, values of PEtsPEg0 and PEtsPEg5 were adjusted downwards to values of 0.75 and 0.45 from their initial values of 1.0 and 0.5 in order to obtain a calibrated SWD time series for Canberra Airport, based on dry sclerophyll forests in the sub-montane climate zone. The values of the parameter DMAX was also adjusted downwards from 1.0 to 0.5 to reflect the slower drainage of water out of the red podzolic soils underlying dry sclerophyll forests. The value of Dc was also set at 8 to reflect slow drainage out of the soil.

In the upper Cotter River catchment, the value of PEtsPEg0 was left unchanged at 1.0. This higher value characterizes the higher evaporation found in the more productive forests within the moister montane climate zone. The parameter PEtsPEg5 was adjusted downwards to 0.60 in order to obtain the best correlation between values of SWD produced by the F-DSWBM and the RSDI models. The values of D_{MAX} and D_C were set to 1 and 4 respectively to reflect the better soil drainage in the more friable soils found in the upper Cotter River catchment.

Table A3.1 Model parameters and final values for the Fowler daily soil water balance model

Parameter	Description of parameter	Values for Canberra Airport	Values for the upper Cotter River catchment
*INT0P	Effective rainfall threshold (mm)	0.2	0.2
*INT1P, INT1Peff	Rainfall and effective rainfall values for hinge point 1 (mm)	3, 2.6	3, 1.8
*INT2P, INT2Peff	Rainfall and effective rainfall values for hinge point 2 (mm)	7, 5.0	7, 4.5
*PEtsPEg0	Overall potential dry canopy evaporation as a proportion of E_P estimated from Priestley Taylor equation. (mm)	0.75	1.0
*PEtsPEg5	potential dry canopy evaporation set for particular vegetation types	0.45	0.60
*EiPEts	Evaporation effectiveness ratio on a wet day (mm)	3	3
*AWC	Available water capacity (mm)	165	200
*AWCup	Starting available water capacity (AWC) (mm)	200	0
*SWD_0	Starting soil water deficit (mm)	0	0
$SWCup_0$	Starting AWC (mm)	0	0
*D_{MAX}	Amount of drainage when soil water (SW) exceeds available water capacity (AWC) (mm)	0.5	1
Dc	Drainage function parameter C	8	4
SSC	Surface storage capacity (mm)	0.5	1.0
IAa	Initial abstraction parameter	1.0	1.0
*SRF_RL	Threshold at which soil water resistance commences (mm)	25	25
QQ_0	Starting quickflow value (mm)	5	5
QQa, QQb	Quickflow recession parameters	4, 1, 31	4, 1, 31
QQprop	Proportion of quickflow in relation to total runoff (Q)	0.8	0.8
QB_0	Starting baseflow value (mm)	0.3	0.3
QBa, QBb	User defined baseflow recession parameters	35, 0.8	35, 0.8

Notes: (1) * denotes variables varied in the Fowler daily water balance model in this study. Interception (E_I) values found for a dry sclerophyll forest type near Canberra Airport were employed to calibrate the interception values in the F-DSWBM model. Runoff values were not adjusted due to a lack of suitable run-off data needed to calibrate these parameters.

(2) The last five parameters relating to run-off were left unadjusted in the calibration procedure.

Appendix 4: Calculations of Fire Weather Index (FWI) for Canberra Airport

Refer to CD-ROM.